

AD-A192 429

NASA

Technical Memorandum 4024

AVSCOM

Technical Report 87-B-4

Acoustic Measurements From a Rotor Blade-Vortex Interaction Noise Experiment in the German-Dutch Wind Tunnel (DNW)

R. M. Martin

*Langley Research Center
Hampton, Virginia*

W. R. Splettstoesser

*Deutsche Forschungs- und
Versuchsanstalt fur
Luft- und Raumfahrt
Braunschweig, West Germany*

J. W. Elliott

*Aerostructures Directorate
USAARTA-AVSCOM
Langley Research Center
Hampton, Virginia*

K.-J. Schultz

*Deutsche Forschungs- und
Versuchsanstalt fur
Luft- und Raumfahrt
Braunschweig, West Germany*

NASA

National Aeronautics
and Space Administration

Scientific and Technical
Information Division

1988

This document has been approved
for public release and sale in
distribution is unlimited.

Contents

Abstract 1

Introduction 1

Symbols 1

Experimental Apparatus and Procedures 2

 Wind Tunnel 2

 Model Rotor Test Apparatus 2

 Model Test Stand and Support 2

 Model Rotor 3

 Rotor Performance Data Acquisition and Reduction 3

 Matrix of Test Conditions 3

 Acoustic Instrumentation 4

 Microphone Array Traverse System 4

 Fuselage-Mounted Microphones 4

 Acoustic Data Reduction and Analysis 5

 Data Quality 5

 Tunnel Flow Quality 5

 Rotor Performance Data 5

 Background Noise 5

 Acoustic Reflections 6

 Acoustic Shielding by Fuselage 7

 Steadiness and Repeatability of Rotor Acoustic Data 7

 Testing Procedures and Measurement Accuracy 7

Presentation of Data 8

References 8

Tables 9

Figures 11

Averaged Acoustic Signals 23

Accession For	
NTIS GRA&I	<input checked="" type="checkbox"/>
DTIC TAB	<input type="checkbox"/>
Unannounced	<input type="checkbox"/>
Justification	
By _____	
Distribution/	
Availability Codes	
Dist	Avail and/or Special
A-1	



Abstract

Acoustic data are presented from a 40-percent-scale model of the four-bladed BO-105 helicopter main rotor, tested in a large aeroacoustic wind tunnel. Rotor blade-vortex interaction (BVI) noise data in the low-speed flight range were acquired using a traversing in-flow microphone array. The experimental apparatus, testing procedures, calibration results, and experimental objectives are fully described. A large representative set of averaged acoustic signals are presented.

Introduction

The primary objectives of the test program reported here were (1) to acquire a comprehensive data base to improve the definition of the directivity patterns of rotor blade-vortex interaction (BVI) impulsive noise, (2) to investigate more fully retreating-side BVI noise, and (3) to improve knowledge of the locations of BVI noise sources. Secondary objectives of the program were (1) to access the far field of rotor BVI noise, (2) to extend the investigation of reference 1 into the scalability from model- to full-scale of the BVI signal at high advance ratio, (3) to explore the parametric effects of advance ratio, tip-path-plane angle, and thrust coefficient on BVI noise, and (4) to acquire a noise data base for future development of a BVI noise prediction methodology.

The test was performed in the open test section of the Duits-Nederlandse Windtunnel (DNW), a large aeroacoustic test facility, utilizing a four-bladed, 40-percent dynamically scaled model of the Messerschmitt-Bölkow-Blohm GmbH BO-105 helicopter main rotor. The experiment was performed jointly with research personnel of the German Aerospace Research Establishment, the Deutsche Forschungs- und Versuchsanstalt für Luft- und Raumfahrt (DFVLR). The model rotor and the rotor test stand were provided and operated by research personnel of the Rotary Wing Aircraft Branch of the DFVLR Institute of Flight Mechanics. Acoustic instrumentation support was provided by research personnel of the Technical Acoustics Division of the DFVLR Institute of Design Aerodynamics.

High quality acoustic data were acquired due to the excellent fluid dynamic and acoustic properties of the DNW. In particular, the tunnel has quite low in-flow background noise and turbulence levels and a sizable anechoic open test section. The importance of low turbulence airflow on rotor acoustic testing is stressed in reference 2, a comparison of acoustic results from a model rotor tested in both the DNW and the French CEPRA-19 tunnel.

An extensive range of in-flow acoustic measurements were acquired in a plane underneath and upstream of the rotor model using a traversing nine-microphone array. A digital acoustic data acquisition system was employed to guide the choice of the test matrix and identify optimum measurement locations by using on-line identification of strong BVI noise test conditions. The BVI directivity was investigated by using an array of microphones traversing in a large plane under and upstream of the rotor. A high quality data base for acoustic localization techniques was acquired through a large range of measurement locations. The occurrence of BVI acoustic signals created on the retreating side of the rotor was pursued by positioning the microphone array under and downstream of the rotor, in positions previously found to best measure the phenomenon (ref. 3).

This paper addresses the general philosophy and experimental approach of this program. Test results on acoustic directivity, retreating-side BVI, and BVI source locations have been presented in references 4 to 6. In the present paper, the model test rig, instrumentation, data acquisition and reduction, acoustic calibrations, and experimental procedures are fully documented. A large representative set of the averaged acoustic signals are presented.

Symbols

C_T	rotor thrust coefficient, $T/\pi\rho\omega R^4$
f_c	filter cutoff frequency, Hz
r	radial distance from rotor hub to microphone (see fig. 1), m
M_H	hover tip Mach number
R	rotor radius, 2.0 m
T	rotor thrust, N
V	flow speed, m/sec
X_w	streamwise location of traversing array relative to hub, positive upstream (see fig. 1), corrected for streamwise movement of hub due to model pitch, m
Y_w	cross stream location of traversing array microphones relative to hub, positive under advancing side (see fig. 1), m
Z_w	vertical location of traversing array, positive above hub (see fig. 1), m
α_{shaft}	angle of rotor shaft from vertical, deg
α_{TPP}	rotor tip-path-plane angle, positive nose up (see fig. 1), deg

Δf	spectral bandwidth, Hz
θ	polar angle, angle centered at hub from tip-path plane to microphone location, positive down (see fig. 1), deg
μ	advance ratio, $V/\omega R$
ρ	density, kg/m^3
ψ	azimuth angle in tip-path plane from rotor hub to microphone location, zero over tail, 90° over rotor advancing side (see fig. 1), deg
ω	rotational speed of rotor, cycles/sec

Abbreviations:

ATD	analog-to-digital
BVI	blade-vortex interaction
DFVLR	Deutsche Forschungs- und Versuchsanstalt für Luft- und Raumfahrt
DNW	Duits-Nederlandse Windtunnel (German-Dutch Wind Tunnel)
DTA	digital-to-analog
Mic	microphone
rms	root-mean-square quantity
rpm	revolutions per minute
SPL	sound pressure level, dB referenced to 2×10^{-5} Pa rms

Experimental Apparatus and Procedures

Wind Tunnel

The test was performed in the open test section of the Duits-Nederlandse Windtunnel (DNW), located in the North East Polder, The Netherlands. The DNW is a subsonic, atmospheric, closed circuit wind tunnel with three interchangeable, closed test section configurations and one open configuration. The open configuration employs an 8×6 m contraction section, shown in figure 2, and a 19-m-long test section, surrounded by a large anechoic hall of about $30\,000 \text{ m}^3$ lined with absorptive acoustic wedges. The tunnel has excellent fluid dynamic qualities, fully described in references 7 to 10.

Model Rotor Test Apparatus

Model Test Stand and Support

The DFVLR rotor test stand (refs. 11-13) is shown installed in the DNW open test section in figure 3. Details of the rotor test stand are given in

figure 4 and table I. The stand consists of three major subsystems: the hydraulic drive system, the rotor balance system, and the rotor control system. During this test, the stand was housed within an acoustically insulated fiberglass shell and was attached to the computer-controlled, hydraulic sting support mechanism.

The rotor drive system consists of a seven-piston axial drive motor connected by hydraulic lines to a remotely located electrically driven pump. The axial hydraulic motor is connected directly to the rotor shaft and has a power capability of 100 kW at 1050 rpm.

The rotor balance system is a six-component balance containing separate measuring elements for static and dynamic load components. The balance consists of a lower and an upper plate connected through transmission rods. Seven load cells on the lower plate measure the static components. The dynamic components are measured by means of piezoelectrical transducers connected to the transmission rods. A separate load cell is provided to measure the rotor torque and is located between the upper and lower balance plates. This ensures that no undesired coupling between the rotor balance and the drive shaft occurs.

The rotor control system is of a swashplate system consisting of three electric actuators attached to the upper plate, the swashplate, and the rotating blade pitch control rods. The actuators provide collective and cyclic blade pitch control by moving the nonrotating part of the swashplate and are remotely controlled. A potentiometer at the root of one of the blades measures the blade angle of incidence during rotation.

The fuselage is constructed of a 4-mm-thick reinforced fiberglass shell covered on the inside with a heavy 3.5-mm-thick layer of sound-damping material and a 30-mm-thick layer of open cell sound-absorbing foam. The outer side of the fuselage is lined with 50-mm-thick open-cell foam to minimize acoustic reflections. The overall sound pressure level transmission losses through the fuselage were 27 dB for simulated hydraulic drive noise and 30 dB for white noise. To maximize the transmission loss, special care was taken to shield both the gap between the rotating rotor head and the top of the fuselage and the gap between the fuselage and sting.

The model rotor rig was supported by the computer-controlled, hydraulically actuated sting. Prior to the test, a thorough analysis was made of the dynamic behavior of the rotor test rig and sting combination to ensure that a ground resonance problem would not be encountered. The sting was covered with a streamlined sound absorptive lining to

minimize acoustic reflections. The sting control system was programmed to keep a model reference point at a preselected height in the test section, for the range of angle of attack (α_{shaft}). However, it was not possible to maintain the reference point at a fixed streamwise location for the range of angle of attack.

Model Rotor

The rotor is a 40-percent, dynamically scaled model of a four-bladed, hingeless BO-105 rotor (fig. 5). The rotor has a diameter of 4 m with a root cutout of 0.350 m and a chord length of 0.121 m. The rotor blade is constructed of an NACA 23012 airfoil, with the trailing edge modified to form a 5-mm-long tab, to match the geometry of the full-scale rotor. The rotor blades have -8° of linear twist, a standard square tip, and a solidity of 0.077. Further details are given in table I and reference 11. The nominal rotor operating speed was 1040 rpm, giving an acoustic blade-passage frequency of about 70 Hz. The nominal hover tip Mach number was 0.64. The rotor blades are made of glass-fiber-reinforced plastic and have essentially the same mass and stiffness distributions as the full-scale rotor. However, the blade chord length ($0.061R$) is a slightly larger scale than the full-scale chord ($0.054R$) in order to maintain the proper Locke number scaling (ratio between the aerodynamic forces and the mass and elastic forces, ref. 11). Each blade is equipped with a small tab located at 70 percent of the radius, measuring 60×10 mm (shown in fig. 5). These tabs, in addition to the pitch rods, are used to adjust the track of each blade in the rotor system. Strain gages installed near the root of each blade are used to measure the blade flapping, lagging, and torsional moments.

Rotor Performance Data Acquisition and Reduction

The rotor performance data were obtained from the rotating and fixed systems of the DFVLR test stand control system (ref. 12). The rotating system acquired the signals of the strain gages on the rotor blades (flapping, lagging, and torsional moments), on the control rods (pitch link forces), on the rotor shaft (bending moment), and on the blade root potentiometer (blade pitch angle).

The rotating signals were transmitted by two 16-channel pulse-code-modulated (PCM) encoders on the rotating rotor head. The data were multiplexed, converted to a digital form, and then formatted into two serial data streams for transmission through slip rings. Subsequently, both serial data streams were reformatted into parallel signals by two decoders followed by digital-to-analog (DTA) conversion and

filtering. The rotating data were then merged with the fixed system data via a 64-channel encoder.

The fixed system also has a 32-channel capacity. Signals from the displacement transducers, the static and dynamic balance transducers, the shaft torque transducer, the shaft rpm encoder (360-per-revolution), and the shaft position encoders (once-per-revolution and 512-per-revolution) were transmitted to a PCM data acquisition system. The data acquisition system consists of a central processor unit, a coprocessor, a random access memory unit, and a magnetic tape recorder and has a useful frequency range up to 250 Hz.

Details of the rotor data processing are given in reference 13 and are summarized here. For all signals, 20 revolutions of time domain data were written to digital tape. For on-line analysis and control the central processor performed a Fourier analysis of the data of a single revolution. A second processor fed with selected analog input of the fixed and rotating system provided continuous on-line display of the rotor control parameters: hover tip Mach number, thrust, hub moments, blade bending, and pitch link loads. The final processing of the rotor performance data was done off-line by averaging the results of the 20 revolutions of stored data. These results include such parameters as collective pitch, cyclic pitch, coning angle, rotor power and thrust, and both the steady and the dynamic components of the rotor forces, moments, and longitudinal and lateral flapping angles.

Matrix of Test Conditions

A nominal test plan was developed to investigate the three primary test objectives and concentrated on two thrust coefficients, 0.0044 and 0.0030, and the forward speed range of 20 to 40 m/sec ($\mu = 0.09$ to 0.18) at a range of tip-path-plane angles for constant nominal hover tip Mach number of 0.64. The value of 0.0044 is the nominal thrust coefficient for the full-scale BO-105, while the value of 0.0030 was chosen as a lower limit of thrust level. To investigate the secondary test objectives, a smaller set of conditions included velocities of 50 and 60 m/sec, thrust coefficients ranging from 0.0036 to 0.0056, and hover tip Mach numbers ranging from 0.56 to 0.72.

To determine the optimum test conditions for strong BVI noise generation and the optimum measurement locations for the traversing microphone array, an initial exploratory approach was used. To minimize testing time during this exploratory phase, acoustic data were acquired with an on-line ATD system and were not recorded on analog tape. The on-line analysis performed during this exploratory

matrix was used to fine-tune the final, more extensive, test matrix, for which acoustic data were recorded on analog tape for postprocessing. Data from the initial exploratory matrix are presented in references 4 and 6, and the final expanded test matrix is presented in table II. The data presented here are the postprocessed acoustic signals from the final expanded matrix.

Acoustic Instrumentation

The acoustic instrumentation consisted of a nine-microphone in-flow array mounted on a traversing system and two in-flow microphones mounted on the rotor fuselage as shown in figure 3(b). The microphones were 1/2-in. pressure-type condenser microphones equipped with standard "bullet" nose cones. Each complete microphone system (microphone, preamplifier, and adapter) was calibrated using the electrostatic actuator method to document its frequency response. This response was found to be flat between 5 and 5000 Hz, sufficient for the frequency range of the BVI noise (approximately 500 to 4000 Hz for model scale).

Signal conditioning of the microphones was performed by computer-controlled amplifier and filter systems. The amplitude and phase characteristics of the two-pole Butterworth filters were investigated before the test for high-pass filtering at three nominal cutoff frequencies. The amplitude response is flat in the passband. The phase shift is 180° at the cutoff frequency f_c , is approximately 40° at $5f_c$, and negligible at approximately $10f_c$. The filters were found to be well matched in their phase characteristics, within 1° in the passband.

The acoustic data, the rotor once-per-revolution and 512-per-revolution signals, and a time code were recorded on a 14-track analog frequency-modulated recorder. The data were recorded at a tape speed 30 inches per second, which yielded a useful frequency response to about 20 kHz.

To verify the frequency response of the entire measurement system in situ (from preamplifier to tape recorder), a white noise signal was inserted simultaneously into each preamplifier and recorded on tape. The auto and cross power spectral densities of the white noise signal were checked to ensure flat frequency response and to document phase lag between channels.

The digital amplifier and filter settings were transmitted to a second, larger computer. During testing, up to 10 microphone channels could be digitized using a 12-bit, high-speed simultaneous analog-to-digital (ATD) converter. The computer was employed to control the ATD converter, to store calibration and amplification factors, and to perform on-line

time domain and spectral analysis. A two-channel fast Fourier transform analyzer was also employed for quick-look analysis during testing.

Microphone calibrations were performed using a sound level calibrator at the beginning and end of the test. All microphone gains were adjusted to produce 500-mV rms output for an acoustic level of 114 dB at 1000 Hz. In addition, a daily calibration of a 1000-Hz, 500-mV rms signal was recorded on all channels by signal insertion at the tape recorder inputs.

Microphone Array Traverse System

The microphone array traverse system consisted of a horizontal wing with its span normal to the flow direction and a traverse system with a total range in the flow direction of 8.2 m (7 m upstream, 1.2 m downstream of the hub, see fig. 3). The microphones were arranged symmetrically with respect to the tunnel centerline, spaced 540 mm apart. The array vertical position was nominally 2.1 m below the rotor hub, although a small set of data was acquired at 1.6 and 2.6 m below the hub.

The microphone holders employed a "soft" vibration-isolating mounting. A cross section of the wing is shown in figure 6. The total height of the entire structure was such that only the streamlined wing support struts crossed through the shear layer. The wing and support struts were covered with a 25-mm-thick, open-cell foam airfoil section; and the supporting structure was covered with a 100-mm-thick foam lining except at the base which was covered with 800-mm foam wedges.

The traverse mechanism was powered by a variable-speed dc electrical motor. Control and positioning was obtained with a servo position controller. The positioning accuracy was 2 mm. Prior to data acquisition, the alignment of the traversing array was calibrated over its range of motion. The alignment in the cross flow direction was ± 2 mm; in the vertical direction, less than ± 1 mm. The deflection of the traversing array due to aerodynamic drag was on the order of 9 mm in the streamwise direction at 60 m/sec. The accuracy of this correction is estimated to be ± 3 mm. These deflections were calculated off-line and applied to the measured array position data to correct the calculated microphone positions.

Fuselage-Mounted Microphones

Two microphones were mounted on the fuselage, one under each side of the rotor disk, at azimuth angles of approximately 90° and 270° . The microphones were mounted in vibration isolation mounts

similar to the mounts for the traversing array microphones (fig. 6). These microphones were mounted with a small negative angle (approximately 5°) to the tunnel free stream. This was an attempt to minimize wind-induced background noise due to the free-stream velocity, because most of the data were at positive rotor shaft angles. These microphones are still subjected to the influence of the induced flow of the rotor system, which cannot be calibrated.

Acoustic Data Reduction and Analysis

Before being recorded on analog tape, the microphone data were high-pass filtered at 4 Hz to remove very low-frequency content. The microphone and blade position reference signals (once-per-revolution and 512-per-revolution) were conditionally digitized using a sample rate keyed to the 512-per-revolution signal, which yielded 1024 data points per revolution, or a sample rate of about 18000 samples per second. An antialiasing filter was employed at 9 kHz. This conditional sampling technique is used to ensure that the acoustic samples are acquired when the rotor blades are in the same azimuthal position for every revolution sampled. The time histories were digitized in this manner, and then 40 revolutions were averaged to obtain an average acoustic waveform and standard deviation for each test condition. The average time history and its standard deviation were stored on computer disk.

To obtain spectra, the data of four sequential rotor revolutions were transformed to the frequency domain using a 4096-point fast Fourier transform algorithm. This procedure was performed 40 times, requiring the data of 160 revolutions, and the results were averaged to obtain an average narrow-band spectrum, also stored on computer disk. Considering each power spectrum as a chi-squared random variable, the statistical accuracy of the spectral results is 0.8 to -1.0 dB for an 80-percent confidence interval.

A time domain window was not applied to these data. The conditional sampling approach employed minimizes leakage of the acoustic energy at the blade-passage frequency and its harmonics, and thus a time domain window is not required to improve the spectral estimates at those frequencies.

Data Quality

Tunnel Flow Quality

The DNW has very good aerodynamic qualities when operated in the open throat mode (refs. 7-10). A potential core of uniform flow (mean flow velocity $\pm 0.5\%$) has been defined as a 5×3 m core within

the 8×6 m nominal test section, at 7 m from the jet exit. Turbulence intensities in both the streamwise and the cross stream direction are less than 0.5 at this location.

In the low-speed range, the open-jet configuration can exhibit a low-frequency, low-amplitude pulsation of the mean flow, similar to the pulsations previously observed in other open-jet tunnels (ref. 14). This pulsation occurred at certain velocities between 20 and 28 m/sec, with a maximum amplitude of ± 0.75 m/sec and a period of about 10 seconds. In some cases this pulsation caused problems in achieving stable rotor performance parameters, so that some parts of the test matrix had to be redesigned or omitted. Overall, this pulsation was of sufficiently low frequency to be considered quasi-steady compared with the analysis time for both the rotor performance and the acoustic data.

Rotor Performance Data

The nominal thrust coefficients tested were 0.0030 and 0.0044. The actual average thrust coefficients were 0.0029 and 0.00435 with standard deviations of 3% and 1.4%, respectively. The nominal hover tip Mach number was 0.64, with average and standard deviation of 0.636 and 0.5%. The first harmonics of lateral and longitudinal flapping angles were generally less than 0.3° . During the pretest calibrations, a check was made to ensure that a change in the traversing array position in the test section did not affect the rotor performance by requiring changes to the rotor control inputs.

Background Noise

The background noise data were acquired with all testing and model hardware installed in the tunnel. The blades were not installed, but the hub was spinning at nominal speed (1040 rpm).

Effect of tunnel speed. Background noise was measured for a range of tunnel speeds at a fixed nominal traverse position 3 m upstream of the hub. Examples of the spectra for microphone 1 at 20, 40, and 60 m/sec are shown in figure 7(a). Each of the nine microphones located on the traversing array shows generally the same background noise levels as microphone 1 at this position ($X_w = 3$ m). The low-frequency levels of the traverse microphones increase about 28 dB (from 82 to 110 dB) due to increasing the speed from 20 to 60 m/sec. Data for fuselage microphone 10 is shown in figure 7(b). The levels increase only about 15 dB (from 90 to 105 dB) with an increase in speed from 20 to 60 m/sec. The low-frequency background noise levels of the fuselage

microphones at the lower tunnel speeds are higher than those measured by the traversing microphones. The higher frequencies of the spectra are about the same for the fuselage and traverse microphones. The higher frequency noise levels for all microphones start at about 35 dB at 20 m/sec and increase to about 55 dB at 60 m/sec.

Effect of traversing array position. Background noise was measured at 40 m/sec for $X_w = 1, 3,$ and 5 m and at 60 m/sec for $X_w = -0.7$ and 3 m. The spectral levels increase consistently (by about 10 dB) as the traverse moves downwind and closer to the model ($X_w = 5$ to 1 m). This is illustrated by figure 8, which shows the background noise levels for $X_w = 1, 3,$ and 5 m at 40 m/sec from microphones 1 and 5 and by figure 9, which shows the data for $X_w = -0.7$ and 3 m at 60 m/sec from microphones 1 and 5. This increase in level at the downstream positions is probably due to the increased proximity of the microphones to the bottom shear layer (see fig. 3(a)) and increased proximity to the model system. The levels measured at the fuselage microphones appear to be fairly insensitive to the traverse position, indicating that the traverse itself is not creating additional background noise.

Background tones. Discrete tones were measured by some of the traverse microphones, particularly at tunnel speeds of 30, 40, and 50 m/sec, in the range of 2 to 5 kHz. The tone frequencies are not related to tunnel speed. An example can be seen in figure 8(b) for microphone 5 at 40 m/sec at two traverse positions. The highest levels of these tones appear to be about 70 dB, which is typically much lower than the rotor signals in that frequency range (see the following section on signal-to-noise ratio). The tones have the largest amplitude at upstream locations, although they are present at lower levels at $X_w = 1$ and -0.7 m. These tones are not measured by all the traverse microphones at once, indicating that the sources are localized.

Effect of rotor shaft angle. Background noise levels were studied for $X_w = 3$ and -0.7 m for rotor shaft angles of $-5^\circ, 0^\circ, 5^\circ,$ and 10° . No significant effect was seen in the traverse microphone data. The data for a fuselage microphone (microphone 10) exhibited slightly lower levels at -5° , which was expected due to the preset microphone angle of 5° (see "Fuselage-Mounted Microphones").

Acoustic signal-to-noise ratio. From the above results, the highest background noise for the traverse microphones occurs when the traverse is the farthest

downstream at the highest tunnel speed. The highest background noise for the fuselage-mounted microphones probably occurs at the largest shaft angle and highest tunnel speed. Several test conditions fitting these conditions were chosen and the rotor signals were compared with the background noise. The rotor spectra and the background spectra are almost identical at the first spectral line (20 Hz), but above this point the rotor spectrum is at least 5 dB higher than the background spectrum and typically 20 dB higher in the frequency range dominated by BVI noise, as shown in figure 10. The results indicate that the background noise levels are not a contaminant for any of the microphone measurements.

The effect of the spurious tones observed by the traverse microphones at the higher tunnel speeds and upstream positions was also investigated. These data are seen in figure 10, which shows that although the background tones are just below the rotor signal, they do not appear to be a significant contaminant.

Acoustic Reflections

To measure the potential contamination of the rotor signal due to reflections, small explosive charges were specially mounted on the model rotor test rig and detonated to create an impulsive noise source. The explosives generate peak pressure levels of approximately 148 dB at a distance of 4 m. The charges were mounted in a three-rod mock-up rotor, with 10 charges on each rod, mounted between 80 and 100 percent of the rotor radius. The mock-up rotor was installed on the rotor head with the three rods located at $60^\circ, 180^\circ,$ and 300° azimuth (ψ). Approximately 30 charges were ignited to assess the acoustic reflections for the following tunnel configurations: tunnel speeds of 0 and 60 m/sec, X_w of 4, 2, 1, and -0.7 m, and Z_w of $-0.5, 0, 0.3,$ and 0.5 m.

The acoustic signals were recorded on analog tape and analyzed on-site. For all the tested configurations, the reflected signals were generally less than 10 percent of the direct blast signal, or 20 dB down from the direct signal, and in many cases were of negligible amplitude. The effect of increasing tunnel speed was found to be negligible, as was the effect of rotor hub vertical position. An example of the blast signals measured at 60 m/sec by microphones 1, 3, 5, 7, and 9 at $X_w = 4$ m is shown in figure 11 for a blast located at $\psi = 300^\circ$. The difference in the maximum pressure measured at microphones 1, 3, and 5 can be attributed to distance from the source. The signals at microphones 7 and 9 have been shielded by the fuselage, as discussed in the next section.

Acoustic Shielding by Fuselage

Acoustic diffraction for the traversing array microphones was identified and is due to the presence of the fuselage. When the traversing array is moved close to the model, the microphones at one end of the traverse are shielded from the acoustic signal from the opposite side of the rotor disk. This was quantified by comparing the known propagation distances (from the source to each microphone) with the measured blast signal arrival times, amplitudes, and model geometry.

From the geometry of the test hardware, a free acoustic path to all the microphones exists at $X_w = 2$ m, and all the array microphones receive a directly propagated blast signal. However, the amplitudes measured at microphones 1, 2, and 3 when the source is located at $\psi = 60^\circ$ are attenuated to a larger degree than can be attributed to spherical spreading. (This is also observed at microphones 7, 8, and 9 when the source is located at $\psi = 300^\circ$.) This indicates that the fuselage is causing diffraction of the acoustic signal for this particular geometry. For traverse positions that are close to and under the model, the blast signals received by the "shielded" microphones are not the direct signal but a combination of a reflected and a diffracted signal, with significantly lower amplitudes. This can be seen in the data of microphones 7 and 9 in figure 11, for $X_w = 1$ m and the blast located at $\psi = 300^\circ$. The delay time, attenuation, and distortion of the blast waveform can be seen in the shielded microphones.

These results indicate that the directivity or absolute levels of advancing- or retreating-side BVI cannot be accurately determined from the shielded microphone locations. The conclusions can be summarized in the table below.

Source azimuth, deg	X_w , m	Shielded microphones
60	2.0	1, 2, 3, 10
	1.0	1, 2, 3, 4, 10
	-7	1, 2, 3, 4, 10
300	2.0	7, 8, 9, 11
	1.0	6, 7, 8, 9, 11
	-7	6, 7, 8, 9, 11

Steadiness and Repeatability of Rotor Acoustic Data

To illustrate the steadiness of the rotor signals, several cases were chosen for comparison. Two of these cases, at $\mu = 0.092$ and $\mu = 0.138$, are shown

in figure 12. At $\mu = 0.092$, figure 12 shows both the instantaneous data (fig. 12(a)) acquired using the on-line ATD system and the 40-average time history (fig. 12(b)) obtained from the postprocessing. The general features of the instantaneous data are consistently seen in the averaged waveform. Particular features to note are the small impulses approximately 0.01 period after the major impulses of the first three blade passages and the large impulse 0.01 period before the third major impulse. An equally good comparison, particularly in the BVI characteristics, can be found for $\mu = 0.138$ in figures 12(c) and 12(d).

The repeatability of the rotor signal was studied for several test conditions repeated during the experiment. An example of the instantaneous data acquired using the on-line system at different times during the experiment is given in figure 13, for $\mu = 0.138$ and $\alpha_{\text{TPP}} = 1.8^\circ$. These data were filtered by a 500-3000 Hz band-pass filter (ref. 5). While there is considerable random noise evident in these data, the general amplitudes and features of the major impulses can be seen in the two measurements.

Testing Procedures and Measurement Accuracy

Corrections to the free-stream flow angle and speed due to the presence of the lifting rotor in the test section were calculated according to the method of Heyson (ref. 15) and applied to the measured data off-line to obtain the corrected tip-path-plane angles presented here. These corrections are considered reasonable estimates of the true flow angle at moderate tunnel speeds, but become less reliable as the correction increases at the lower tunnel speeds, less than 20 m/sec.

Because of the pivoting of the support sting to achieve a specified shaft angle, the center of the rotor hub experiences both a vertical and a streamwise translation. The sting controller was programmed to reposition the hub at the same vertical position for any shaft angle. The streamwise movement of the rotor hub could not be corrected by repositioning the sting, but is calculated off-line and is accounted for in the calculation of microphone locations. The streamwise position of the microphones X_w is thus corrected for the movement of the hub due to model pitch angle.

In addition to the kinematic motion of the sting support, the actual rotor hub position was also influenced by vertical deflections due to its weight, the rotor angle, the rotor thrust level, and aerodynamic drag. These effects were calibrated before data acquisition by measuring the rotor hub position for the ranges of shaft angle, rotor thrust, and tunnel speed contained in the test matrix. These corrections were

then applied to the data off-line. The accuracy of the rotor hub position measurements is ± 2 mm.

The rotor parameters—tip-path-plane angle, hover tip Mach number, and thrust—were set using the digital displays at the rotor controls. The rotor operator set the rotor speed for the desired value of hover tip Mach number, simultaneously adjusting collective pitch to obtain the desired thrust. The rotor was operated so that the first harmonics of the shaft bending moments and of lateral and longitudinal flapping were as close to zero as possible. In this case, and neglecting blade bending, the measured rotor shaft angle was thus equivalent to the tip-path-plane angle.

Presentation of Data

The data presented in the plots at the end of this paper are a representative set of the postprocessed results of the final test matrix defined by table II. Preceding these plots is a detailed table of test conditions corresponding to the plots. Each plot presents the averaged time histories of traversing array microphones 1, 3, 5, 7, and 9. Spectral results are not presented here but averaged narrow-band spectra have been calculated for all test conditions. Both the averaged time histories and the spectral results are available to the research community for their use in rotor noise work and can be provided in the form of plots, computer listings, tapes, or computer disks as required. Interested persons should contact the principal author of this document.

NASA Langley Research Center
Hampton, VA 23665-5225
December 23, 1987

References

1. Spletstoesser, W. R.; Schultz, K. J.; Boxwell, D. A.; and Schmitz, F. H.: *Helicopter Model Rotor-Blade Vortex Interaction Impulsive Noise: Scalability and Parametric Variations*. NASA TM-86007, USAAVSCOM TM-84-A-7, 1984.
2. Boxwell, D. A.; Schmitz, F. H.; Spletstoesser, W. R.; Schultz, K. J.; Lewy, S.; and Caplot, M.: *A Comparison of the Acoustic and Aerodynamic Measurements of a Model Rotor Tested in Two Anechoic Wind Tunnels*. NASA TM-88364, USAAVSCOM TM-86-A-6, 1986.
3. Leighton, Kenneth P.; and Harris, Wesley L.: *On Mach Number Scaling of Blade/Vortex Noise Produced by Model Helicopter Rotors at Moderate Tip Speeds*. FDRL Rep. 84-3, Dep. of Aeronautics and Astronautics, Massachusetts Inst. of Technology, Oct. 1984.
4. Martin, Ruth M.; and Spletstoesser, Wolf R.: *Acoustic Results of the Blade-Vortex Interaction Acoustic Test of a 40 Percent Model Rotor in the DNW*. *Proceedings of the National Specialists' Meeting on Aerodynamics and Aeroacoustics*, American Helicopter Soc., c.1987.
5. Martin, R. M.; Spletstoesser, W. R.; Elliott, J. W.; and Schultz, K.-J.: *Advancing-Side Directivity and Retreating-Side Interactions of Model Rotor Blade-Vortex Interaction Noise*. NASA TP-2784, USAVSCOM TR 87-B-3 1988.
6. Spletstoesser, W. R.; Schultz, K. J.; and Martin, Ruth M.: *Rotor Blade-Vortex Interaction Impulsive Noise Source Identification and Correlation With Rotor Wake Predictions*. AIAA-87-2744, Oct. 1987.
7. Van Ditshuizen, J. C. A.; Courage, G. D.; Ross, R.; and Schultz, K.-J.: *Acoustic Capabilities of the German-Dutch Wind Tunnel DNW*. AIAA-83-0146, Jan. 1983.
8. *Compilation of Calibration Data of the German-Dutch Wind Tunnel*. MP-82.01, Duits-Nederlandse Windtunnel, Mar. 13, 1982.
9. Ross, R.; Van Nunen, J. W. G.; Young, K. J.; Allen, R. M.; and Van Ditshuizen, J. C. A.: *Aero-Acoustic Calibration of DNW Open Jet*. DNW TR 82.03, German-Dutch Windtunnel (DNW) (North East Polder, Netherlands), July 1982. (Also available as Boeing Document D6-51501, 1983.)
10. Seidel, M.; and Maarsingh, R. A.: *Test Capabilities of the German-Dutch Wind Tunnel DNW for Rotors, Helicopters and V/STOL Aircraft*. *Proceedings of the Fifth European Rotorcraft and Powered Lift Aircraft Forum*, Sept. 1979, pp. 17-1-17-22.
11. Langer, H. J. (SCITRAN, transl.): *DFVLR Rotorcraft—Construction and Engineering*. NASA TM-77740, 1984.
12. Langer, H.-J. (Leo Kanner Assoc., transl.): *Data Input, Processing and Presentation*. NASA TM-77739, 1984.
13. Breustedt, Wolfgang (SCITRAN, transl.): *Data Analysis on the Rotor Test Stand Program for Interactive Processing*. NASA TM-77948, 1985.
14. Applin, Zachary T.: *Modification to the NASA Langley 4- by 7-Meter Tunnel for Improved Rotorcraft Aerodynamics and Acoustics*. NASA paper presented at the American Helicopter Society National Specialist's Meeting on Helicopter Testing Technology (Williamsburg, VA), Oct. 29-Nov. 1, 1984.
15. Heyson, Harry H.: *Use of Superposition in Digital Computers To Obtain Wind-Tunnel Interference Factors for Arbitrary Configurations, With Particular Reference to V/STOL Models*. NASA TR R-302, 1969.

Table I. Details of the BO-105 Model Main Rotor and Rotor Test Stand

Main rotor:	
Rotor diameter, m	4
Blade airfoil section	NACA 23012
Number of blades	4
Blade solidity	0.077
Blade tip speed, m/sec	218
Flapping frequency ratio	1.111
Lagging frequency ratio	0.785
Nominal rotational speed, rpm	1040
Nominal rotor thrust, N	3600
Nominal rotor thrust coefficient	0.0044
Drive system:	
Shaft power, kW	100
Rotor drive moment, N-m	900 at 1050 rpm
Power (electric)	3 phase, 380 V at 300 A
Balance load range:	
Axial force, N	1000
Side force, N	2000
Thrust force, N	7000 static \pm 1500 dynamic
Rolling moment, N-m	700
Pitching moment, N-m	700
Control system:	
Blade setting angle range, deg	-4 to 14

Table II. Final Test Matrix

Comment	C_T	V , m/sec	μ	α_{shaft} , deg	X_w , m	Z_w , m	M_H
α sweep	0.0044	17	0.078	^a 7 to 10	5.0	-2.1	0.636
		20	.092	6 to 10	2.5		
		25	.115	4 to 8	2.5		
		30	.138	2 to 6	1.0		
		32	.147	0 to 4	1.0		
		37	.170	-2 to 2	2.5		
μ sweep	0.0044	^b 33 to 41	0.152 to 0.187	0	2.5	-2.1	0.636
		28 to 36	0.129 to 0.166	2.0	1.0		
		25 to 35	0.115 to 0.161	4.0	1.0		
		20 to 26	0.092 to 0.120	6.0	2.5		
		17 to 22	0.078 to 0.101	8.0	2.5		
		13 to 21	0.060 to 0.097	10.0	5.0		
X_w sweep	0.0044	38	0.175	0.5	^c - 1.2 to 6.0	-2.1	0.636
		35	.161	3.0			
		31	.143	5.0			
		25	.115	5.5			
		20	.092	8.0			
		19	.087	10.0			
α sweep	0.0044	30	0.138	^a 4 to 7	-1.15	-2.1	0.636
μ sweep	0.0044	^b 28 to 34	0.129 to 0.156	5.0	-1.15	-2.1	0.636
X_w sweep	0.0044	30	0.138	5.0	^d - 1.2 to 4.4	-2.1	0.636
α sweep	0.0030	30	0.138	^a 1 to 7	-1.15	-2.1	0.636
		40	.184	-1 to 3			
μ sweep	0.0030	^b 28 to 35	0.129 to 0.161	2.8	-1.15	-2.1	0.636
		36 to 44	0.166 to 0.202	1.2			
X_w sweep	0.0030	30	0.138	2.8	^d - 1.2 to 4.4	-2.1	0.636
		40	.184	1.2			
Near/far-field data	0.0044	19	0.087	10.0	^e 1.5 to 6.0	-1.6	0.636
		31	.143	5.0	^e 1.5 to 6.0	-1.6	
		19	.087	10.0	^f 2.5 to 6.2	-2.6	
		31	.143	5.0	^f 2.5 to 6.2	-2.6	
High μ	0.0044	50	0.230	-5 to 1	2.5	-2.1	0.636
		60	.276	-7 to 1	2.5	-2.1	
		60	.276	-7 to 0	2.57	-2.6	
		60	.276	-7 to 0	3.68	-2.6	
M_H sweep	0.0044	^g 27 to 35	0.140	5.0	4.5	-2.1	^h 0.56 to 0.72
C_T sweep	0.0036 to 0.0056	31	0.140	5.0	4.5	-2.1	0.636
M_H sweep	0.0044	^g 17.5 to 22.5	0.090	8.0	4.0	-2.1	^h 0.56 to 0.72
C_T sweep	0.0036 to 0.0056	20	0.090	8.0	4.0	-2.1	0.636
M_H sweep	0.0044	^g 33.3 to 42.8	0.175	0.5	4.0	-2.1	^h 0.56 to 0.72
C_T sweep	0.0036 to 0.0056	38	0.175	0.5	4.0	-2.1	0.636

^a Varied in increments of 0.5.

^b Varied in increments of 1.

^c Varied as follows: 6.0, 5.2, 4.4, 3.6, 2.8, 2.0, 1.5, 0.8, 0, -0.7, -1.2.

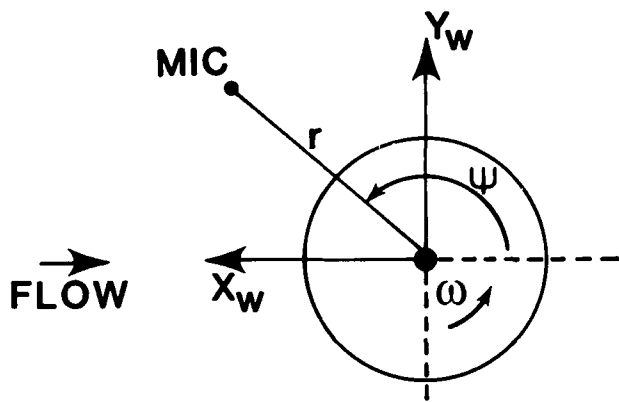
^d Varied as follows: 4.4, 2.8, 2.0, 1.2, 0.4, 0, -0.4, -0.7, -1.2.

^e Varied as follows: 1.5, 2.1, 2.7, 3.3, 4.0, 4.6.

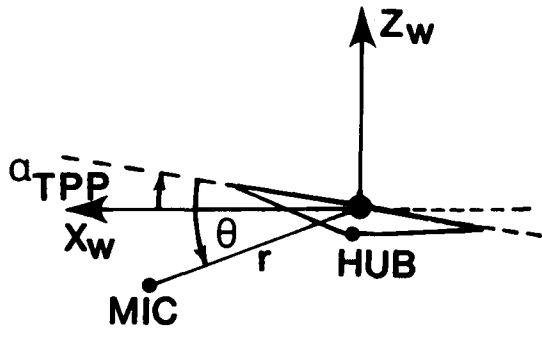
^f Varied as follows: 2.5, 3.5, 4.4, 5.4, 6.2.

^g Varied in increments of 2.

^h Varied in increments of 0.04.

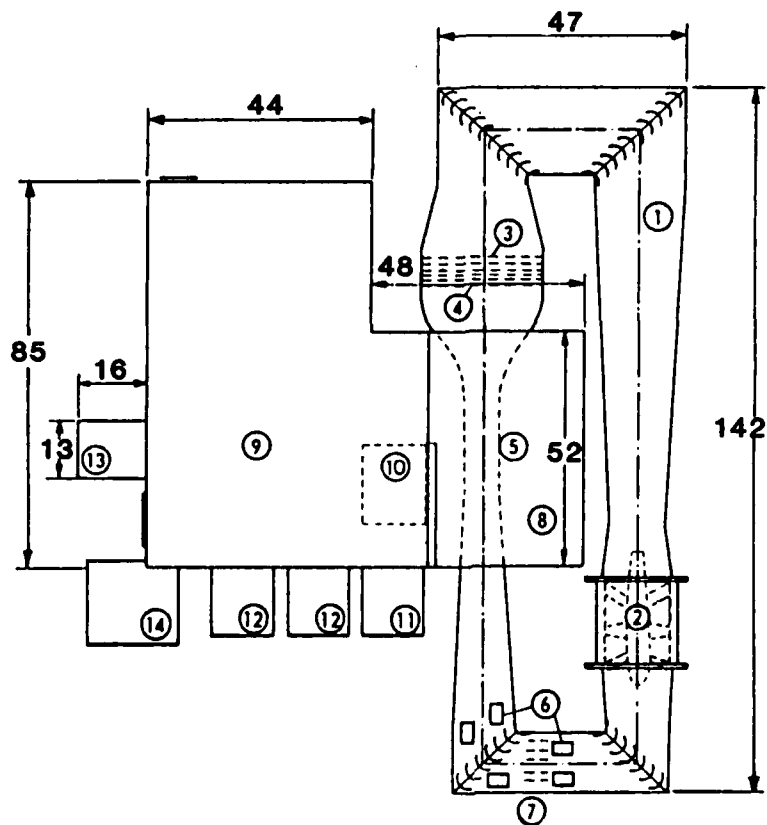


TOP VIEW



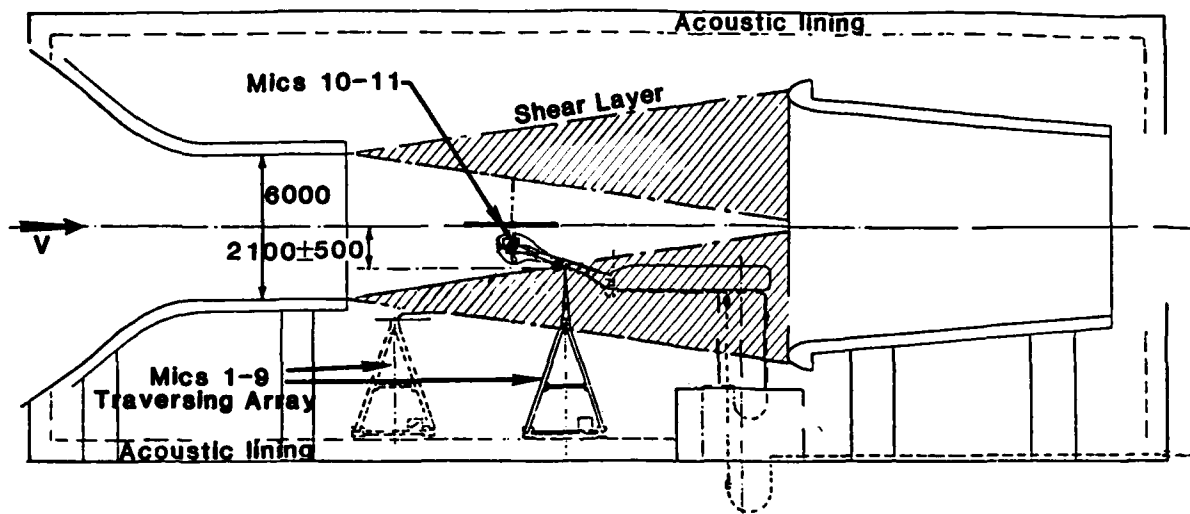
SIDE VIEW

Figure 1. Diagram of coordinate system and test geometry.

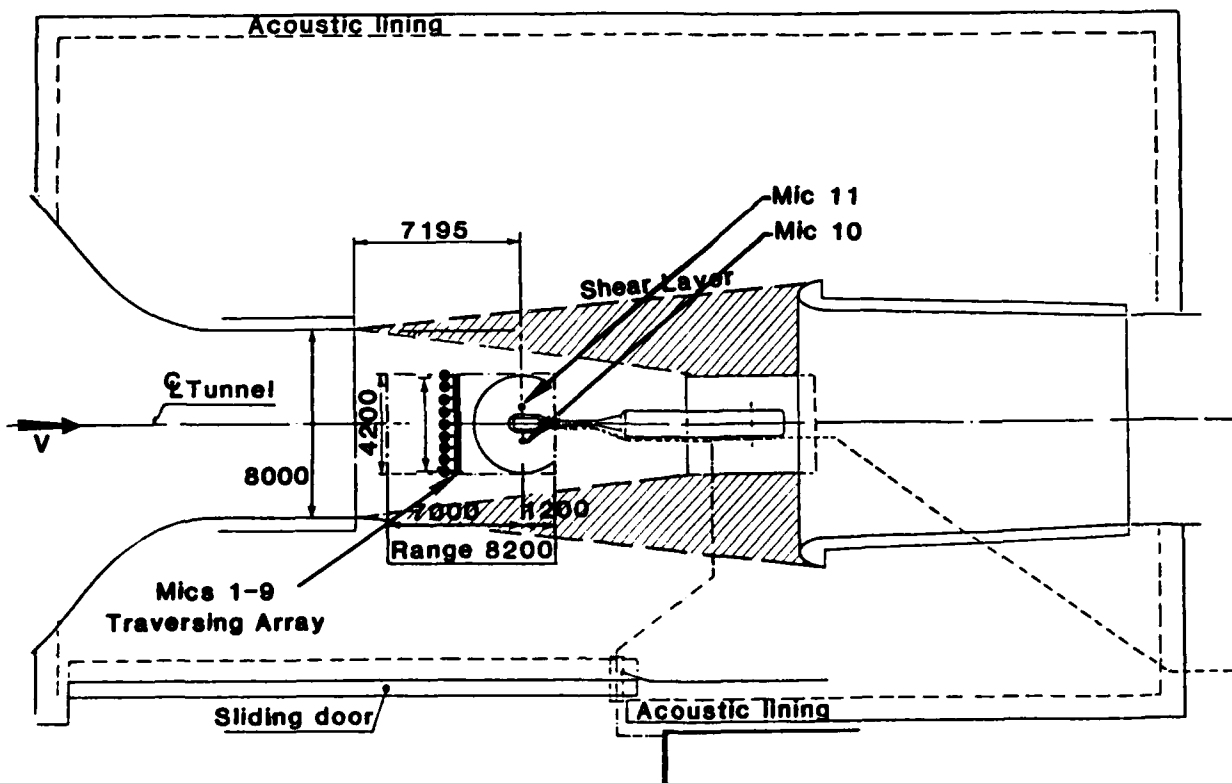


- ① Prefabricated concrete circuit
- ② Eight-bladed fan with electric drive (nominal 12.5MW)
- ③ Heat exchanger (11MW) with flow rectifier
- ④ Anti-turbulence screens
- ⑤ Exchangeable test sections: $9.5 \times 9.5 \text{m}^2$, $8 \times 6 \text{m}^2$, $6 \times 6 \text{m}^2$, open jet
- ⑥ Air exchange hatches
- ⑦ Throttling device
- ⑧ Acoustically treated testing hall: $52 \times 30 \times 20 \text{m}^3$
- ⑨ Parking hall
- ⑩ Control room
- ⑪ Experiment hall
- ⑫ Model assembly hall
- ⑬ Calibration hall
- ⑭ Office building

Figure 2. Plan view of the DNW facility.

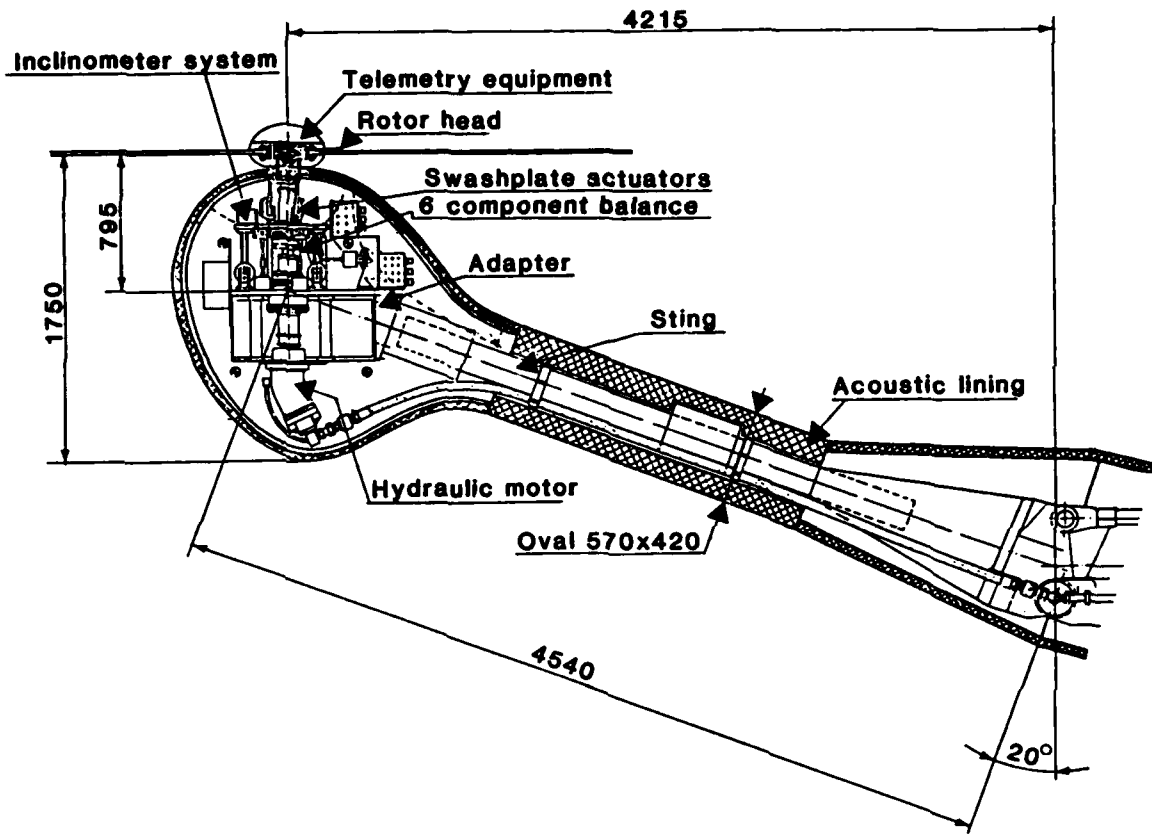


(a) Side view.

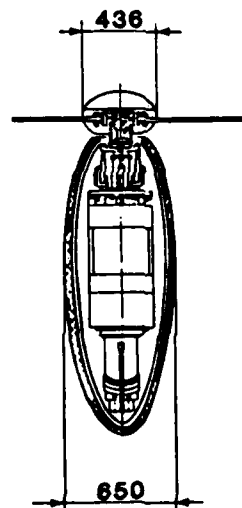


(b) Plan view.

Figure 3. Diagram of experimental apparatus installed in the DNW open test section. All dimensions are in millimeters.



(a) Side view.



(b) Front view.

Figure 4. Diagram of the DFVLR rotor test stand. All dimensions are in millimeters.

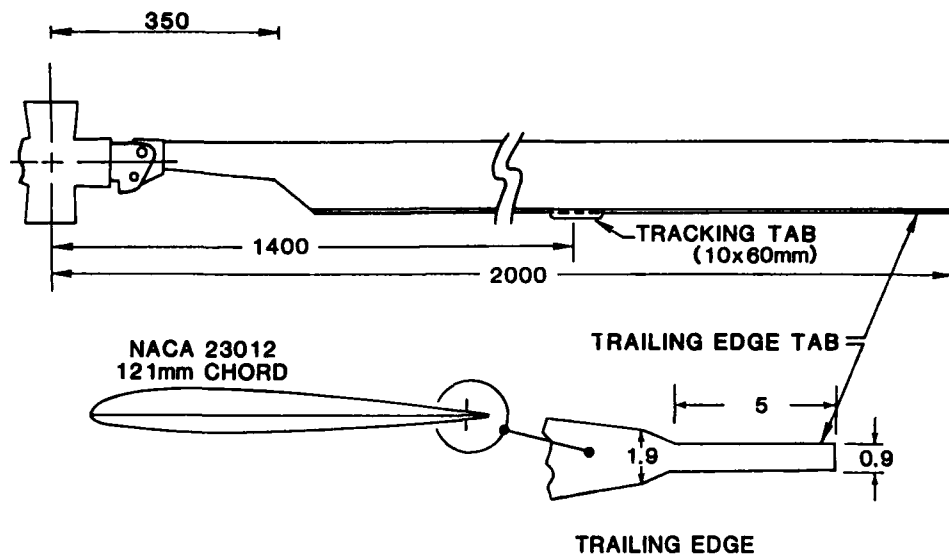


Figure 5. Model BO-105 rotor blade geometry.

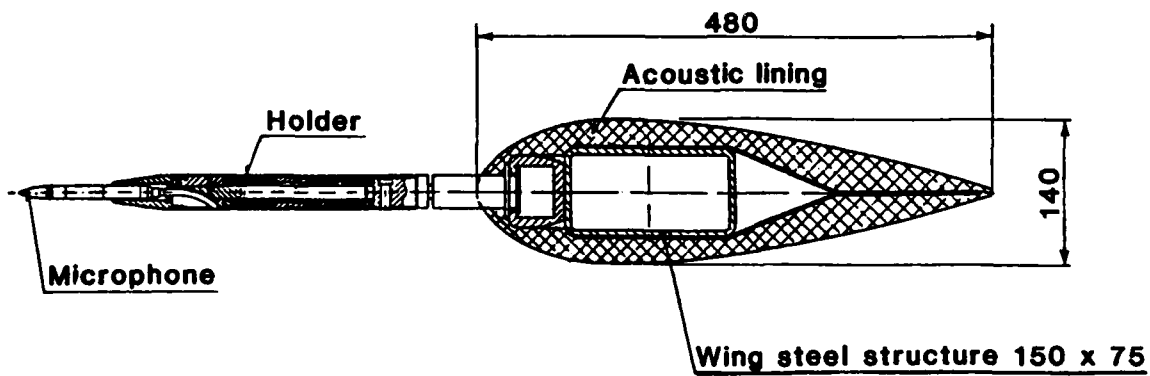
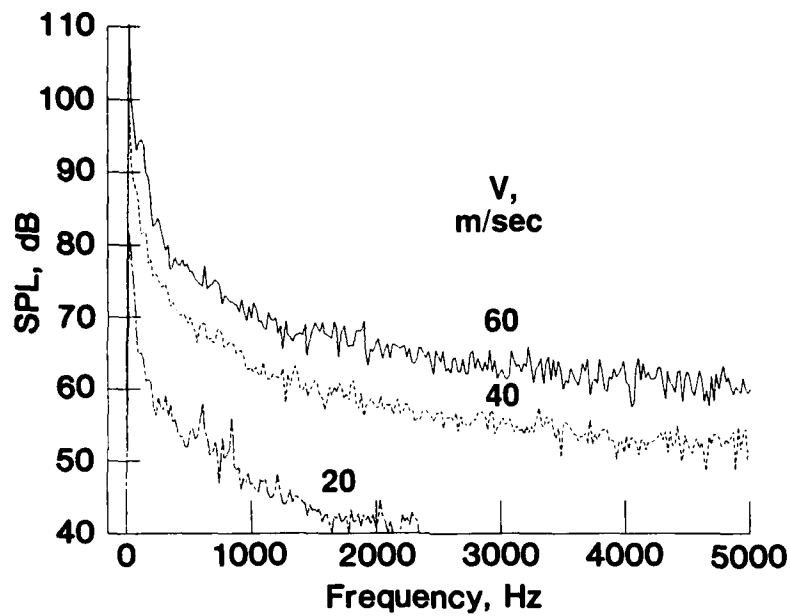
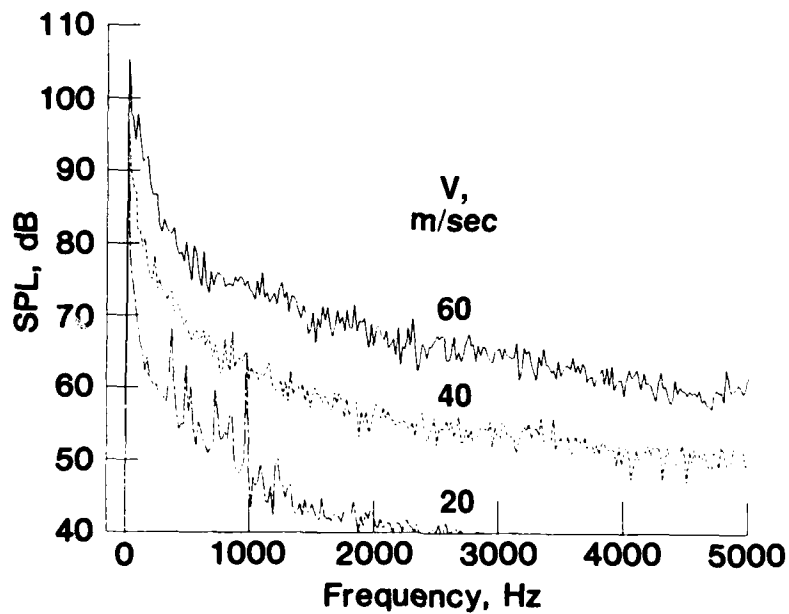


Figure 6. Cross section of traversing microphone array wing and microphone holder. All dimensions are in millimeters.

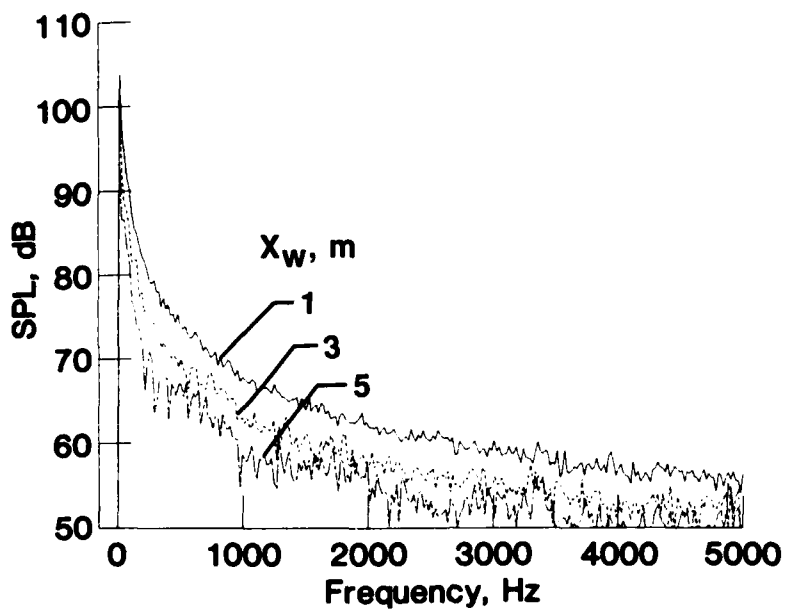


(a) Microphone 1.

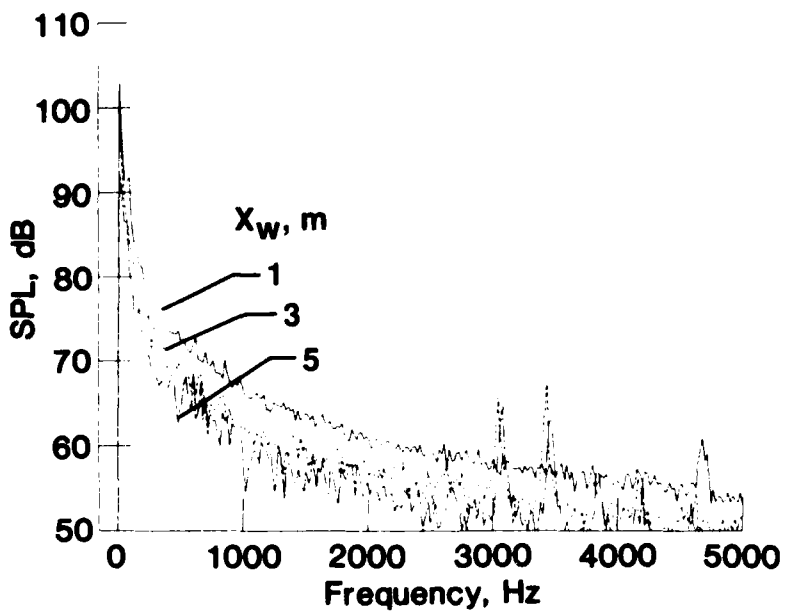


(b) Microphone 10.

Figure 7. Background noise at $X_w = 3$ m, as a function of tunnel speed. $\Delta f = 20$ Hz.

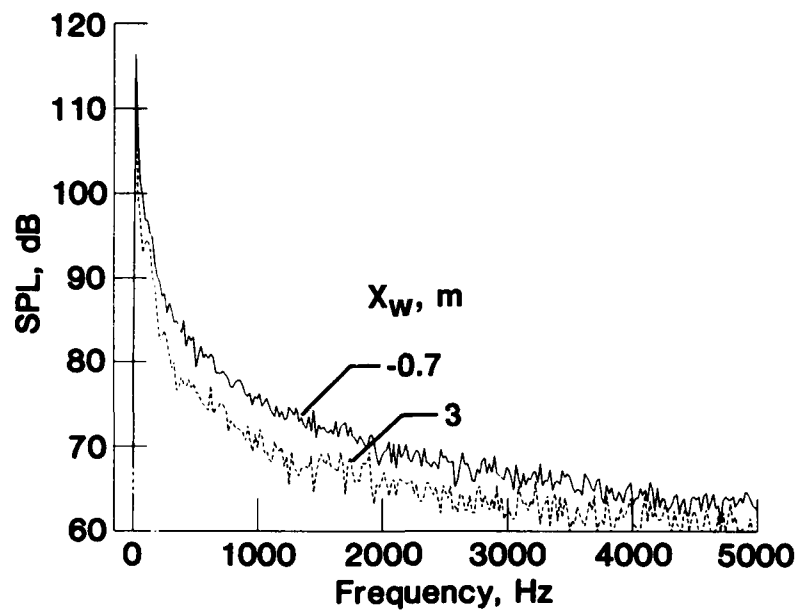


(a) Microphone 1.

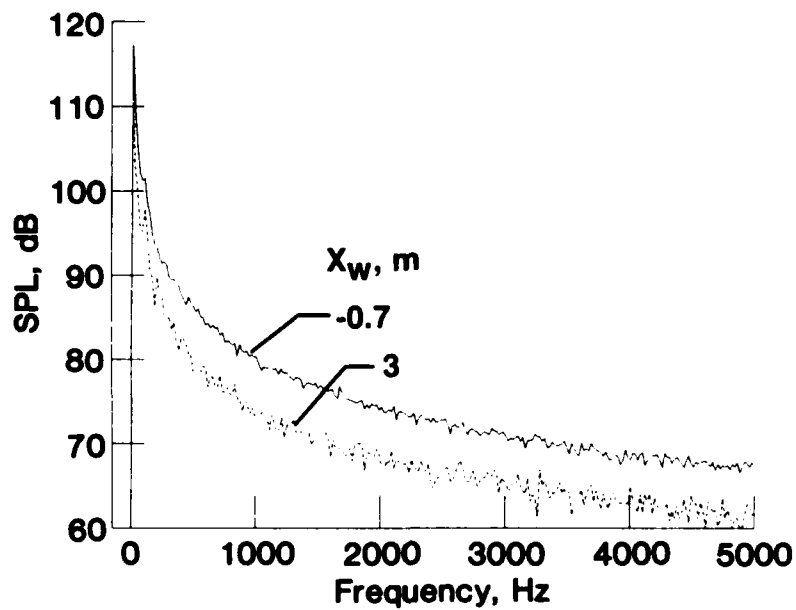


(b) Microphone 5.

Figure 8. Background noise at $V = 40$ m/sec as a function of traversing array position. $\Delta f = 20$ Hz.



(a) Microphone 1.



(b) Microphone 5.

Figure 9. Background noise at $V = 60$ m/sec as a function of traversing array position. $\Delta f = 20$ Hz.

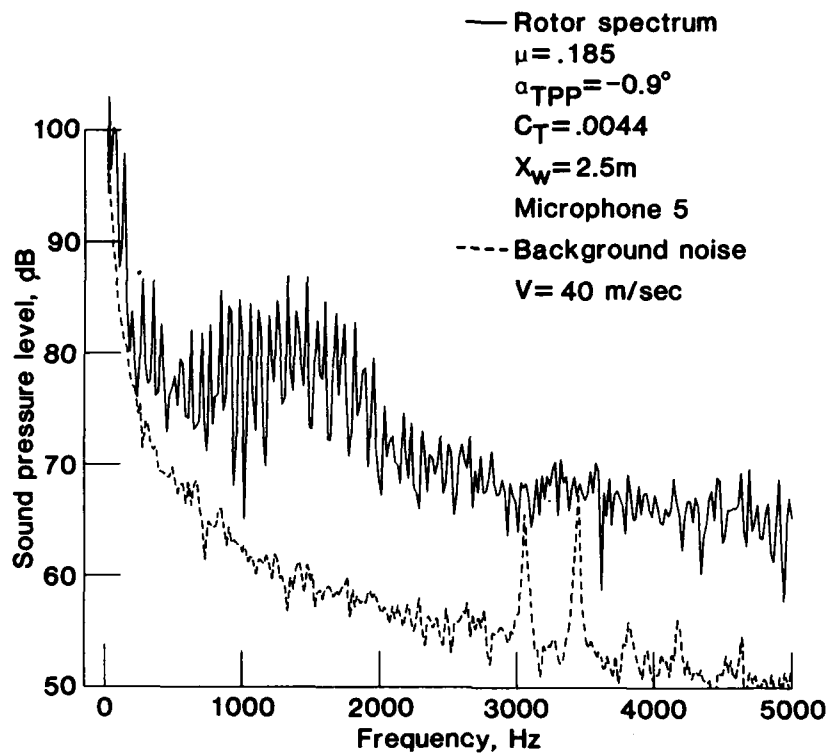


Figure 10. Comparison of typical rotor spectrum with background noise. $\Delta f = 20 \text{ Hz}$.

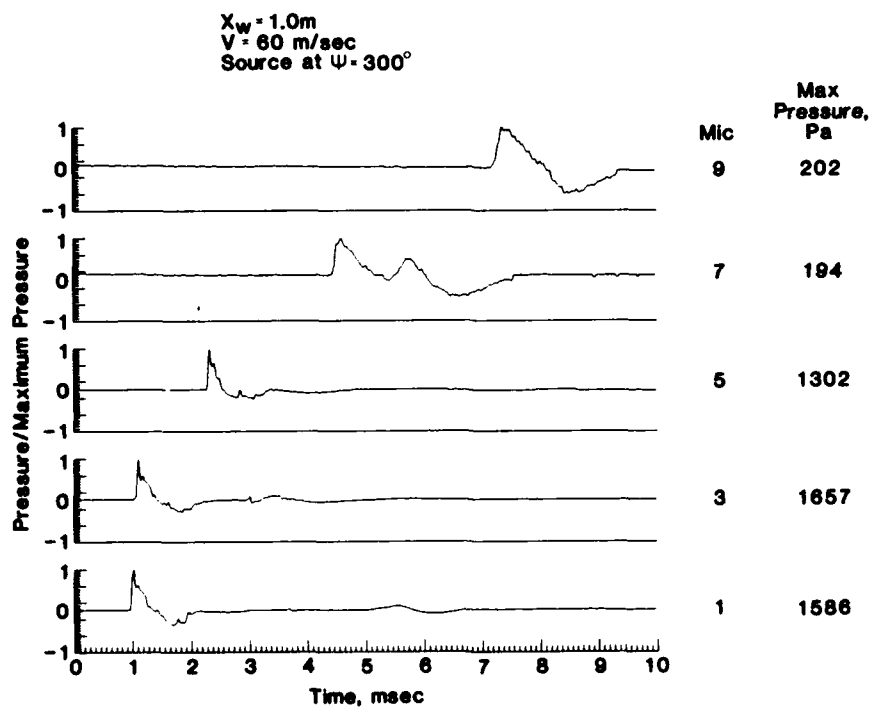
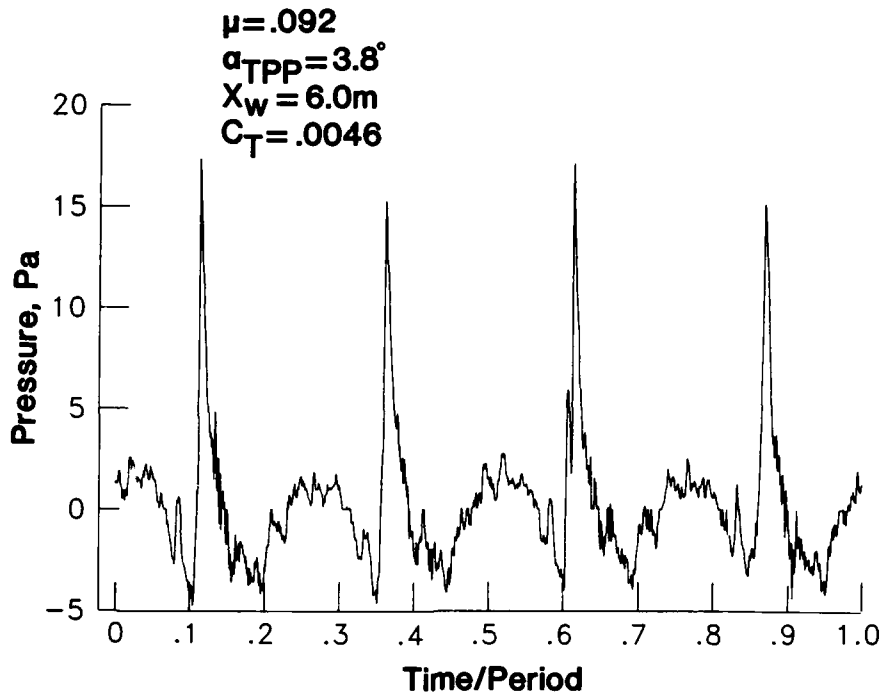
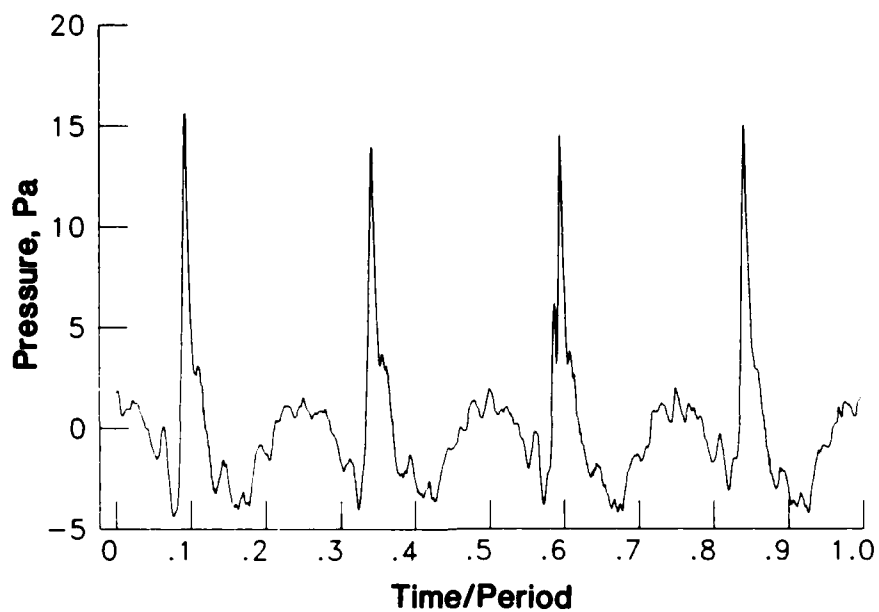


Figure 11. Example of blast calibration data, showing shielded microphones 7 and 9.

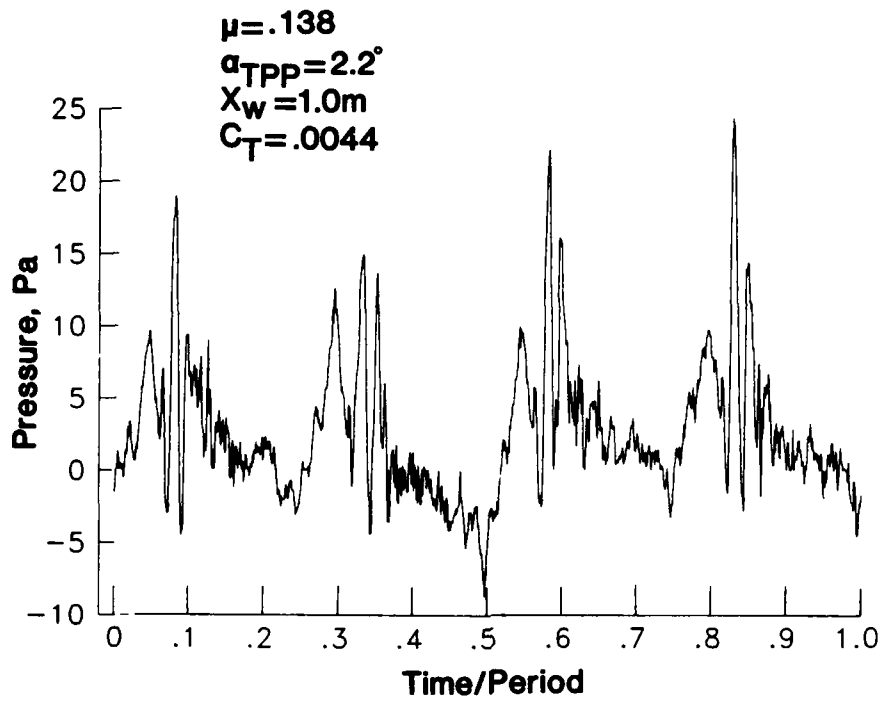


(a) Unaveraged on-line data at $\mu = 0.092$.

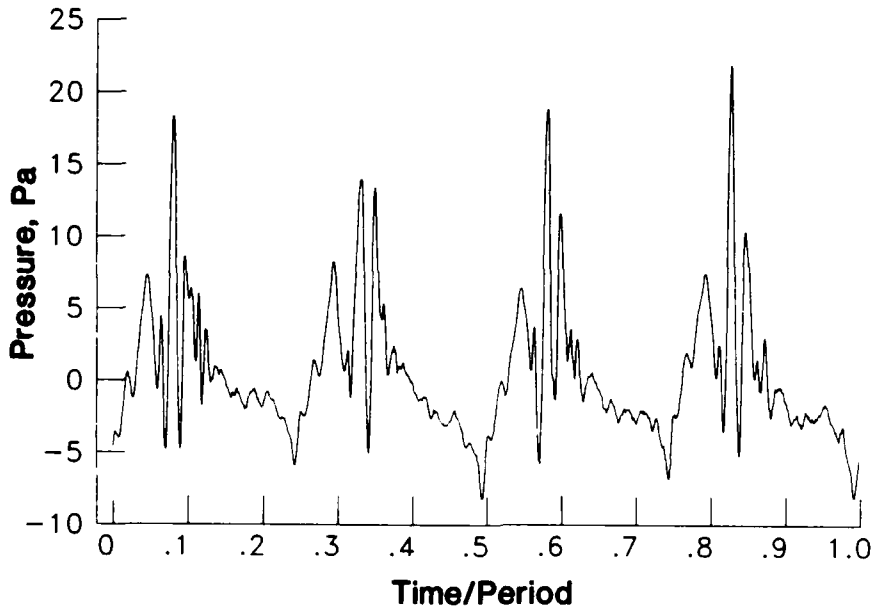


(b) Averaged postprocessed data at $\mu = 0.092$.

Figure 12. Comparison of instantaneous on-line acoustic data with averaged postprocessed results (microphone 5).

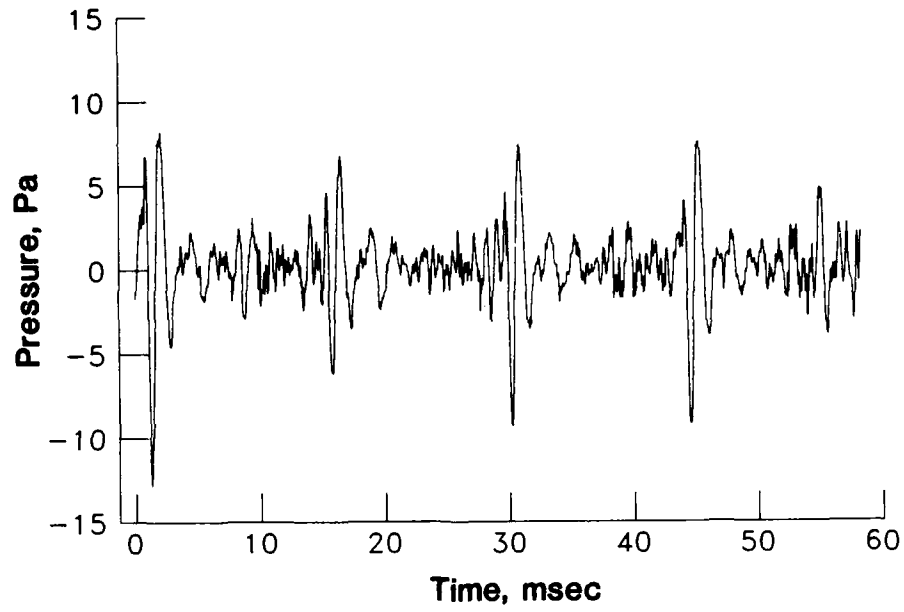


(c) Unaveraged on-line data at $\mu = 0.138$.

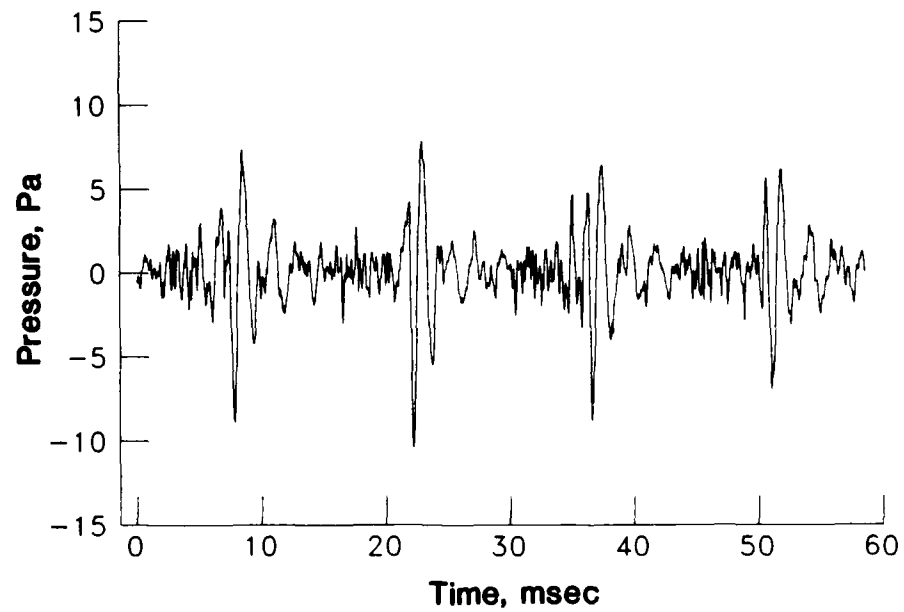


(d) Averaged postprocessed data at $\mu = 0.138$.

Figure 12. Concluded.



(a) Data point 411.



(b) Data point 429.

Figure 13. Repeatability of filtered on-line data. $\mu = 0.138$; $\alpha_{TPP} = 1.8^\circ$; $X_w = 1.0$ m; $C_T = 0.0030$; microphone 1; $f_c = 448$ Hz.

Averaged Acoustic Signals

The data presented in the following plots are a representative set of the postprocessed results of the final test matrix defined by table II. Each plot presents the averaged time histories of traversing array microphones 1, 3, 5, 7, and 9. The following table is an index of test conditions for the plots and page numbers.

Test Conditions for Plots of Averaged Acoustic Signals

V , m/sec	μ	α_{TPP} , deg	${}^a X_w$, m	Z_w , m	C_T	Point	M_H	Page
≈17.0	≈0.078	$b_{1.7}$	≈5.3	-2.1	≈0.00435	210	≈0.636	27
≈17.0	≈.078	$b_{3.0}$	≈5.3	↓	↓	264	↓	28
≈17.0	≈.078	$b_{4.6}$	≈5.3	↓	↓	267	↓	29
≈20.0	≈.092	$b_{2.1}$	≈2.8	↓	↓	225	↓	30
≈20.0	≈.092	$b_{4.1}$	↓	↓	↓	221	↓	31
≈20.0	≈.092	$b_{6.1}$	↓	↓	↓	217	↓	32
≈25.0	≈.115	1.5	↓	↓	↓	226	↓	33
≈25.0	≈.115	3.5	↓	↓	↓	230	↓	34
≈25.0	≈.115	5.5	↓	↓	↓	234	↓	35
≈30.0	≈.138	.2	≈1.1	↓	↓	244	↓	36
≈30.0	≈.138	2.2	↓	↓	↓	239	↓	37
≈30.0	≈.138	4.3	↓	↓	↓	235	↓	38
≈32.0	≈.147	-1.6	↓	↓	↓	253	↓	39
≈32.0	≈.147	-.1	↓	↓	↓	250	↓	40
≈32.0	≈.147	.9	↓	↓	↓	248	↓	41
≈32.0	≈.147	2.4	↓	↓	↓	245	↓	42
37.0	.170	-3.1	≈2.5	↓	↓	262	↓	43
37.0	.170	-1.1	↓	↓	↓	258	↓	44
37.0	.170	.9	↓	↓	↓	254	↓	45
33.0	.152	-1.4	↓	↓	.00402	318	↓	46
50.0	.160	-1.2	↓	↓	.00417	320	↓	47
39.0	.179	-1.0	↓	↓	≈.00435	324	↓	48
41.0	.187	-.8	↓	↓	↓	326	↓	49
27.5	.130	-.1	≈1.1	↓	↓	309	↓	50
30.3	.139	.1	↓	↓	↓	311	↓	51
32.0	.147	.4	↓	↓	↓	313	↓	52
34.0	.157	.5	↓	↓	.00464	315	↓	53
35.9	.165	.8	↓	↓	≈.00435	317	↓	54
24.8	.113	1.6	≈1.2	↓	↓	297	↓	55
26.5	.125	1.7	≈1.2	↓	↓	299	↓	56

${}^a X_w$ varies with α_{TPP} (see section "Testing Procedures and Measurement Accuracy").

b Accuracy of estimated α_{TPP} deteriorates as V decreases below 20 m/sec (see "Testing Procedures and Measurement Accuracy").

Test Conditions for Plots of Averaged Acoustic Signals Continued

V, m/sec	μ	α_{TPP} , deg	$^a X_w$, m	Z_w , m	C_T	Point	M_H	Page
28.5	0.132	2.2	1.2	-2.1	0.00416	301	≈ 0.636	57
31.2	.142	2.3	↓	↓	≈ 0.00435	303	↓	58
32.8	.150	2.4	↓	↓	↓	305	↓	59
35.0	.159	2.7	↓	↓	↓	308	↓	60
20.1	.092	b2.1	≈ 2.8	↓	↓	290	↓	61
22.0	.101	2.7	↓	↓	↓	292	↓	62
23.8	.110	3.2	↓	↓	↓	294	↓	63
25.6	.120	3.6	↓	↓	↓	296	↓	64
17.3	.079	b2.7	≈ 2.9	↓	↓	284	↓	65
19.1	.087	b3.7	≈ 2.9	↓	↓	286	↓	66
21.0	.095	4.4	≈ 2.9	↓	↓	288	↓	67
13.1	.059	b1.4	≈ 5.5	↓	↓	275	↓	68
16.2	.073	b4.0	↓	↓	↓	278	↓	69
18.3	.083	b5.2	↓	↓	↓	280	↓	70
20.7	.093	6.2	↓	↓	↓	283	↓	71
38.0	$\approx .175$	≈ -5	-1	↓	↓	400	↓	72
↓	↓	↓	.8	↓	↓	402	↓	73
↓	↓	↓	2.0	↓	↓	404	↓	74
↓	↓	↓	3.6	↓	↓	406	↓	75
↓	↓	↓	5.2	↓	↓	408	↓	76
35.0	$\approx .161$	1.7	-1.0	↓	↓	399	↓	77
↓	↓	↓	.5	↓	↓	397	↓	78
↓	↓	↓	2.1	↓	↓	395	↓	79
↓	↓	↓	3.7	↓	↓	393	↓	80
↓	↓	↓	5.3	↓	↓	391	↓	81
31.1	$\approx .143$	≈ 3.3	-9	↓	↓	380	↓	82
↓	↓	↓	.6	↓	↓	382	↓	83
↓	↓	↓	2.2	↓	↓	384	↓	84
↓	↓	↓	3.8	↓	↓	386	↓	85
↓	↓	↓	5.4	↓	↓	388	↓	86
24.8	$\approx .114$	≈ 2.9	-9	↓	↓	379	↓	87
↓	↓	↓	1.0	↓	↓	377	↓	88
↓	↓	↓	3.1	↓	↓	374	↓	89
↓	↓	↓	4.7	↓	↓	372	↓	90
↓	↓	↓	6.3	↓	↓	369	↓	91
20.0	$\approx .092$	b ≈ 3.8	-8	↓	.00476	358	↓	92
↓	↓	b ≈ 3.8	.8	↓	$\approx .00435$	360	↓	93
↓	↓	b ≈ 3.8	2.4	↓	↓	362	↓	94
↓	↓	≈ 4.1	4.0	↓	↓	364	↓	95
↓	↓	≈ 4.1	5.6	↓	↓	366	↓	96
18.9	$\approx .087$	b ≈ 5.7	-6	↓	↓	357	↓	97

^a X_w varies with α_{TPP} (see section "Testing Procedures and Measurement Accuracy").

^bAccuracy of estimated α_{TPP} deteriorates as V decreases below 20 m/sec (see "Testing Procedures and Measurement Accuracy").

Test Conditions for Plots of Averaged Acoustic Signals—Continued

V , m/sec	μ	α_{TPP} , deg	$^a X_w$, m	Z_w , m	C_T	Point	M_H	Page
18.9	≈ 0.087	$^b \approx 5.7$	2.0	-2.1	≈ 0.00435	354	≈ 0.636	98
↓	↓	↓	3.3	↓	.00474	352	↓	99
↓	↓	↓	4.9	↓	≈ 0.00435	350	↓	100
↓	↓	↓	6.5	↓	↓	348	↓	101
≈ 29.8	$\approx .137$	2.3	- .9	↓	↓	476	↓	102
≈ 29.8	$\approx .137$	3.8	↓	↓	↓	473	↓	103
≈ 29.8	$\approx .137$	5.3	↓	↓	↓	470	↓	104
27.7	.127	2.9	↓	↓	↓	512	↓	105
30.0	.136	3.2	↓	↓	↓	510	↓	106
31.9	.145	3.4	↓	↓	↓	508	↓	107
↓	↓	↓	↓	↓	↓	↓	↓	↓
34.1	.154	3.6	↓	↓	↓	506	↓	108
≈ 30.0	$\approx .138$	3.2	- .5	↓	↓	536	↓	109
↓	↓	↓	- .2	↓	↓	538	↓	110
↓	↓	↓	.6	↓	↓	540	↓	111
↓	↓	↓	2.2	↓	↓	542	↓	112
↓	↓	↓	4.6	↓	↓	544	↓	113
↓	↓	- .2	≈ -1.0	↓	$\approx .00290$	460	↓	114
↓	↓	1.3	↓	↓	↓	457	↓	115
↓	↓	3.4	↓	↓	↓	453	↓	116
↓	↓	5.9	↓	↓	↓	448	↓	117
↓	↓	↓	↓	↓	↓	↓	↓	↓
40.0	.184	-1.6	↓	↓	↓	469	↓	118
40.0	.184	.4	↓	↓	↓	465	↓	119
40.0	.184	2.4	↓	↓	↓	461	↓	120
27.4	.126	1.4	↓	↓	↓	489	↓	121
30.9	.142	1.6	↓	↓	↓	492	↓	122
34.6	.159	1.9	↓	↓	↓	496	↓	123
35.6	.164	$\approx .5$	≈ 1.1	↓	↓	497	↓	124
37.6	.173	↓	↓	↓	↓	499	↓	125
39.6	.182	↓	↓	↓	↓	501	↓	126
41.7	.192	↓	↓	↓	↓	503	↓	127
↓	↓	↓	↓	↓	↓	↓	↓	↓
43.5	.200	↓	↓	↓	↓	505	↓	128
30.0	$\approx .138$	1.6	-1.0	↓	↓	515	↓	129
↓	↓	↓	- .3	↓	↓	517	↓	130
↓	↓	↓	.5	↓	↓	519	↓	131
↓	↓	↓	2.1	↓	↓	521	↓	132
↓	↓	↓	4.5	↓	↓	523	↓	133
40.0	$\approx .184$.6	-1.1	↓	↓	532	↓	134
↓	↓	↓	- .4	↓	↓	530	↓	135
↓	↓	↓	.5	↓	↓	528	↓	136
↓	↓	↓	1.3	↓	↓	527	↓	137

^a X_w varies with α_{TPP} (see section "Testing Procedures and Measurement Accuracy").

^bAccuracy of estimated α_{TPP} deteriorates as V decreases below 20 m/sec (see "Testing Procedures and Measurement Accuracy").

Test Conditions for Plots of Averaged Acoustic Signals—Concluded

V, m/sec	μ	α_{TPP} , deg	$^a X_w$, m	Z_w , m	C_T	Point	M_H	Page
40.0	≈ 0.184	0.6	4.5	-2.1	≈ 0.00290	524	≈ 0.636	138
18.5	.085	b5.5	2.6	-1.6	≈ 0.00435	577		139
18.5	.085	b5.5	4.5	-1.6		580		140
30.7	.141	3.3	3.0	-1.6		585		141
30.7	.141	3.3	4.2	-1.6		583		142
18.5	.085	b ≈ 5.5	3.0	-2.6		589		143
18.5	.085	b ≈ 5.5	6.7	-2.6		592		144
30.9	.142	3.3	2.7	-2.6		597		145
30.9	.142	3.3	6.5	-2.6		593		146
49.8	.229	-5.5	≈ 2.4	-2.1		329		147
49.8	.229	-3.5	≈ 2.4		.00409	331		148
49.8	.229	-1.9	≈ 2.4		.00435	333		149
49.8	.229	-5	≈ 2.4		.00435	336		150
60.0	$\approx .276$	-7.3	≈ 2.3		.00435	338		151
60.0	$\approx .276$	-4.8	≈ 2.3		.00418	341		152
60.0	$\approx .276$	-3.8	≈ 2.3		≈ 0.00435	343		153
60.0	$\approx .276$	-1.3	≈ 2.3		≈ 0.00435	346		154
59.6	$\approx .274$	-7.3	≈ 2.4	-2.6	≈ 0.00435	599		155
59.6	$\approx .274$	-5.3	≈ 2.4			601		156
59.6	$\approx .274$	-3.3	≈ 2.4			603		157
59.6	$\approx .274$	-1.3	≈ 2.4			605		158
59.1	.272	-7.3	≈ 3.5			614		159
59.1	.272	-4.3	≈ 3.5			611		160
59.1	.272	-2.3	≈ 3.5			609		161
59.1	.272	-.3	≈ 3.5			607		162
30.9	.142	≈ 3.3	4.7	-2.1		545	.559	163
						547	.636	164
						548	.675	165
					.00357	554	.636	166
					.00399	553	.636	167
					.00548	550	.636	168
≈ 19.6	$\approx .090$	b ≈ 4.1	4.4		.00392	555	.557	169
		b ≈ 4.1			.00428	557	.636	170
		4.6			.00361	560	.636	171
		b3.6			.00466	562	.636	172
		b2.9			.00547	564	.636	173
38.0	$\approx .175$	-.6	4.0		.00431	565	.559	174
		-.5			.00436	567	.636	175
		-.3			.00352	570	.636	176
		-.6			.00469	572	.636	177
		-.8			.00547	574	.636	178

^a X_w varies with α_{TPP} (see section "Testing Procedures and Measurement Accuracy").

^bAccuracy of estimated α_{TPP} deteriorates as V decreases below 20 m/sec (see "Testing Procedures and Measurement Accuracy").

$\mu = 0.79$
 $\alpha_{TPP} = 1.7^\circ$
 $C_T = 0.0043$
 $M_H = 0.634$
 Point = 210

Mic X_w, m Y_w, m Z_w, m

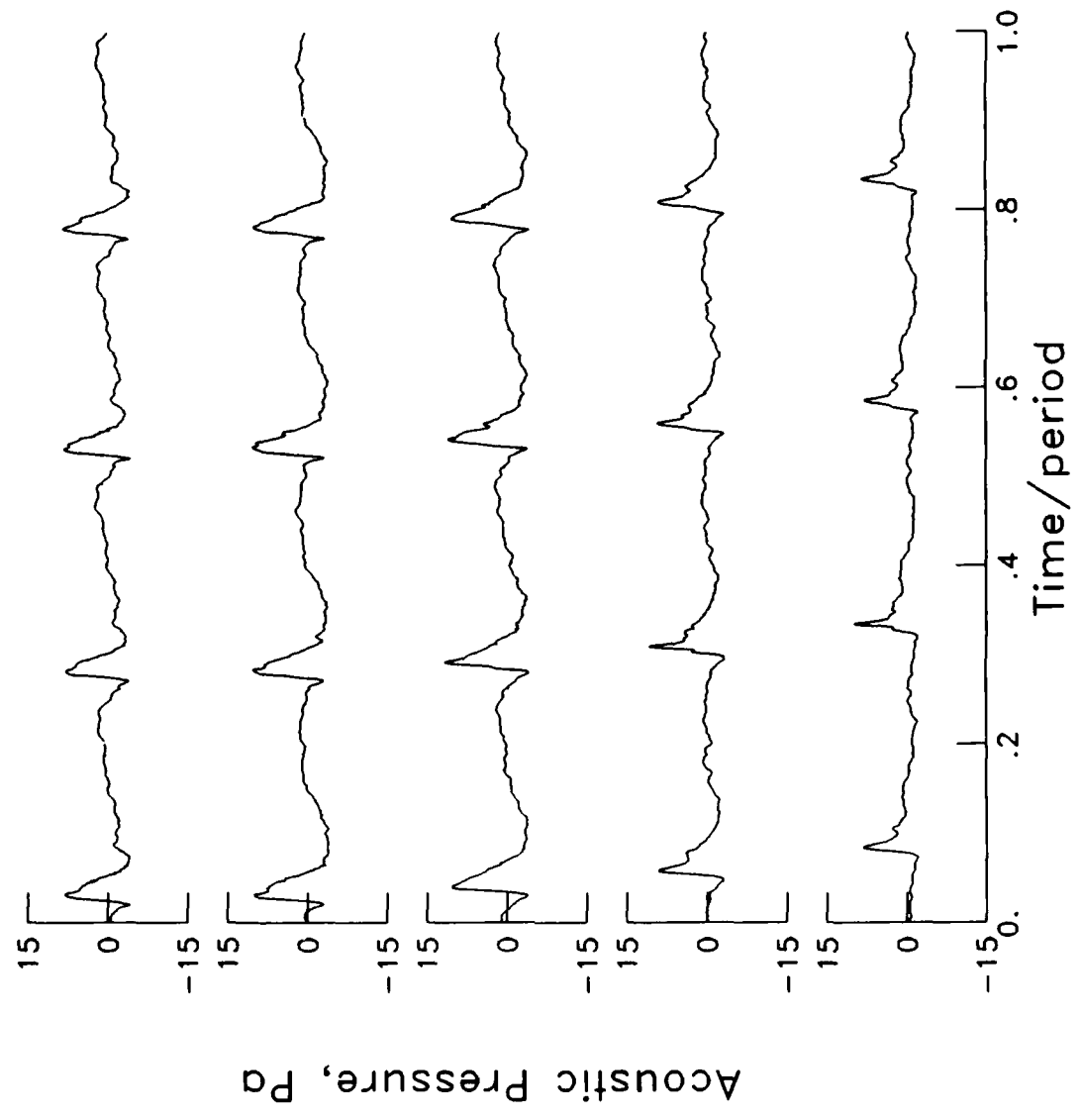
9 5.34 -2.16 -2.10

7 5.34 -1.08 -2.10

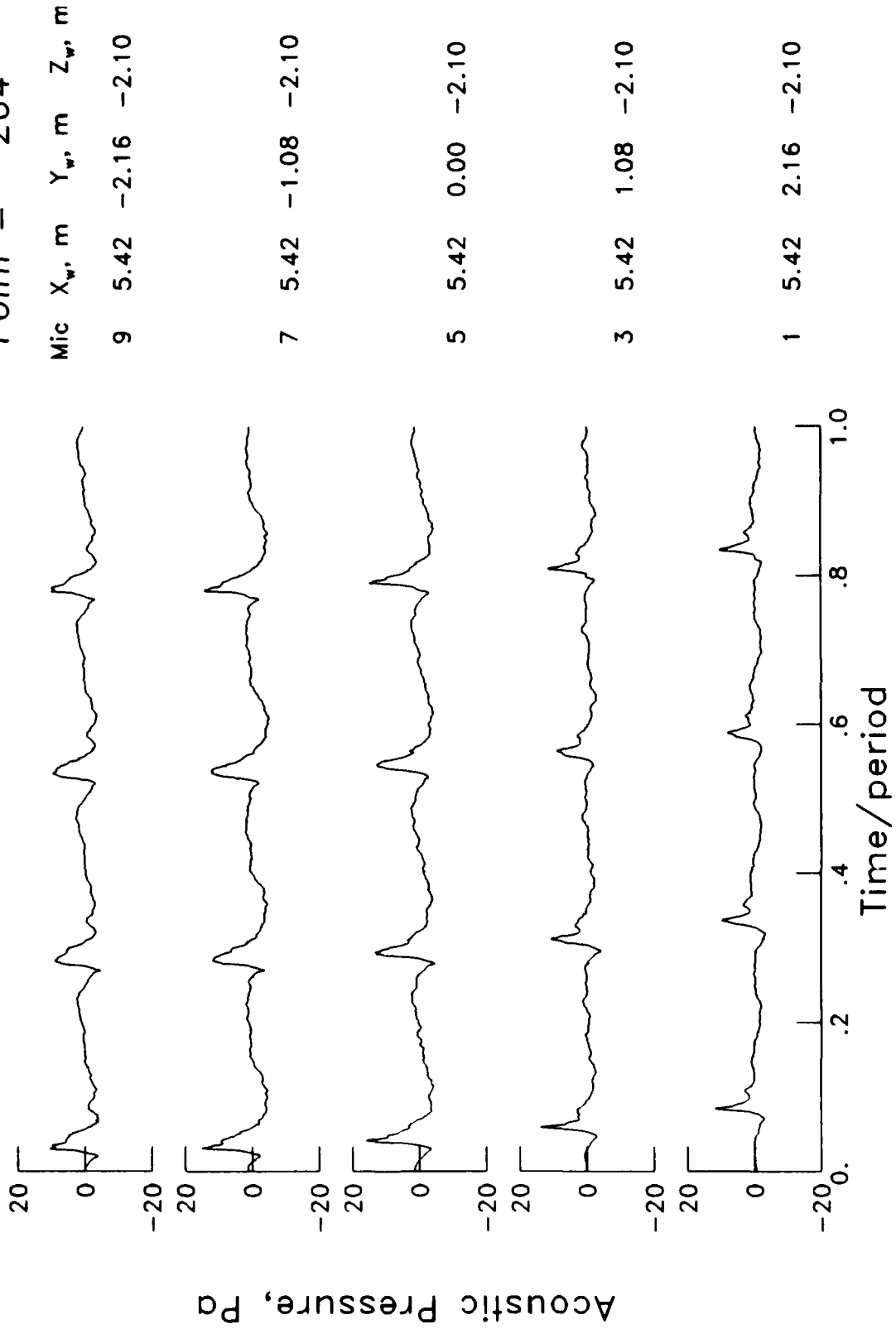
5 5.34 0.00 -2.10

3 5.34 1.08 -2.10

1 5.34 2.16 -2.10



$\mu = .077$
 $\alpha_{TPP} = 3.0^\circ$
 $C_T = 0.0044$
 $M_H = 0.635$
 Point = 264



$\mu = .076$
 $\alpha_{TPP} = 4.6^\circ$
 $C_T = 0.0043$
 $M_{H_i} = 0.635$
 Point = 267

Mic X_w, m Y_w, m Z_w, m

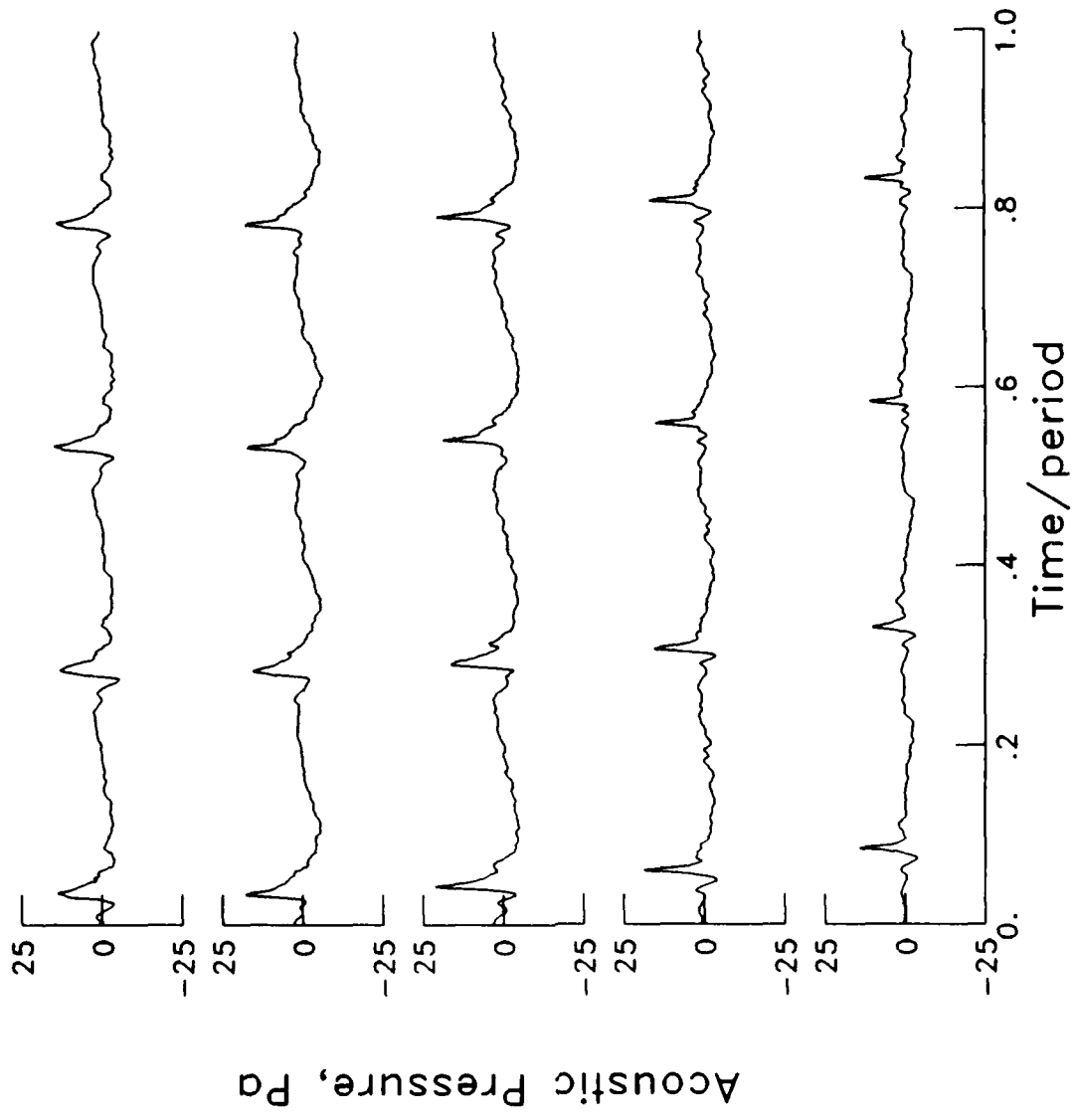
9 5.51 -2.16 -2.10

7 5.51 -1.08 -2.10

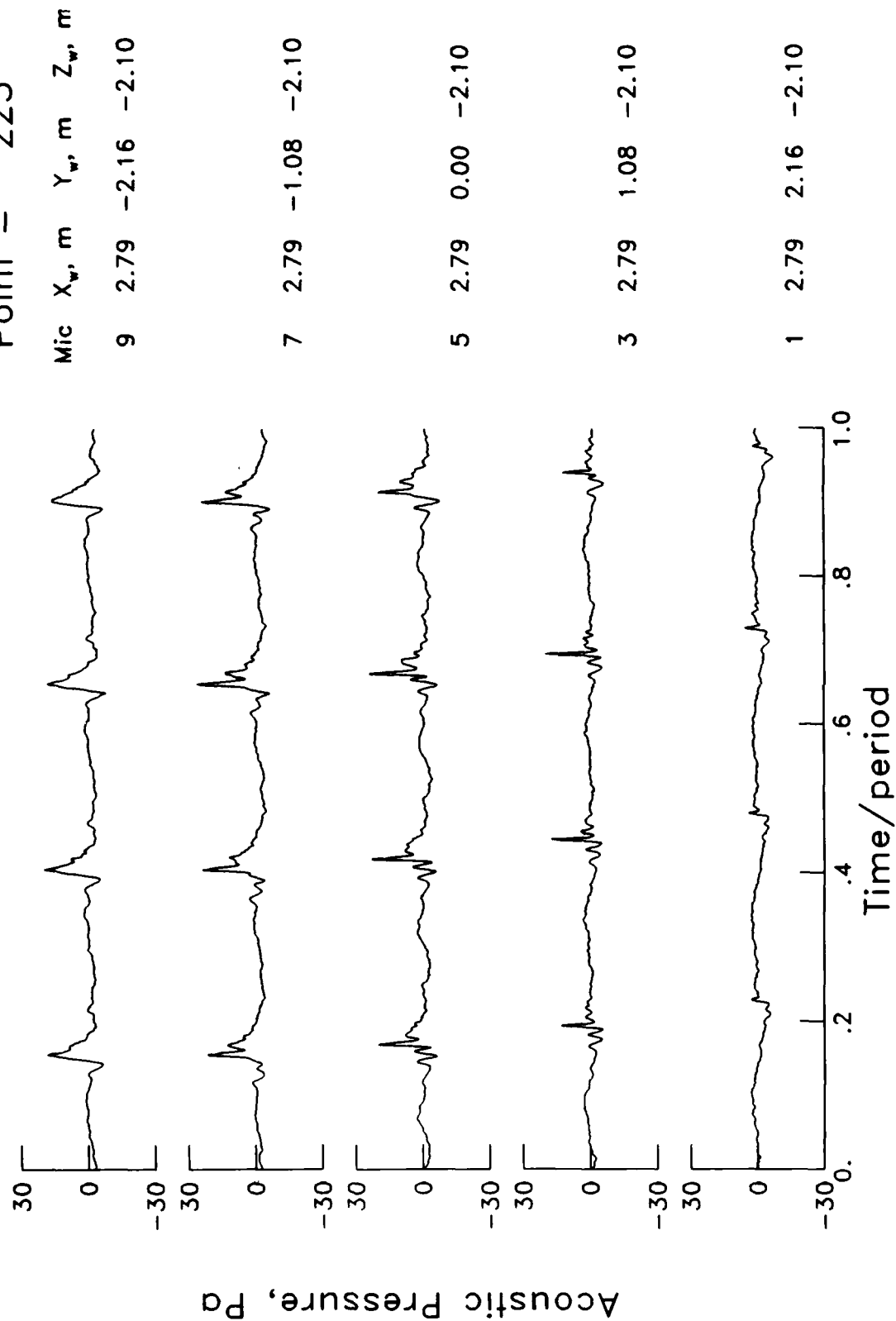
5 5.51 0.00 -2.10

3 5.51 1.08 -2.10

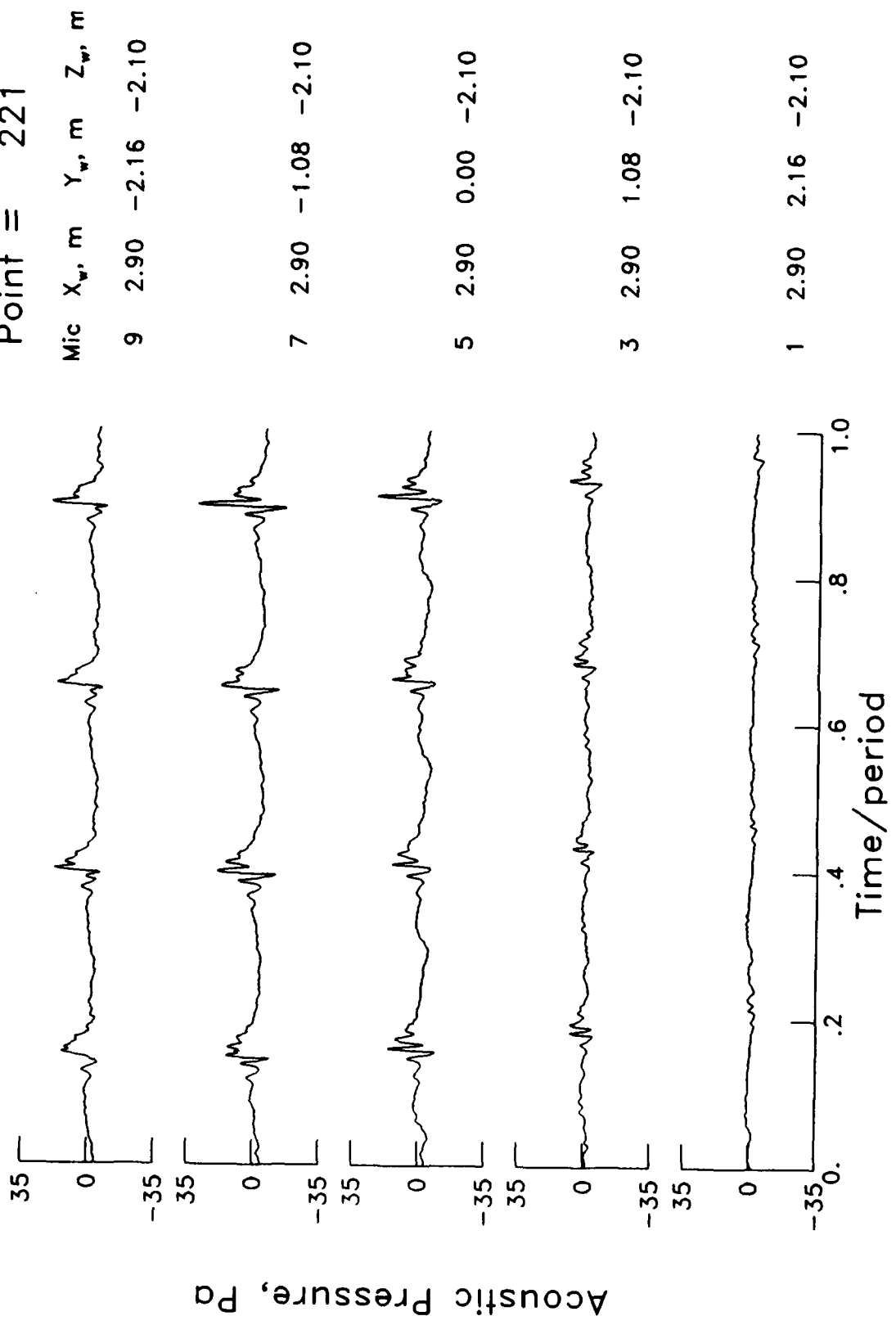
1 5.51 2.16 -2.10



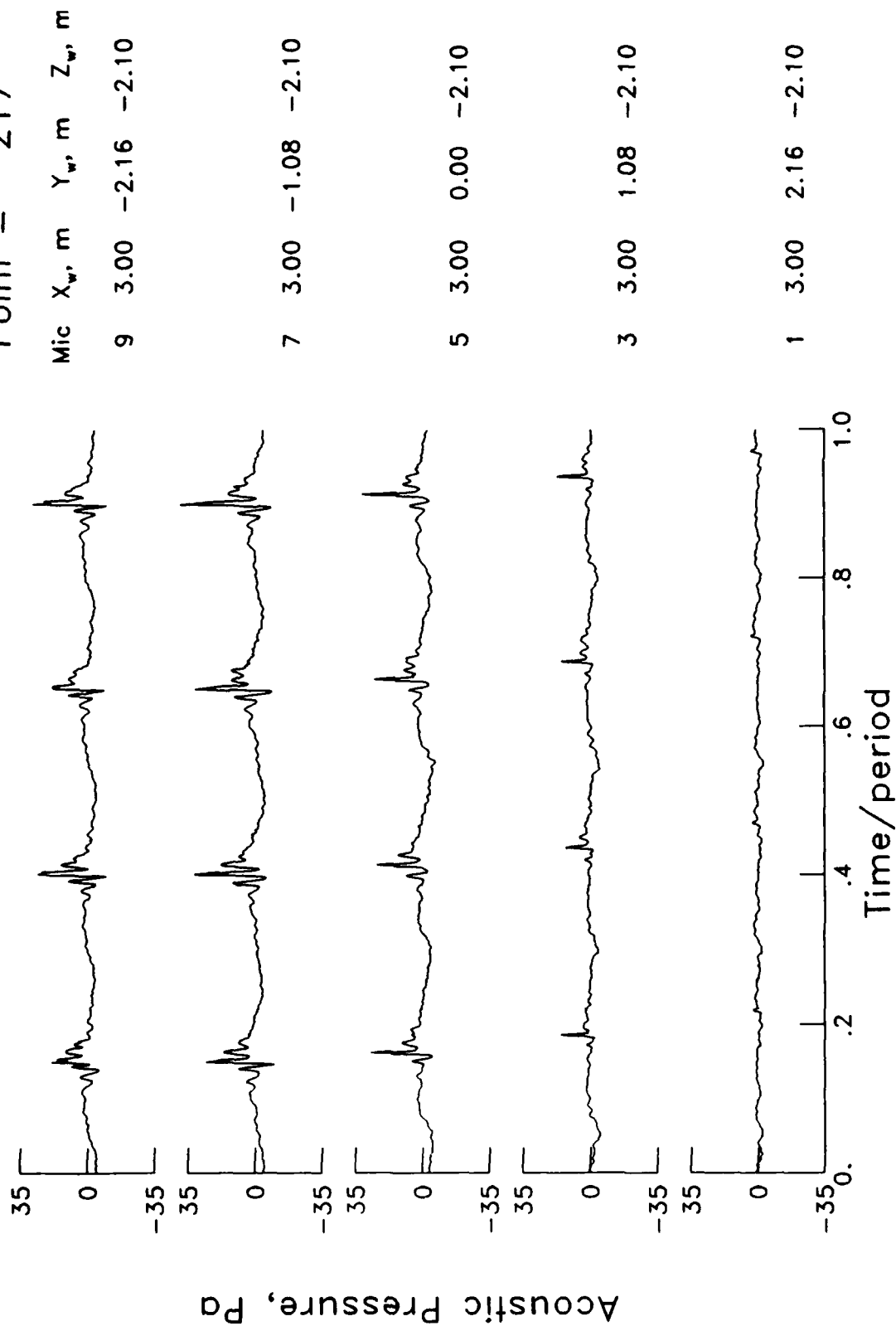
$\mu = .091$
 $\alpha_{TPP} = 2.1^\circ$
 $C_T = 0.0043$
 $M_H = 0.636$
 Point = 225



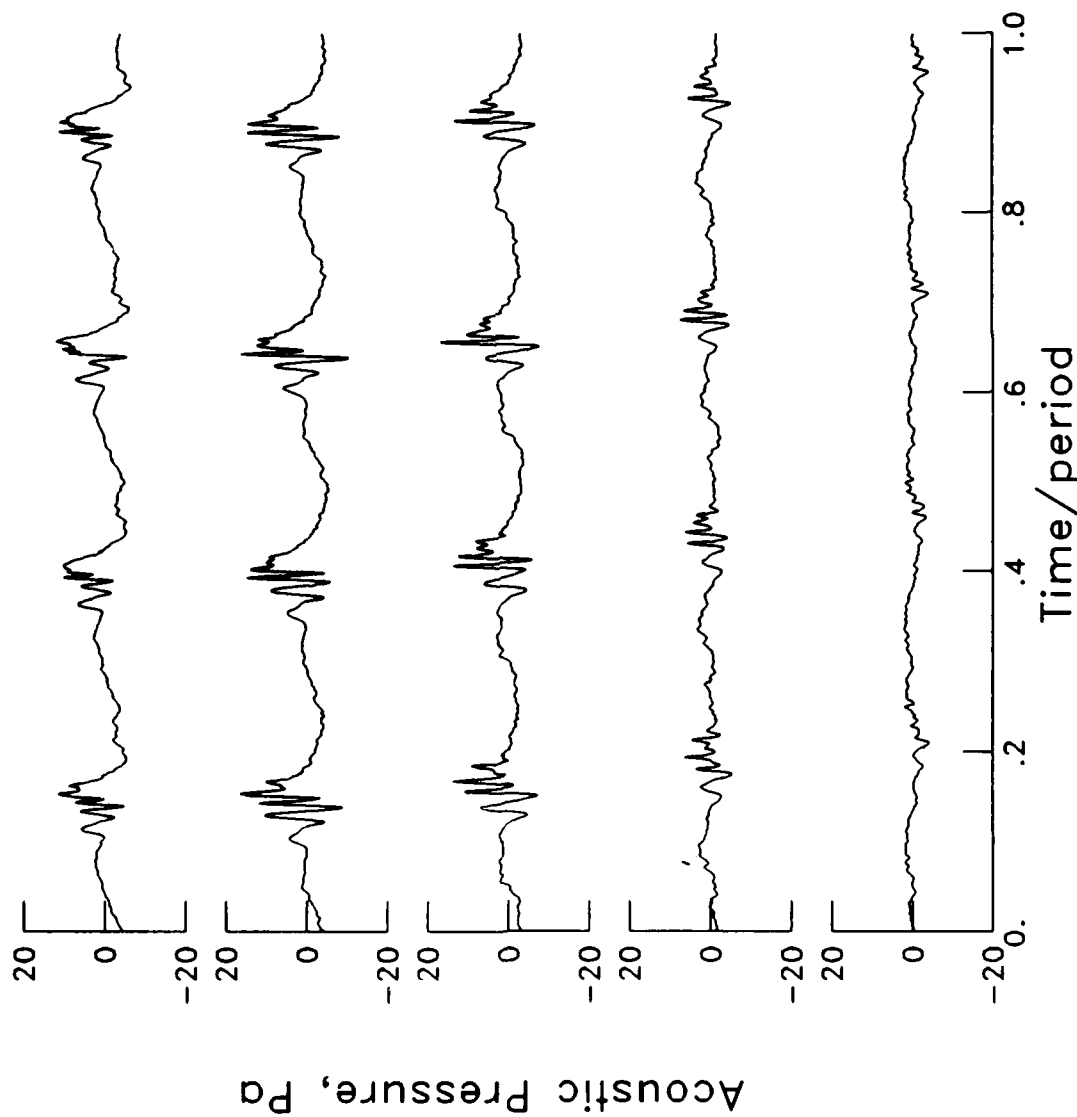
$\mu = .094$
 $\alpha_{TPP} = 4.1^\circ$
 $C_T = 0.0043$
 $M_{H_i} = 0.634$
 Point = 221



$\mu = .093$
 $\alpha_{TPP} = 6.1^\circ$
 $C_T = 0.0043$
 $M_H = 0.634$
 Point = 217

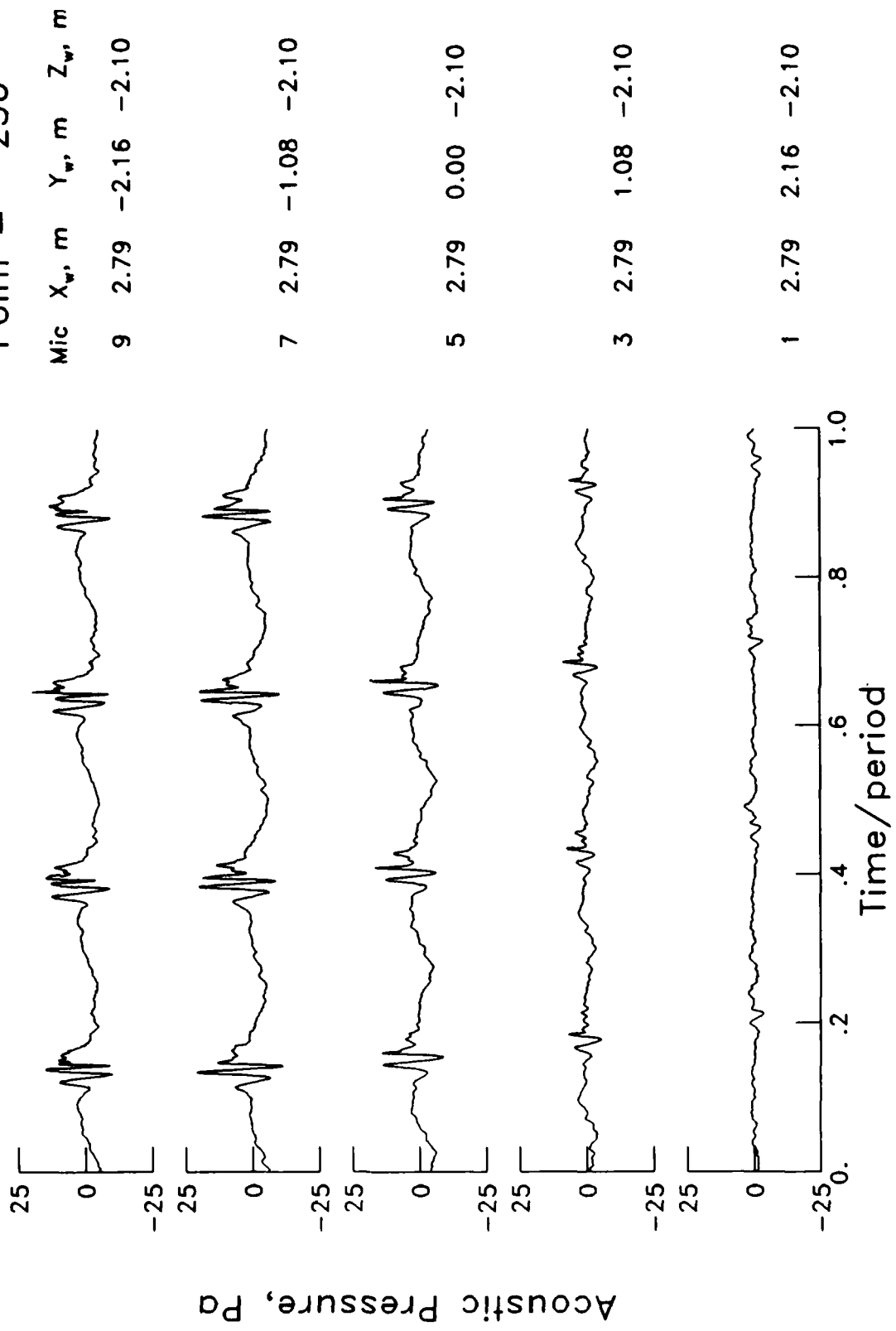


$\mu = .114$
 $\alpha_{TPP} = 1.5^\circ$
 $C_T = 0.0044$
 $M_{H_i} = 0.634$
 Point = 226



Mic	X _w , m	Y _w , m	Z _w , m
9	2.69	-2.16	-2.10
7	2.69	-1.08	-2.10
5	2.69	0.00	-2.10
3	2.69	1.08	-2.10
1	2.69	2.16	-2.10

$\mu = .113$
 $\alpha_{TPP} = 3.5^\circ$
 $C_T = 0.0043$
 $M_{H_i} = 0.635$
 Point = 230



$\mu = .117$
 $\alpha_{TPP} = 5.5^\circ$
 $C_T = 0.0043$
 $M_H = 0.634$
 Point = 234

Mic X_w, m Y_w, m Z_w, m

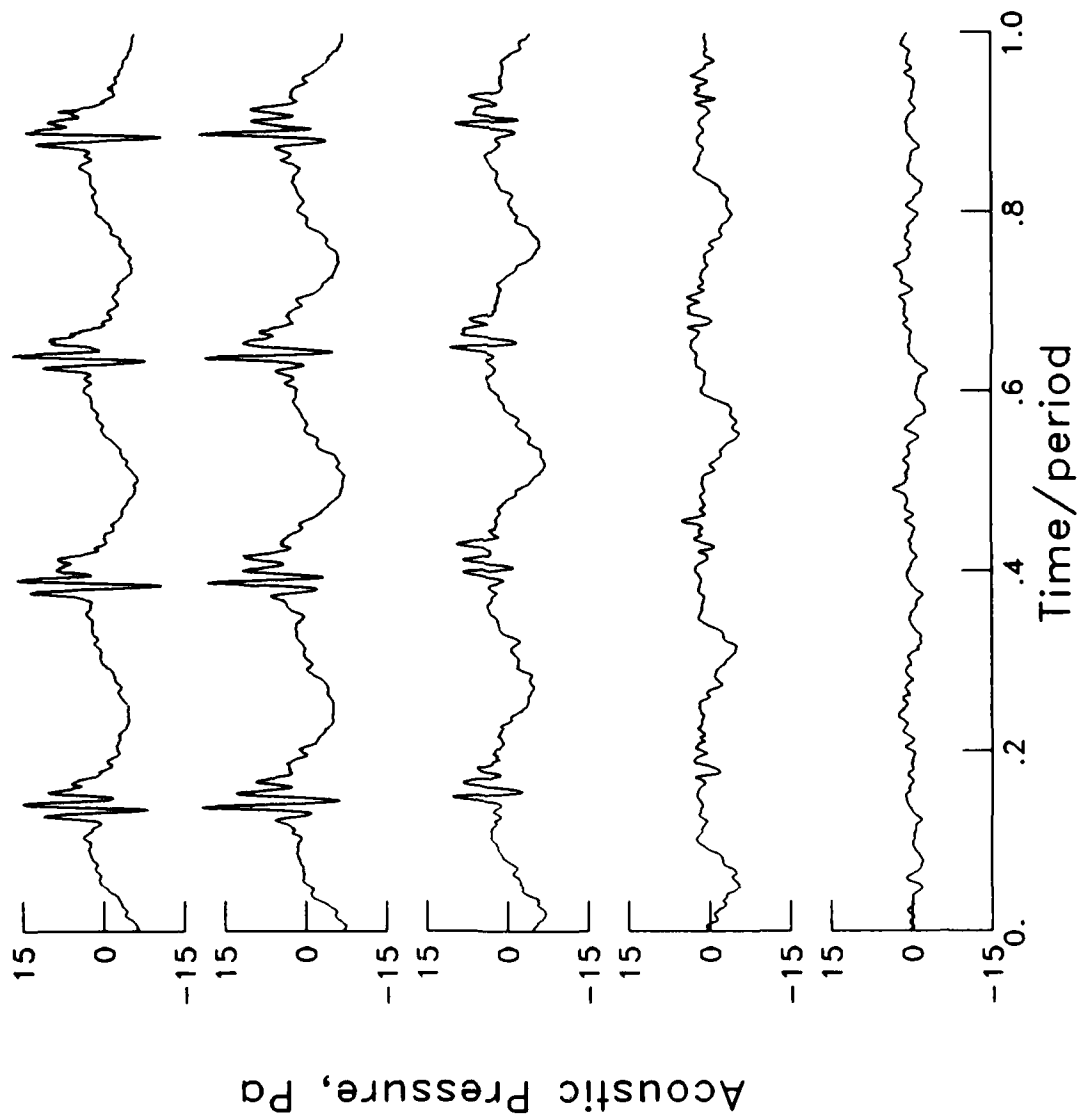
9 2.90 -2.16 -2.10

7 2.90 -1.08 -2.10

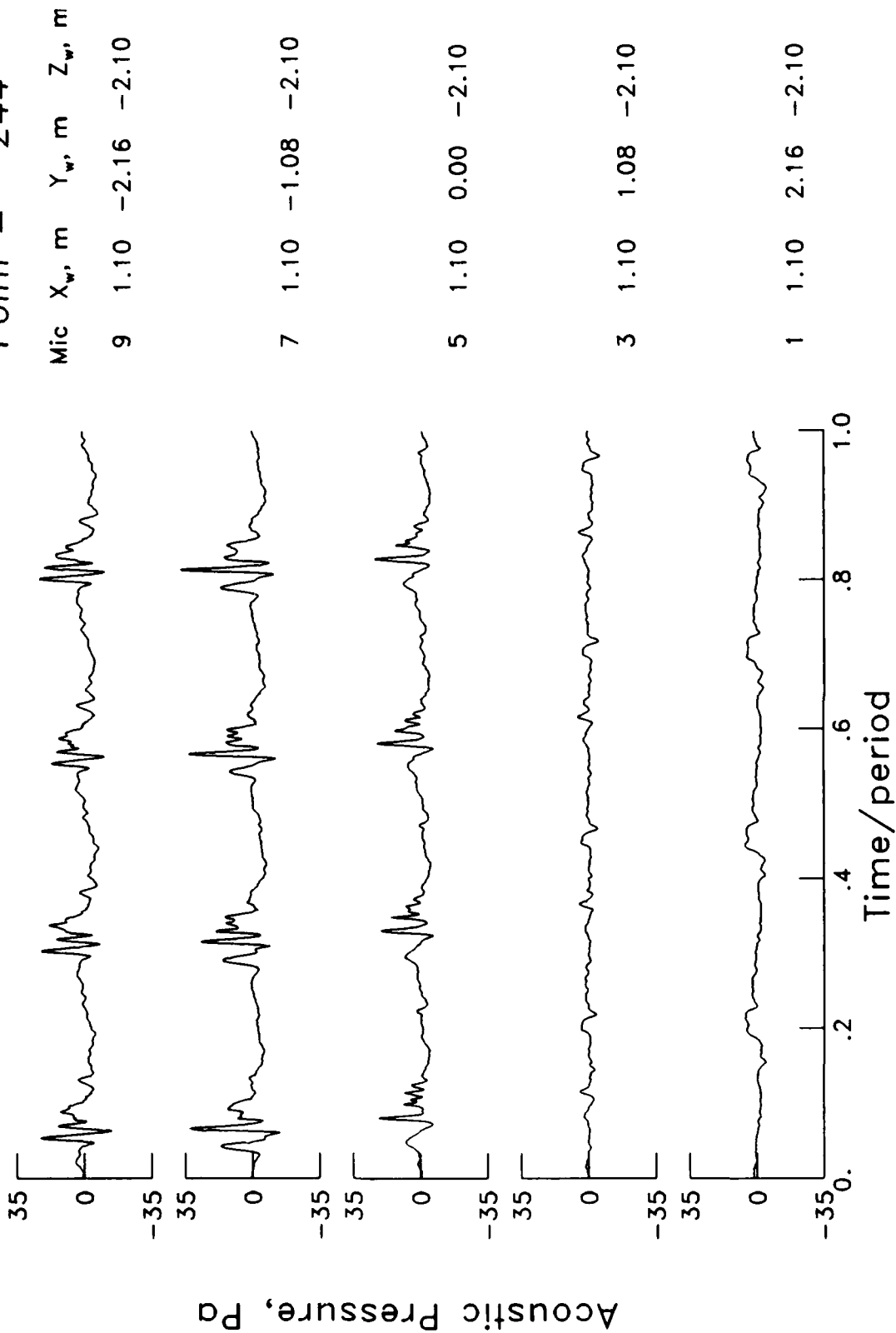
5 2.90 0.00 -2.10

3 2.90 1.08 -2.10

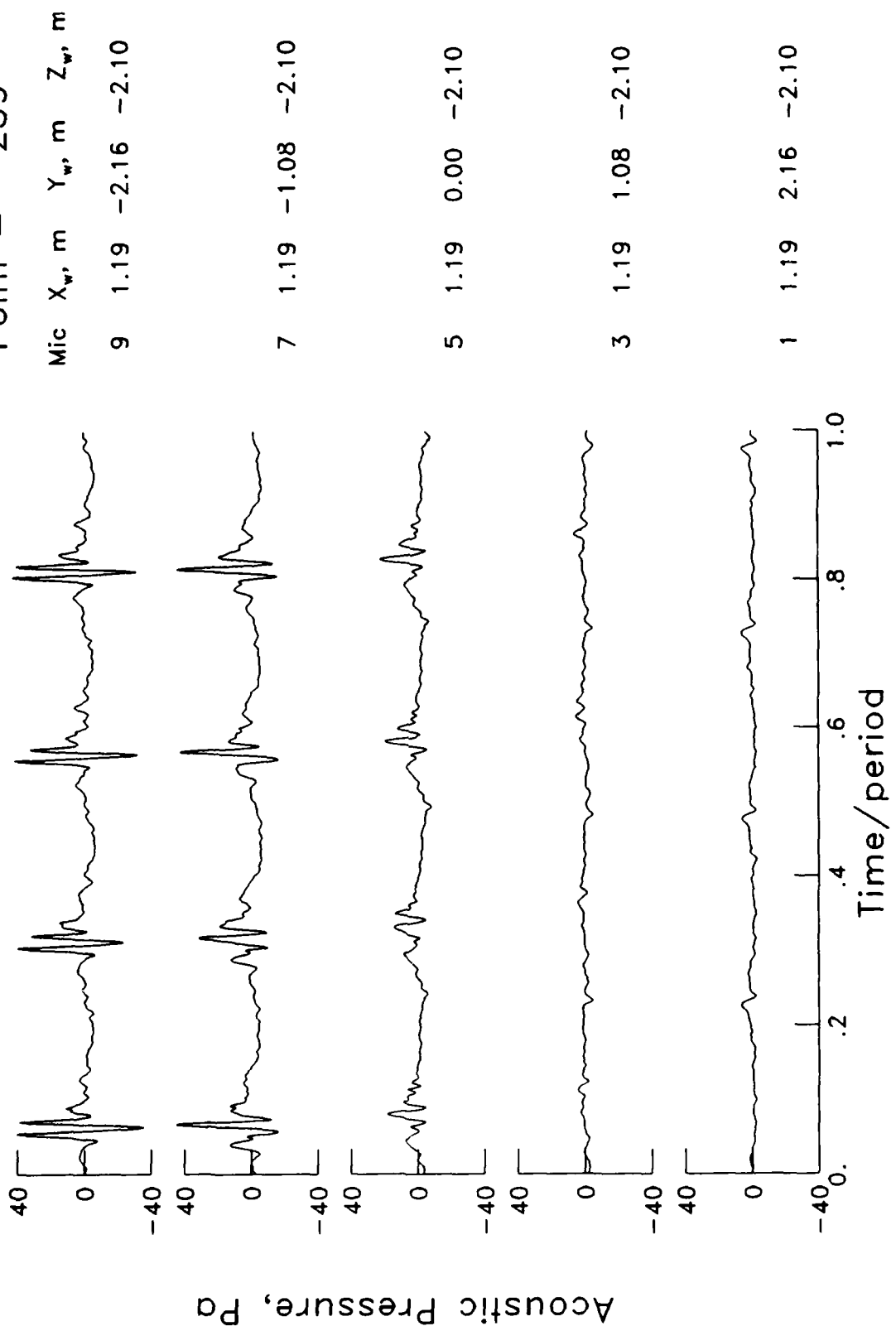
1 2.90 2.16 -2.10



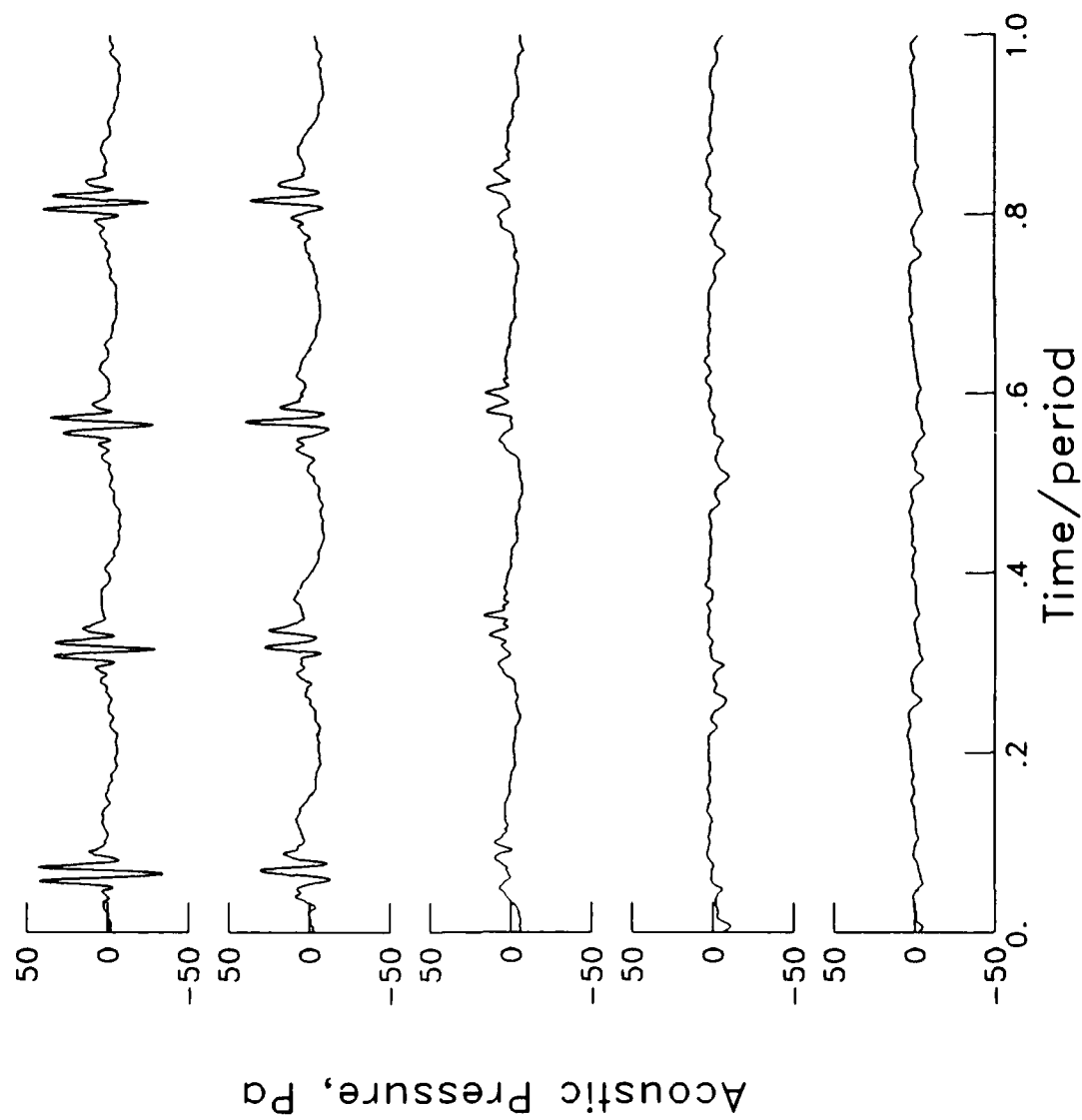
$\mu = .140$
 $\alpha_{TPP} = 0.2^\circ$
 $C_T = 0.0044$
 $M_H = 0.633$
 Point = 244



$\mu = .138$
 $\alpha_{TPP} = 2.2^\circ$
 $C_T = 0.0043$
 $M_H = 0.632$
 Point = 239

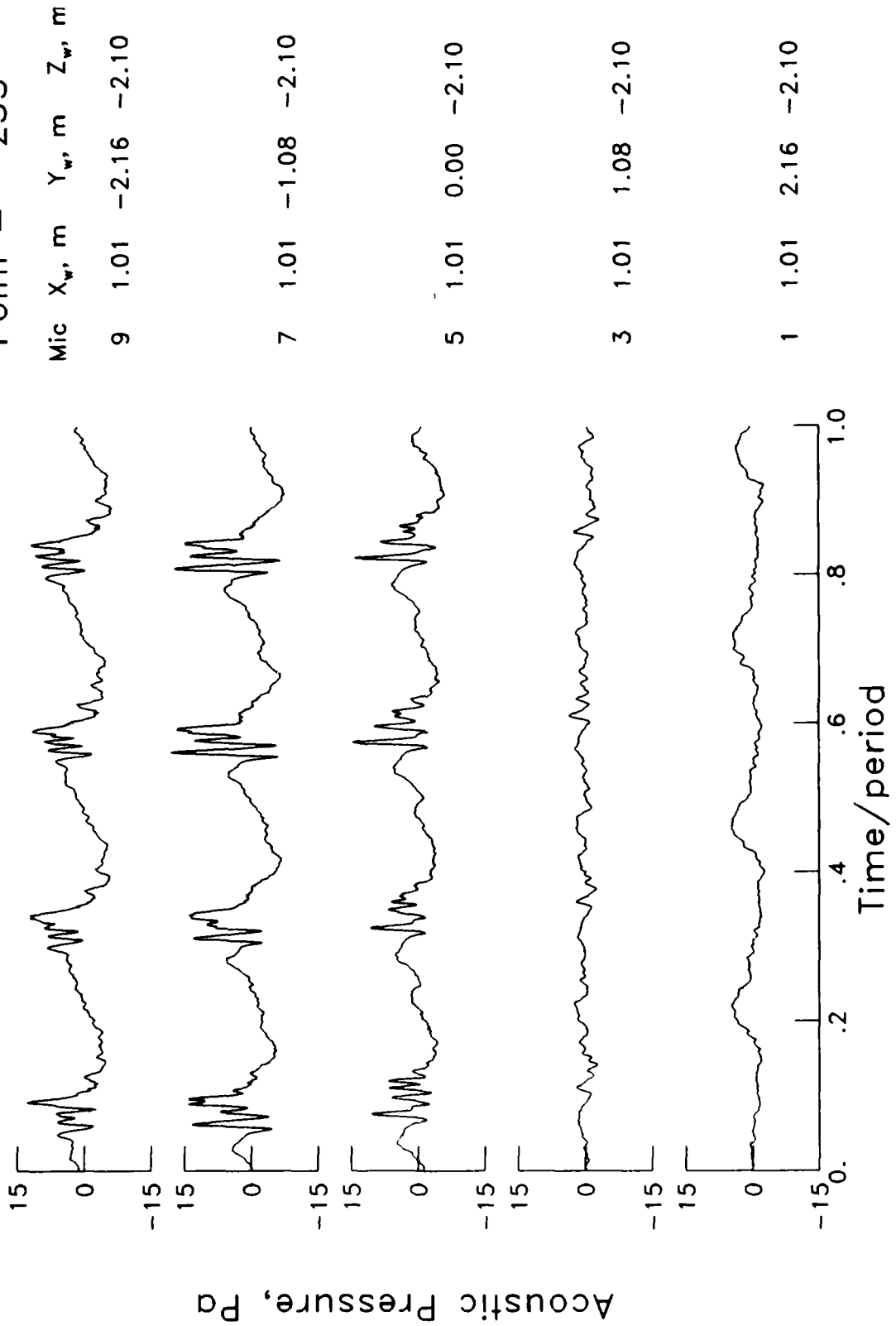


$\mu = .138$
 $\alpha_{\text{TPP}} = 4.3^\circ$
 $C_T = 0.0043$
 $M_{\text{H}} = 0.634$
 Point = 235

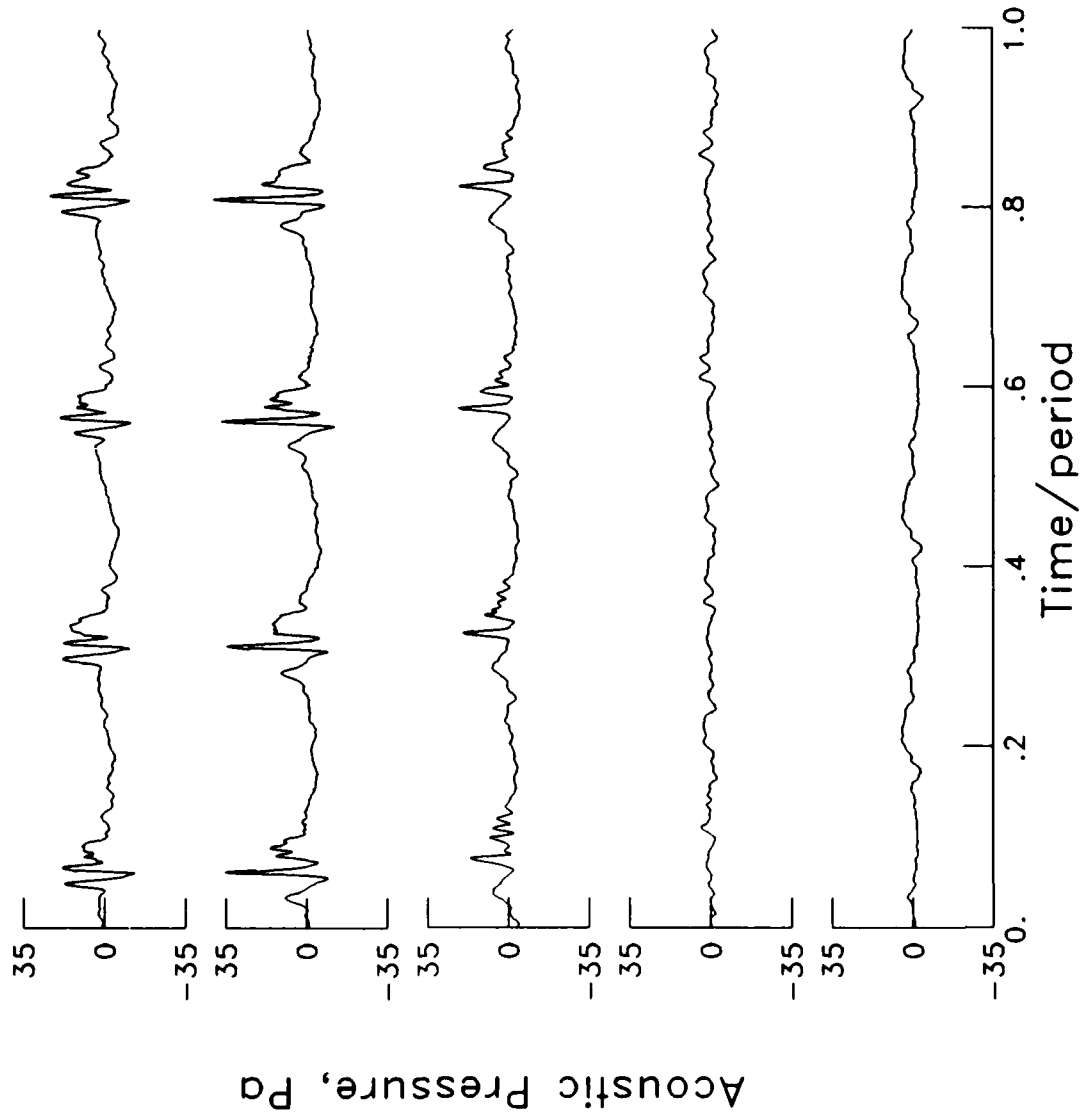


Mic	X_w , m	Y_w , m	Z_w , m
9	1.29	-2.16	-2.10
7	1.29	-1.08	-2.10
5	1.29	0.00	-2.10
3	1.29	1.08	-2.10
1	1.29	2.16	-2.10

$\mu = .147$
 $\alpha_{TPP} = -1.6^\circ$
 $C_T = 0.0043$
 $M_H = 0.633$
 Point = 253

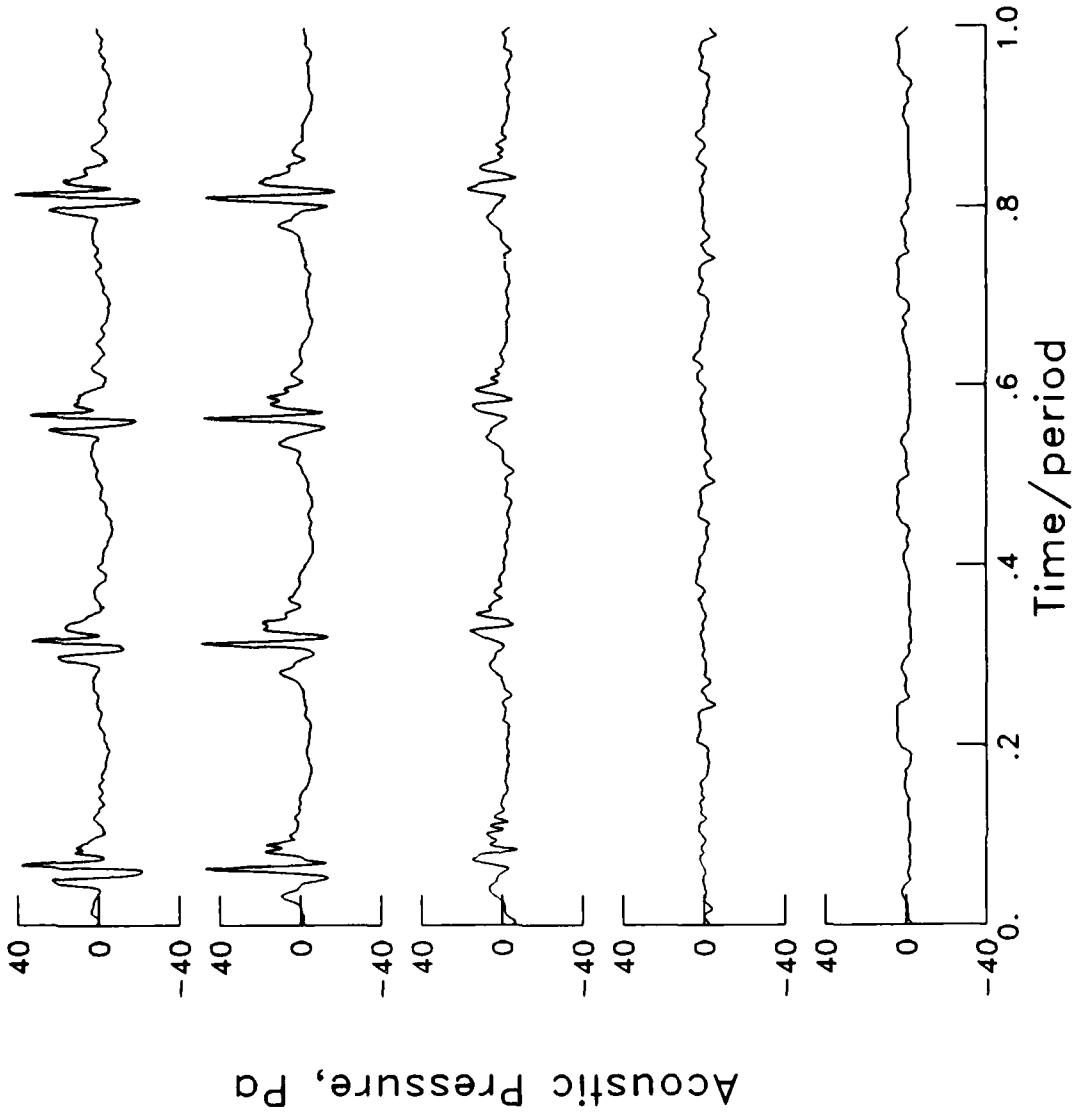


$\mu = .147$
 $\alpha_{TPP} = -0.1^\circ$
 $C_T = 0.0043$
 $M_H = 0.635$
 Point = 250



Mic	X _w , m	Y _w , m	Z _w , m
9	1.07	-2.16	-2.10
7	1.07	-1.08	-2.10
5	1.07	0.00	-2.10
3	1.07	1.08	-2.10
1	1.07	2.16	-2.10

$\mu = .146$
 $\alpha_{TPP} = 0.9^\circ$
 $C_T = 0.0043$
 $M_H = 0.636$
 Point = 248



Mic X_w, m Y_w, m Z_w, m
 9 1.12 -2.16 -2.10

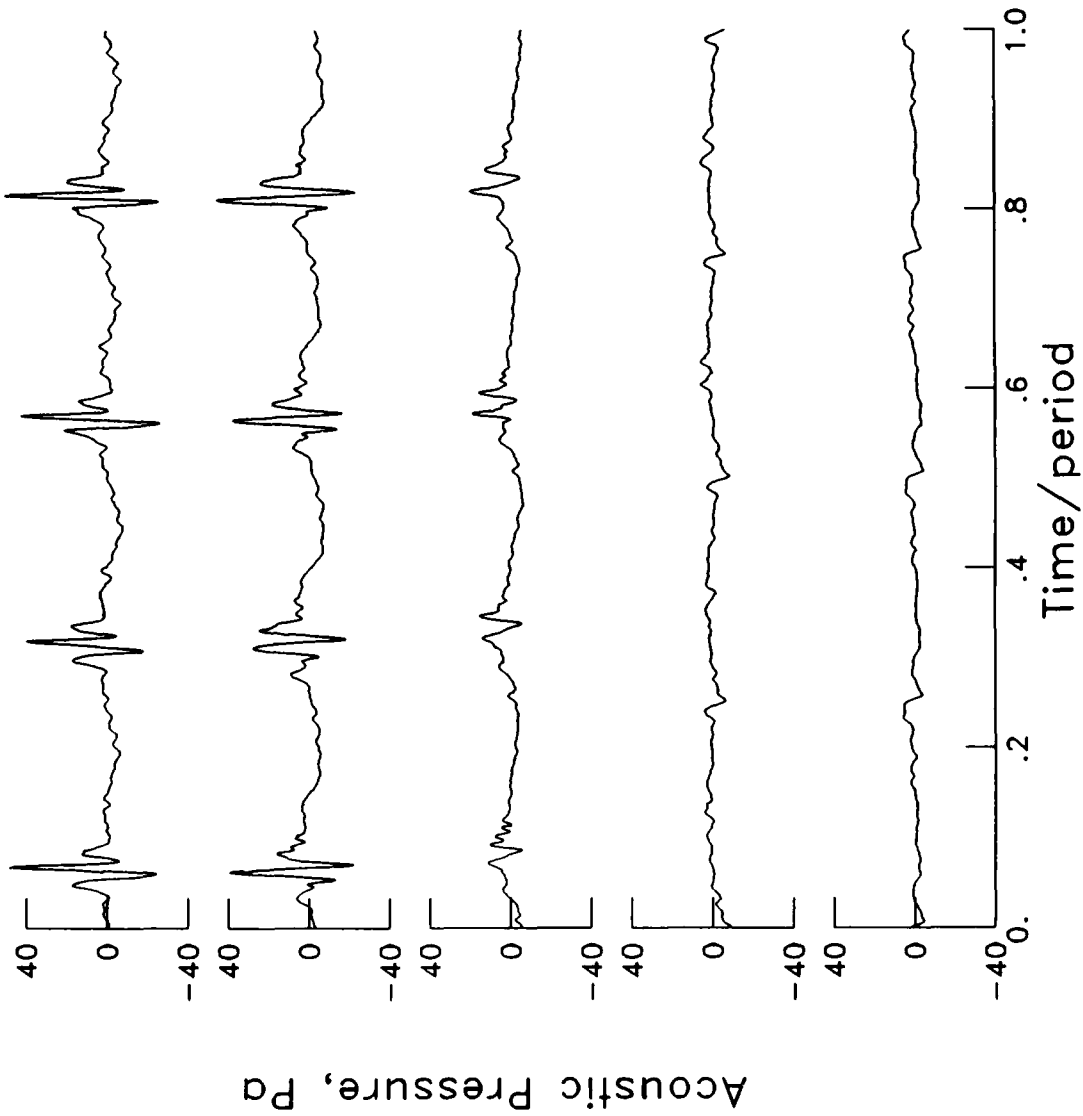
7 1.12 -1.08 -2.10

5 1.12 0.00 -2.10

3 1.12 1.08 -2.10

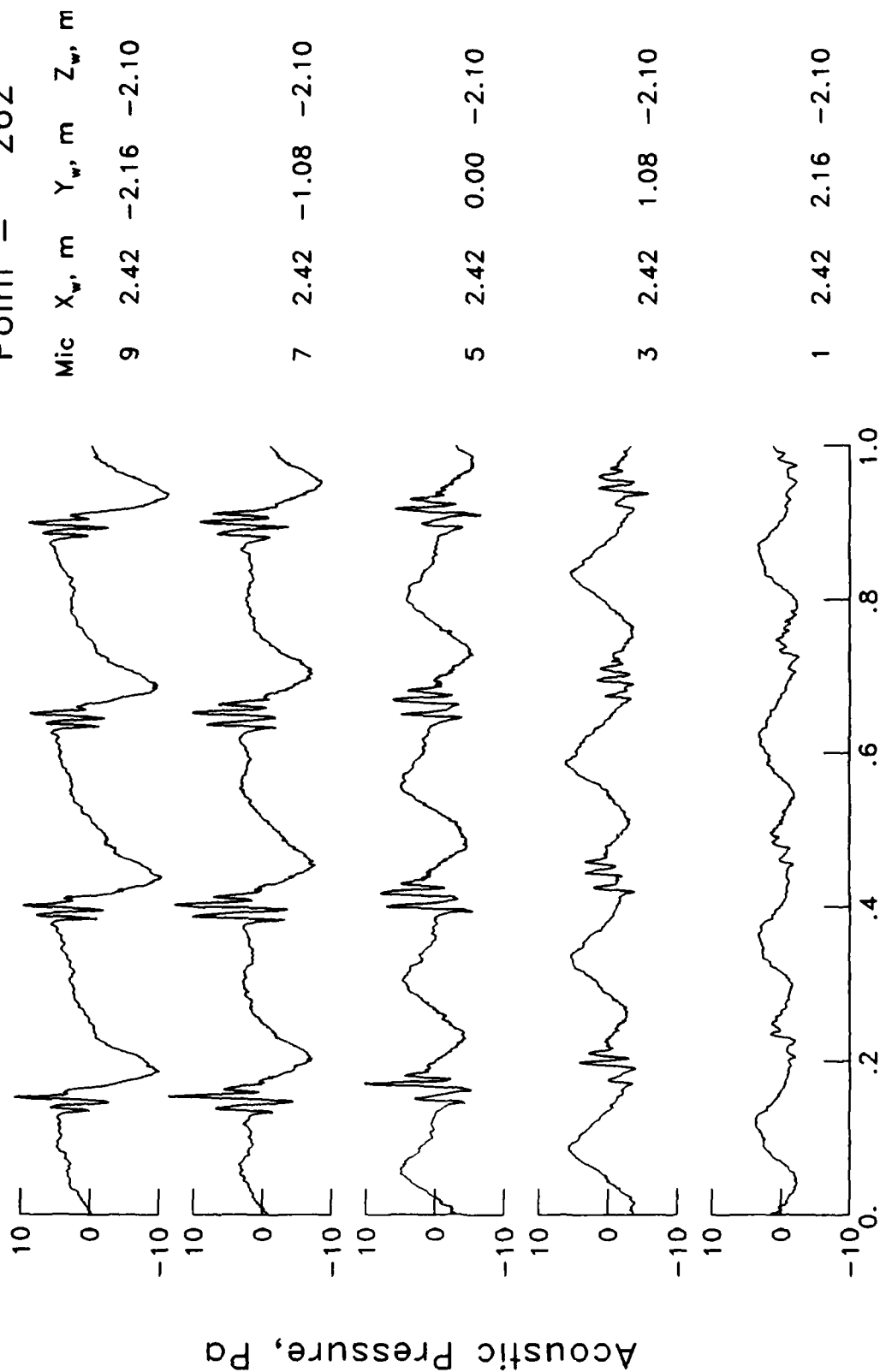
1 1.12 2.16 -2.10

$\mu = .146$
 $\alpha_{TPP} = 2.4^\circ$
 $C_T = 0.0043$
 $M_H = 0.637$
 Point = 245

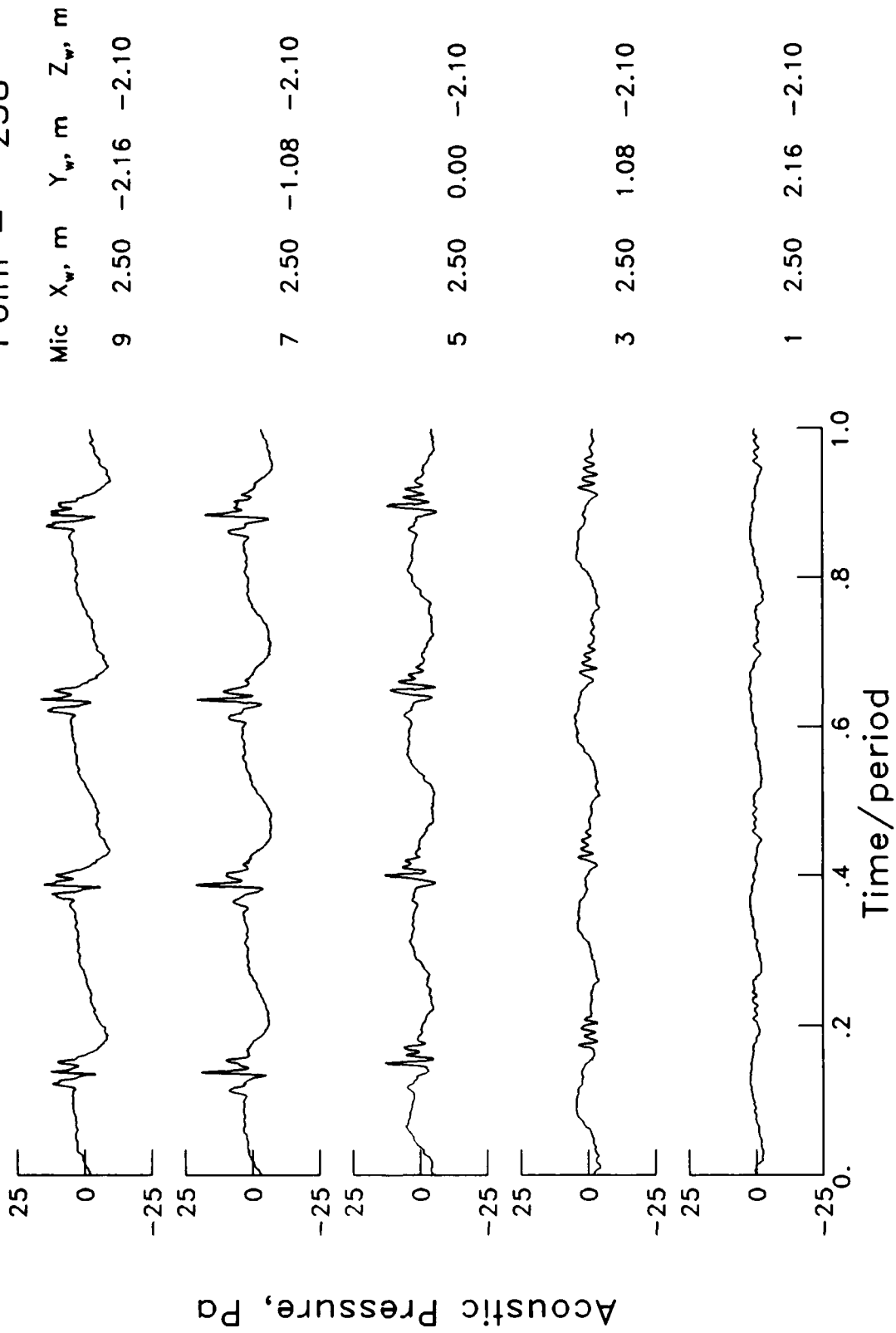


Mic	X_w , m	Y_w , m	Z_w , m
9	1.19	-2.16	-2.10
7	1.19	-1.08	-2.10
5	1.19	0.00	-2.10
3	1.19	1.08	-2.10
1	1.19	2.16	-2.10

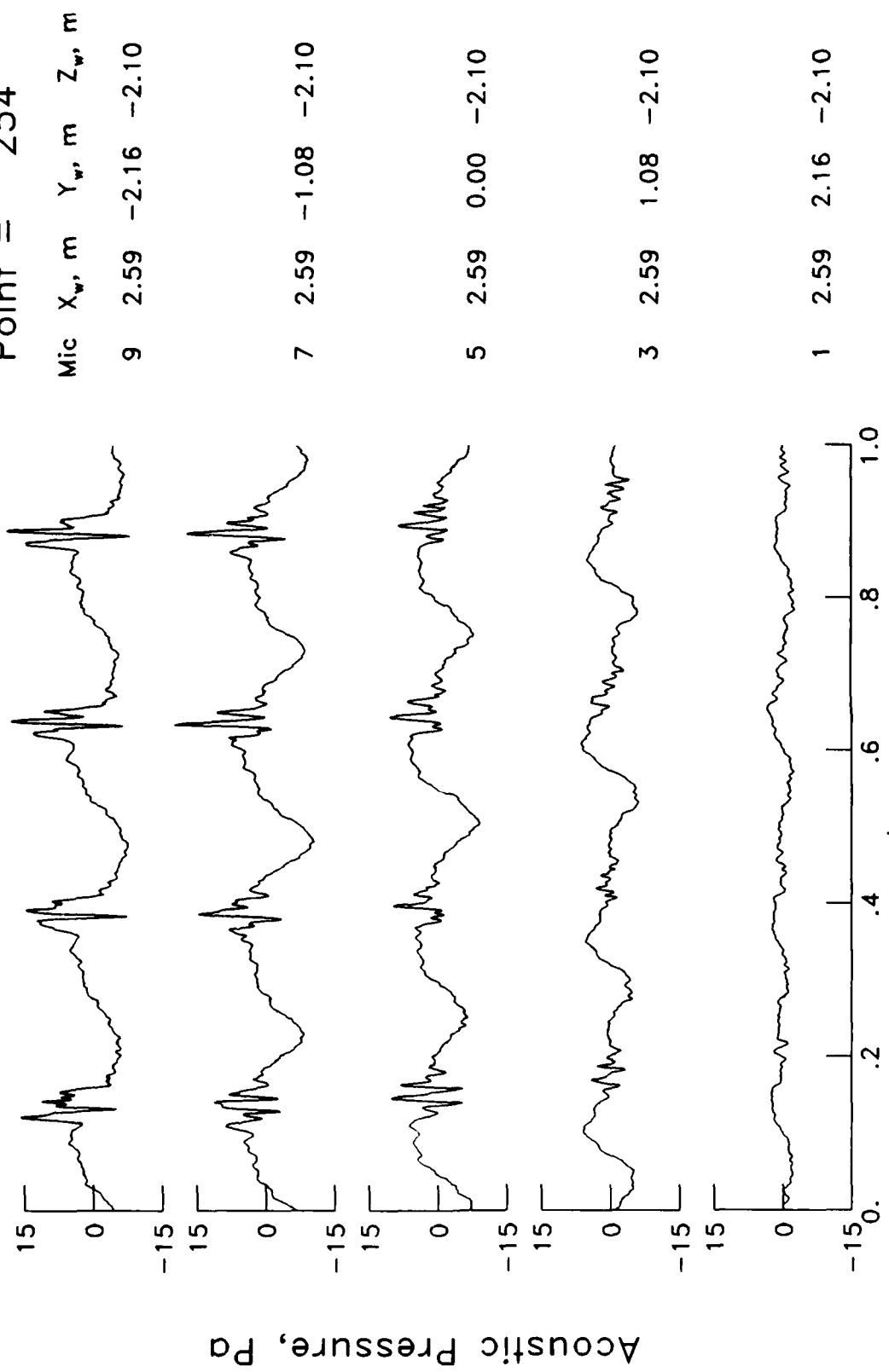
$\mu = .170$
 $\alpha_{TPP} = -3.1^\circ$
 $C_T = 0.0043$
 $M_{H_i} = 0.635$
 Point = 262



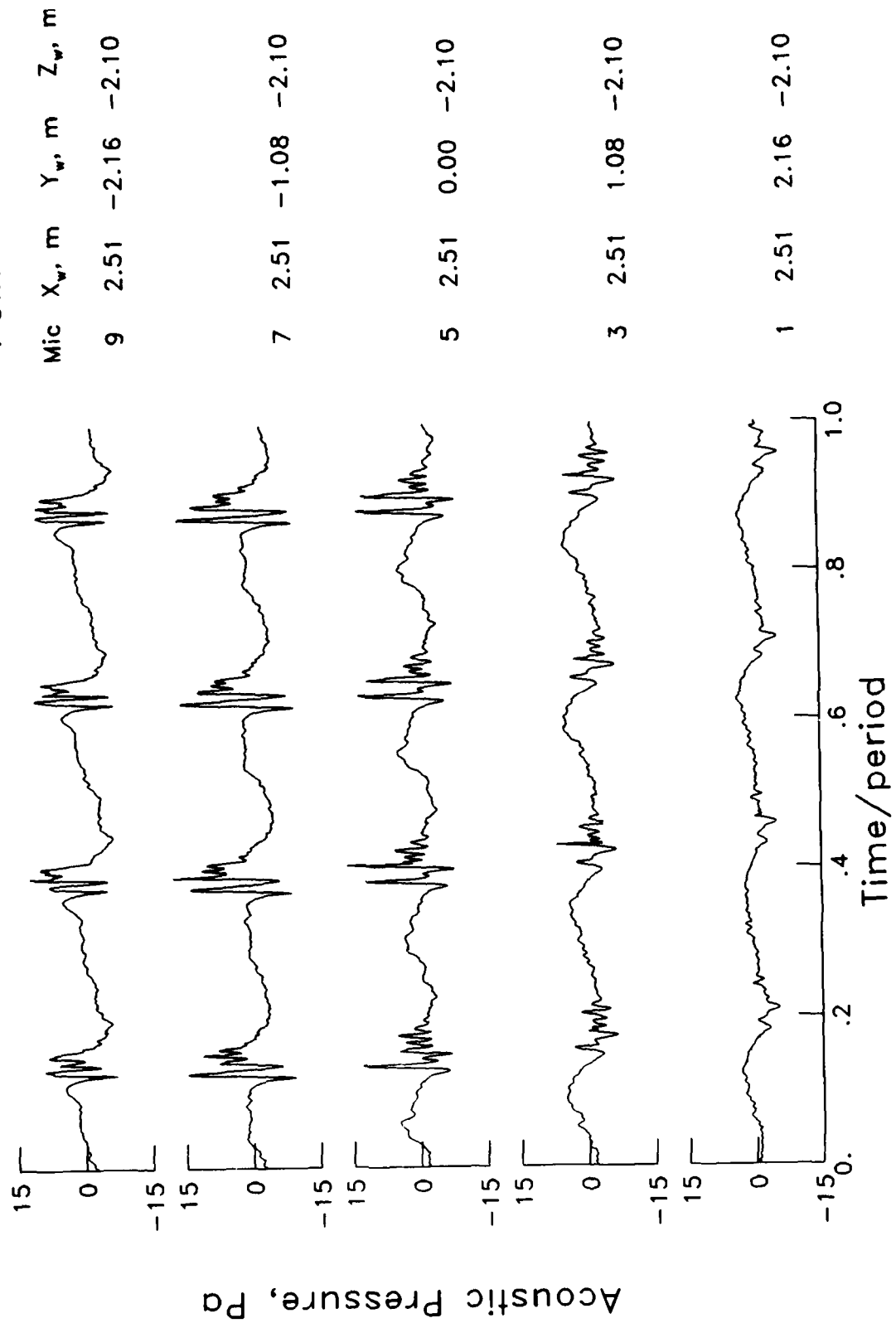
$\mu = .170$
 $\alpha_{TPP} = -1.1^\circ$
 $C_T = 0.0043$
 $M_H = 0.634$
 Point = 258



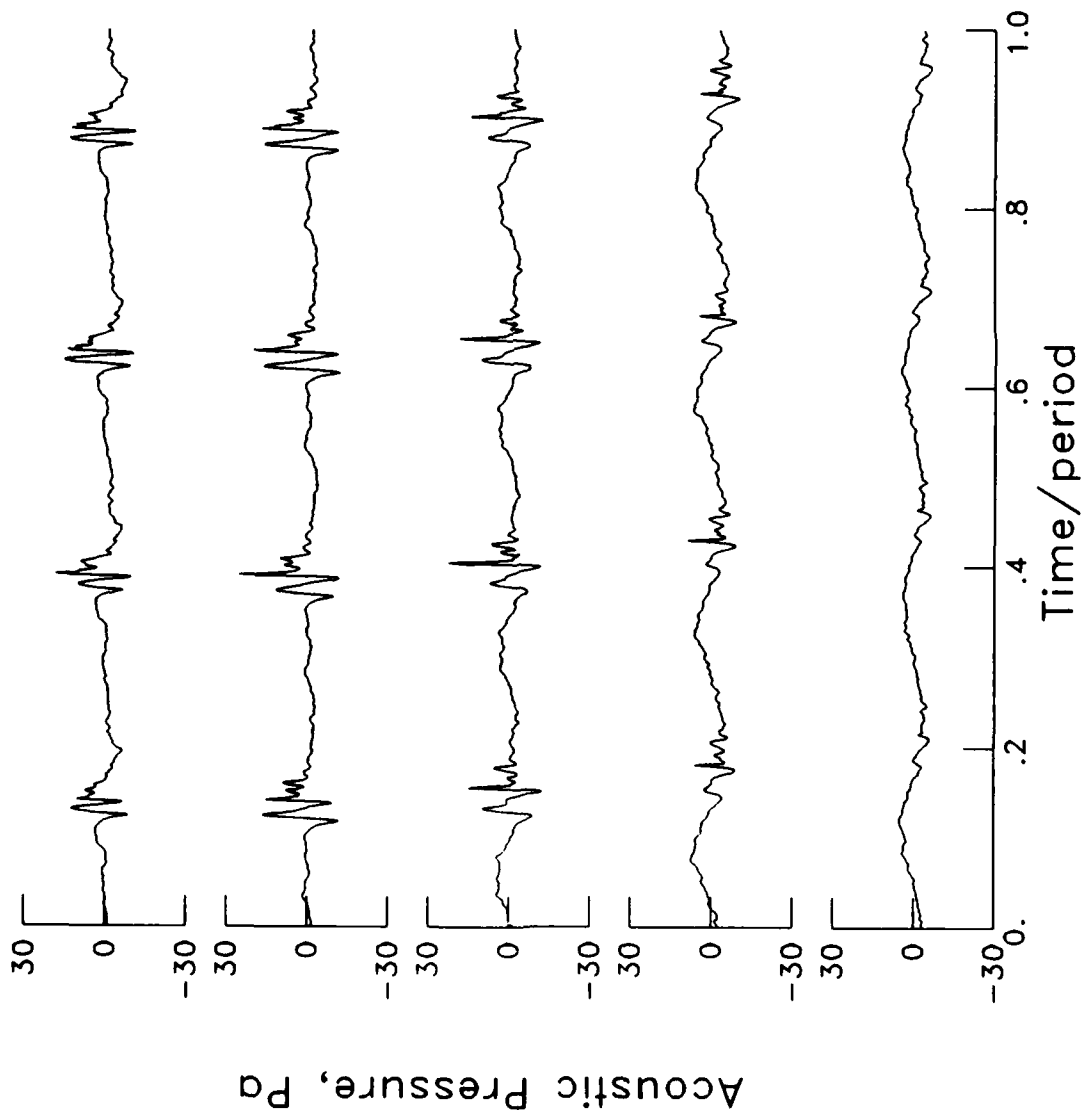
$\mu = .170$
 $\alpha_{TPP} = 0.9^\circ$
 $C_T = 0.0043$
 $M_{H_1} = 0.635$
 Point = 254



$\mu = .152$
 $\alpha_{TPP} = -1.4^\circ$
 $C_T = 0.0040$
 $M_H = 0.633$
 Point = 318



$\mu = .160$
 $\alpha_{TPP} = -1.2^\circ$
 $C_T = 0.0042$
 $M_{H_1} = 0.631$
 Point = 320



Mic X_w, m Y_w, m Z_w, m

9 2.51 -2.16 -2.10

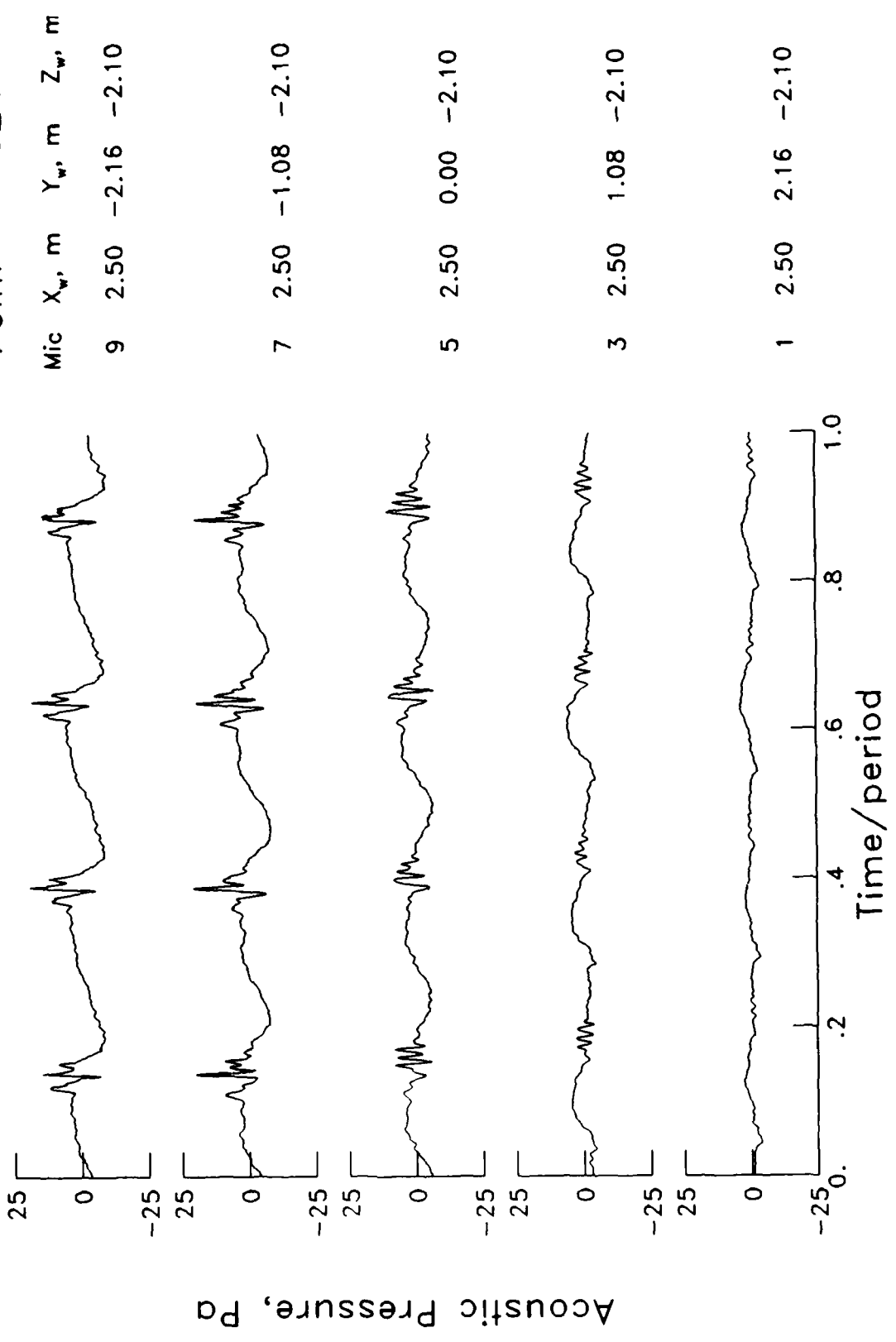
7 2.51 -1.08 -2.10

5 2.51 0.00 -2.10

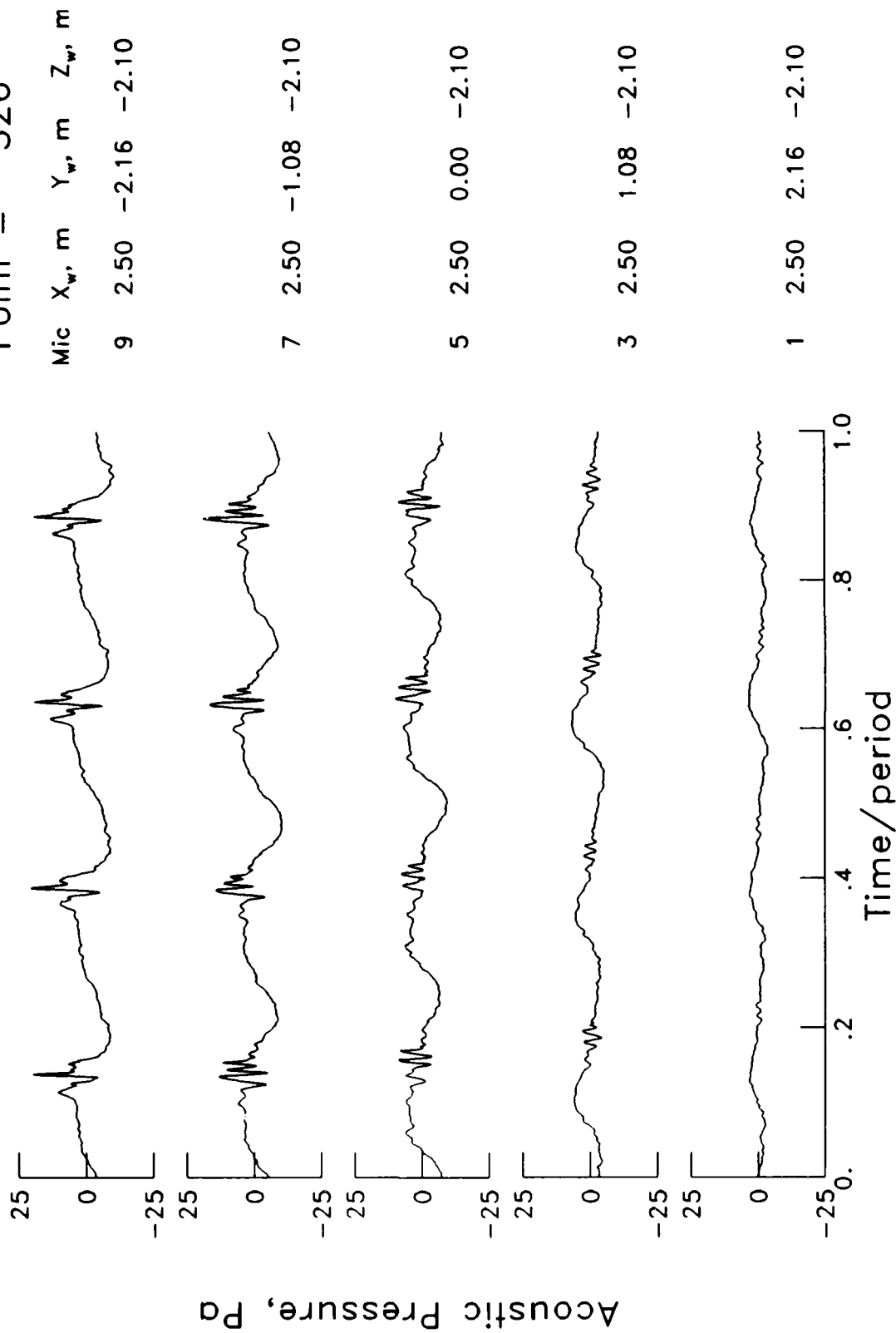
3 2.51 1.08 -2.10

1 2.51 2.16 -2.10

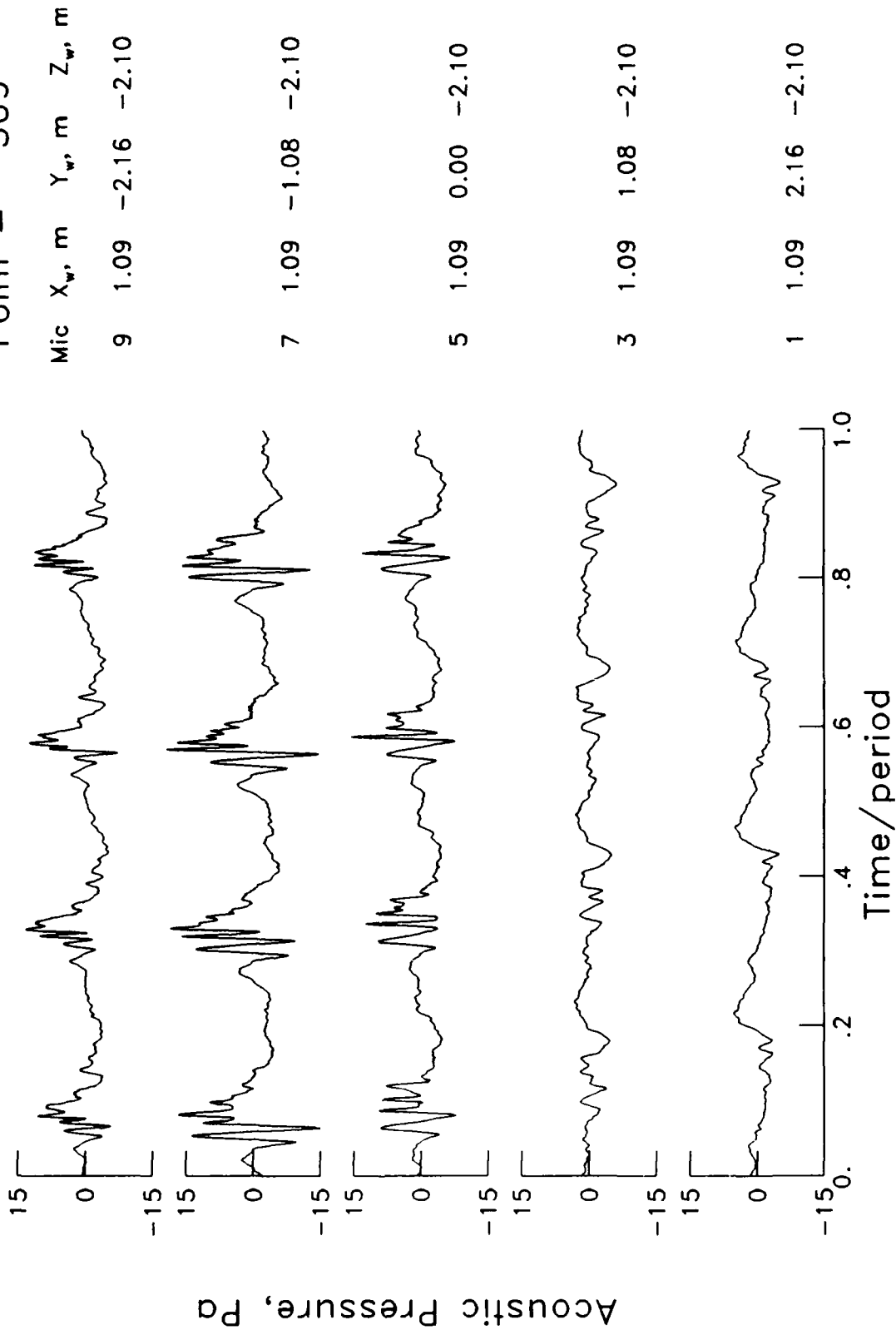
$\mu = .179$
 $\alpha_{TPP} = -1.0^\circ$
 $C_T = 0.0044$
 $M_H = 0.631$
 Point = 324



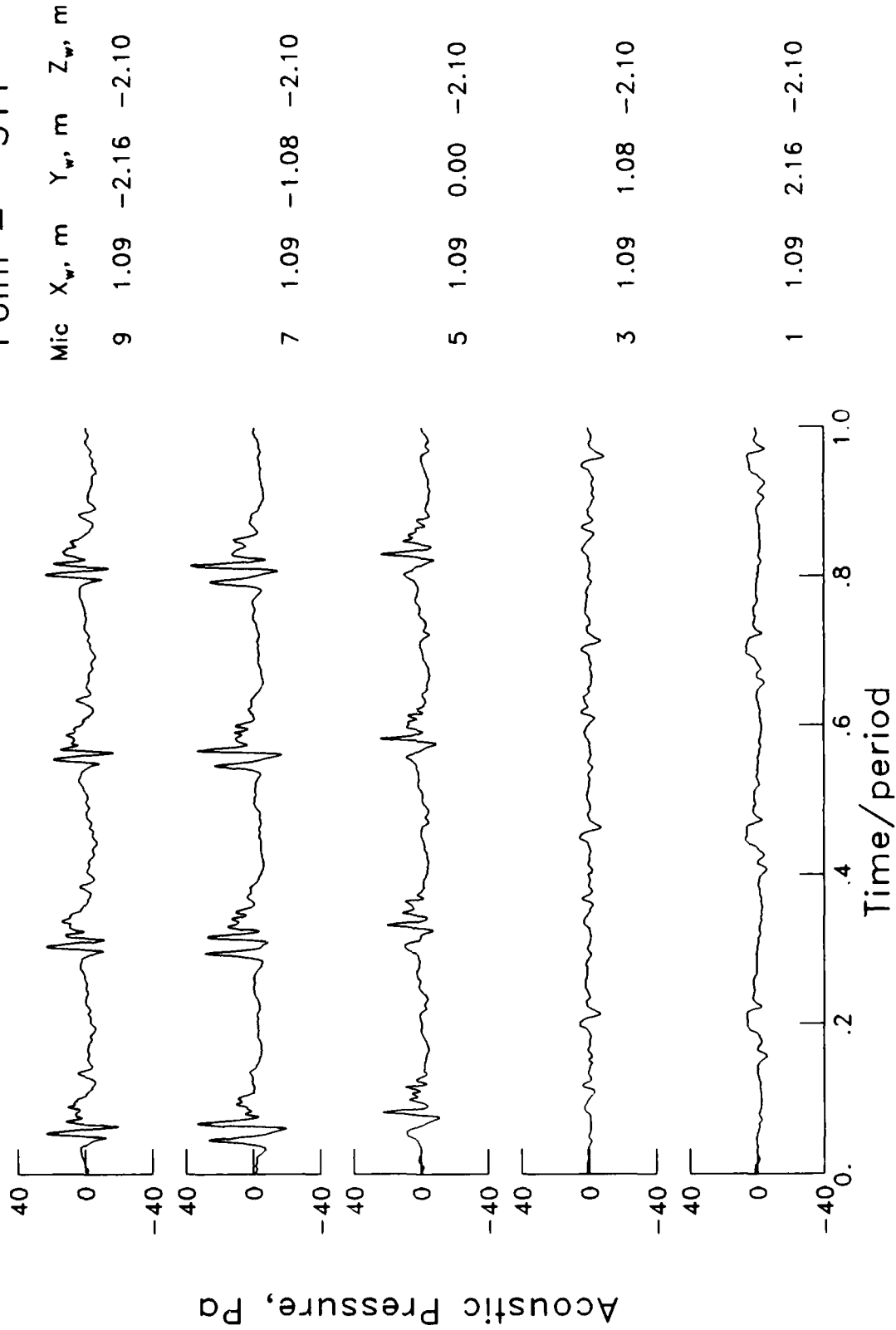
$\mu = .187$
 $\alpha_{TPP} = -0.8^\circ$
 $C_T = 0.0043$
 $M_H = 0.637$
 Point = 326



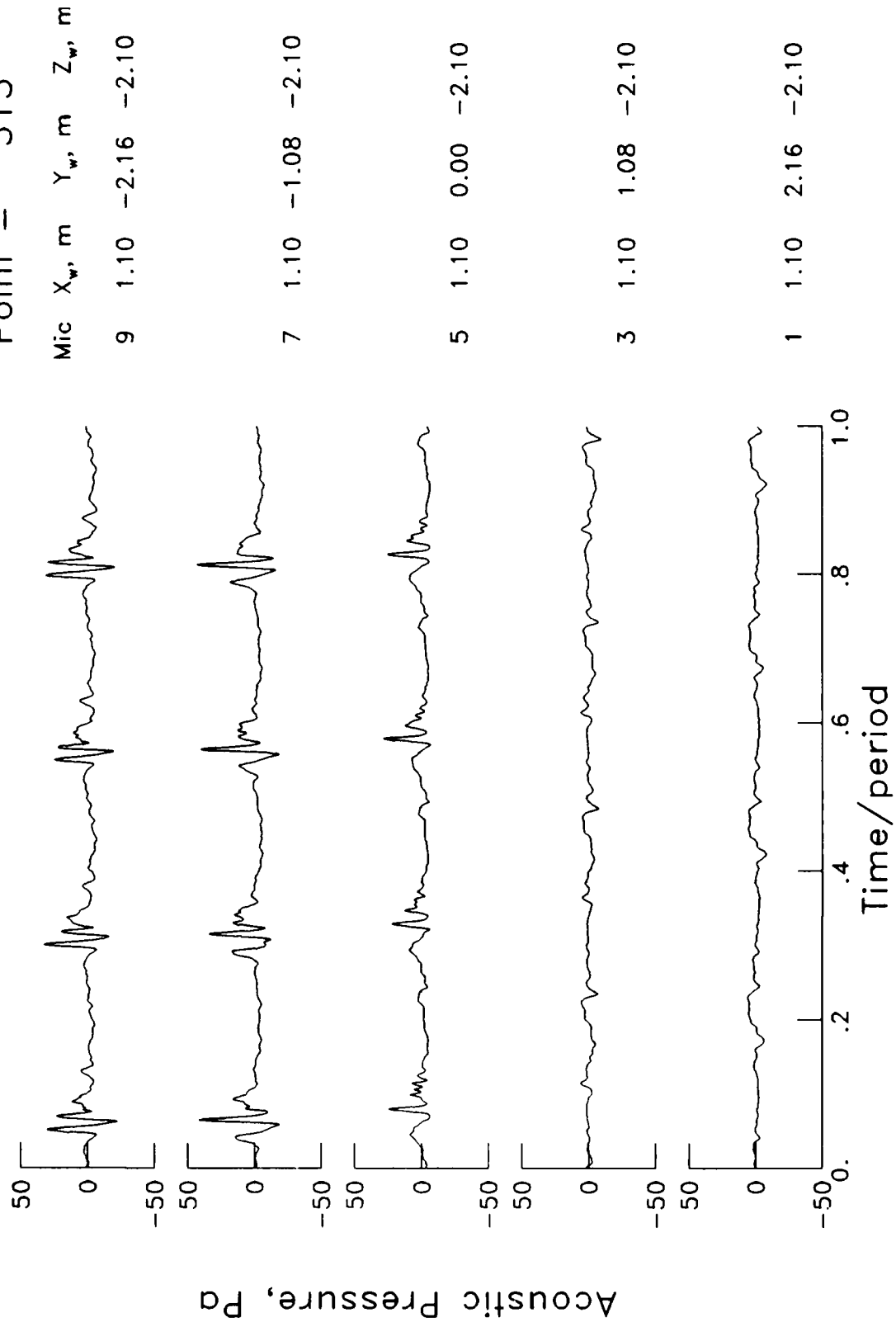
$\mu = .130$
 $\alpha_{TPP} = -0.1^\circ$
 $C_T = 0.0044$
 $M_{H_i} = 0.629$
 Point = 309



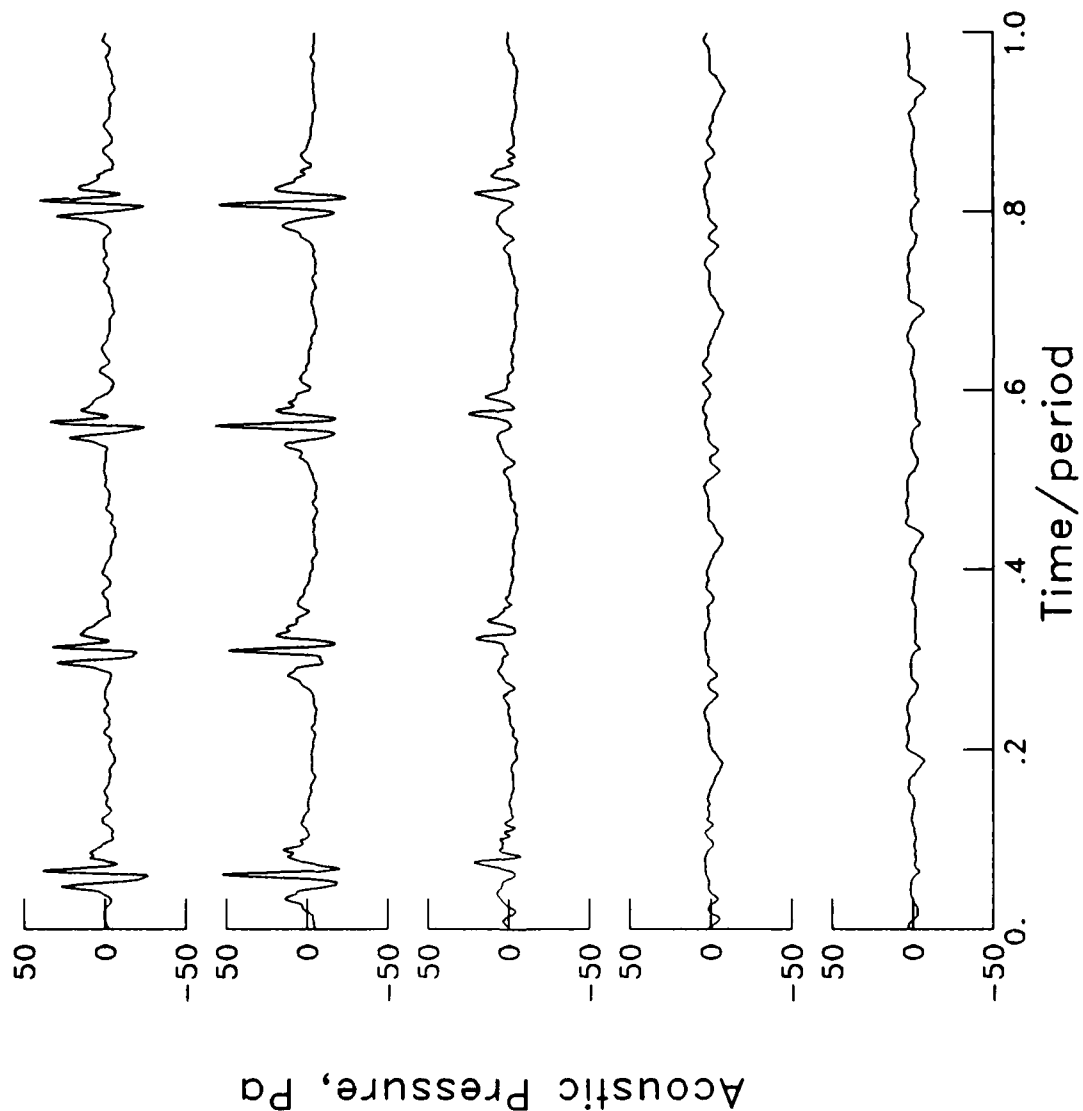
$\mu = .139$
 $\alpha_{TPP} = 0.1^\circ$
 $C_T = 0.0044$
 $M_H = 0.634$
 Point = 311



$\mu = .147$
 $\alpha_{\text{TPP}} = 0.4^\circ$
 $C_T = 0.0043$
 $M_H = 0.633$
 Point = 313

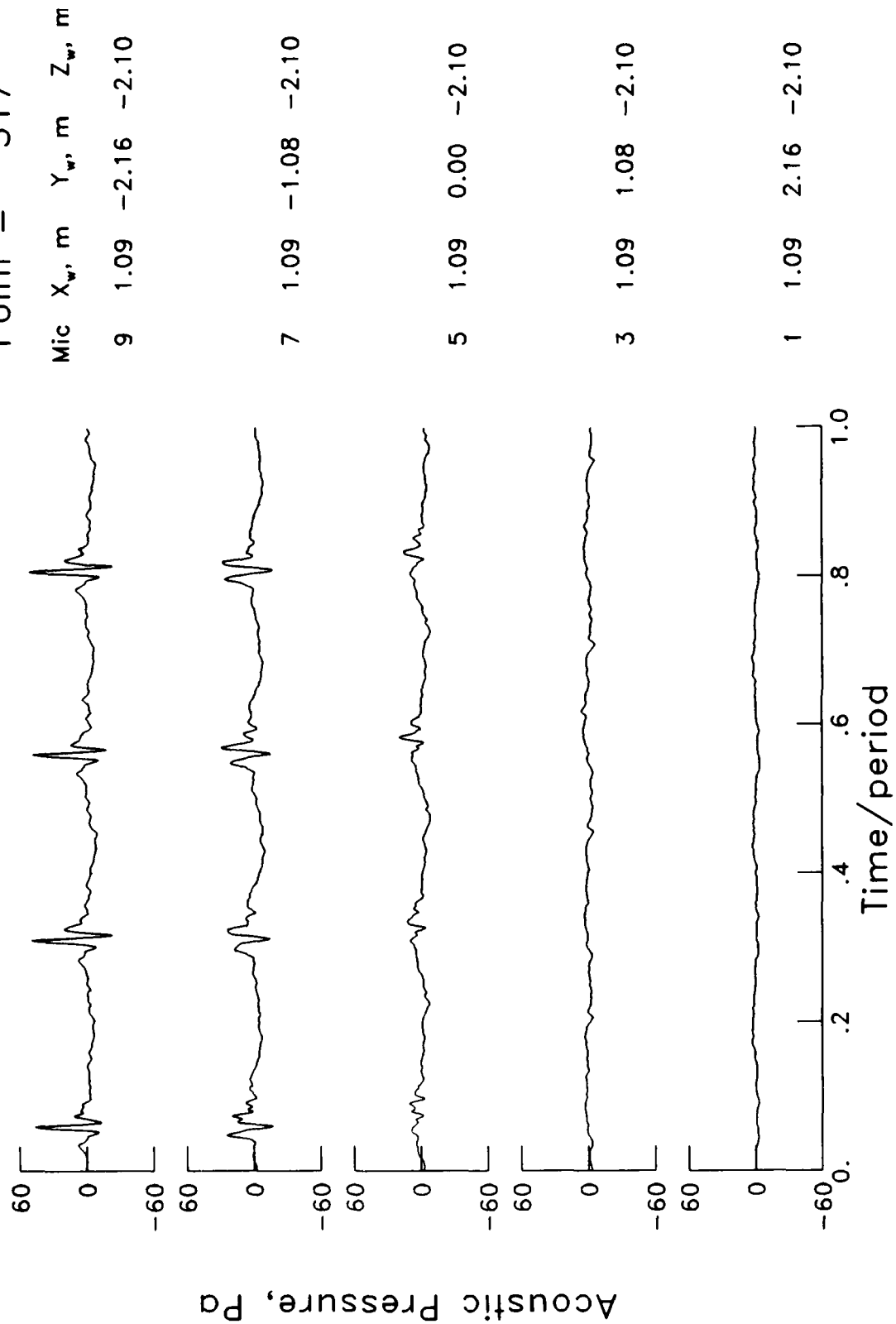


$\mu = .157$
 $\alpha_{TPP} = 0.5^\circ$
 $C_T = 0.0046$
 $M_H = 0.631$
 Point = 315

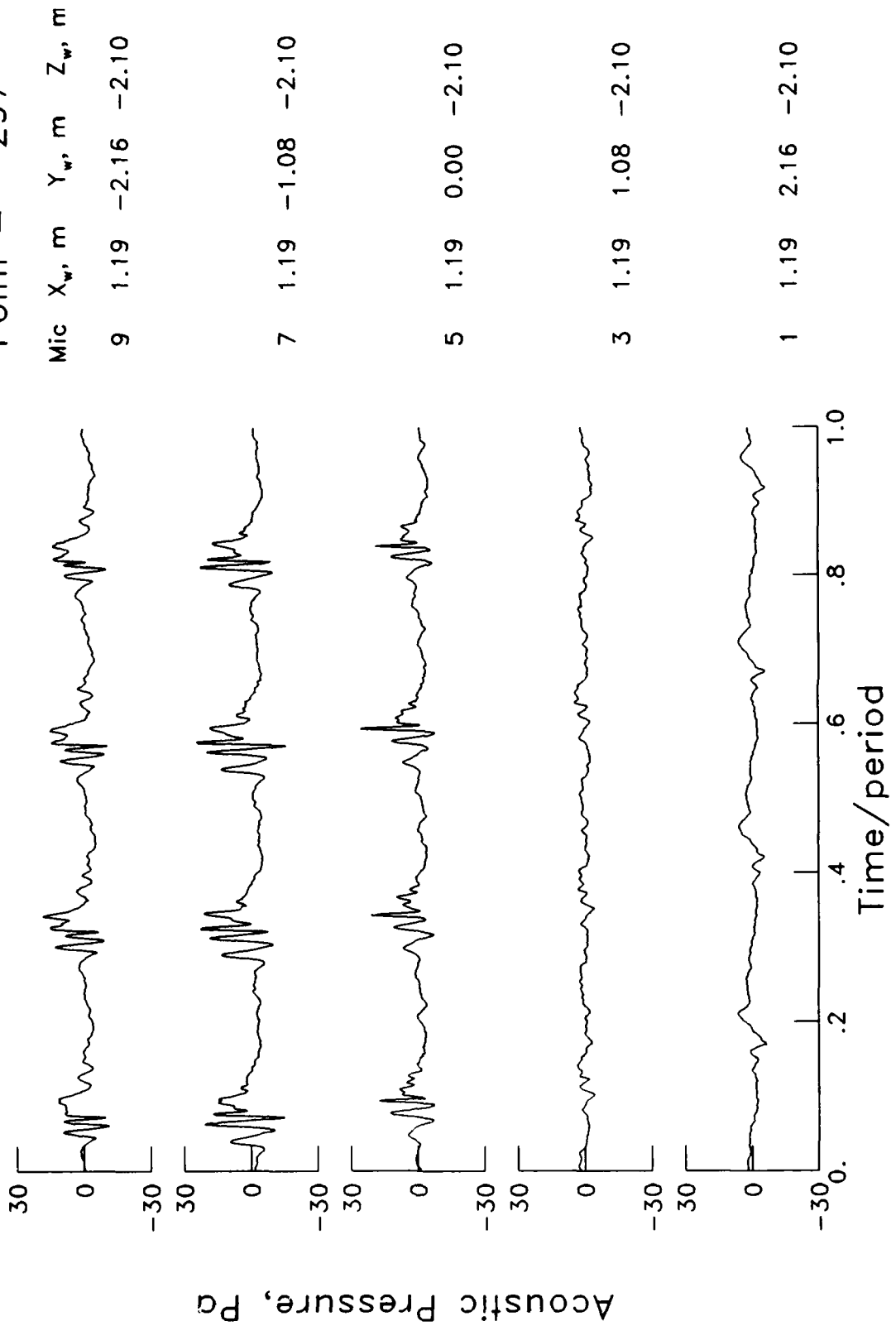


Mic	X _w , m	Y _w , m	Z _w , m
9	1.10	-2.16	-2.10
7	1.10	-1.08	-2.10
5	1.10	0.00	-2.10
3	1.10	1.08	-2.10
1	1.10	2.16	-2.10

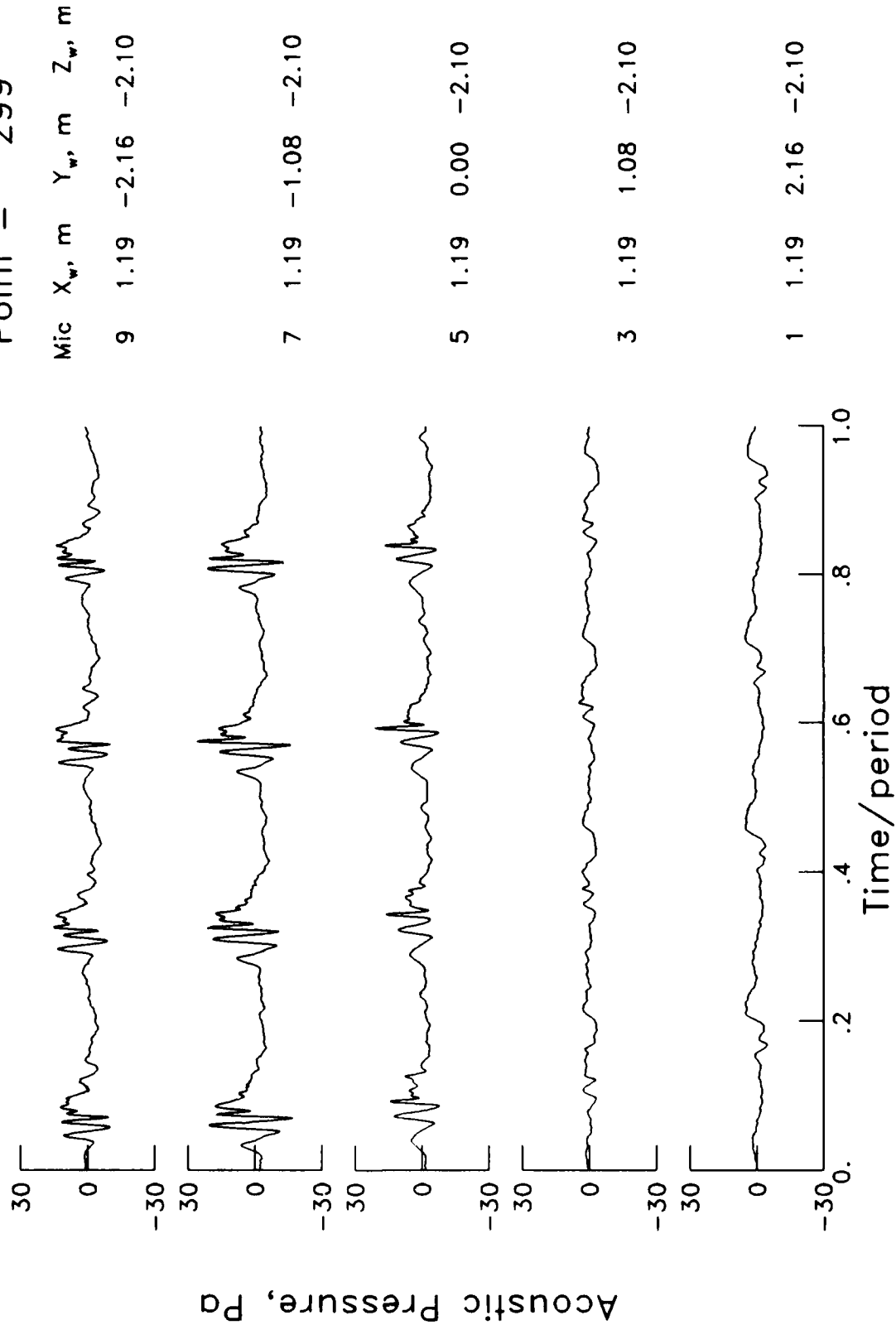
$\mu = .165$
 $\alpha_{TPP} = 0.8^\circ$
 $C_T = 0.0043$
 $M_H = 0.633$
 Point = 317



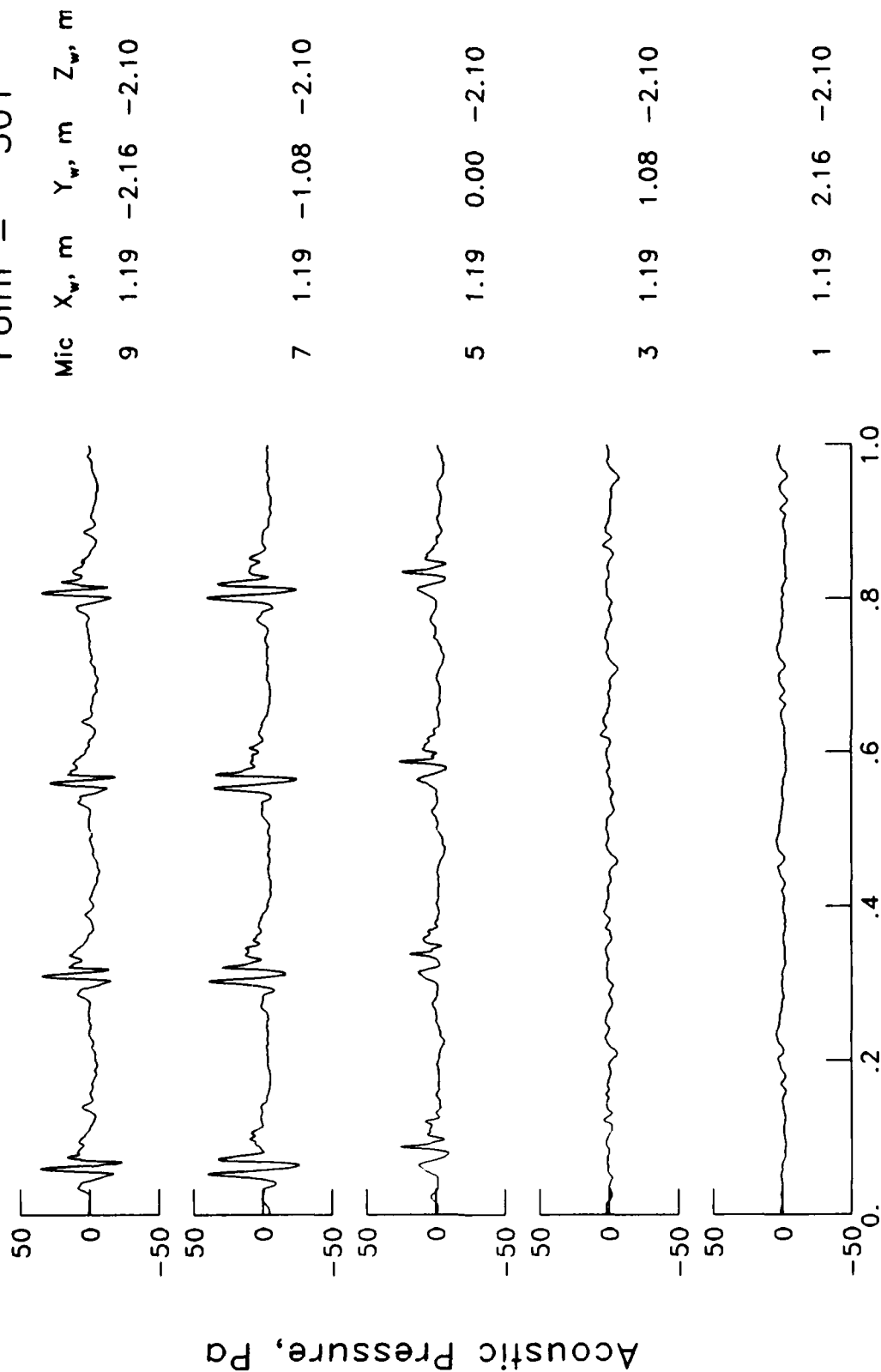
$\mu = .113$
 $\alpha_{TPP} = 1.6^\circ$
 $C_T = 0.0042$
 $M_{H_i} = 0.630$
 Point = 297



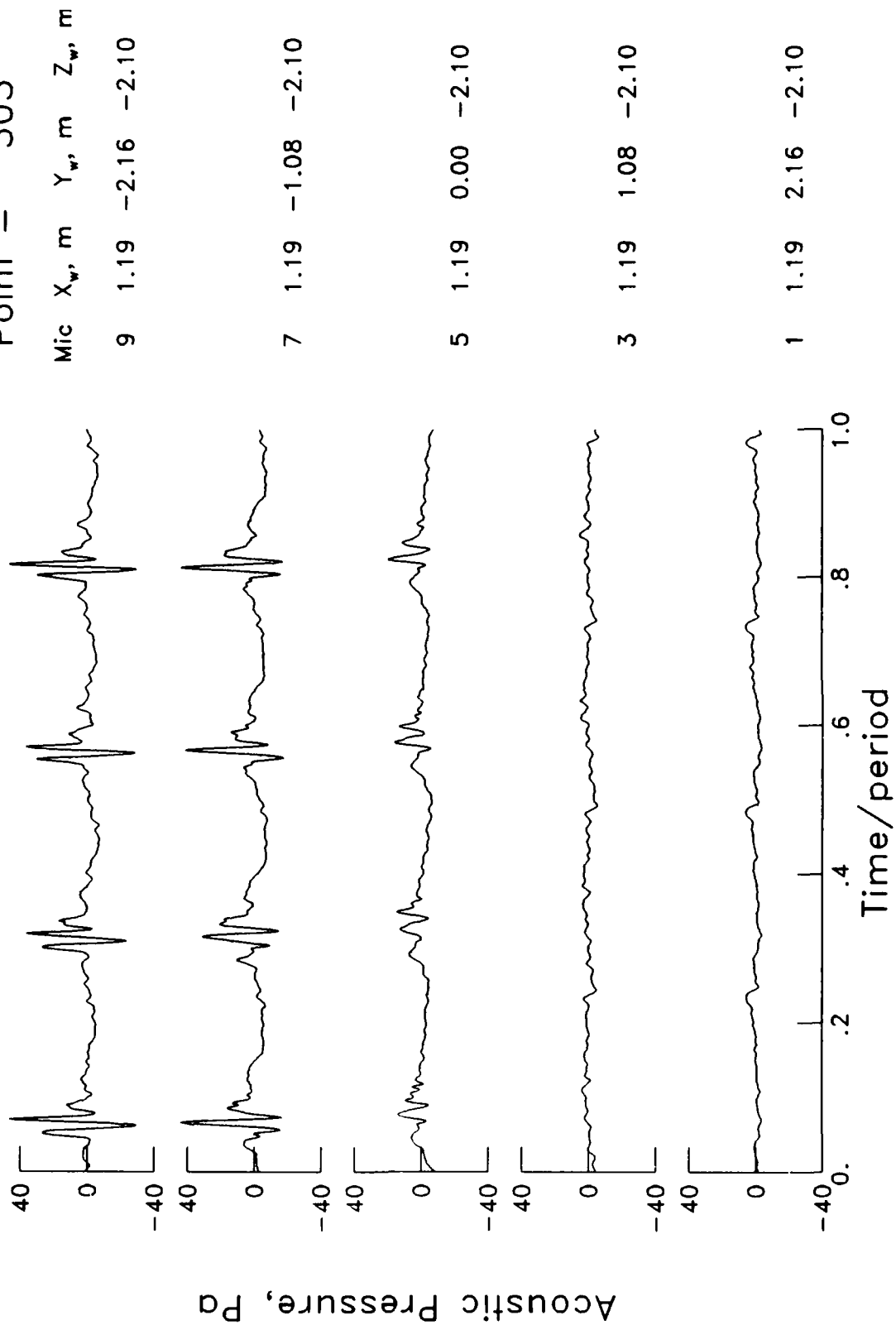
$\mu = .125$
 $\alpha_{TPP} = 1.7^\circ$
 $C_T = 0.0045$
 $M_H = 0.630$
 Point = 299



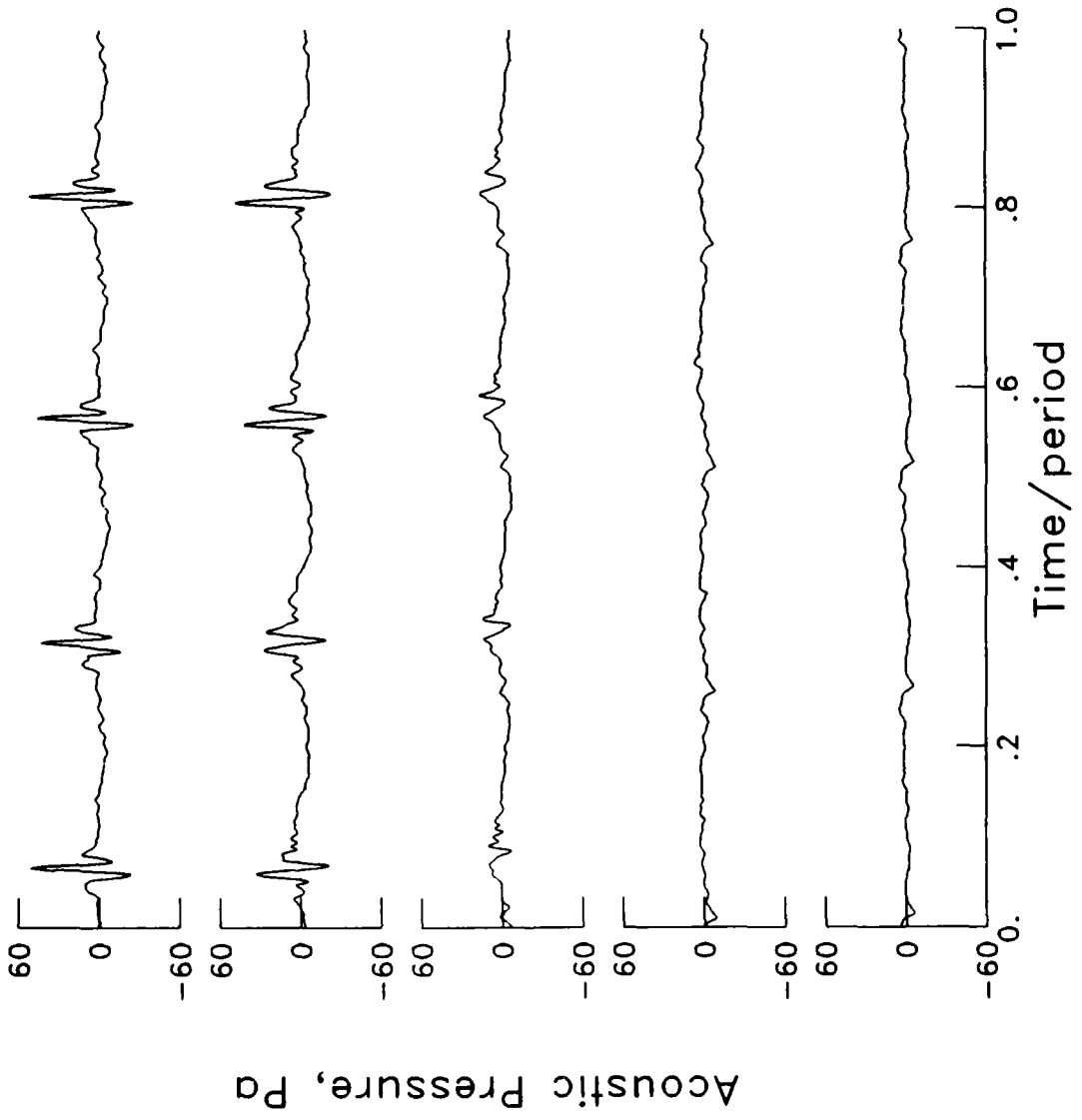
$\mu = .132$
 $\alpha_{TPP} = 2.2^\circ$
 $C_T = 0.0042$
 $M_H = 0.630$
 Point = 301



$\mu = .142$
 $\alpha_{TPP} = 2.3^\circ$
 $C_T = 0.0043$
 $M_H = 0.634$
 Point = 303



$\mu = .150$
 $\alpha_{TPP} = 2.4^\circ$
 $C_T = 0.0044$
 $M_H = 0.635$
 Point = 305



Mic X_w, m Y_w, m Z_w, m
 9 1.19 -2.16 -2.10

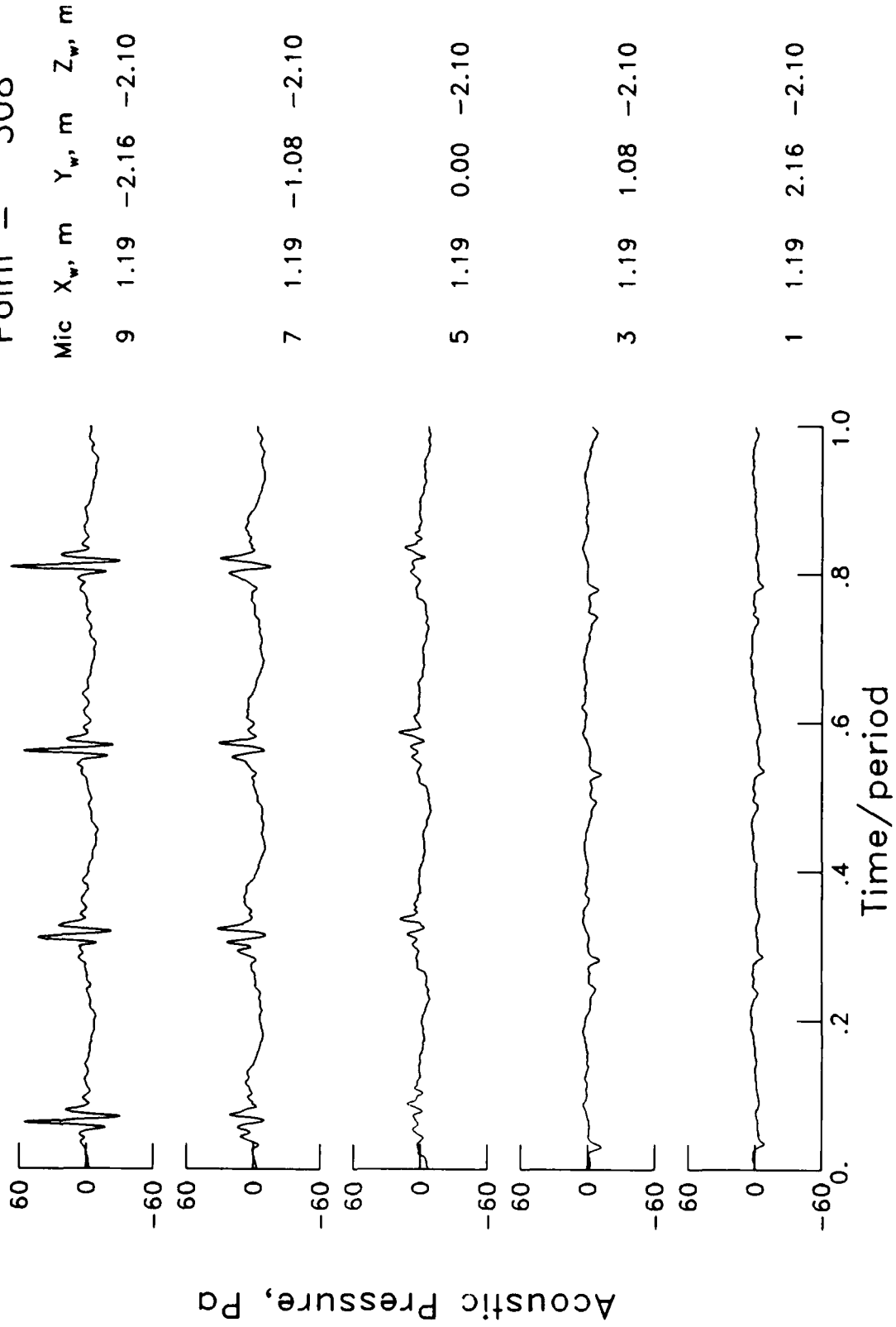
7 1.19 -1.08 -2.10

5 1.19 0.00 -2.10

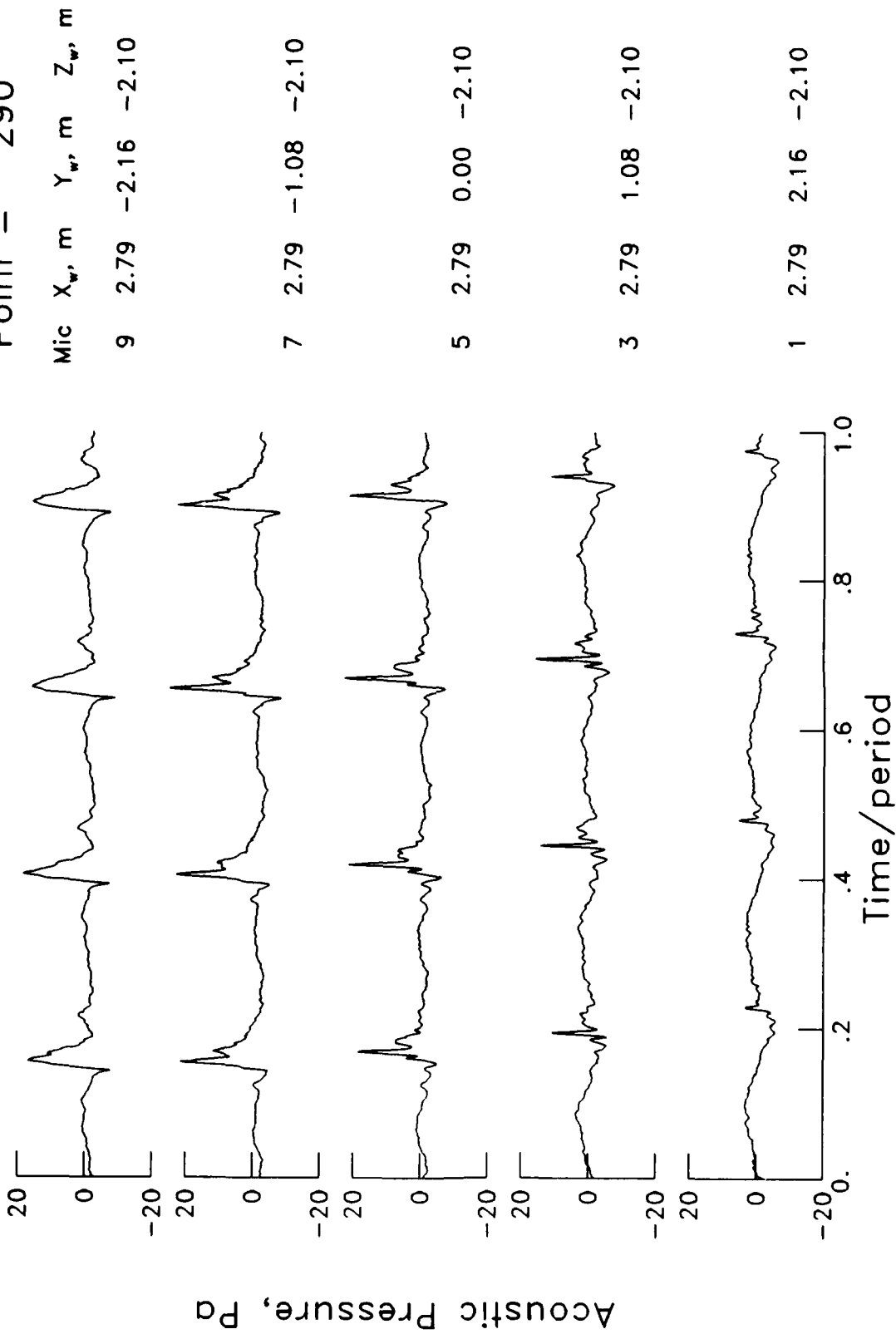
3 1.19 1.08 -2.10

1 1.19 2.16 -2.10

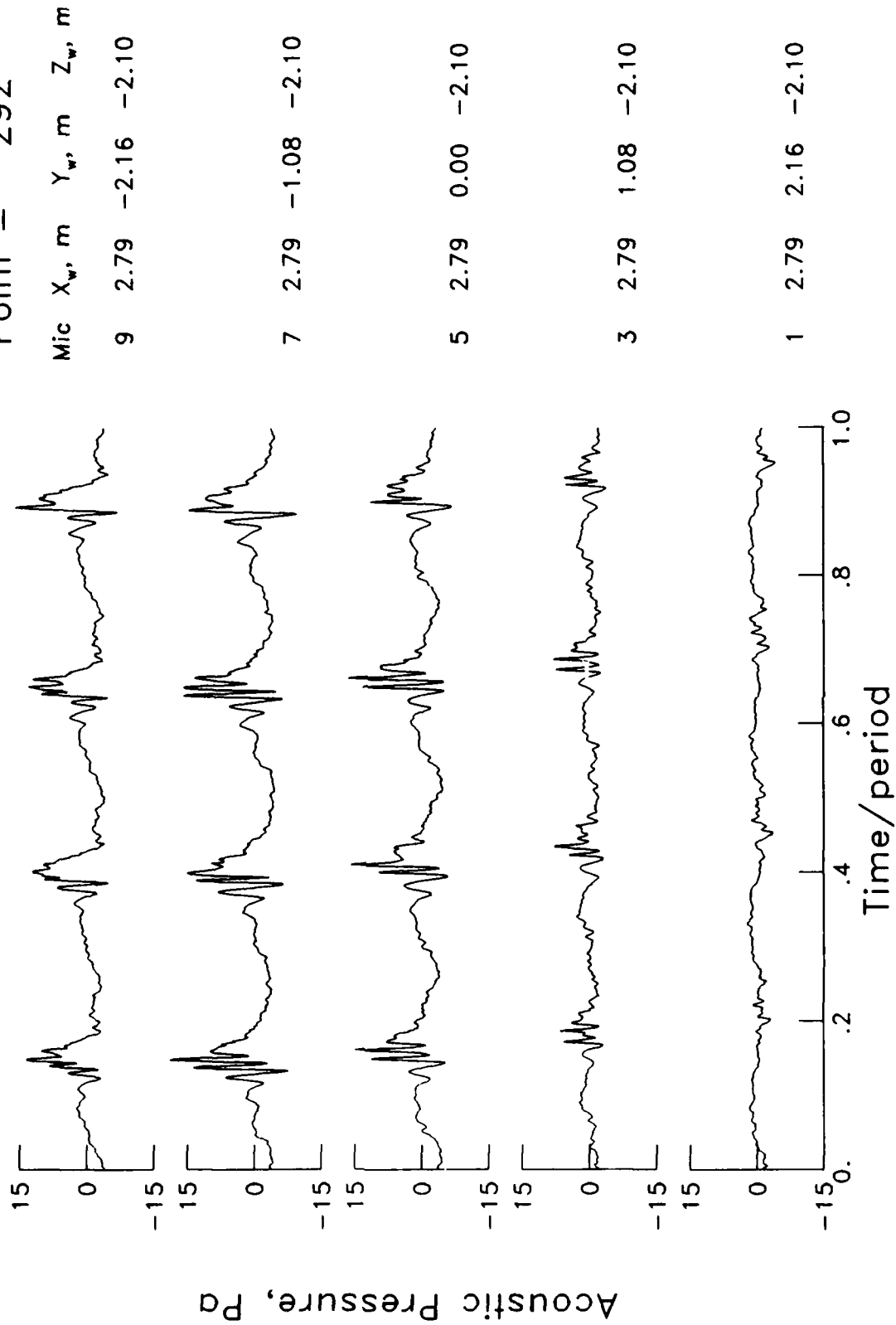
$\mu = .159$
 $\alpha_{TPP} = 2.7^\circ$
 $C_T = 0.0043$
 $M_H = 0.636$
 Point = 308



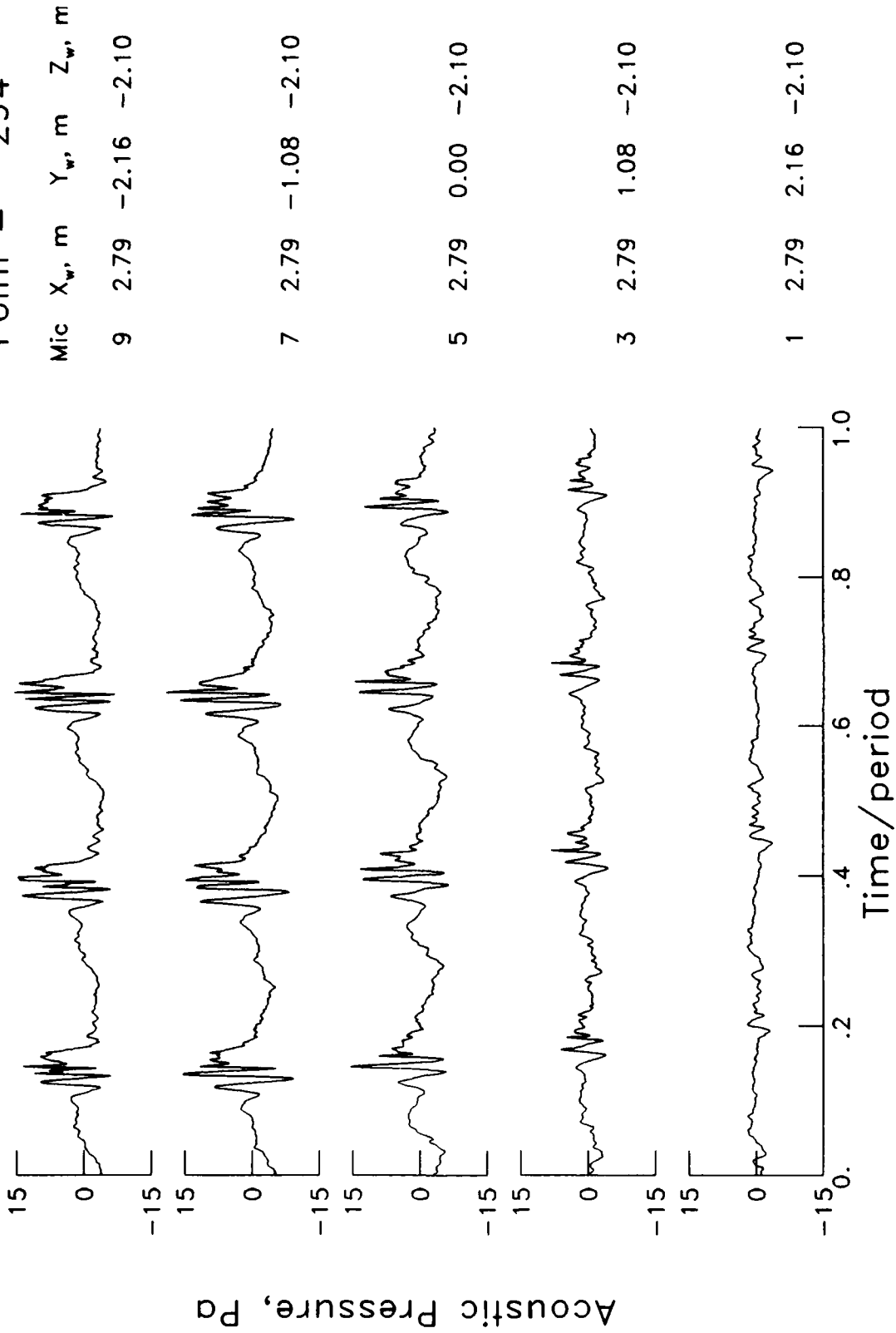
$\mu = .092$
 $\alpha_{TPP} = 2.1^\circ$
 $C_T = 0.0043$
 $M_H = 0.629$
 Point = 290



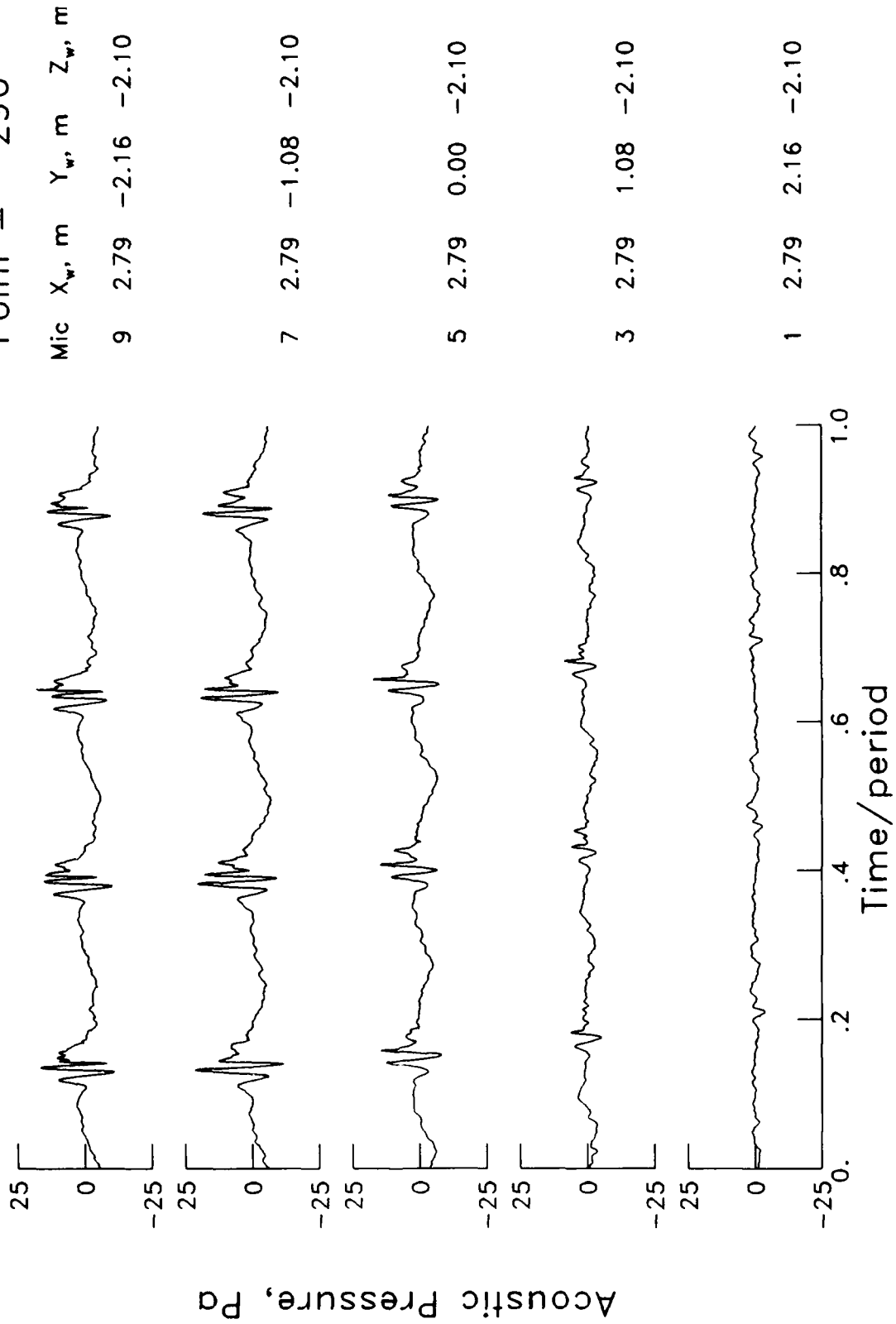
$\mu = .101$
 $\alpha_{TPP} = 2.7^\circ$
 $C_T = 0.0044$
 $M_H = 0.632$
 Point = 292



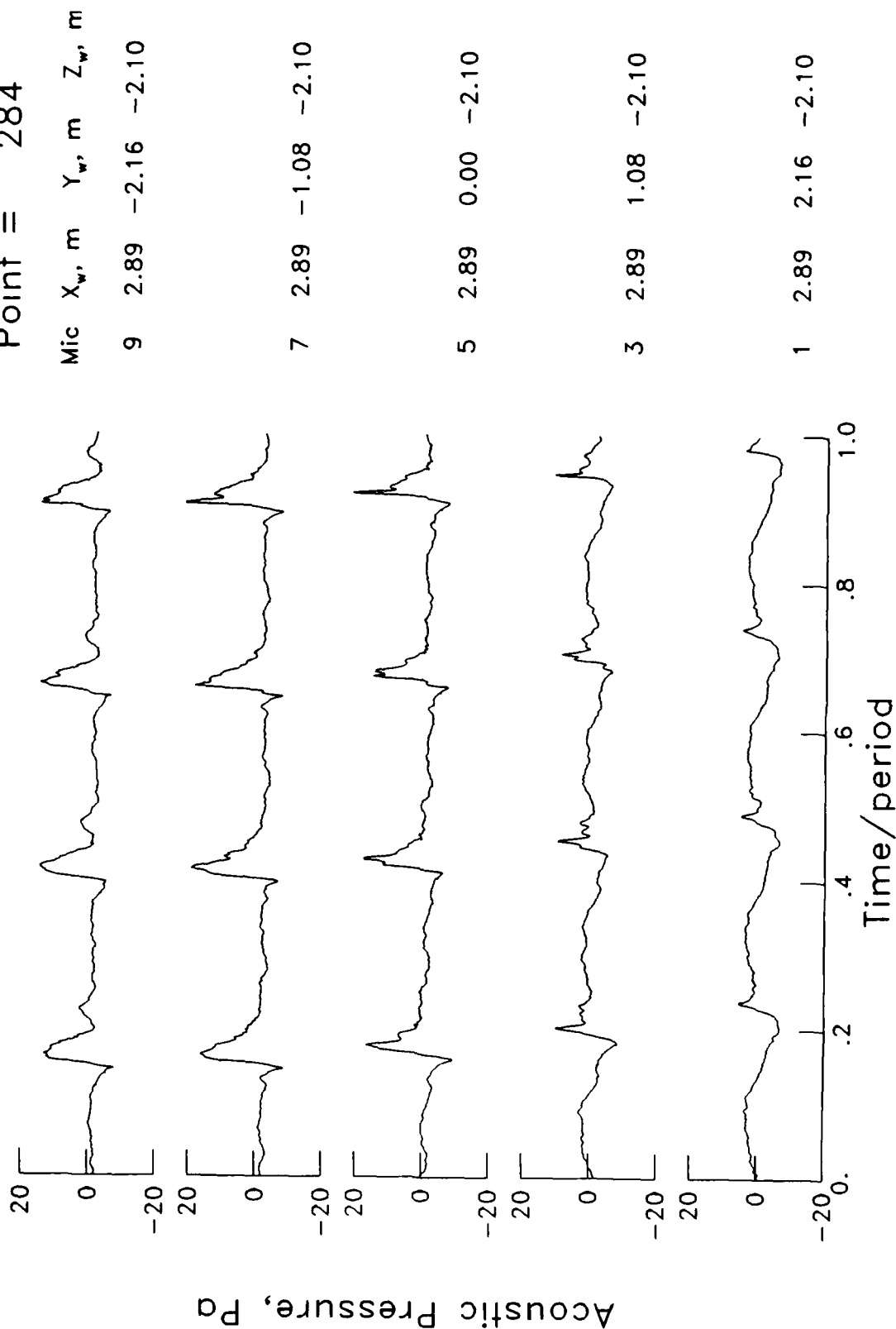
$\mu = .110$
 $\alpha_{TPP} = 3.2^\circ$
 $C_T = 0.0044$
 $M_H = 0.630$
 Point = 294



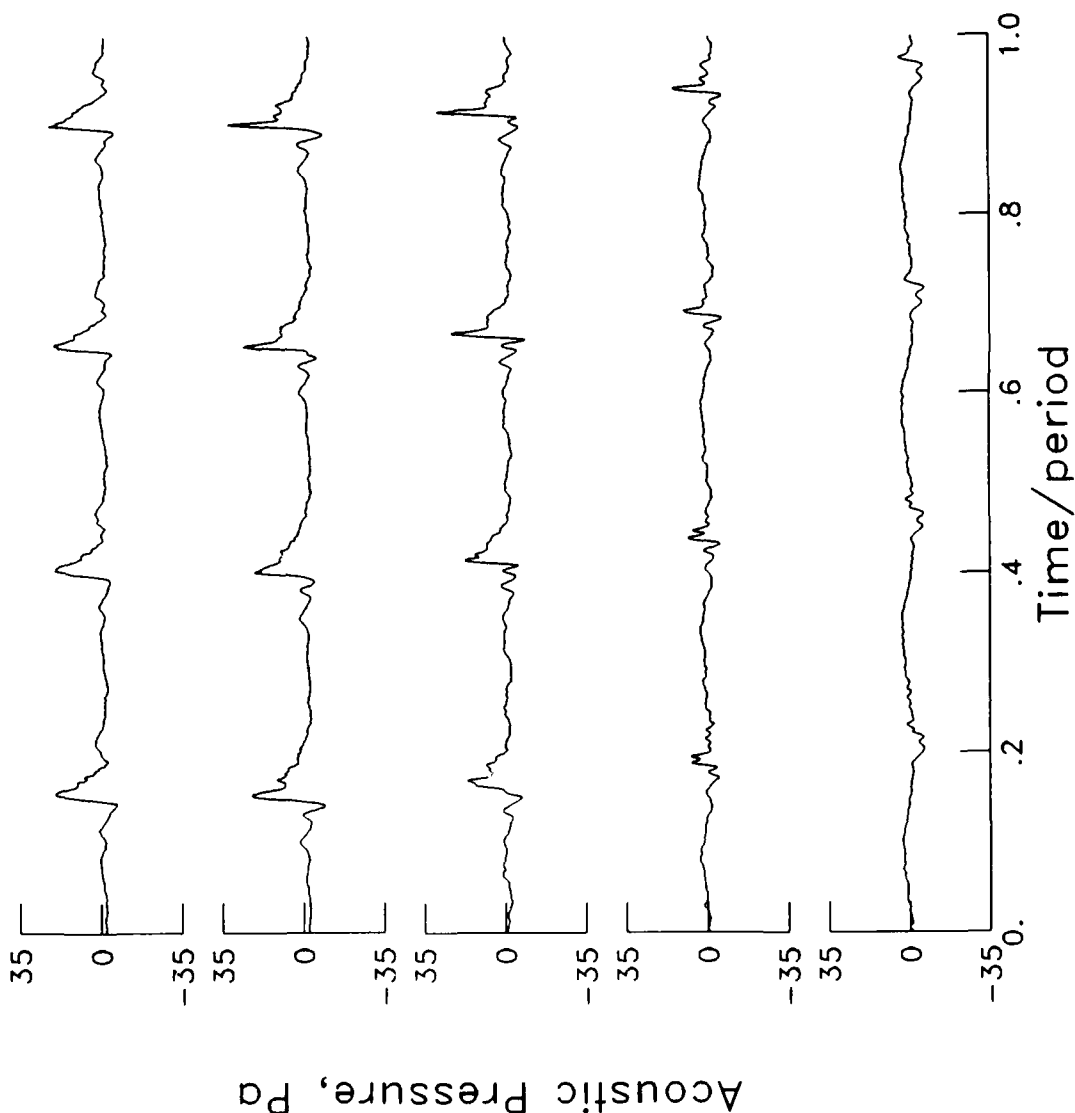
$\mu = .120$
 $\alpha_{TPP} = 3.6^\circ$
 $C_T = 0.0044$
 $M^H = 0.633$
 Point = 296



$\mu = .079$
 $\alpha_{TPP} = 2.7^\circ$
 $C_T = 0.0044$
 $M_{H_i} = 0.629$
 Point = 284

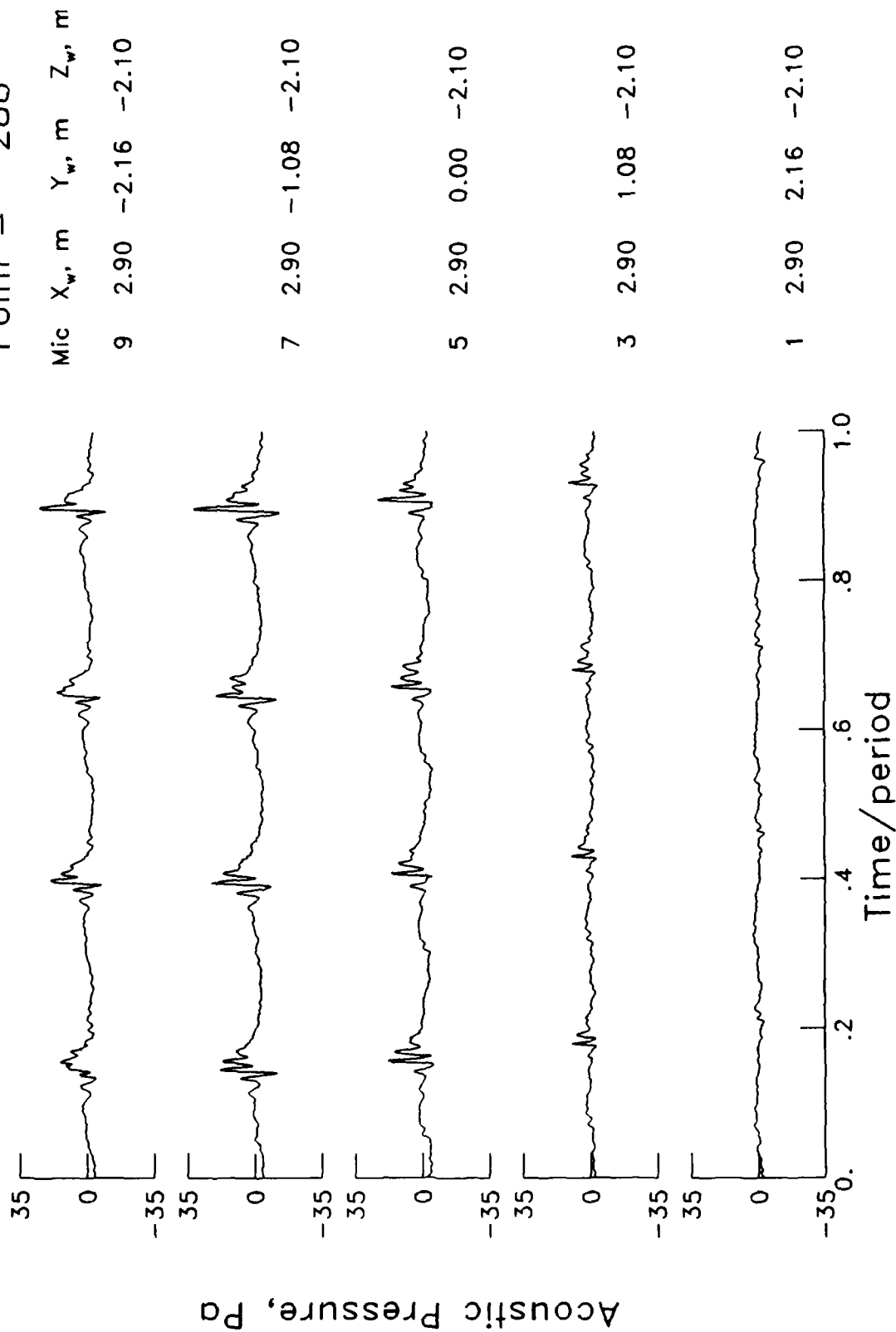


$\mu = .087$
 $\alpha_{TPP} = 3.7^\circ$
 $C_T = 0.0044$
 $M_H = 0.629$
 Point = 286



Mic	X _w , m	Y _w , m	Z _w , m
9	2.90	-2.16	-2.10
7	2.90	-1.08	-2.10
5	2.90	0.00	-2.10
3	2.90	1.08	-2.10
1	2.90	2.16	-2.10

$\mu = .095$
 $\alpha_{TPP} = 4.4^\circ$
 $C_T = 0.0044$
 $M^H = 0.631$
 Point = 288



$\mu = .059$
 $\alpha_{TPP} = 1.4^\circ$
 $C_T = 0.0043$
 $M_H = 0.630$
 Point = 275

Mic X_w, m Y_w, m Z_w, m

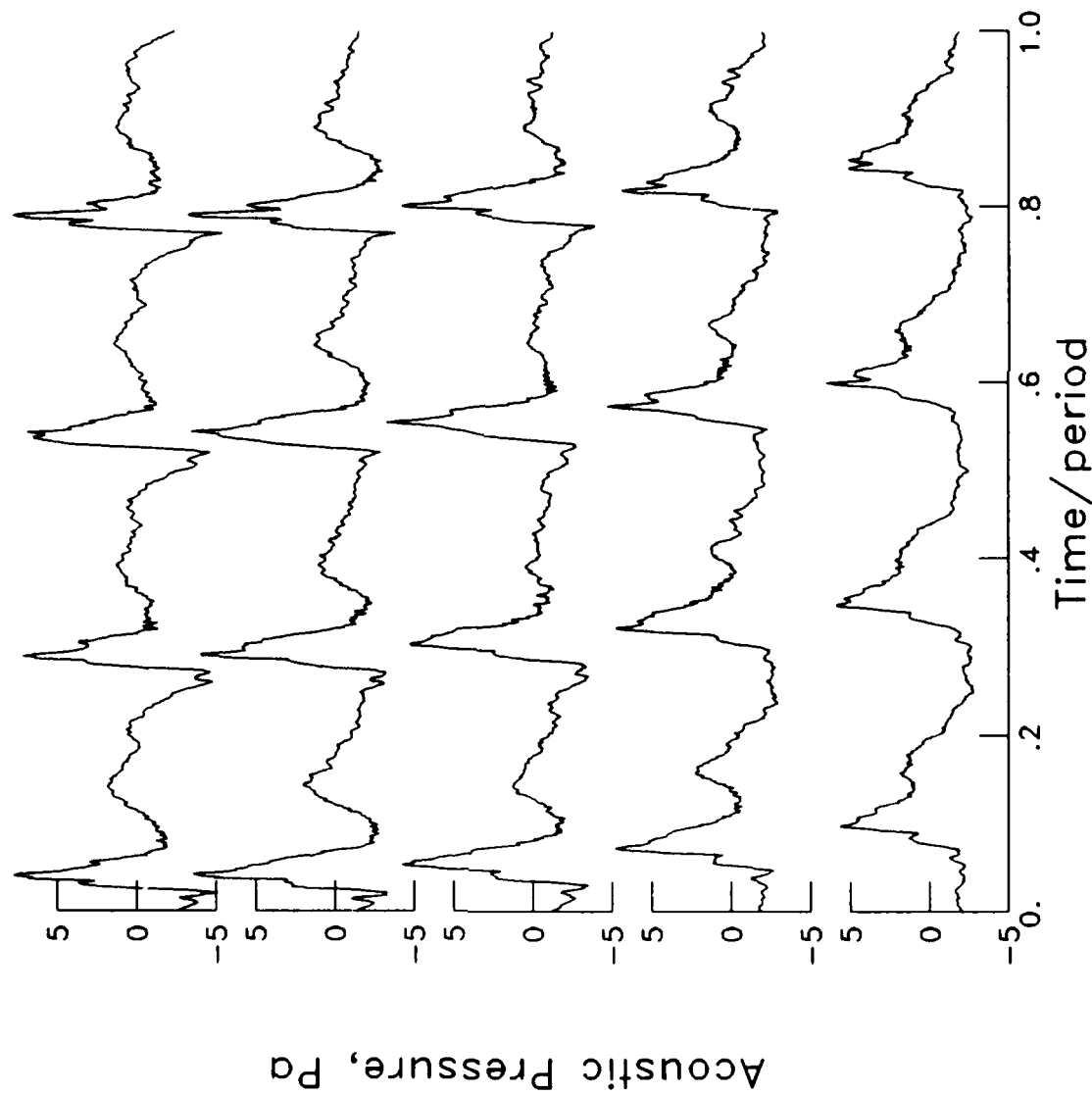
9 5.50 -2.16 -2.10

7 5.50 -1.08 -2.10

5 5.50 0.00 -2.10

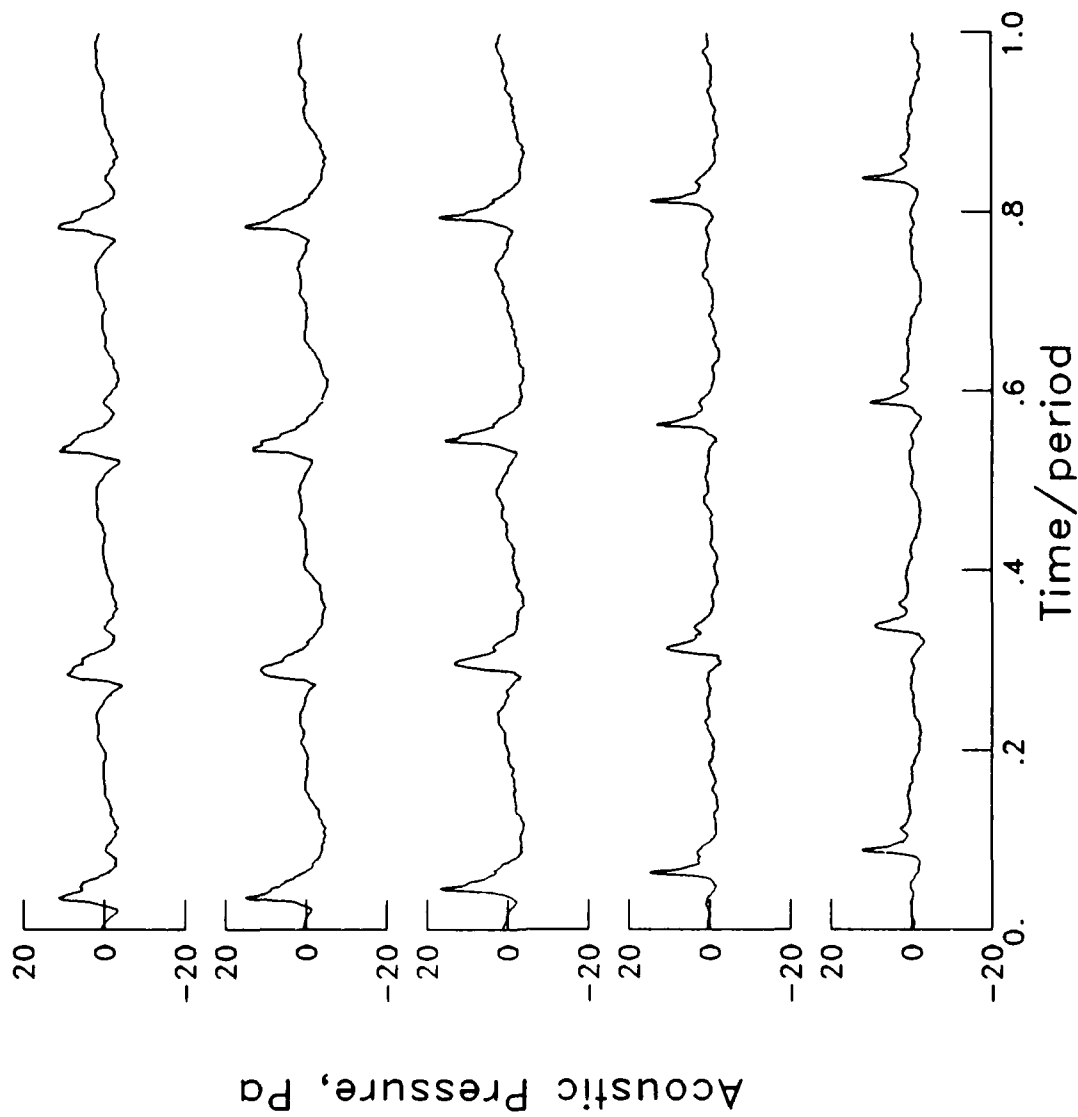
3 5.50 1.08 -2.10

1 5.50 2.16 -2.10

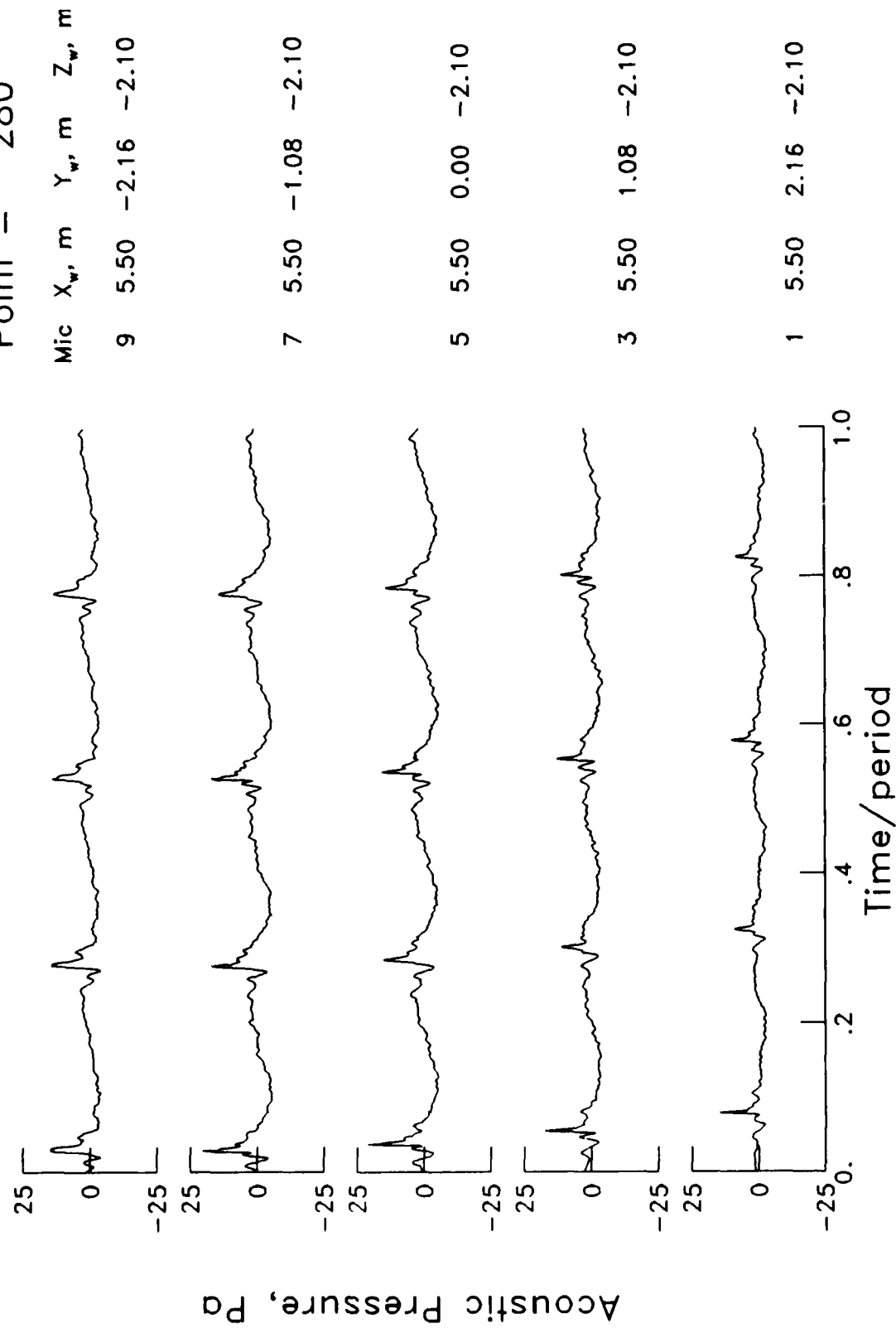


$\mu = .073$
 $\alpha_{TPP} = 4.0^\circ$
 $C_T = 0.0044$
 $M_H = 0.632$
 Point = 278

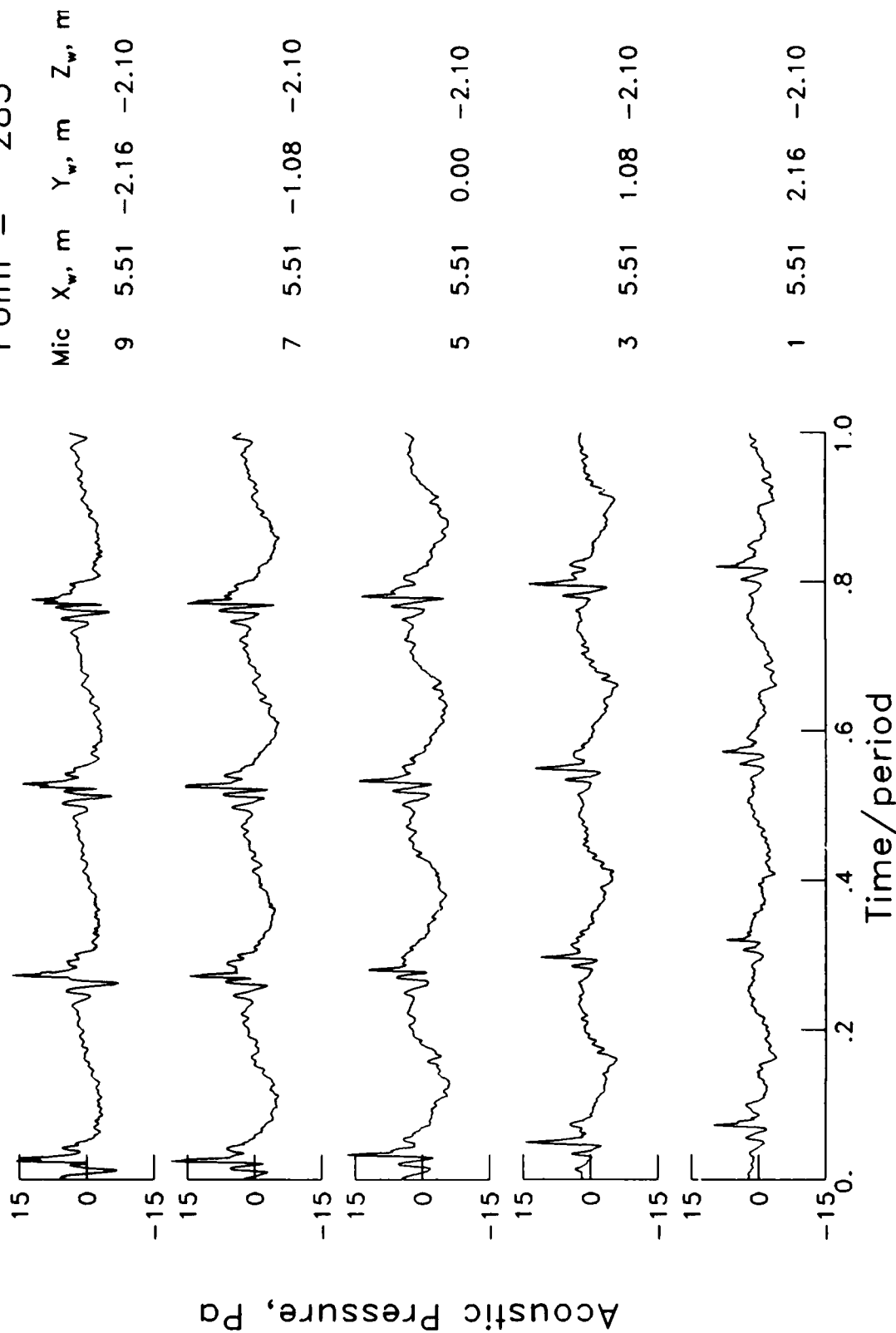
Mic	X _w , m	Y _w , m	Z _w , m
9	5.50	-2.16	-2.10
7	5.50	-1.08	-2.10
5	5.50	0.00	-2.10
3	5.50	1.08	-2.10
1	5.50	2.16	-2.10



$\mu = .083$
 $\alpha_{\text{TPP}} = 5.2^\circ$
 $C_T = 0.0043$
 $M_{\text{H}} = 0.632$
 Point = 280

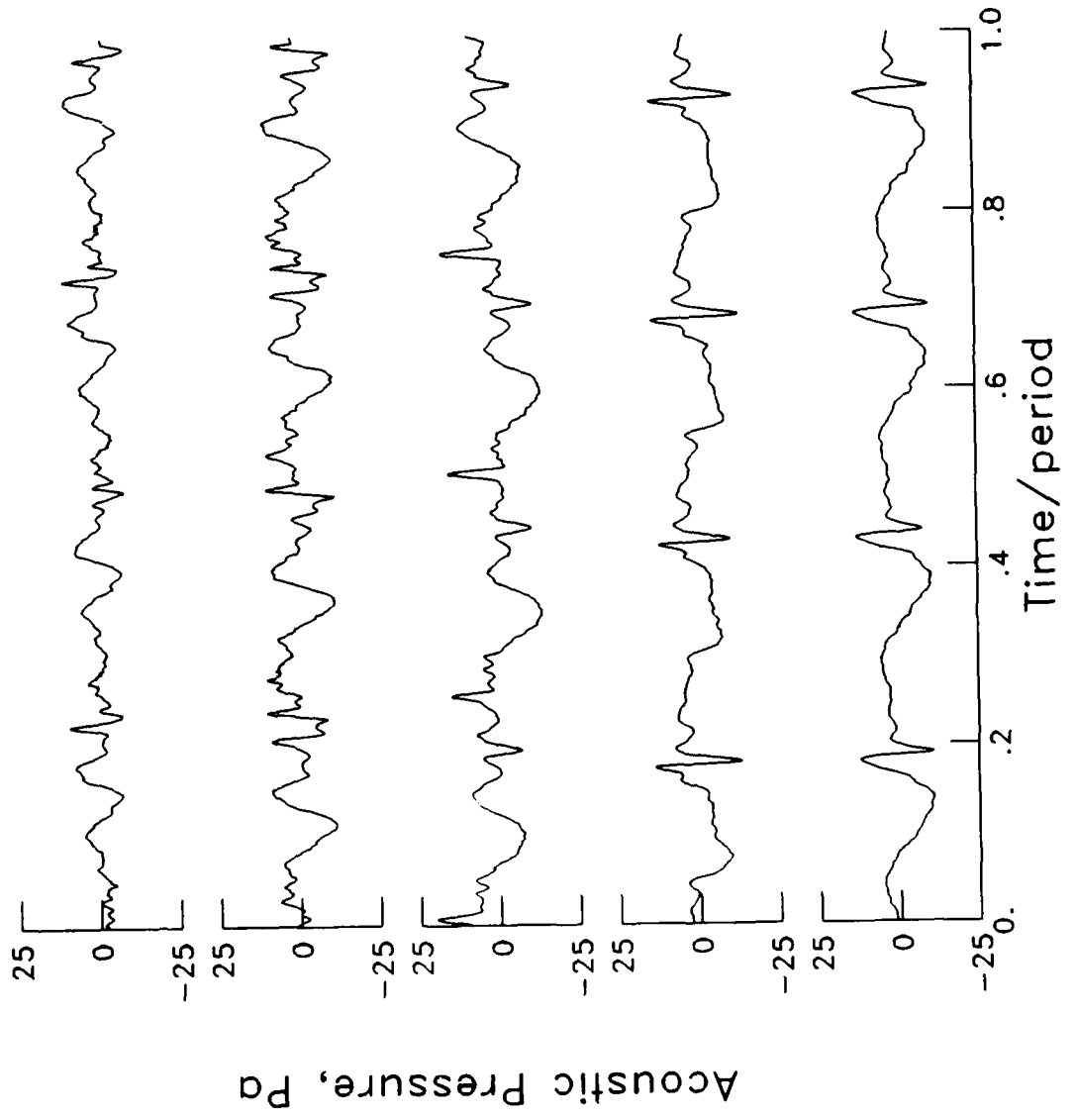


$\mu = .093$
 $\alpha_{TPP} = 6.2^\circ$
 $C_T = 0.0045$
 $M_H = 0.629$
 Point = 283

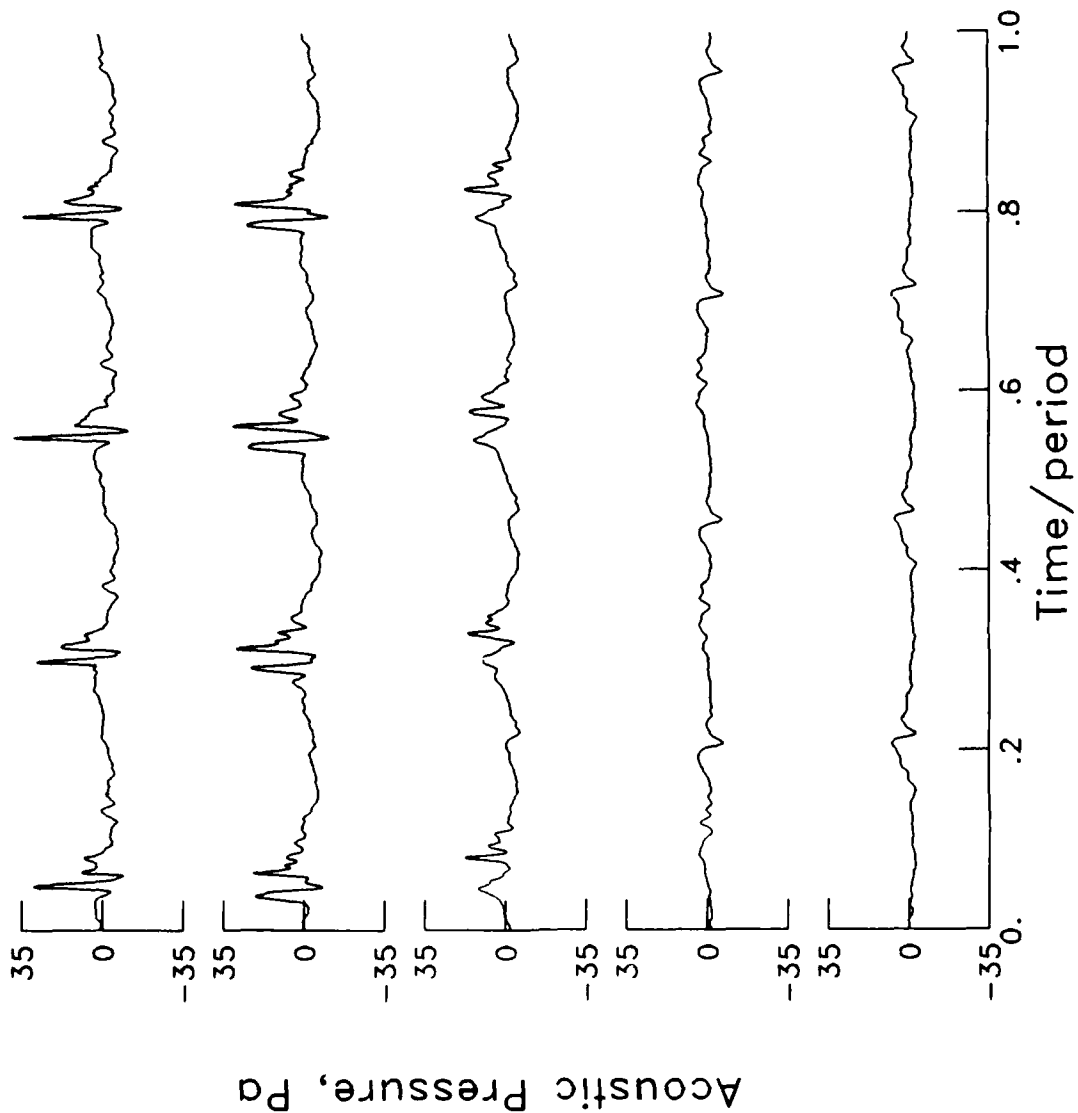


$\mu = .176$
 $\alpha_{TPP} = -0.5^\circ$
 $C_T = 0.0044$
 $M_{H_i} = 0.629$
 Point = 400

Mic	X _w , m	Y _w , m	Z _w , m
9	-1.12	-2.16	-2.10
7	-1.12	-1.08	-2.10
5	-1.12	0.00	-2.10
3	-1.12	1.08	-2.10
1	-1.12	2.16	-2.10

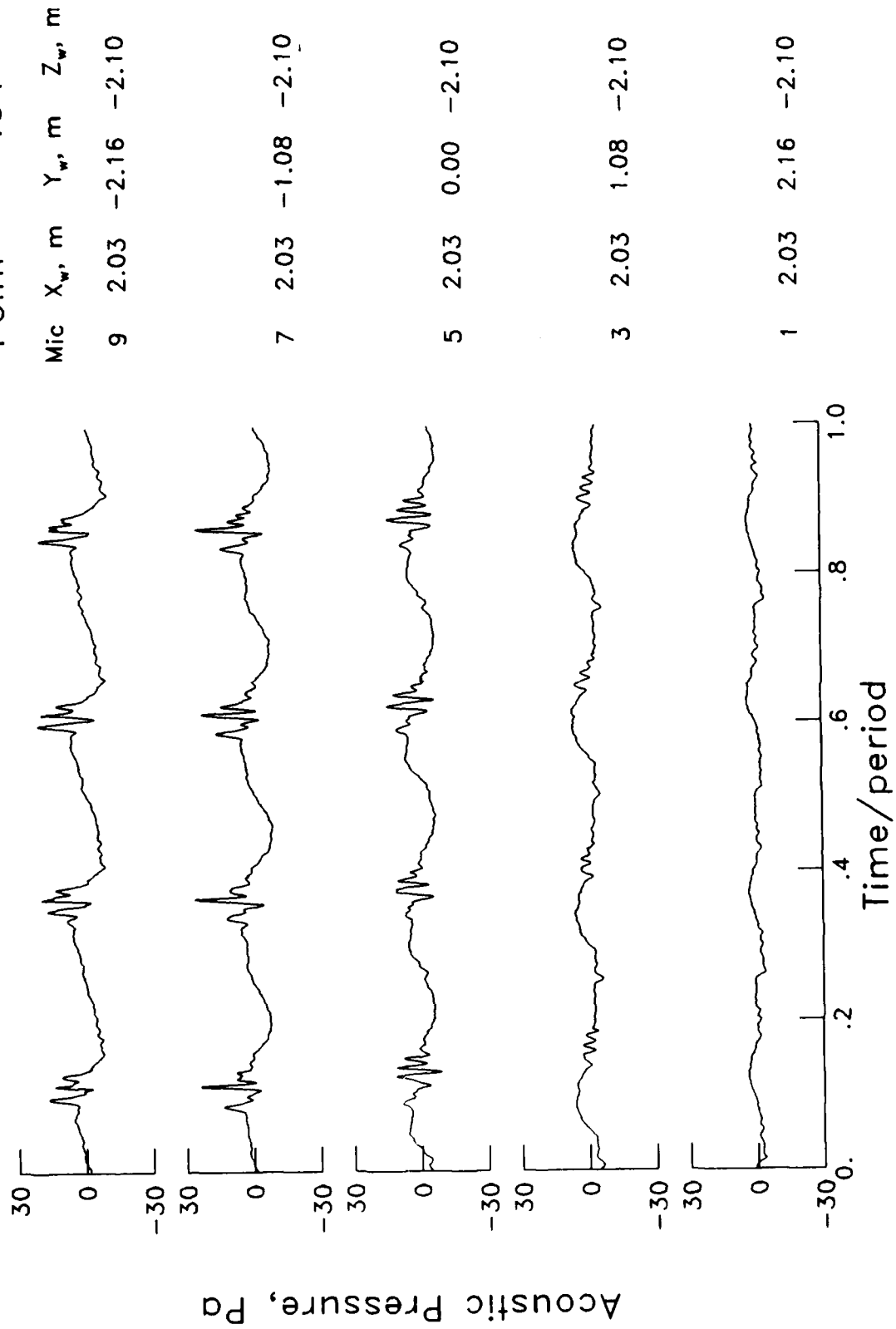


$\mu = .175$
 $\alpha_{TPP} = -0.6^\circ$
 $C_T = 0.0045$
 $M_H = 0.632$
 Point = 402



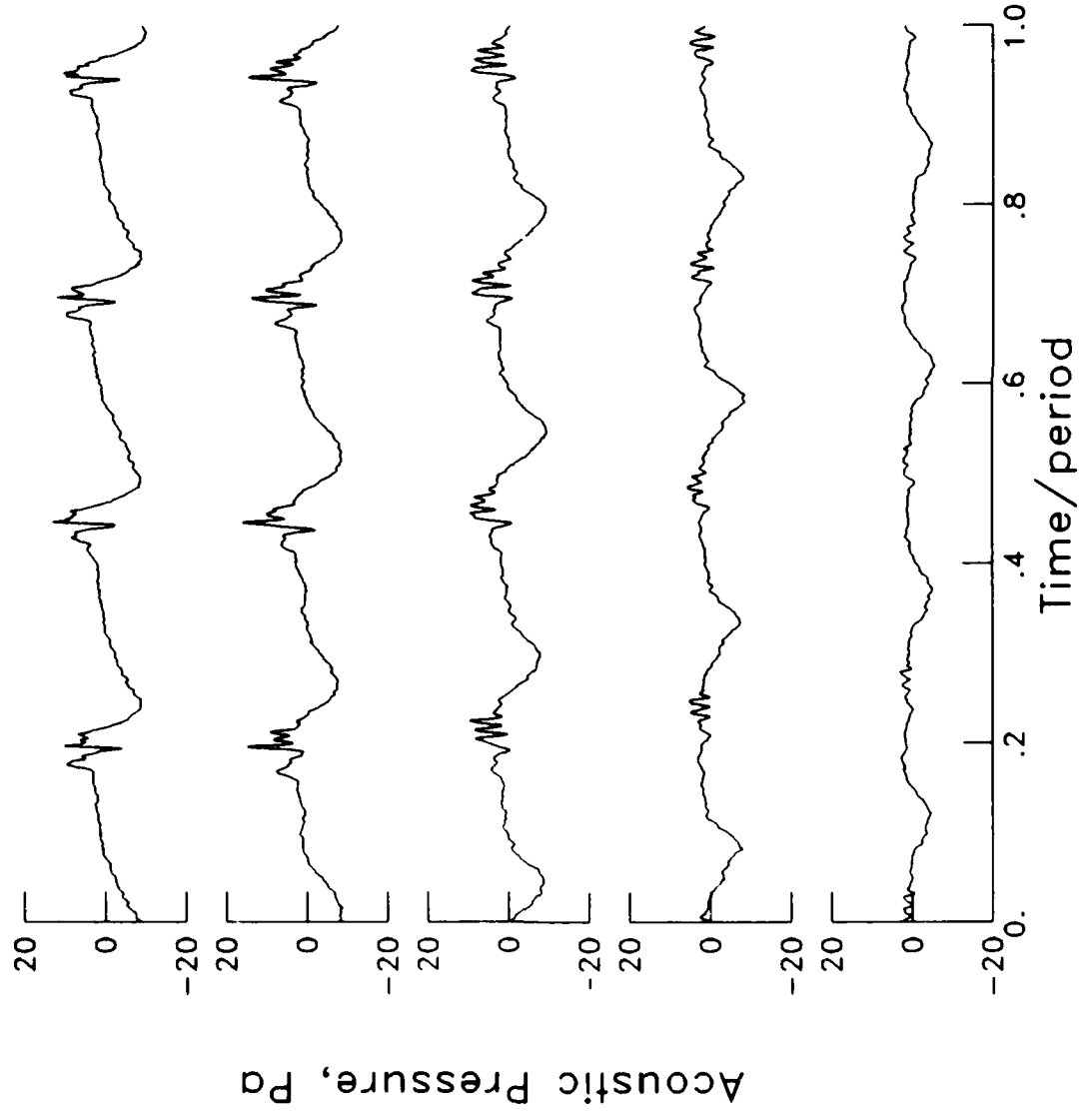
Mic	X _w , m	Y _w , m	Z _w , m
9	0.82	-2.16	-2.10
7	0.82	-1.08	-2.10
5	0.82	0.00	-2.10
3	0.82	1.08	-2.10
1	0.82	2.16	-2.10

$\mu = .176$
 $\alpha_{TPP} = -0.5^\circ$
 $C_T = 0.0043$
 $M_H = 0.633$
 Point = 404

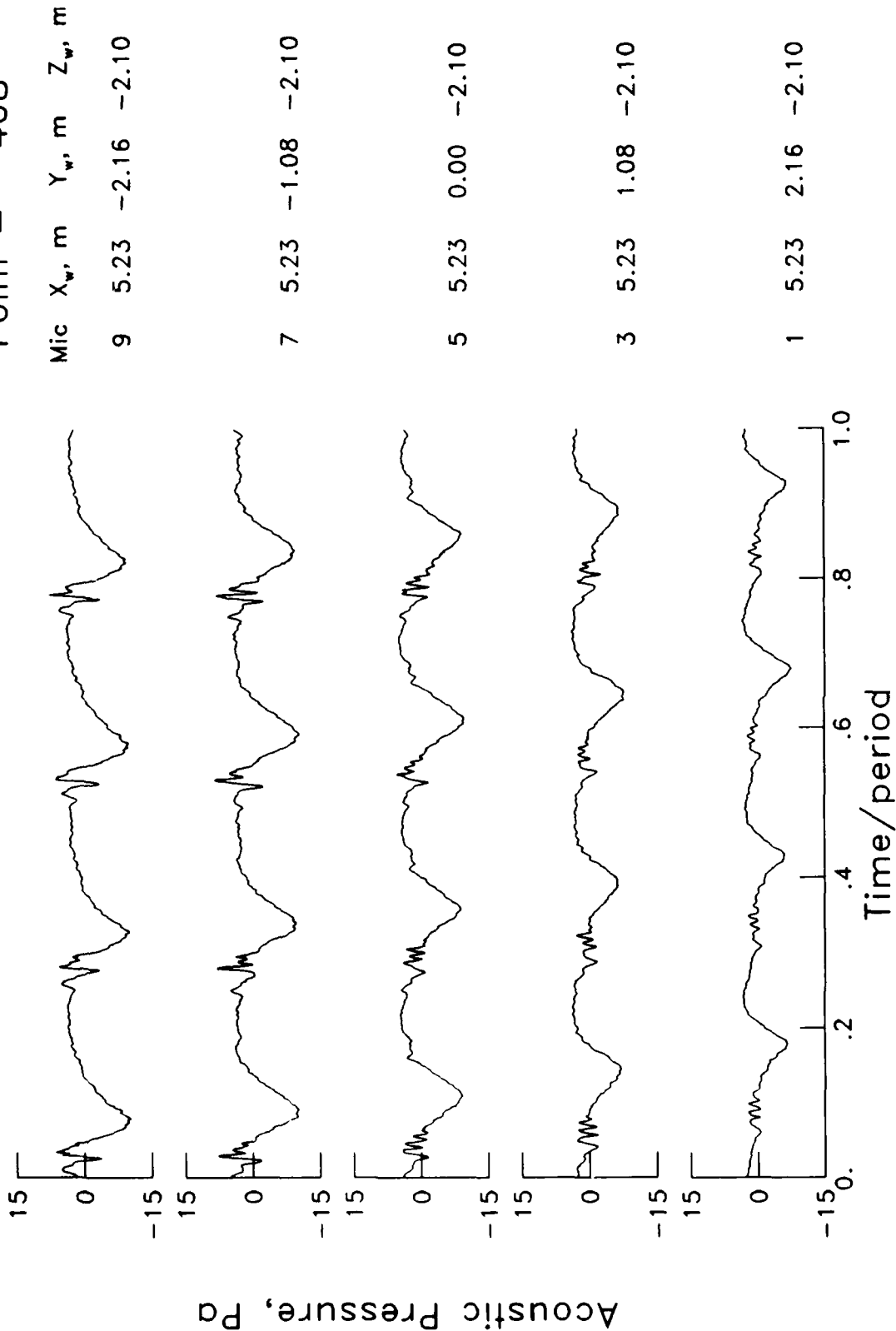


$\mu = .175$
 $\alpha_{TPP} = -0.5^\circ$
 $C_T = 0.0044$
 $M_{H_1} = 0.633$
 Point = 406

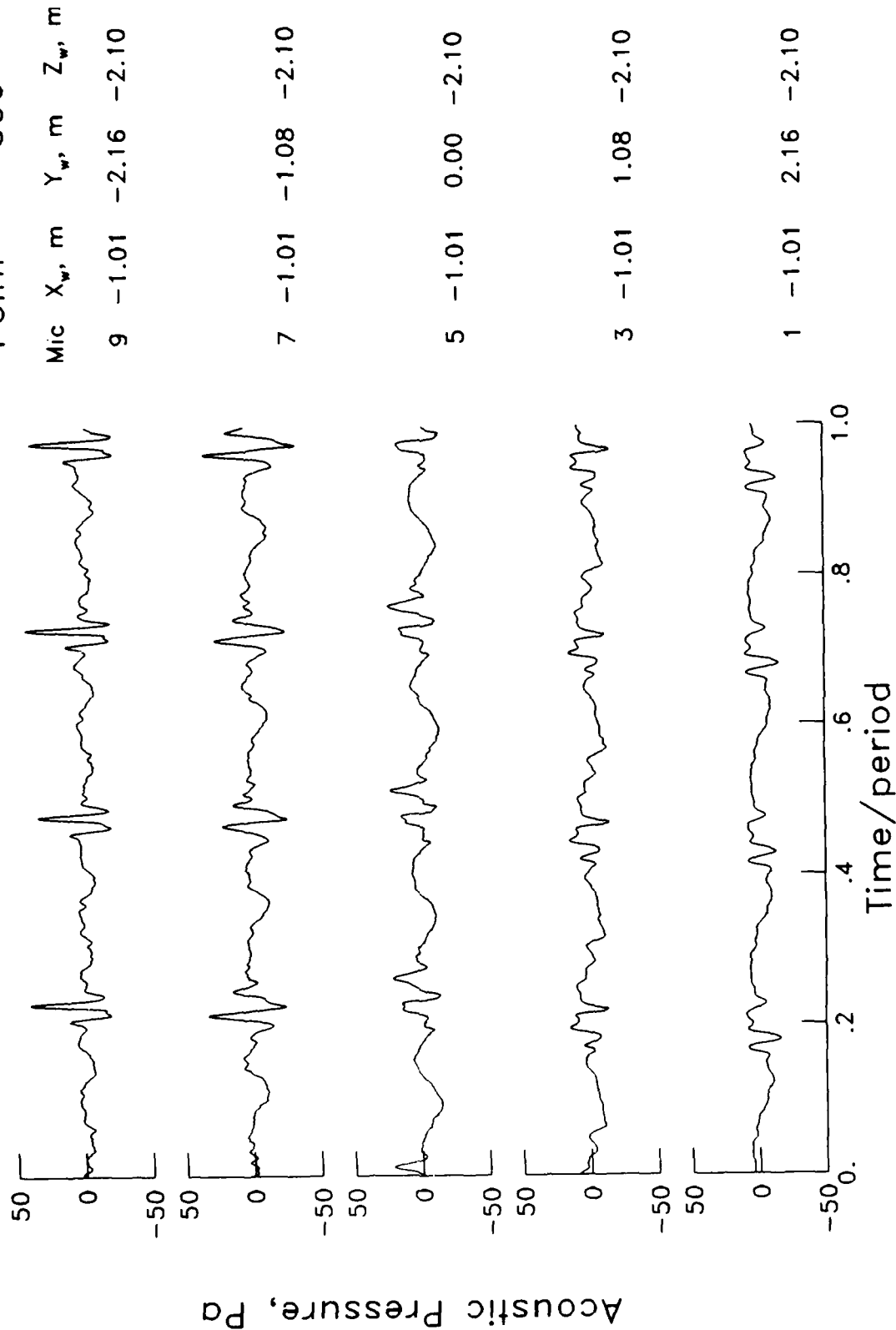
Mic	X _w , m	Y _w , m	Z _w , m
9	3.62	-2.16	-2.10
7	3.62	-1.08	-2.10
5	3.62	0.00	-2.10
3	3.62	1.08	-2.10
1	3.62	2.16	-2.10



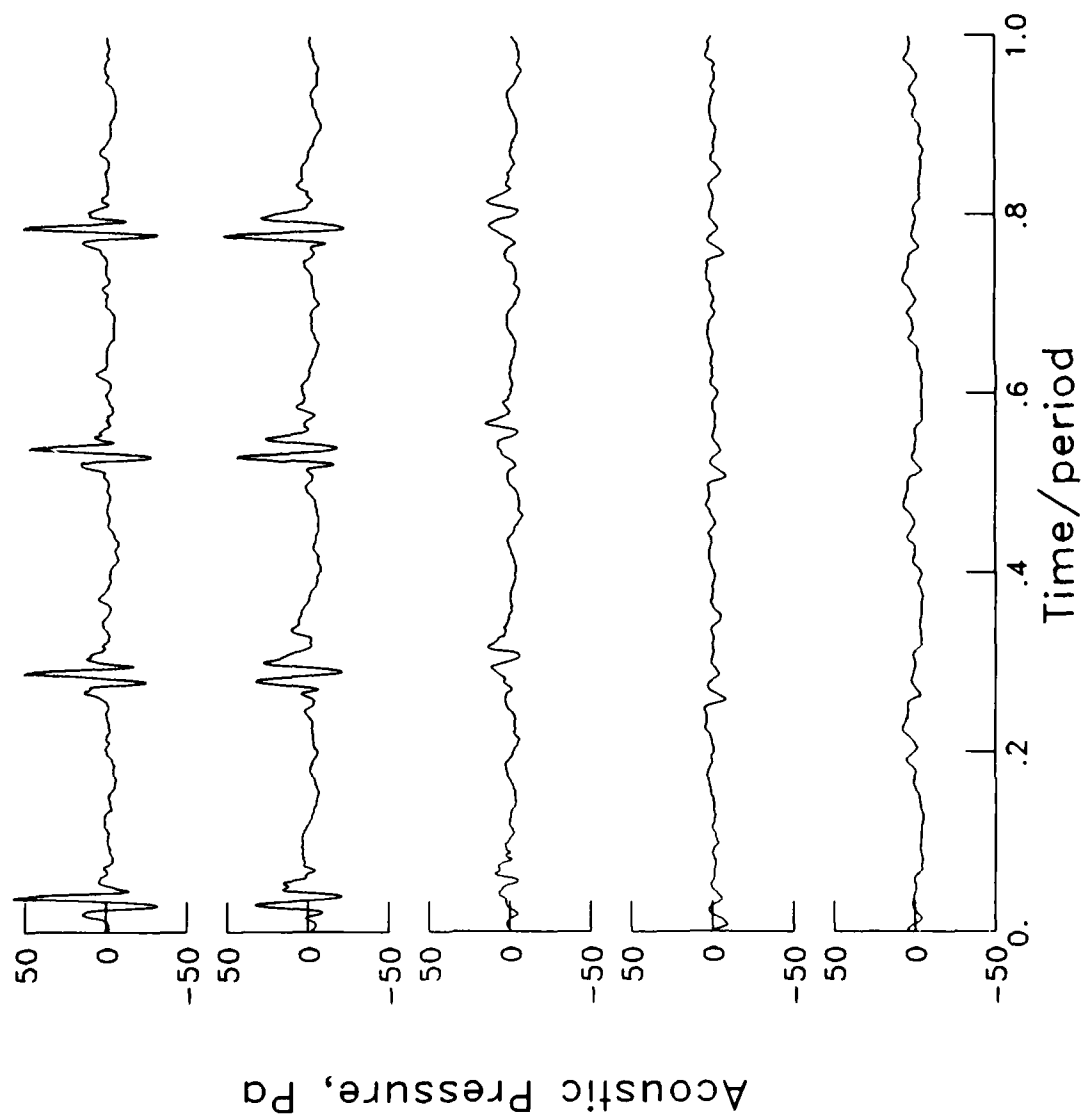
$\mu = .175$
 $\alpha_{TPP} = -0.6^\circ$
 $C_T = 0.0044$
 $M_H = 0.634$
 Point = 408



$\mu = .162$
 $\alpha_{TPP} = 1.7^\circ$
 $C_T = 0.0044$
 $M_{H_i} = 0.631$
 Point = 399

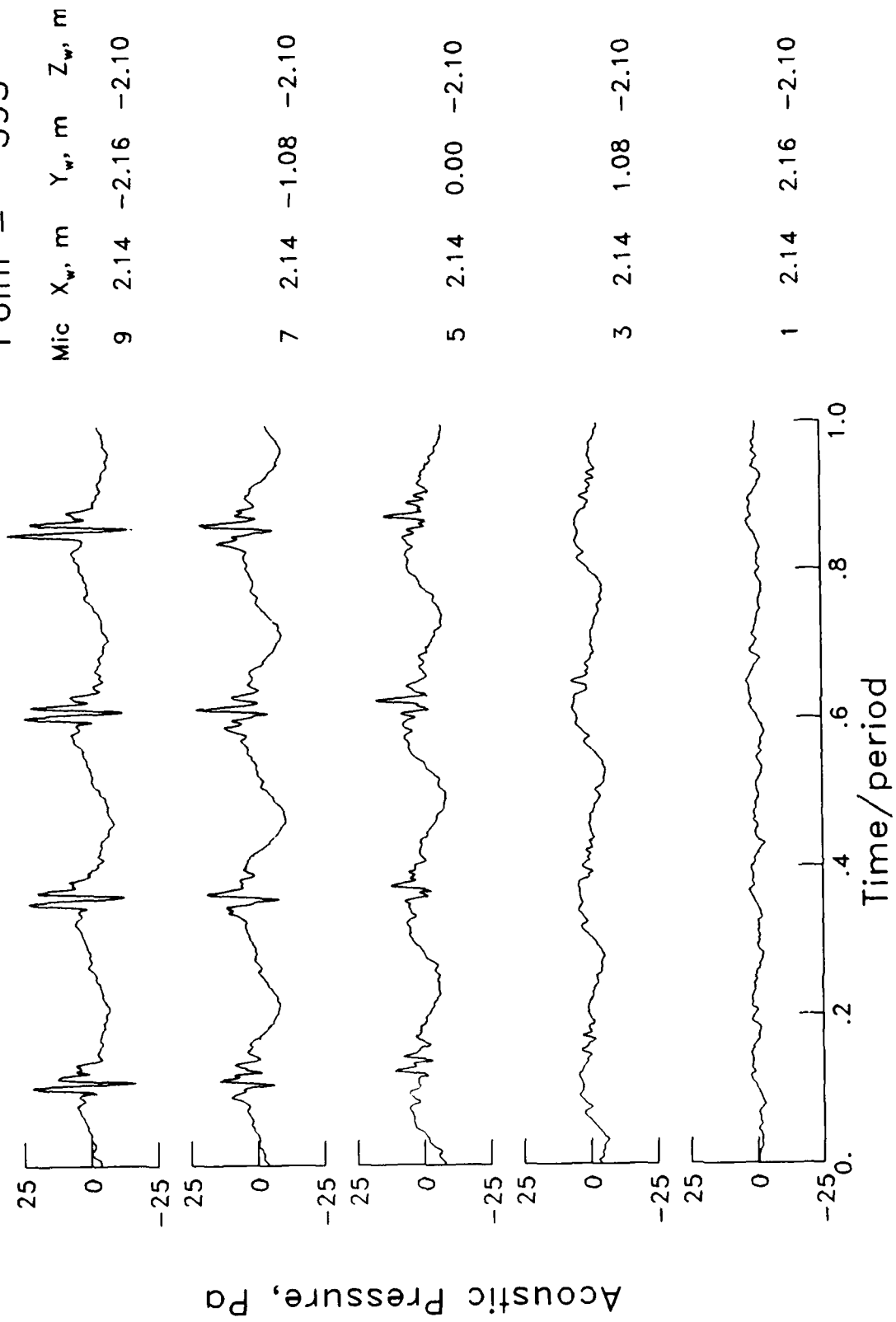


$\mu = .162$
 $\alpha_{TPP} = 1.7^\circ$
 $C_T = 0.0044$
 $M^H = 0.631$
 Point = 397

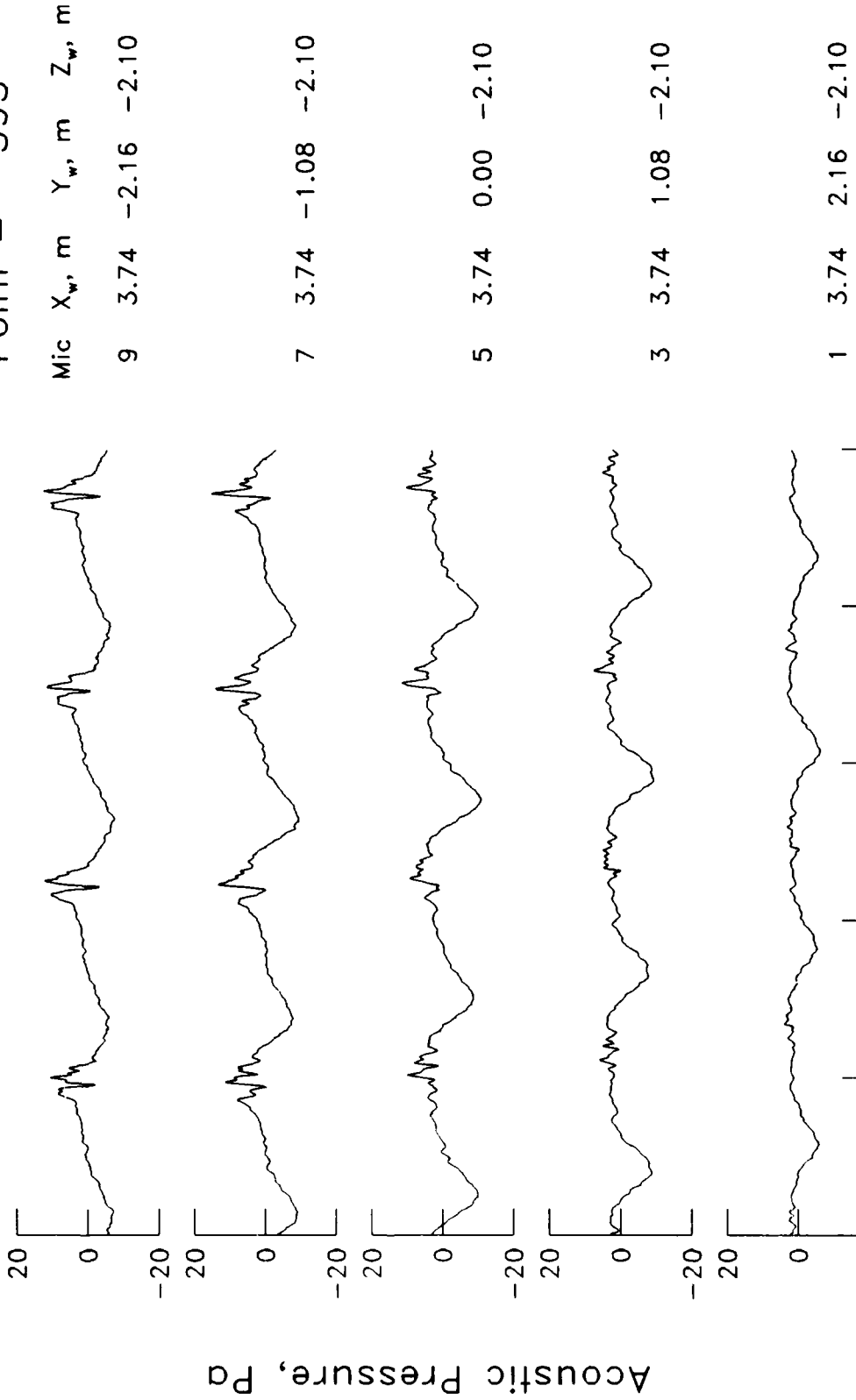


Mic	X _w , m	Y _w , m	Z _w , m
9	0.54	-2.16	-2.10
7	0.54	-1.08	-2.10
5	0.54	0.00	-2.10
3	0.54	1.08	-2.10
1	0.54	2.16	-2.10

$\mu = .161$
 $\alpha_{TPP} = 1.7^\circ$
 $C_T = 0.0044$
 $M_H = 0.632$
 Point = 395



$\mu = .161$
 $\alpha_{TPP} = 1.7^\circ$
 $C_T = 0.0044$
 $M_{H_i} = 0.631$
Point = 393



Acoustic Pressure, Pa

Time/period

$\mu = .161$
 $\alpha_{TPP} = 1.7^\circ$
 $C_T = 0.0043$
 $M_H = 0.632$
 Point = 391

Mic X_w, m Y_w, m Z_w, m

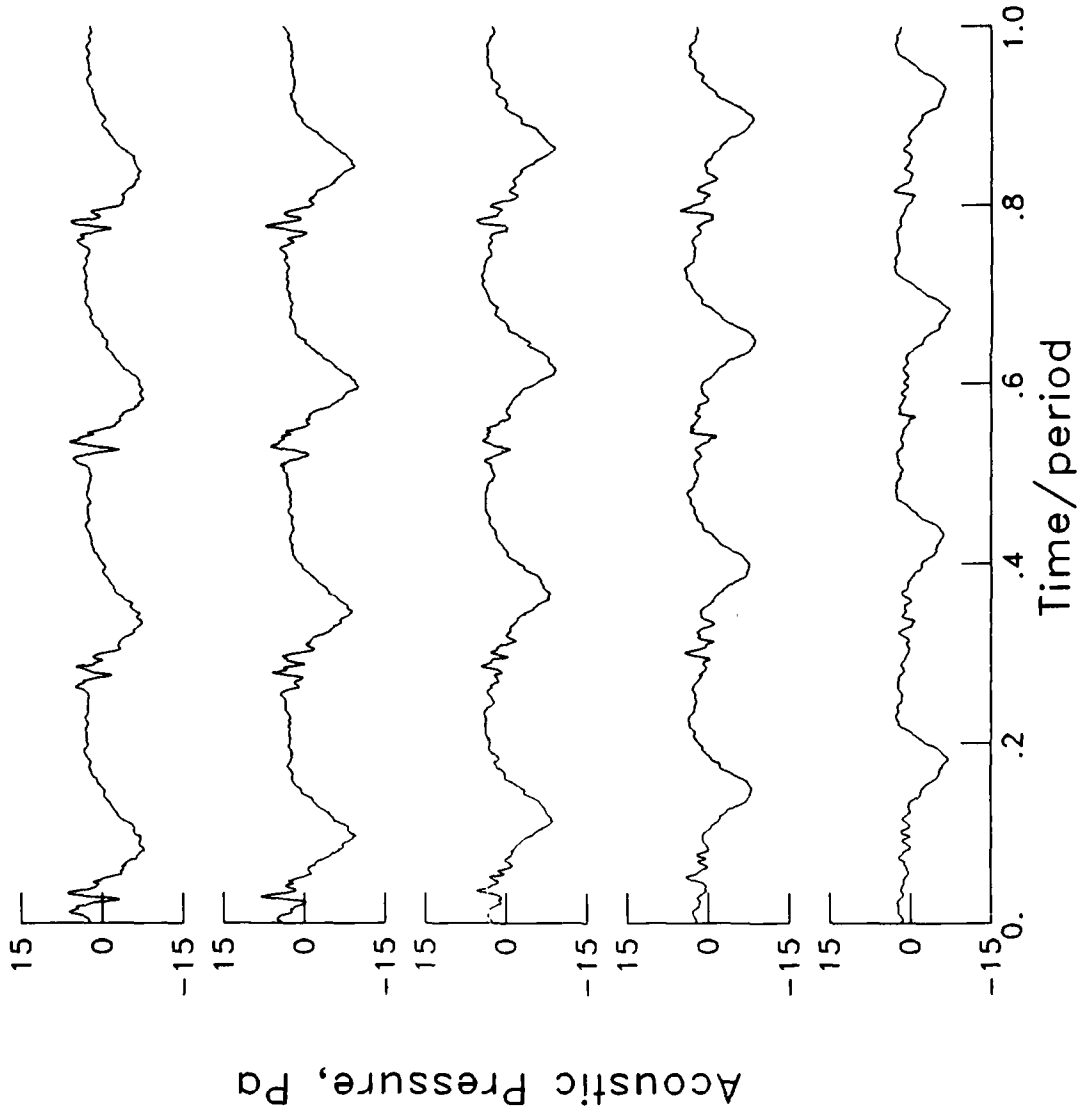
9 5.34 -2.16 -2.10

7 5.34 -1.08 -2.10

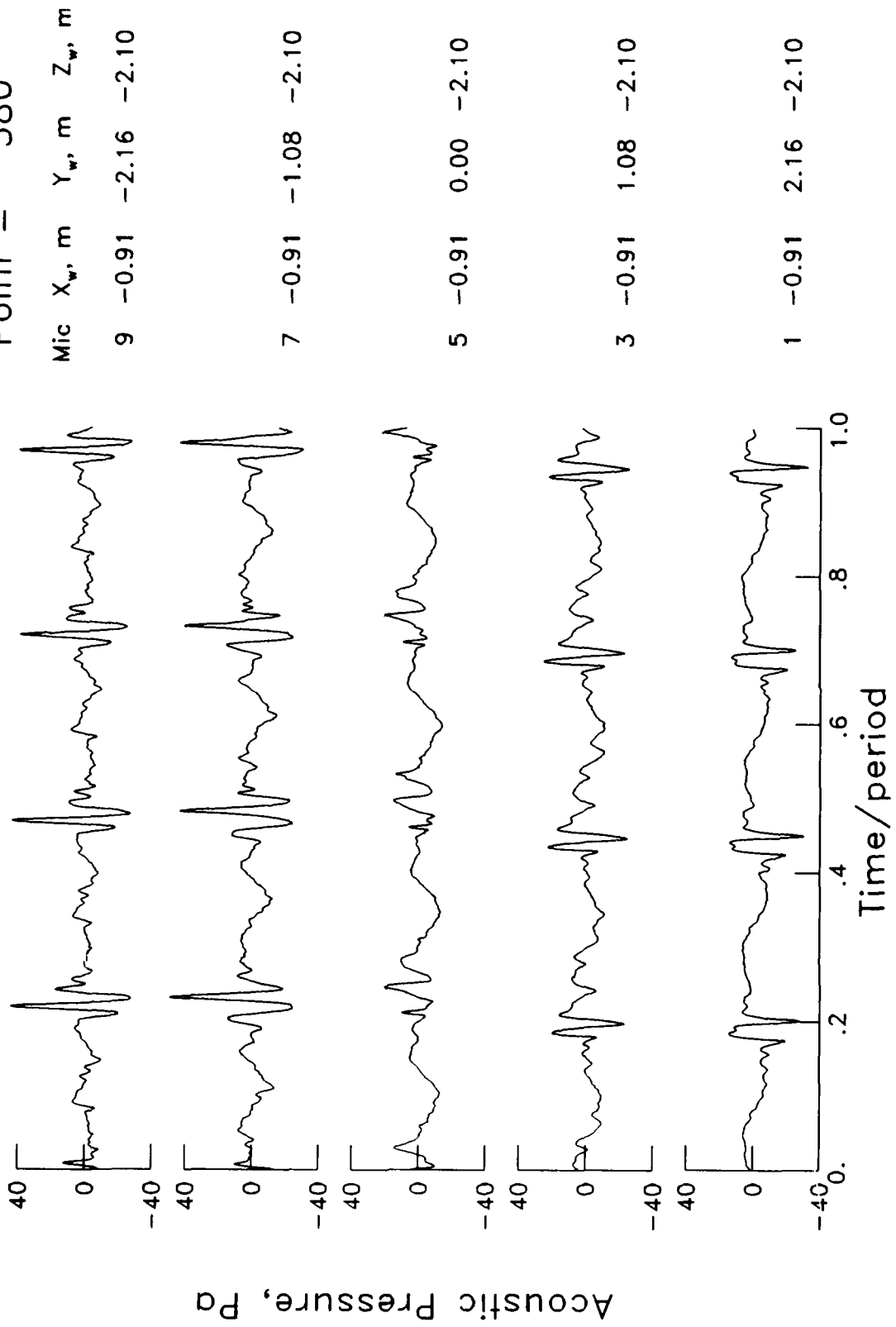
5 5.34 0.00 -2.10

3 5.34 1.08 -2.10

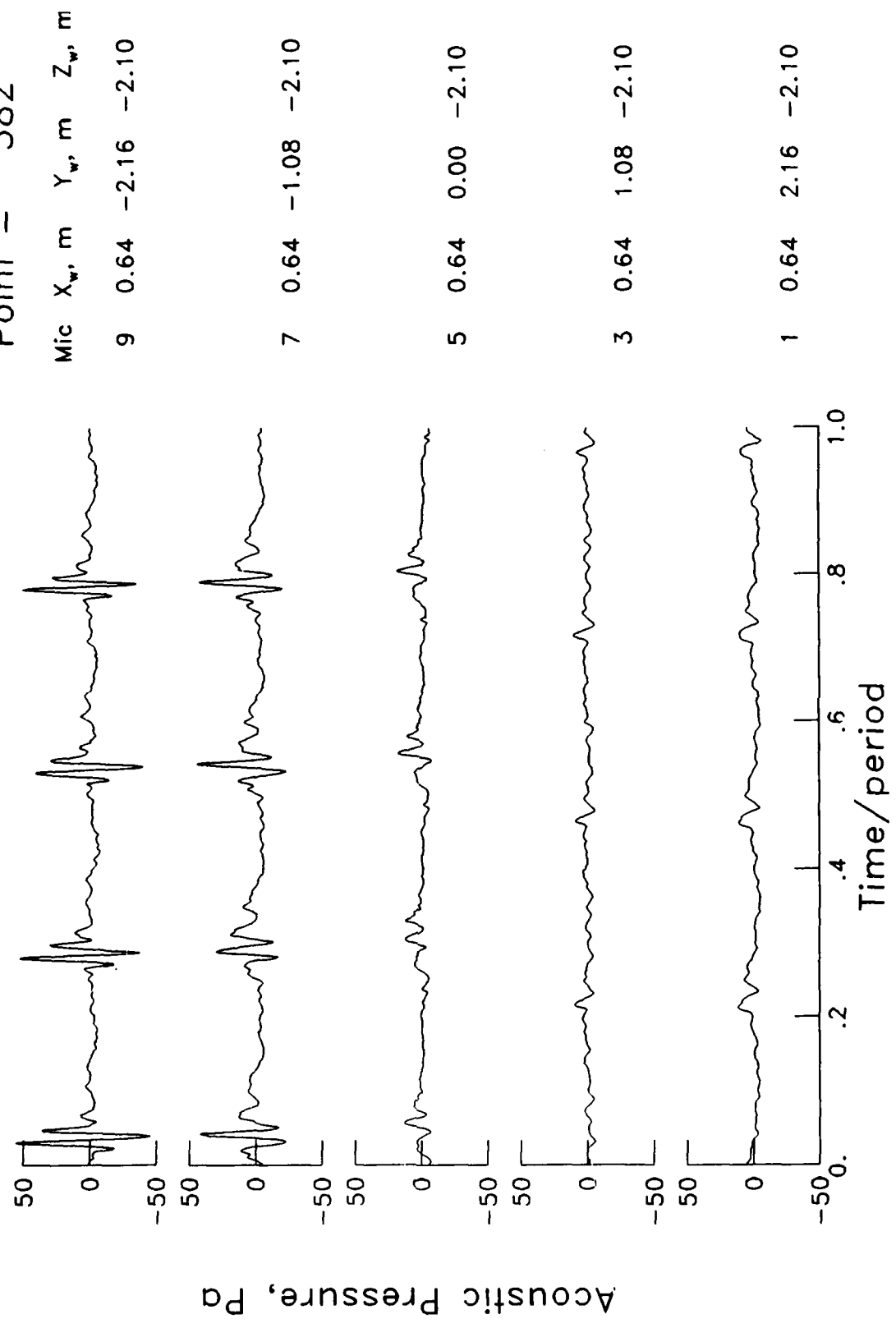
1 5.34 2.16 -2.10



$\mu = .143$
 $\alpha_{TPP} = 3.3^\circ$
 $C_T = 0.0044$
 $M_H = 0.636$
 Point = 380

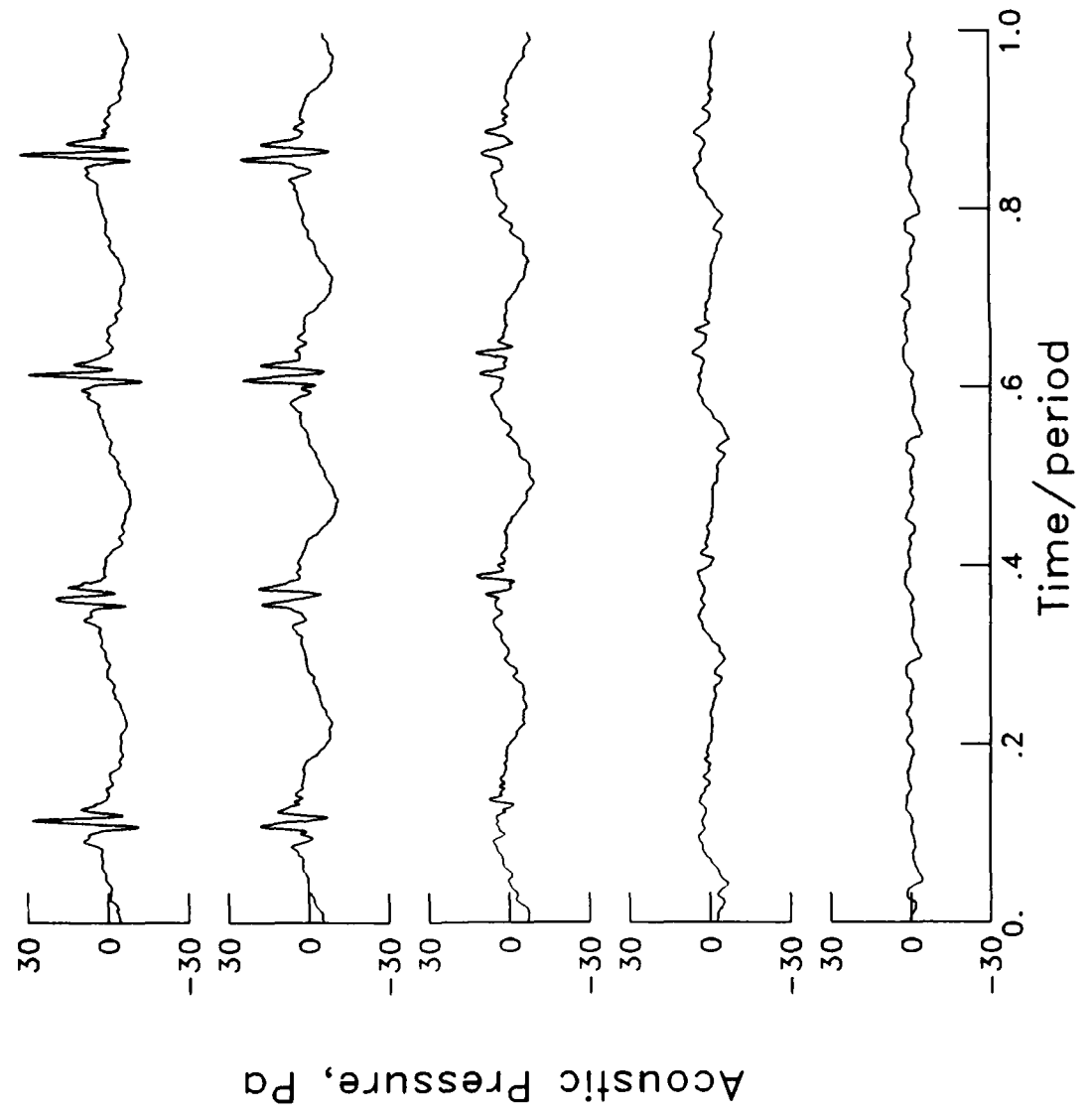


$\mu = .142$
 $\alpha_{TPP} = 3.4^\circ$
 $C_T = 0.0042$
 $M_H = 0.637$
 Point = 382



$\mu = .142$
 $\alpha_{TPP} = 3.3^\circ$
 $C_T = 0.0043$
 $M_{H.} = 0.635$
 Point = 384

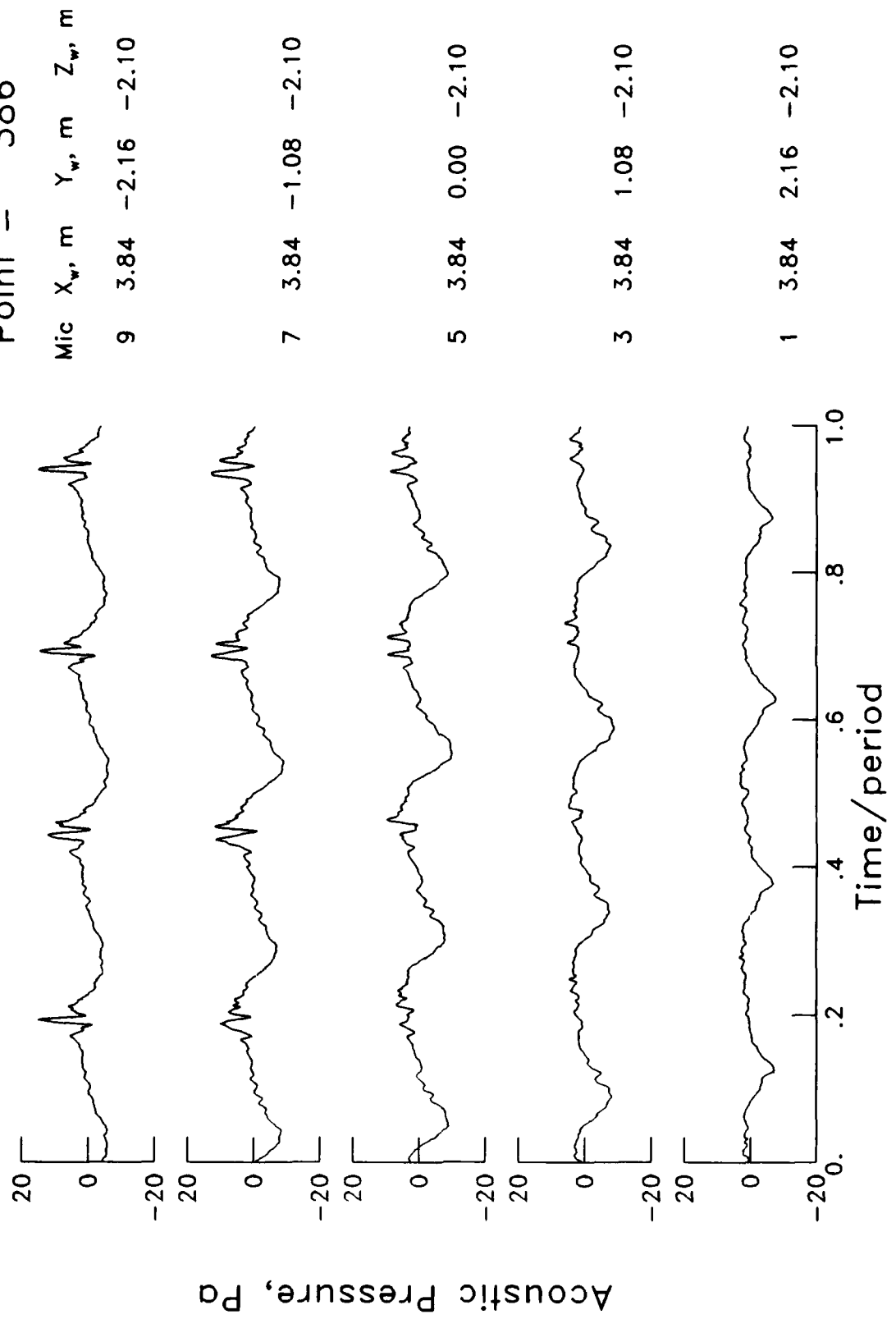
Mic	X _w , m	Y _w , m	Z _w , m
9	2.24	-2.16	-2.10
7	2.24	-1.08	-2.10
5	2.24	0.00	-2.10
3	2.24	1.08	-2.10
1	2.24	2.16	-2.10



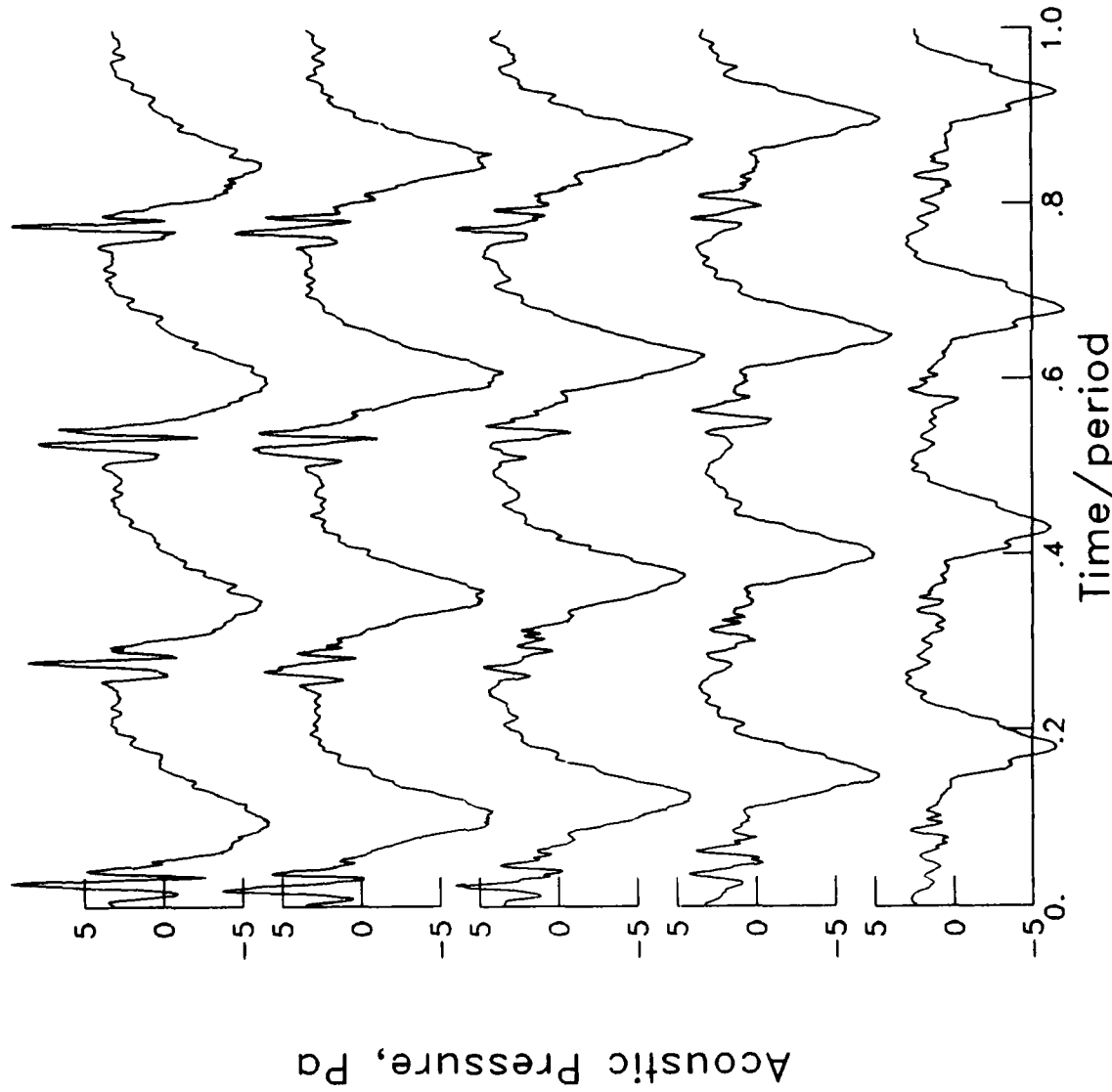
Acoustic Pressure, Pa

Time/period

$\mu = .142$
 $\alpha_{TPP} = 3.3^\circ$
 $C_T = 0.0044$
 $M_H = 0.635$
 Point = 386



$\mu = .142$
 $\alpha_{TPP} = 3.3^\circ$
 $C_T = 0.0044$
 $M_H = 0.636$
 Point = 388



Mic	X _w , m	Y _w , m	Z _w , m
9	5.43	-2.16	-2.10
7	5.43	-1.08	-2.10
5	5.43	0.00	-2.10
3	5.43	1.08	-2.10
1	5.43	2.16	-2.10

$\mu = .114$
 $\alpha_{TPP} = 3.0^\circ$
 $C_T = 0.0043$
 $M_{H_i} = 0.637$
 Point = 379

Mic X_w , m Y_w , m Z_w , m

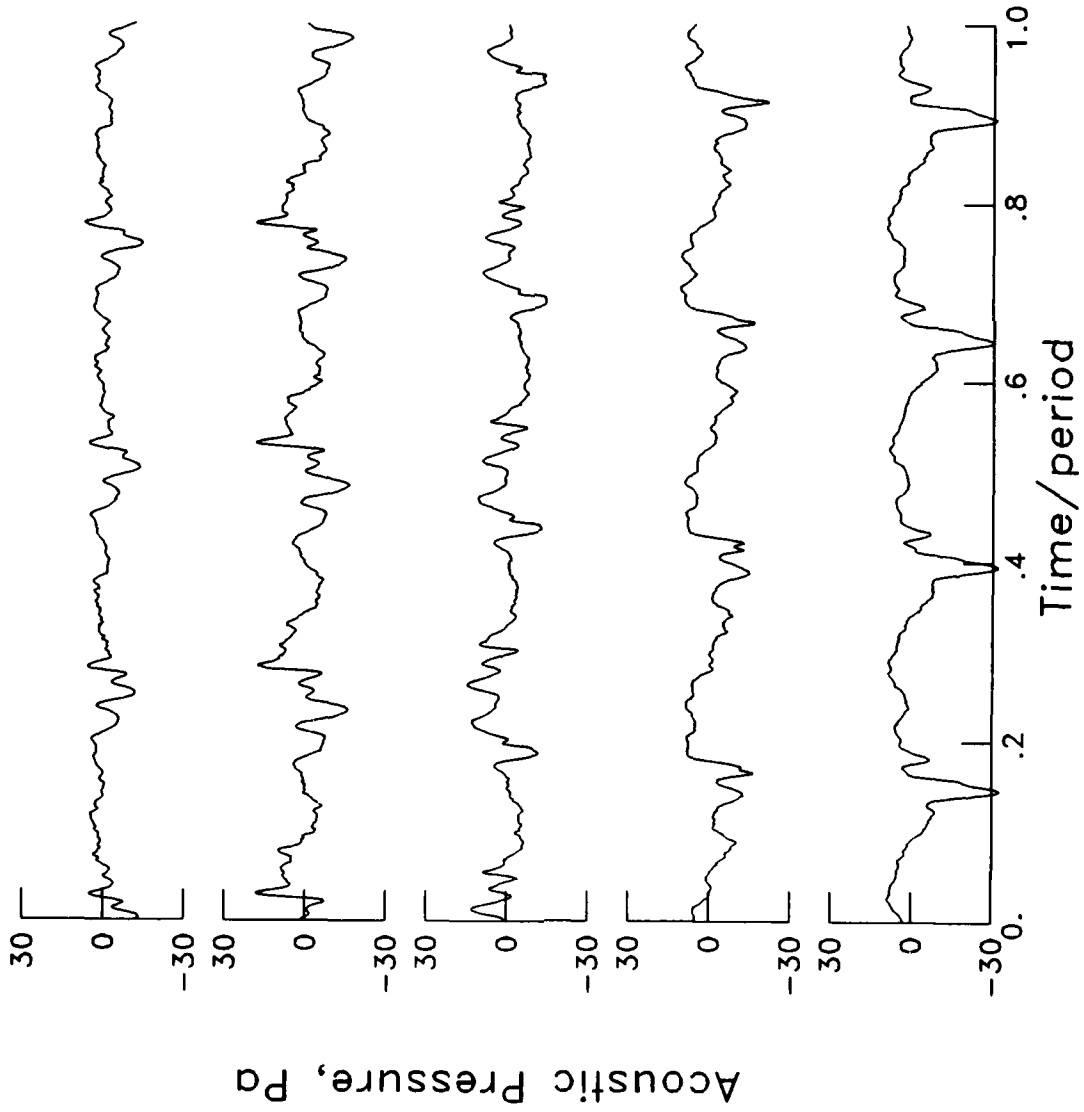
9 -0.88 -2.16 -2.10

7 -0.88 -1.08 -2.10

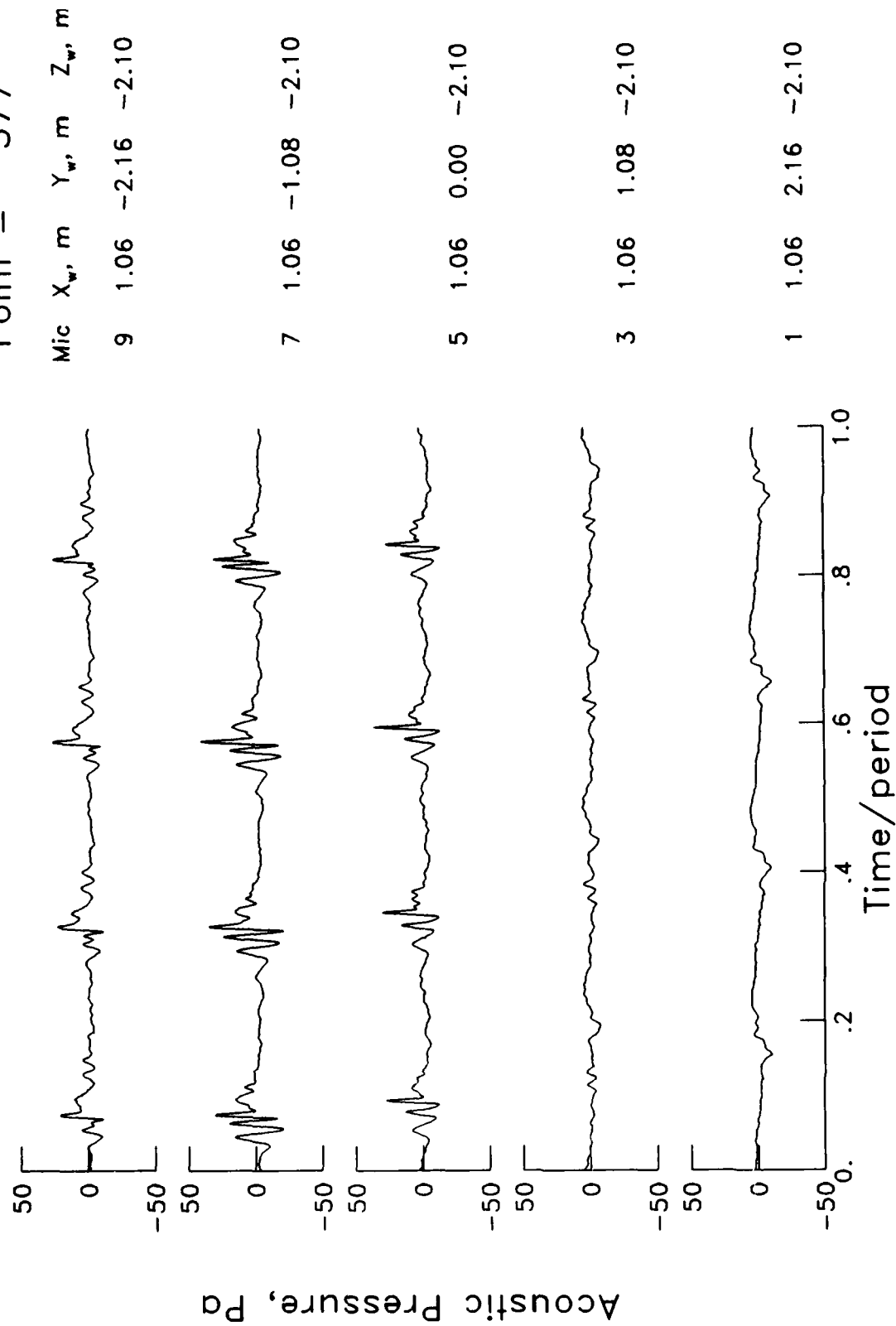
5 -0.88 0.00 -2.10

3 -0.88 1.08 -2.10

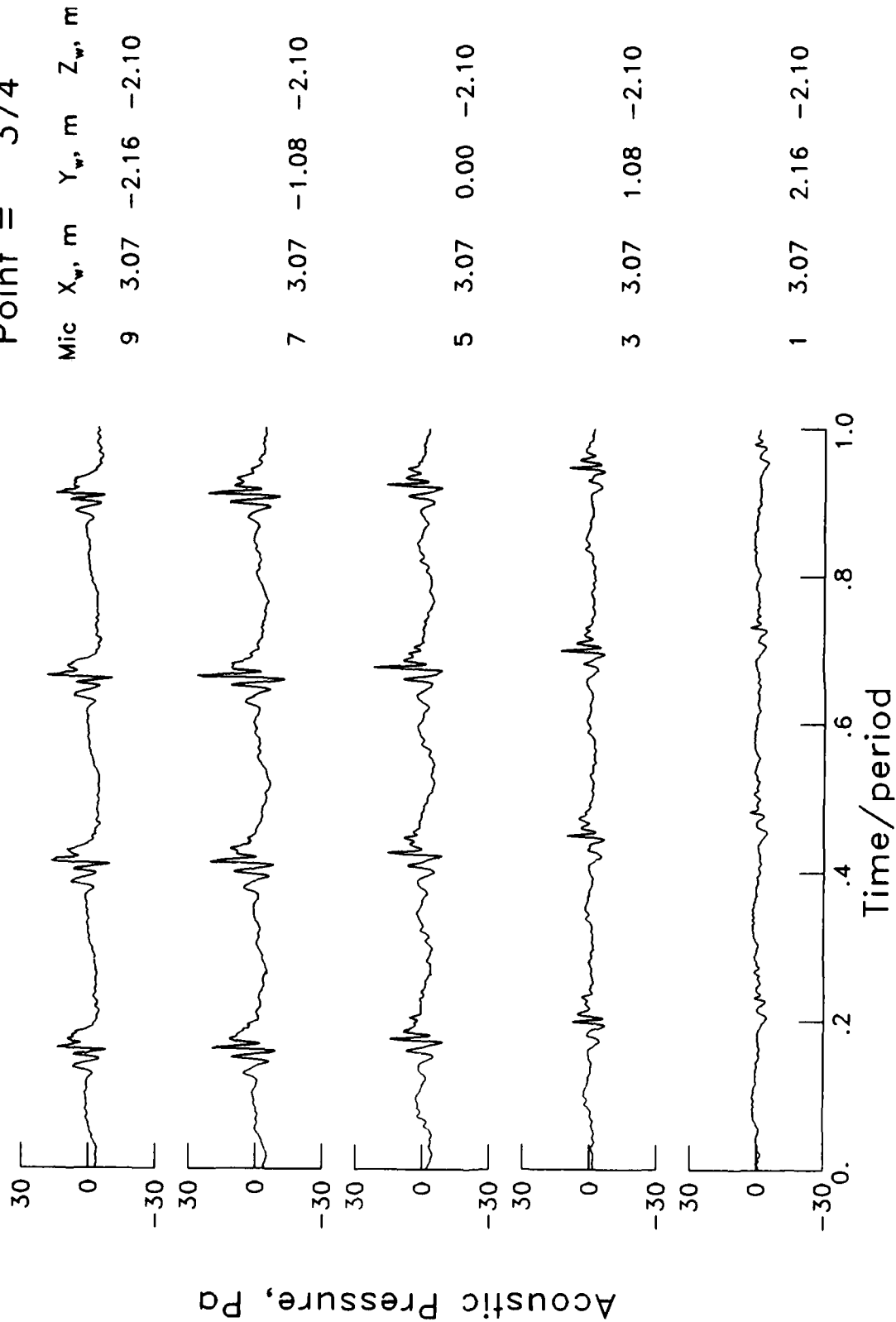
1 -0.88 2.16 -2.10



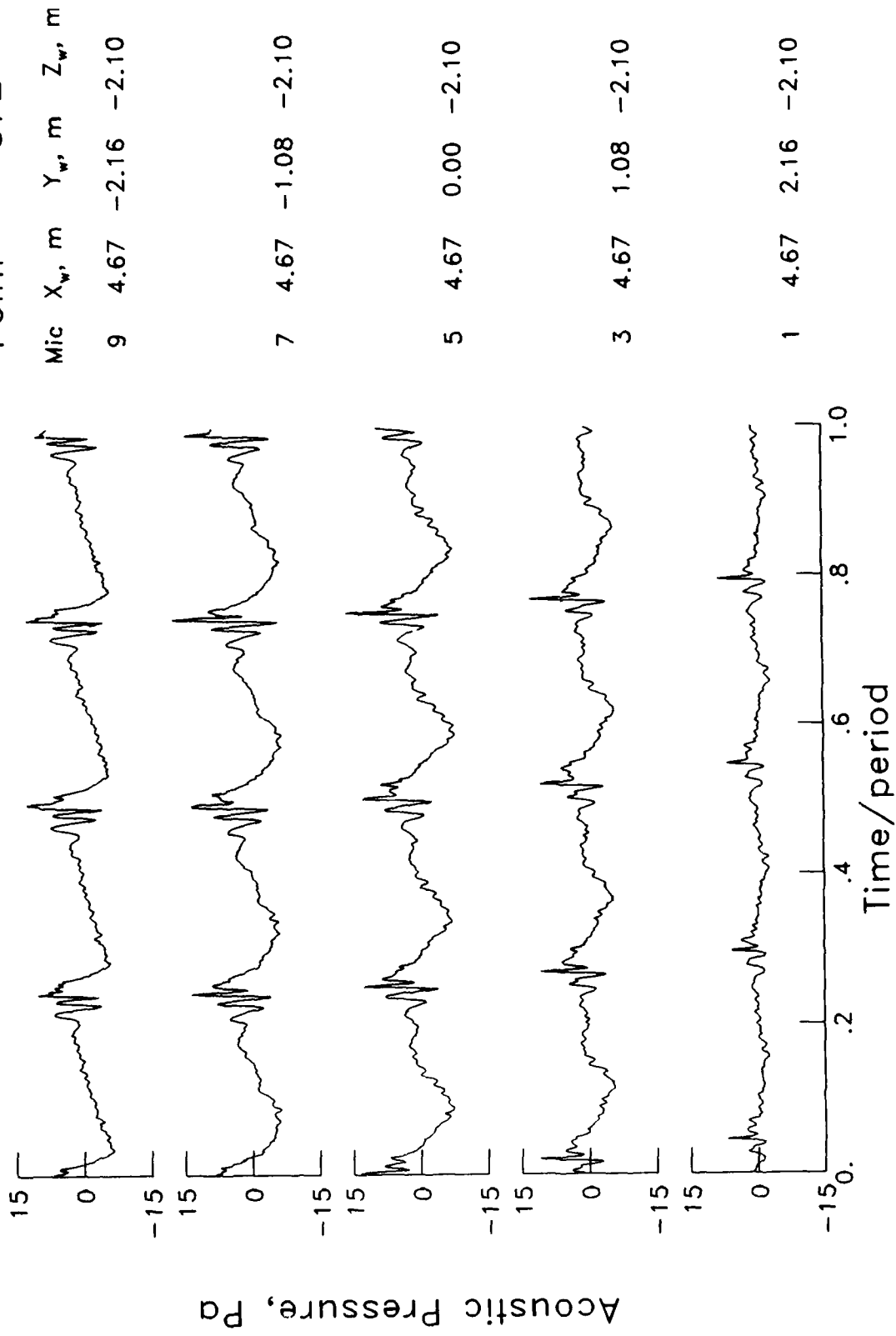
$\mu = .112$
 $\alpha_{TPP} = 2.9^\circ$
 $C_T = 0.0044$
 $M_H = 0.634$
 Point = 377



$\mu = .114$
 $\alpha_{TPP} = 2.9^\circ$
 $C_T = 0.0043$
 $M_H = 0.636$
 Point = 374



$\mu = .112$
 $\alpha_{TPP} = 2.8^\circ$
 $C_T = 0.0044$
 $M_{H.} = 0.636$
 Point = 372



$\mu = .116$
 $\alpha_{TPP} = 2.9^\circ$
 $C_T = 0.0043$
 $M_H = 0.636$
 Point = 369

Mic X_w, m Y_w, m Z_w, m

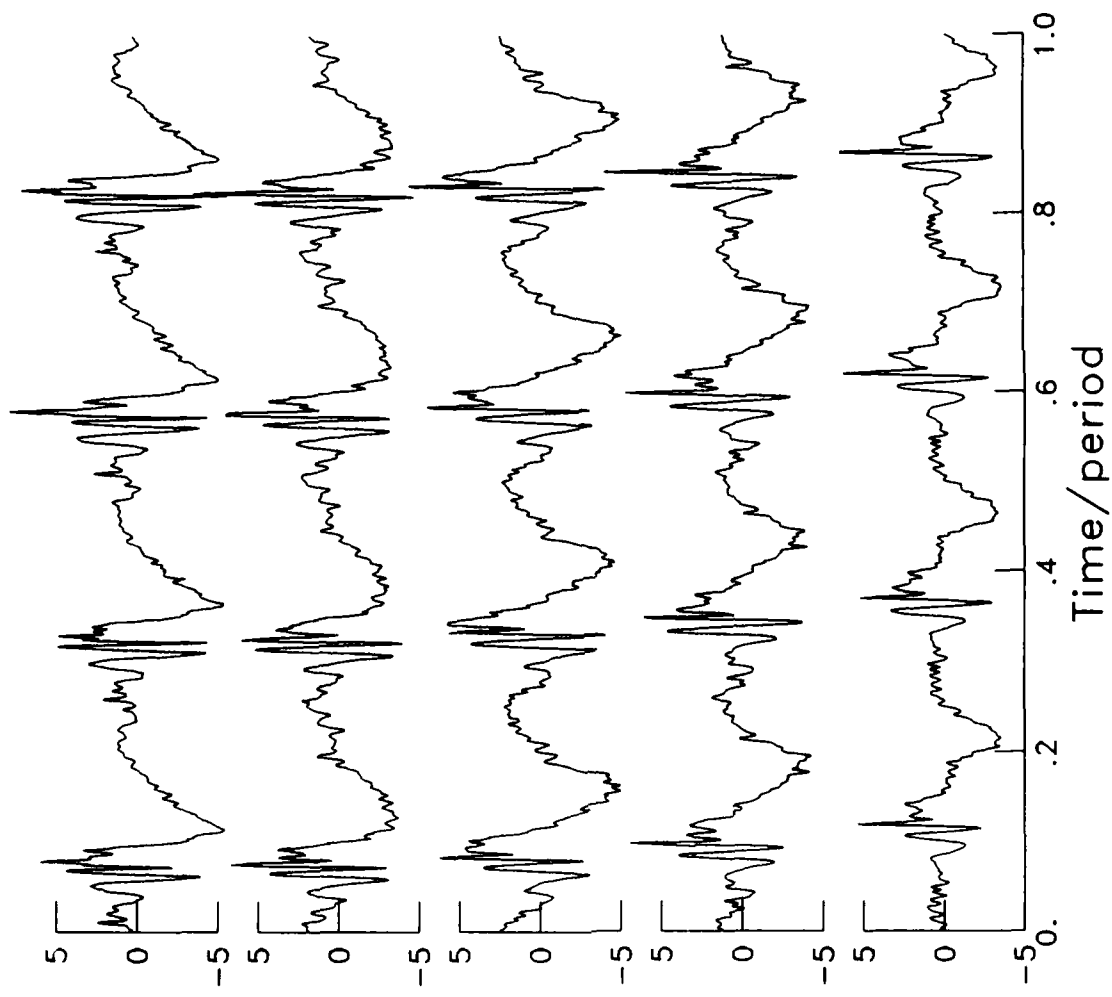
9 6.27 -2.16 -2.10

7 6.27 -1.08 -2.10

5 6.27 0.00 -2.10

3 6.27 1.08 -2.10

1 6.27 2.16 -2.10

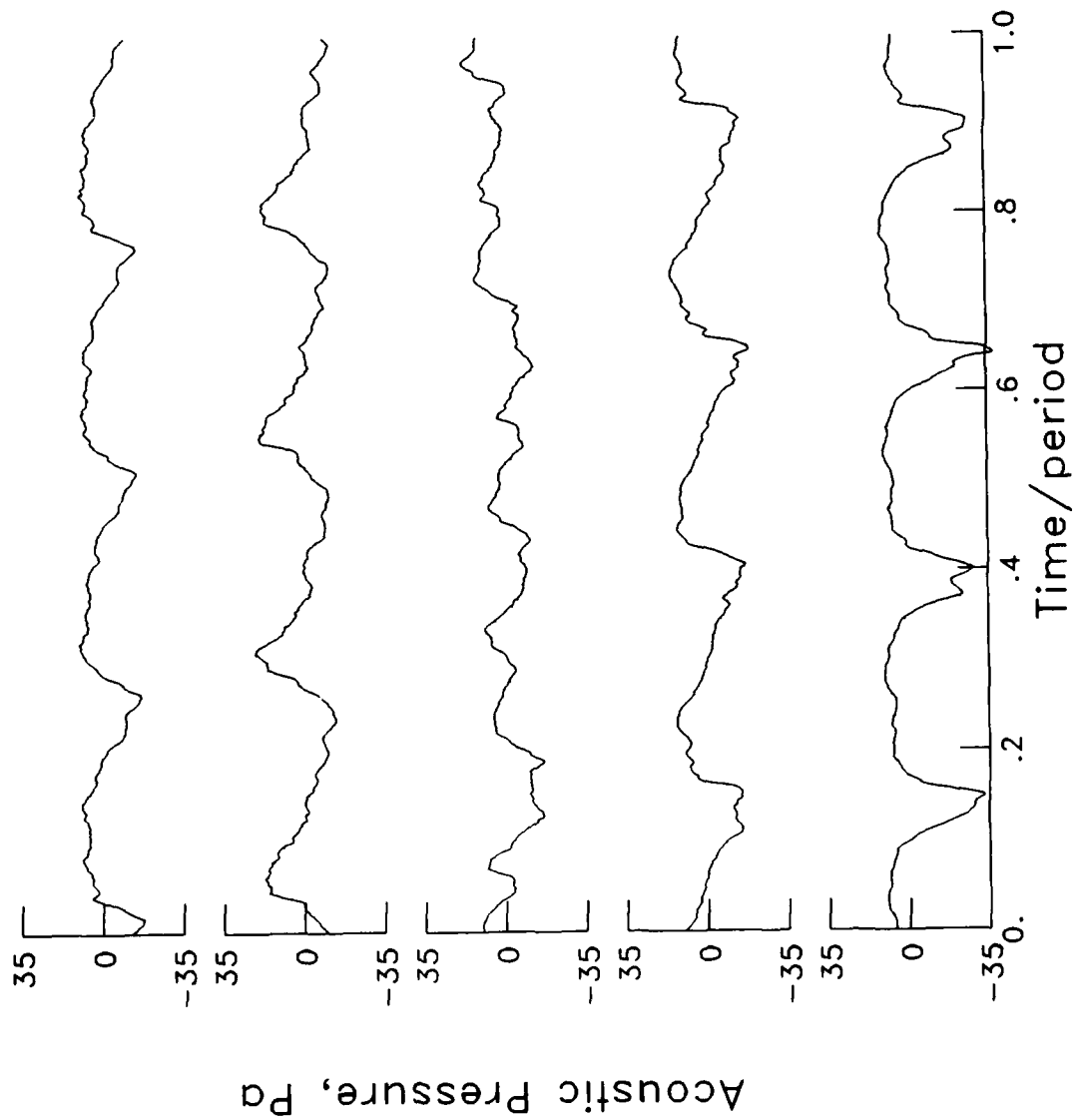


Acoustic Pressure, Pa

Time/period

$\mu = .088$
 $\alpha_{TPP} = 3.6^\circ$
 $C_T = 0.0048$
 $M_H = 0.635$
 Point = 358

Mic	X _w , m	Y _w , m	Z _w , m
9	-0.75	-2.16	-2.10
7	-0.75	-1.08	-2.10
5	-0.75	0.00	-2.10
3	-0.75	1.08	-2.10
1	-0.75	2.16	-2.10



$\mu = .090$
 $\alpha_{TPP} = 3.9^\circ$
 $C_T = 0.0045$
 $M_H = 0.637$
 Point = 360

Mic X_w, m Y_w, m Z_w, m

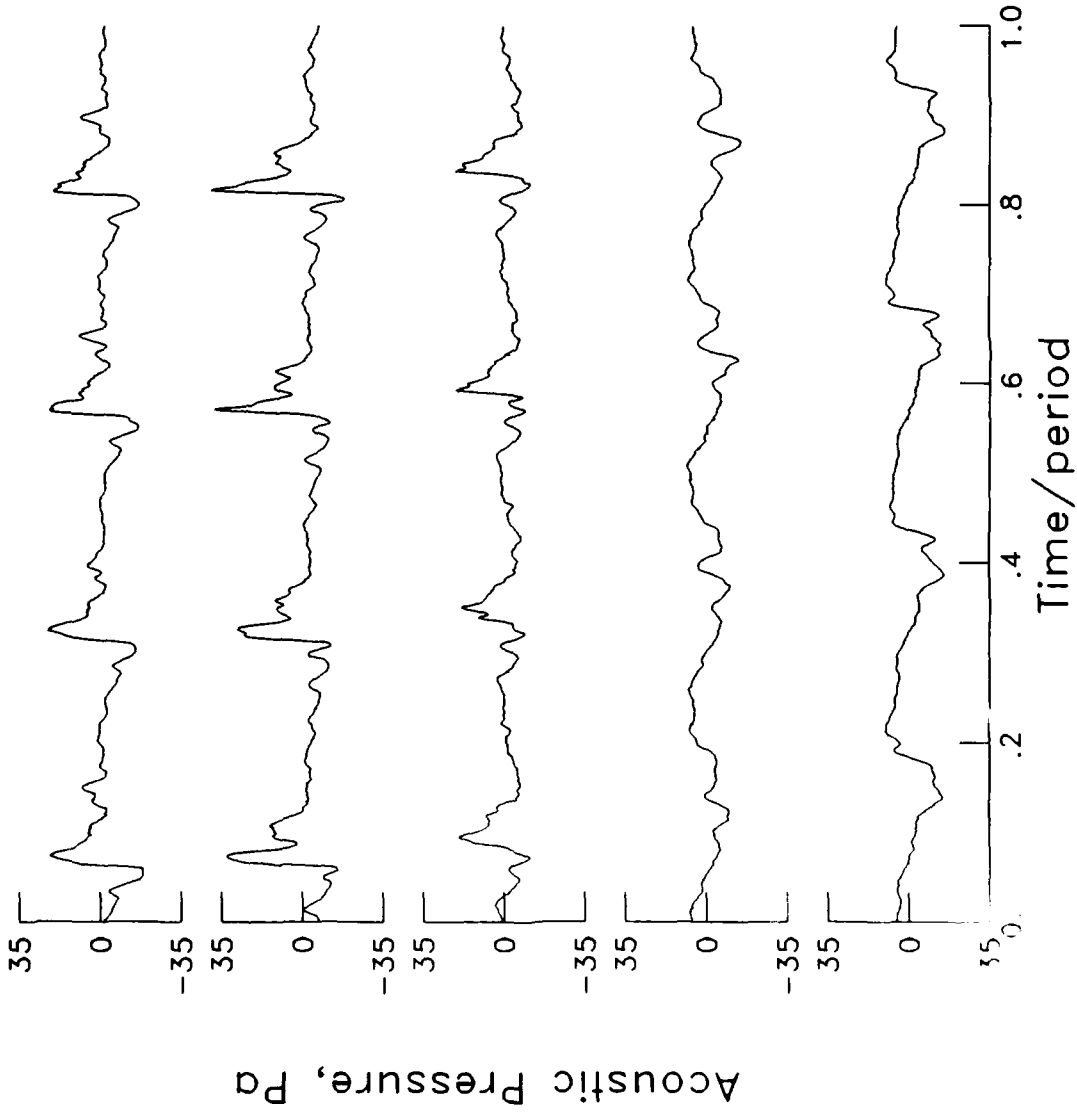
9 0.80 -2.16 -2.10

7 0.80 -1.08 -2.10

5 0.80 0.00 -2.10

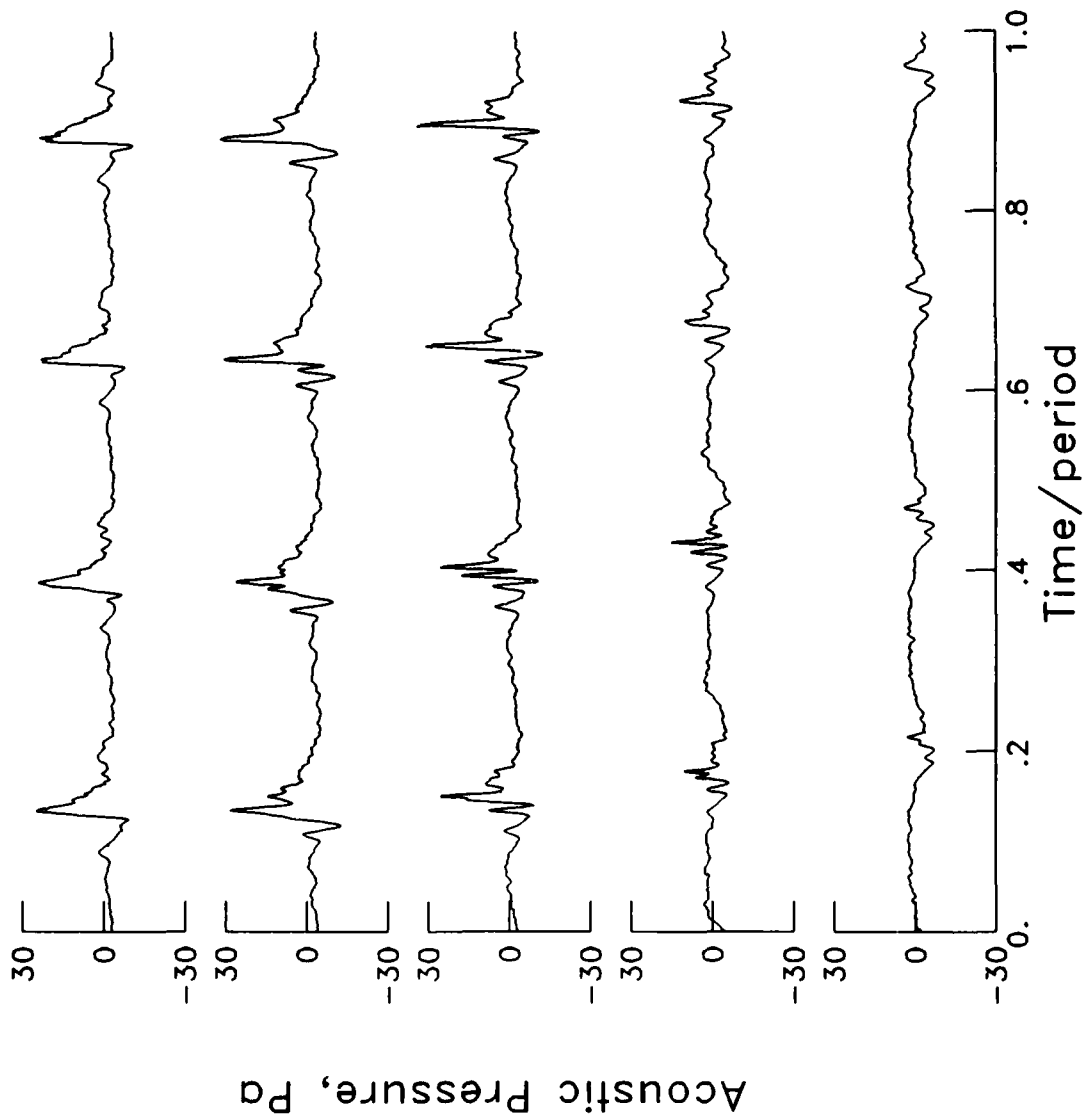
3 0.80 1.08 -2.10

1 0.80 2.16 -2.10

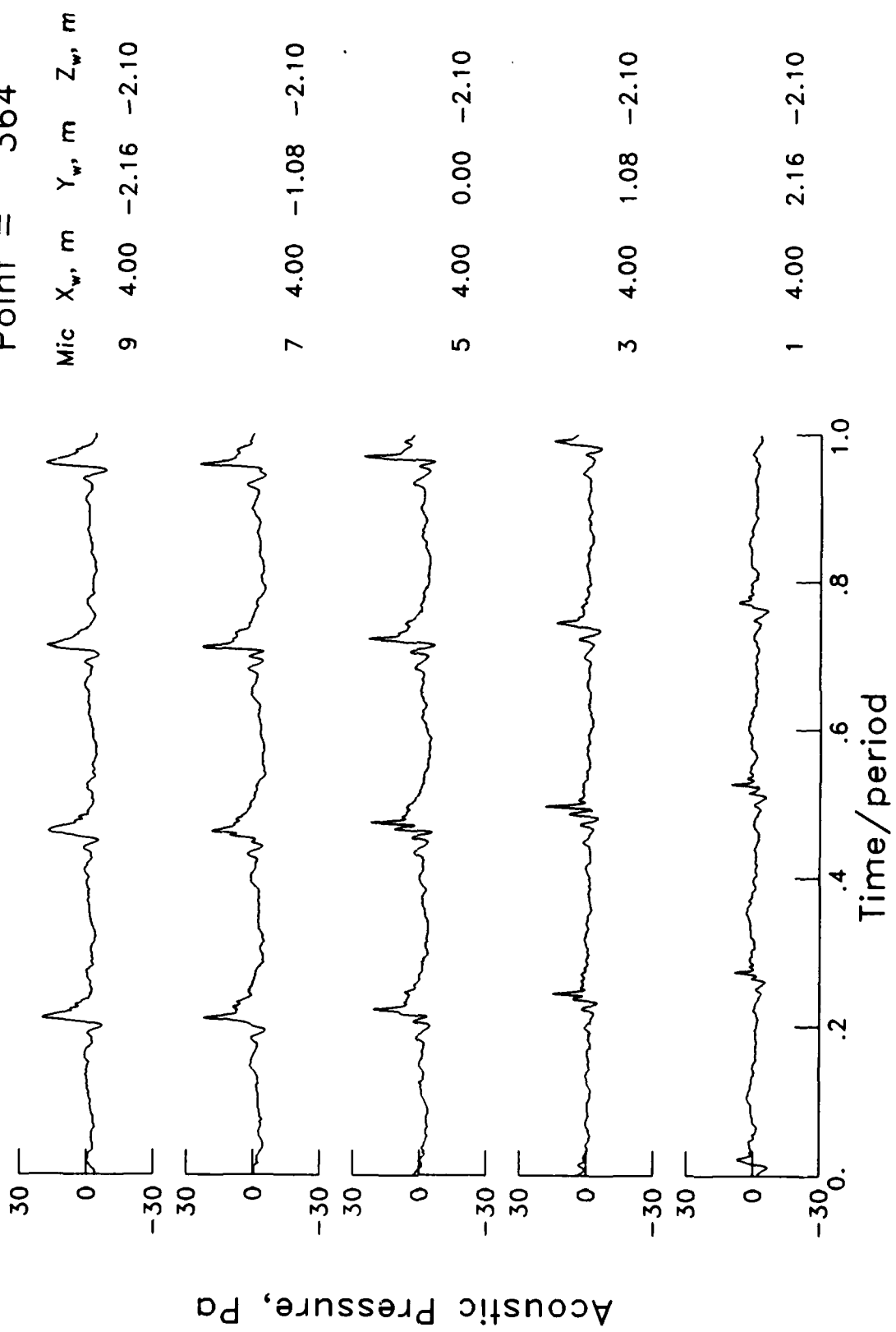


$\mu = .091$
 $\alpha_{TPP} = 4.2^\circ$
 $C_T = 0.0042$
 $M_H = 0.635$
 Point = 362

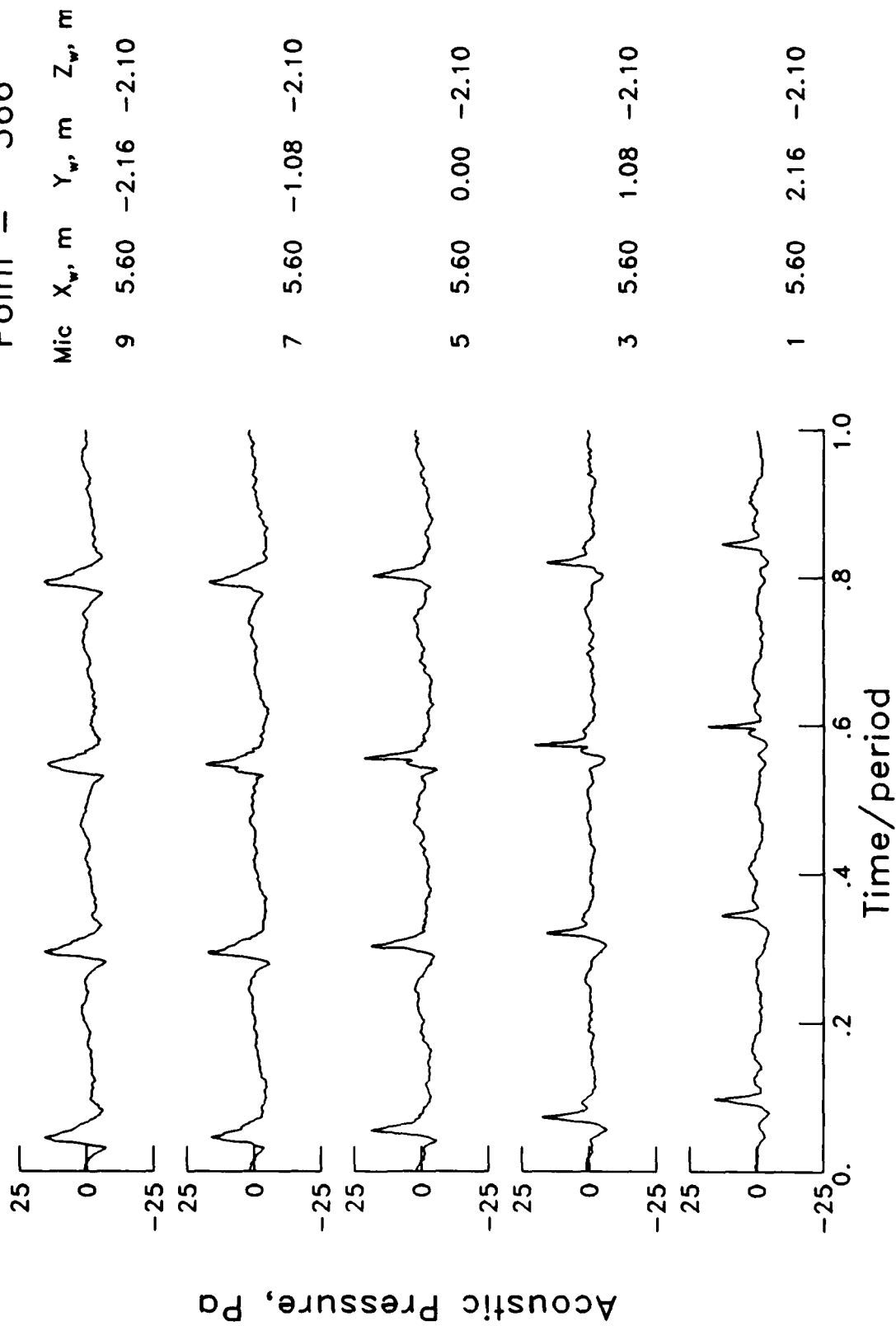
Mic	X _w , m	Y _w , m	Z _w , m
9	2.40	-2.16	-2.10
7	2.40	-1.08	-2.10
5	2.40	0.00	-2.10
3	2.40	1.08	-2.10
1	2.40	2.16	-2.10



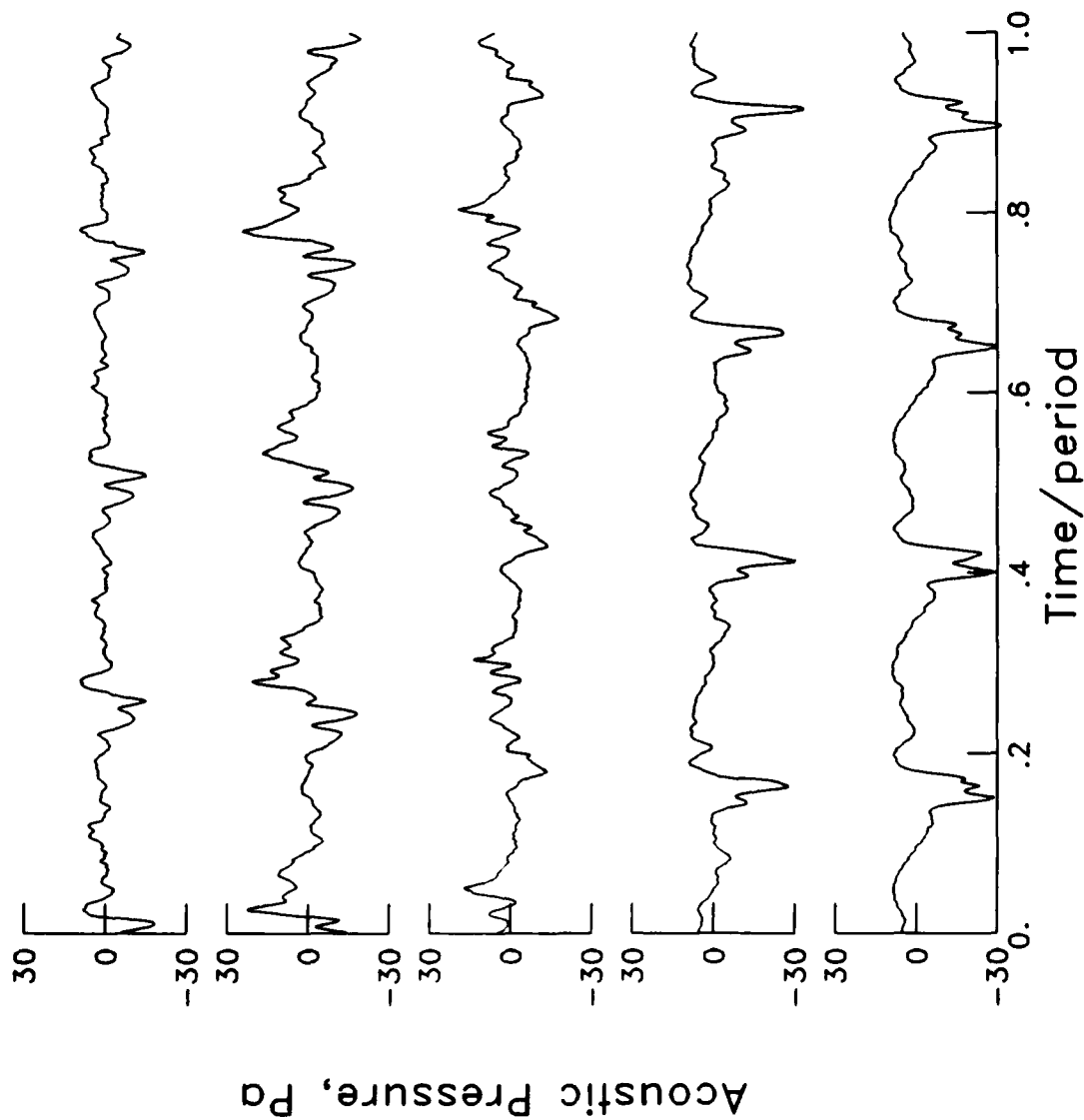
$\mu = .091$
 $\alpha_{\text{TPP}} = 4.1^\circ$
 $C_T = 0.0043$
 $M_H = 0.636$
 Point = 364



$\mu = .090$
 $\alpha_{TPP} = 4.1^\circ$
 $C_T = 0.0043$
 $M_{Hint} = 0.633$
 Point = 366



$\mu = .087$
 $\alpha_{\text{TPP}} = 5.8^\circ$
 $C_T = 0.0044$
 $M_H = 0.635$
 Point = 357



Mic X_w, m Y_w, m Z_w, m

9 -0.64 -2.16 -2.10

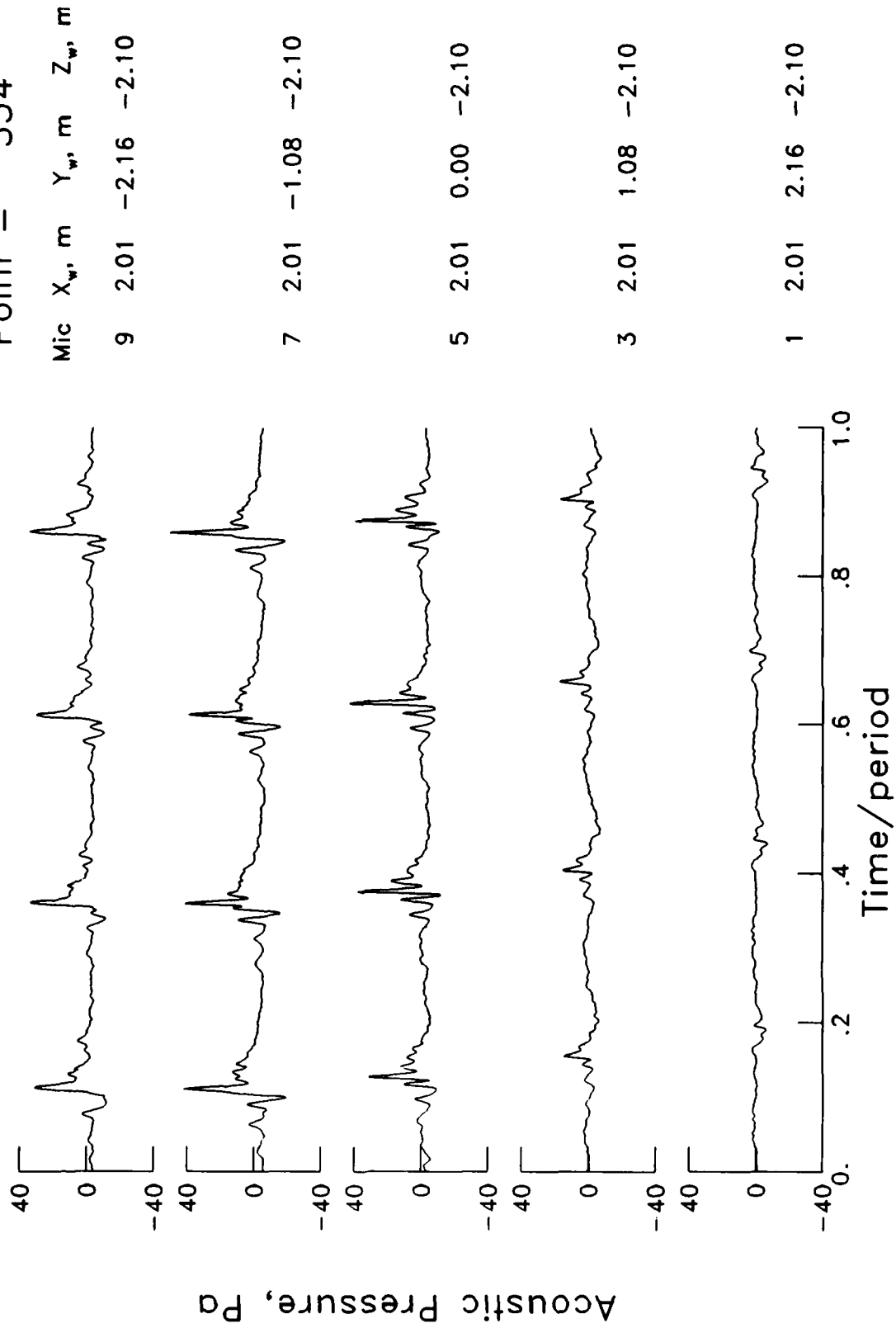
7 -0.64 -1.08 -2.10

5 -0.64 0.00 -2.10

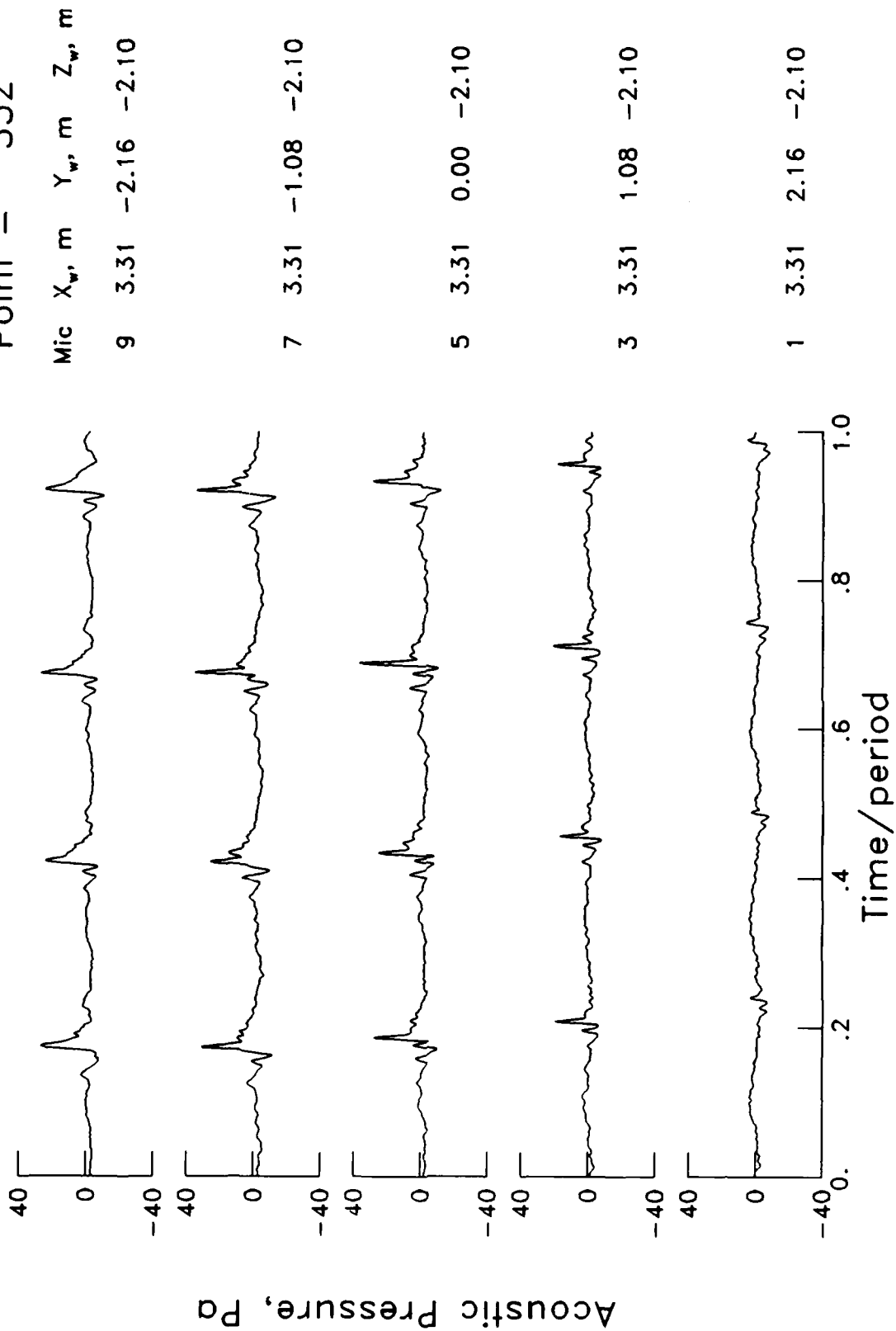
3 -0.64 1.08 -2.10

1 -0.64 2.16 -2.10

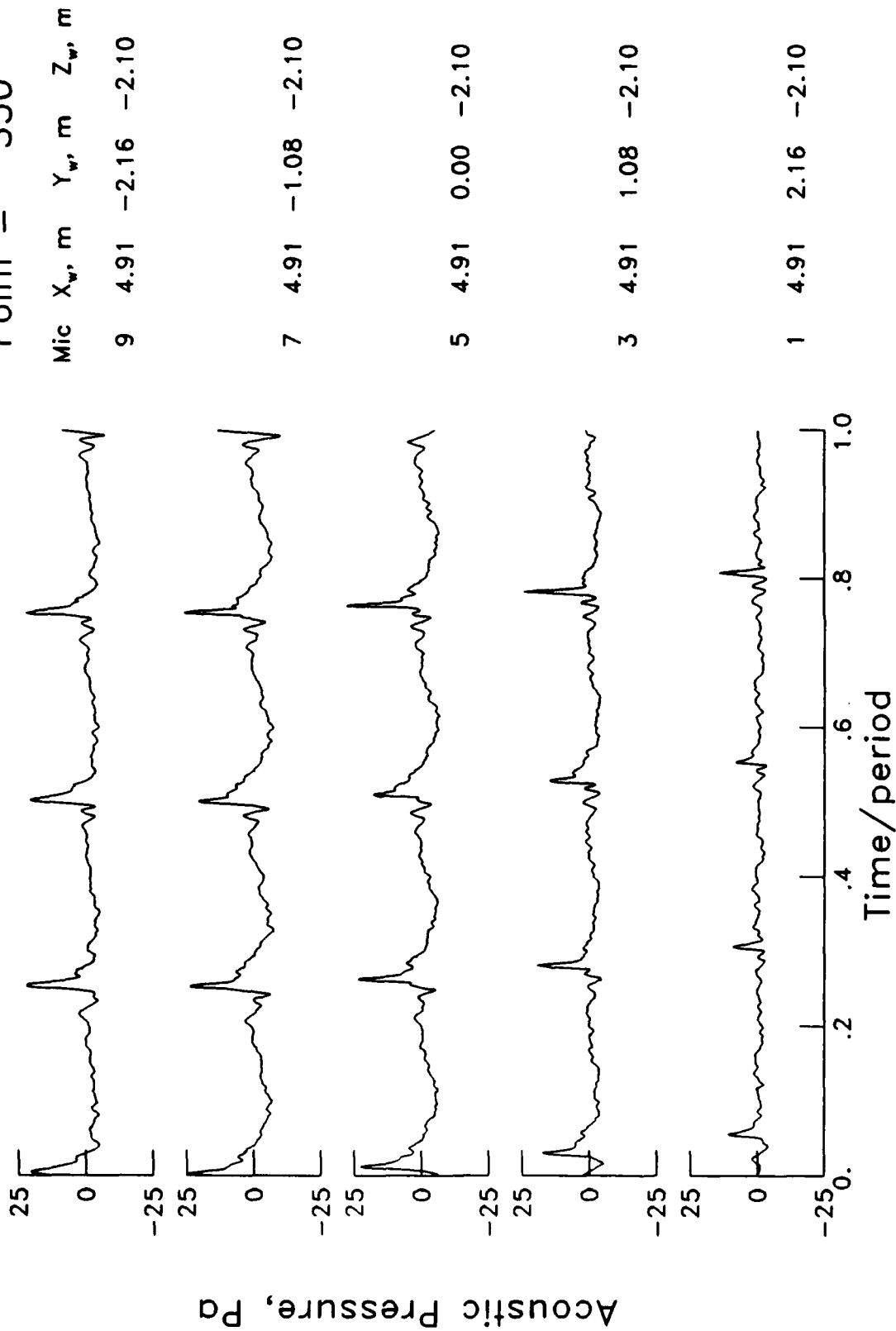
$\mu = .087$
 $\alpha_{TPP} = 5.7^\circ$
 $C_T = 0.0044$
 $M_H = 0.635$
 Point = 354



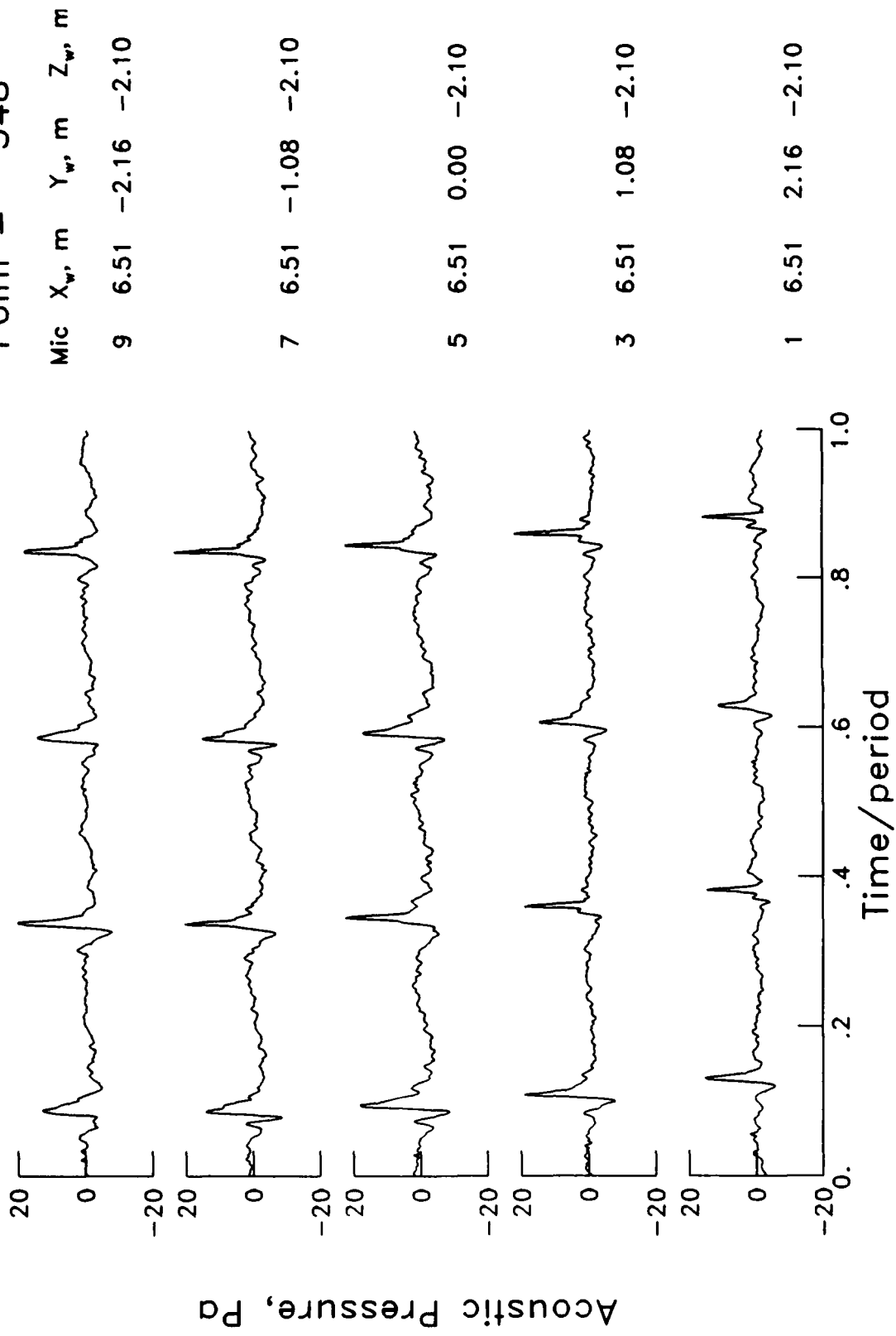
$\mu = .086$
 $\alpha_{TPP} = 5.4^\circ$
 $C_T = 0.0047$
 $M_H = 0.638$
 Point = 352



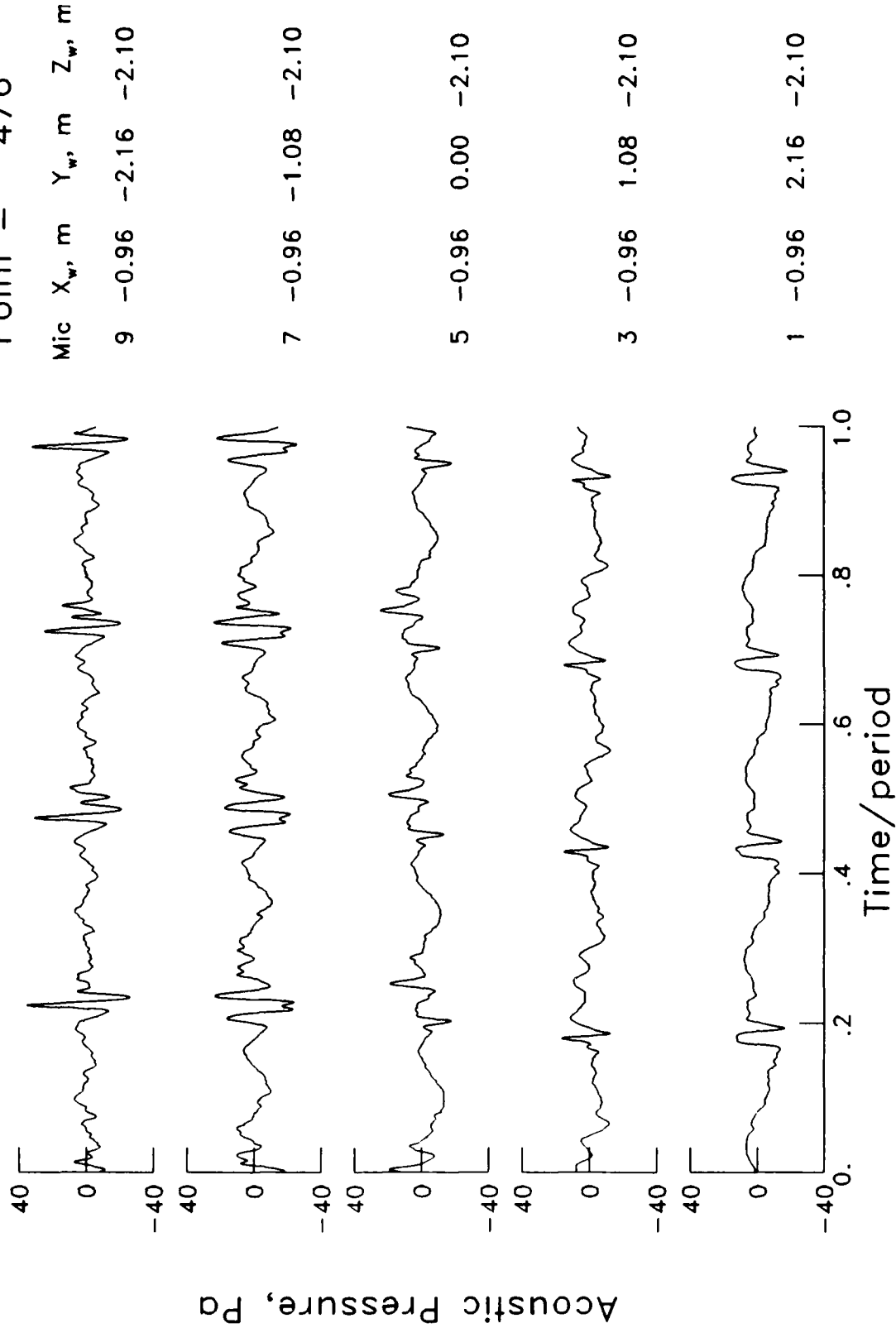
$\mu = .086$
 $\alpha_{TPP} = 5.9^\circ$
 $C_T = 0.0042$
 $M_H = 0.636$
 Point = 350



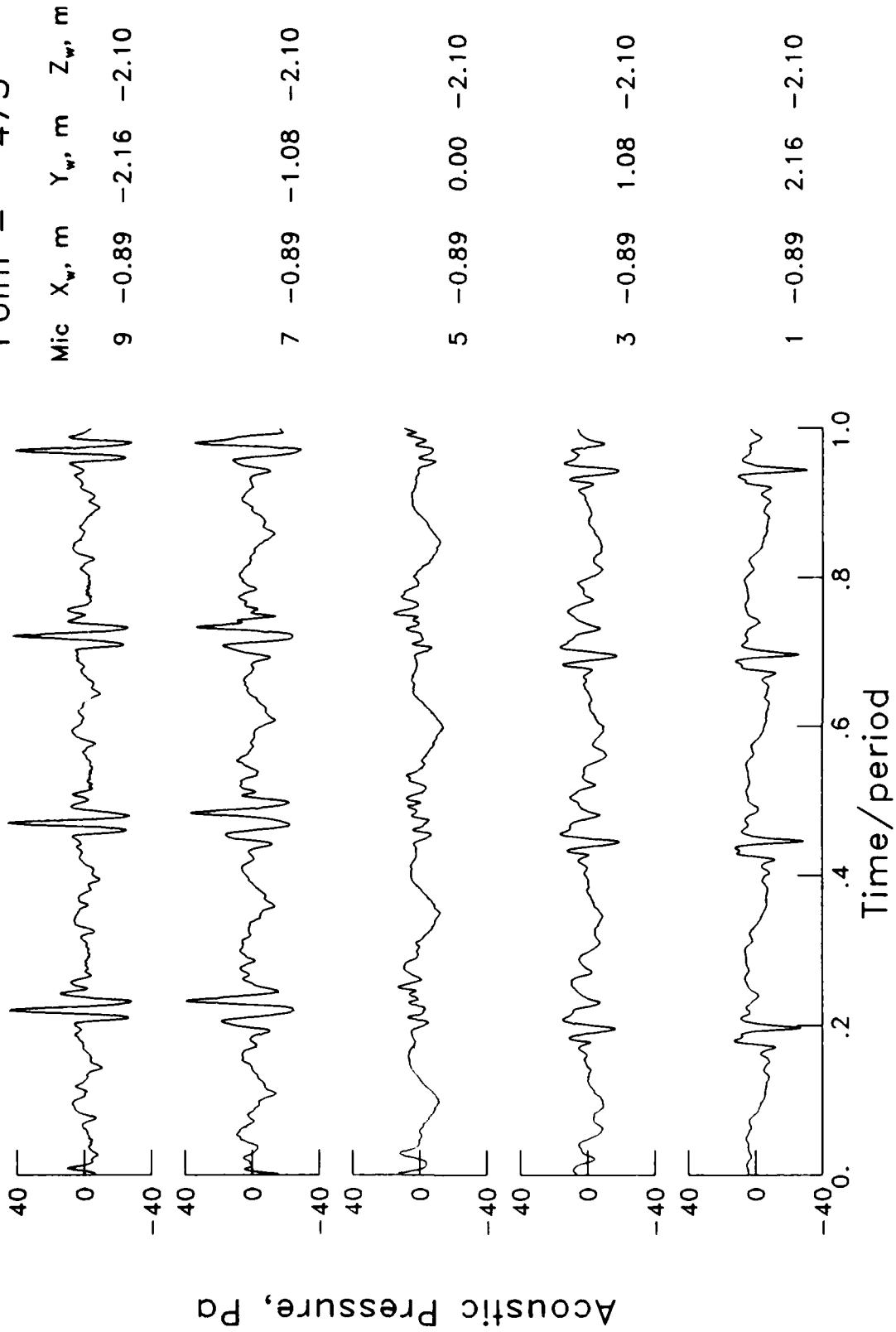
$\mu = .087$
 $\alpha_{TPP} = 5.8^\circ$
 $C_T = 0.0043$
 $M_H = 0.635$
 Point = 348



$\mu = .138$
 $\alpha_{TPP} = 2.3^\circ$
 $C_T = 0.0043$
 $M_H = 0.637$
 Point = 476

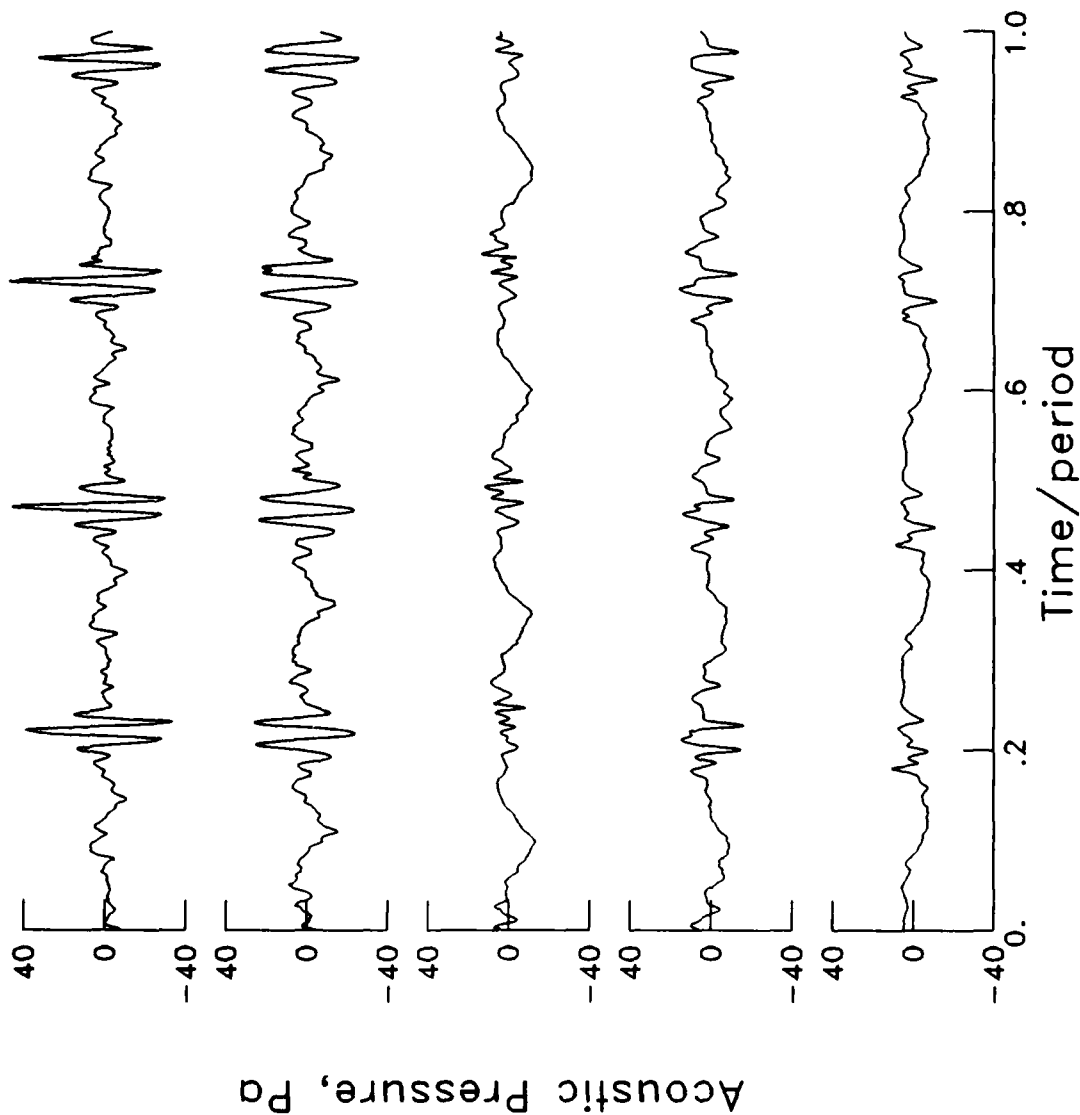


$\mu = .137$
 $\alpha_{TPP} = 3.8^\circ$
 $C_T = 0.0043$
 $M_H = 0.636$
 Point = 473

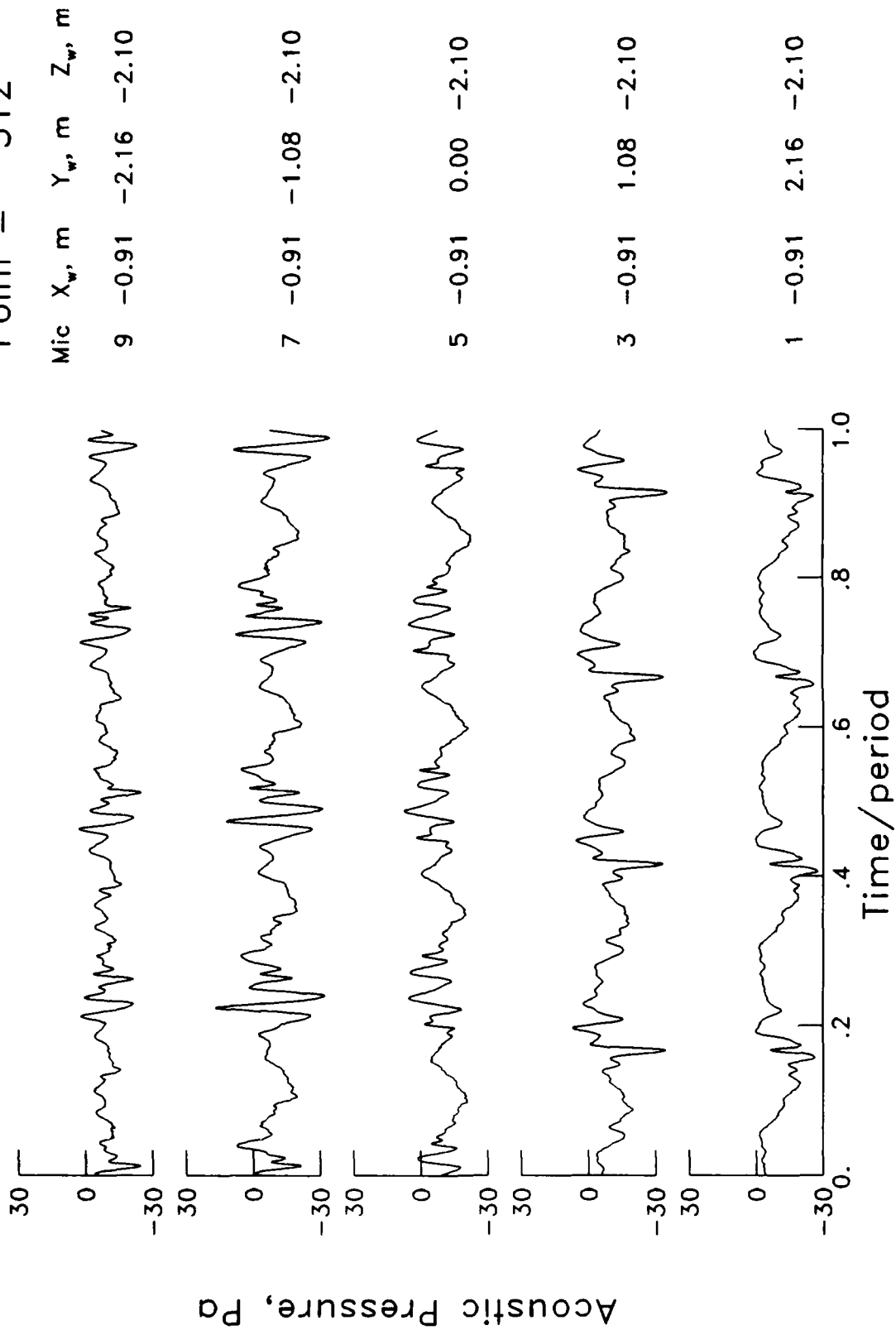


$\mu = .136$
 $\alpha_{TPP} = 5.3^\circ$
 $C_T = 0.0043$
 $M_H = 0.636$
 Point = 470

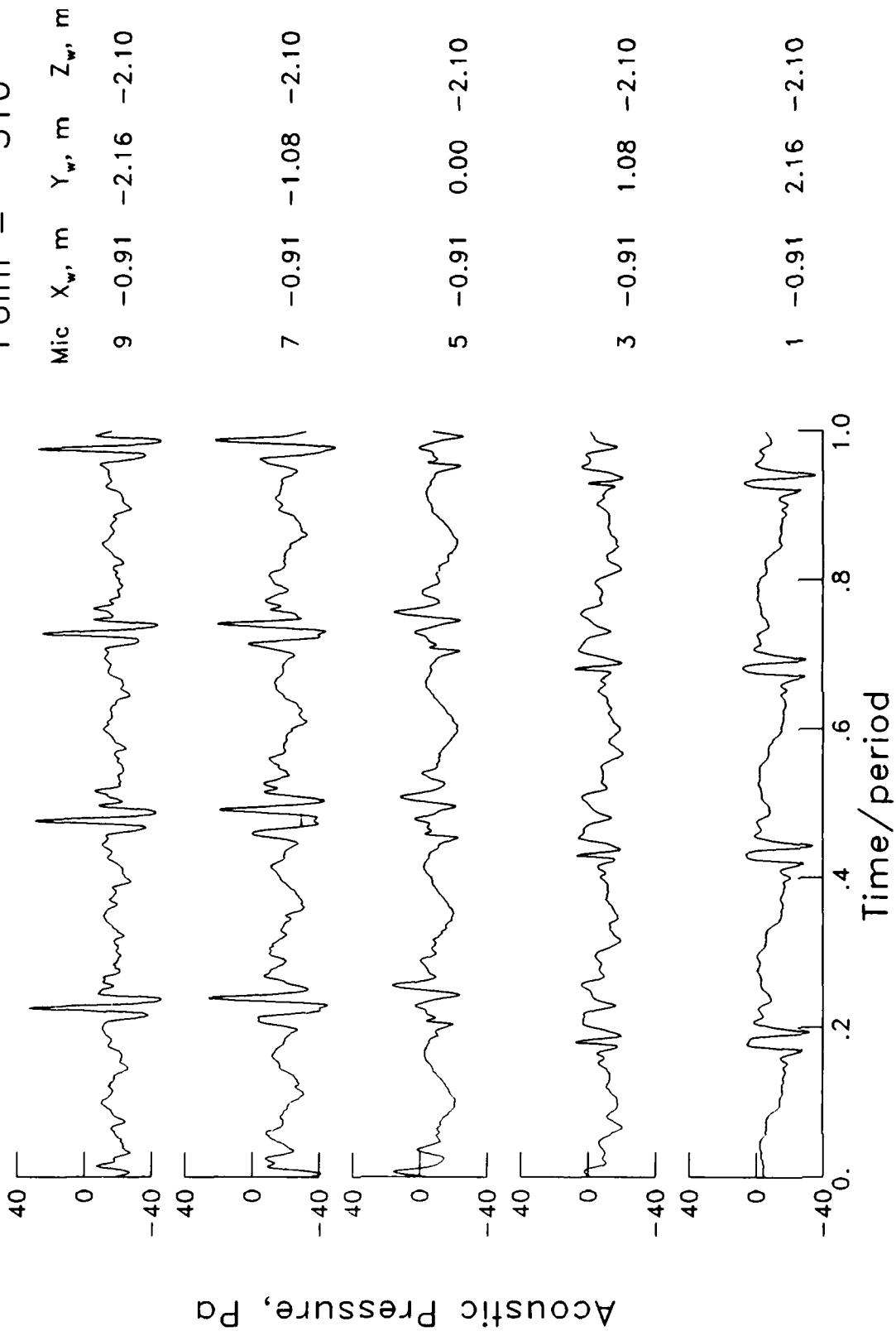
Mic	X _w , m	Y _w , m	Z _w , m
9	-0.81	-2.16	-2.10
7	-0.81	-1.08	-2.10
5	-0.81	0.00	-2.10
3	-0.81	1.08	-2.10
1	-0.81	2.16	-2.10



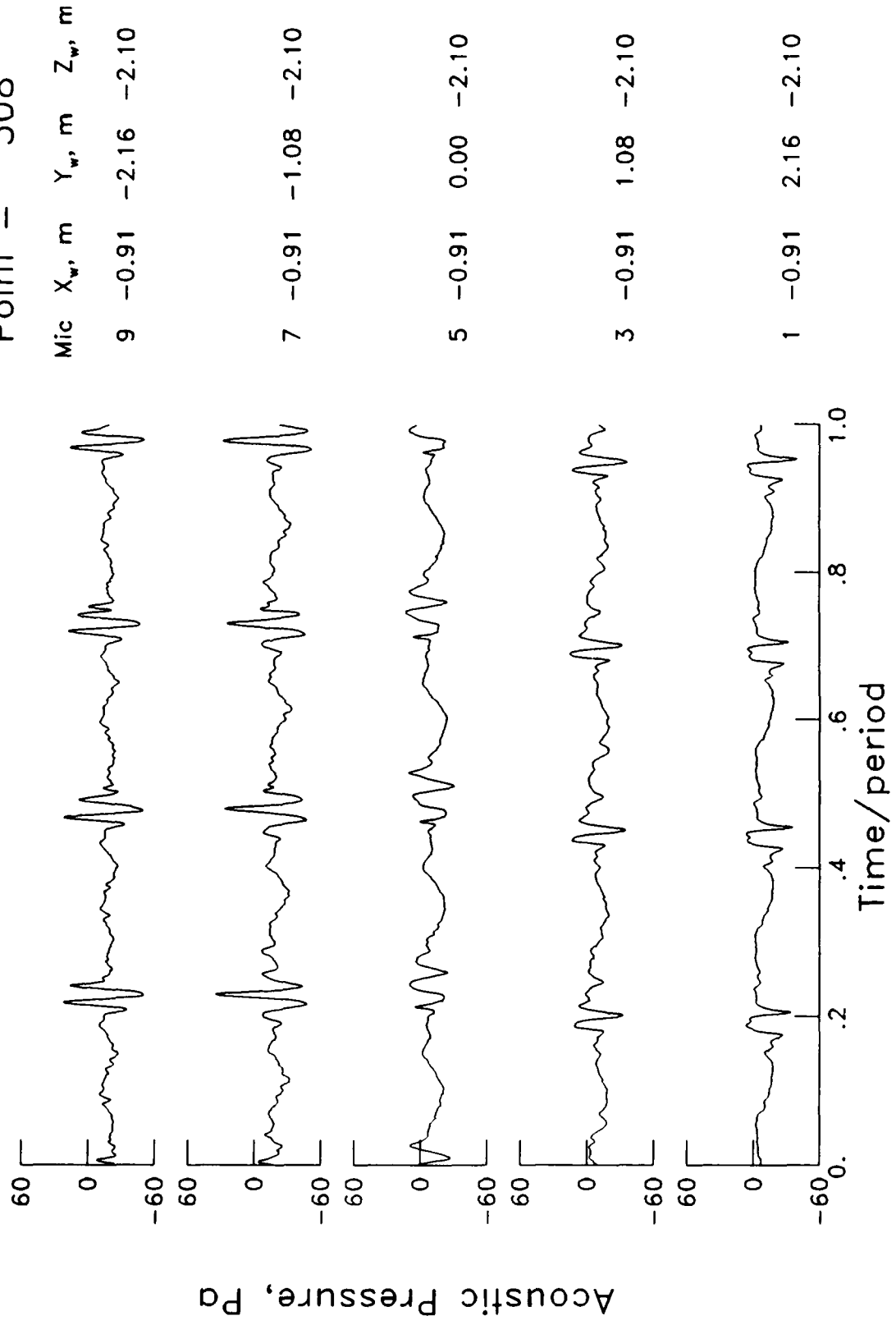
$\mu = .127$
 $\alpha_{TPP} = 2.9^\circ$
 $C_T = 0.0043$
 $M_H = 0.637$
 Point = 512



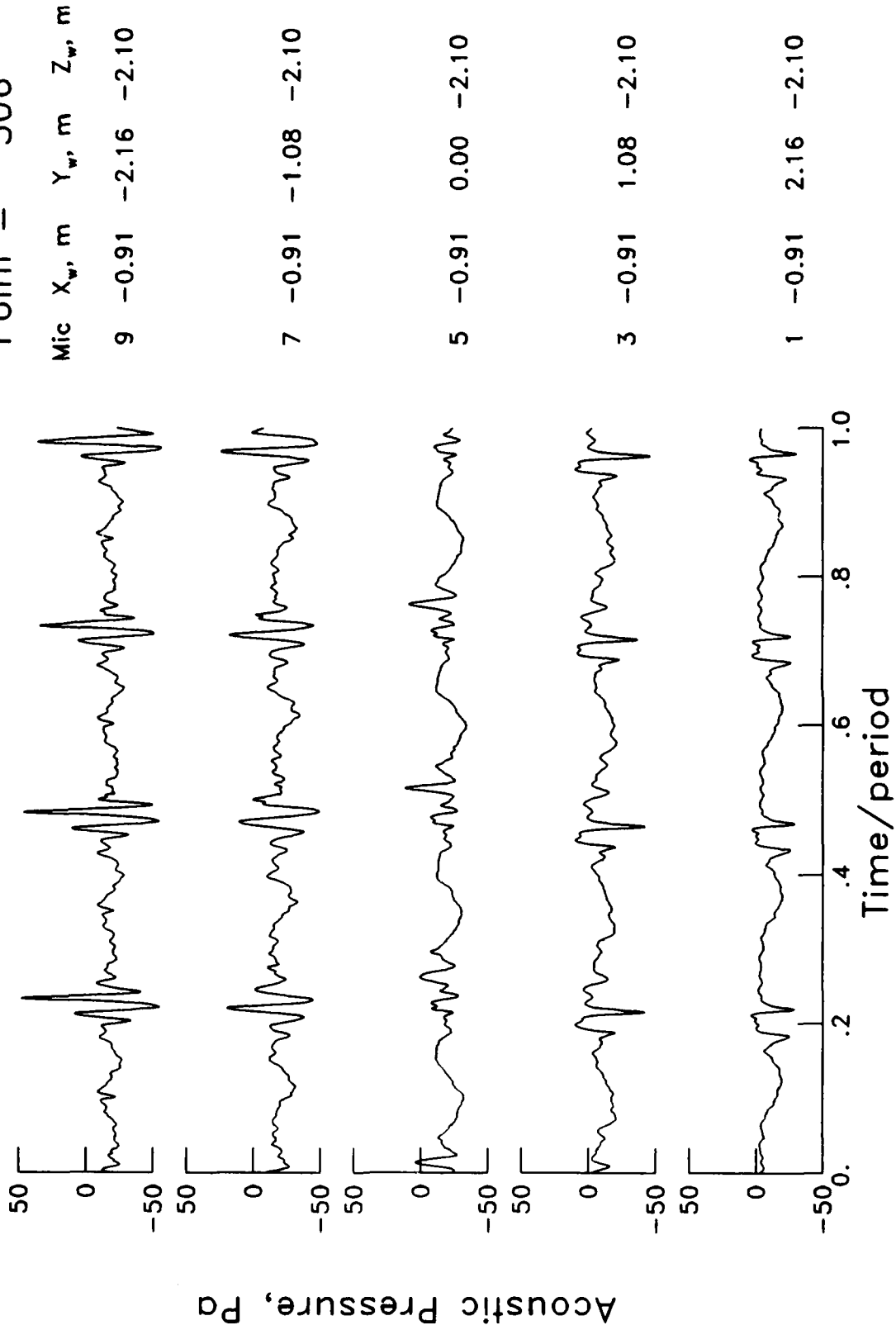
$\mu = .136$
 $\alpha_{TPP} = 3.2^\circ$
 $C_T = 0.0043$
 $M_H = 0.636$
 Point = 510



$\mu = .145$
 $\alpha_{TPP} = 3.4^\circ$
 $C_T = 0.0043$
 $M_{H_i} = 0.637$
 Point = 508



$\mu = .154$
 $\alpha_{TPP} = 3.6^\circ$
 $C_T = 0.0043$
 $M^H = 0.637$
 Point = 506



$\mu = .137$
 $\alpha_{TPP} = 3.2^\circ$
 $C_T = 0.0044$
 $M_H = 0.641$
 Point = 536

Mic X_w, m Y_w, m Z_w, m

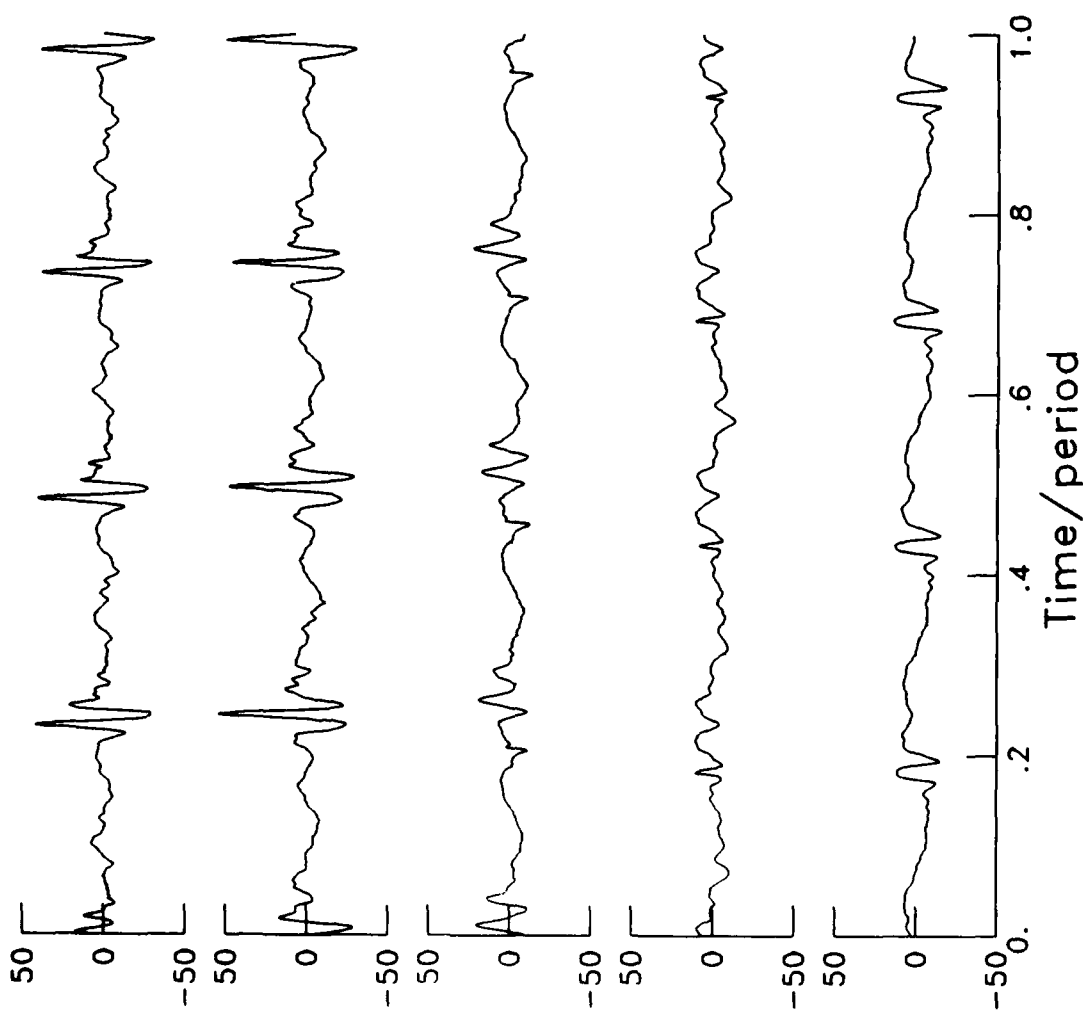
9 -0.46 -2.16 -2.10

7 -0.46 -1.08 -2.10

5 -0.46 0.00 -2.10

3 -0.46 1.08 -2.10

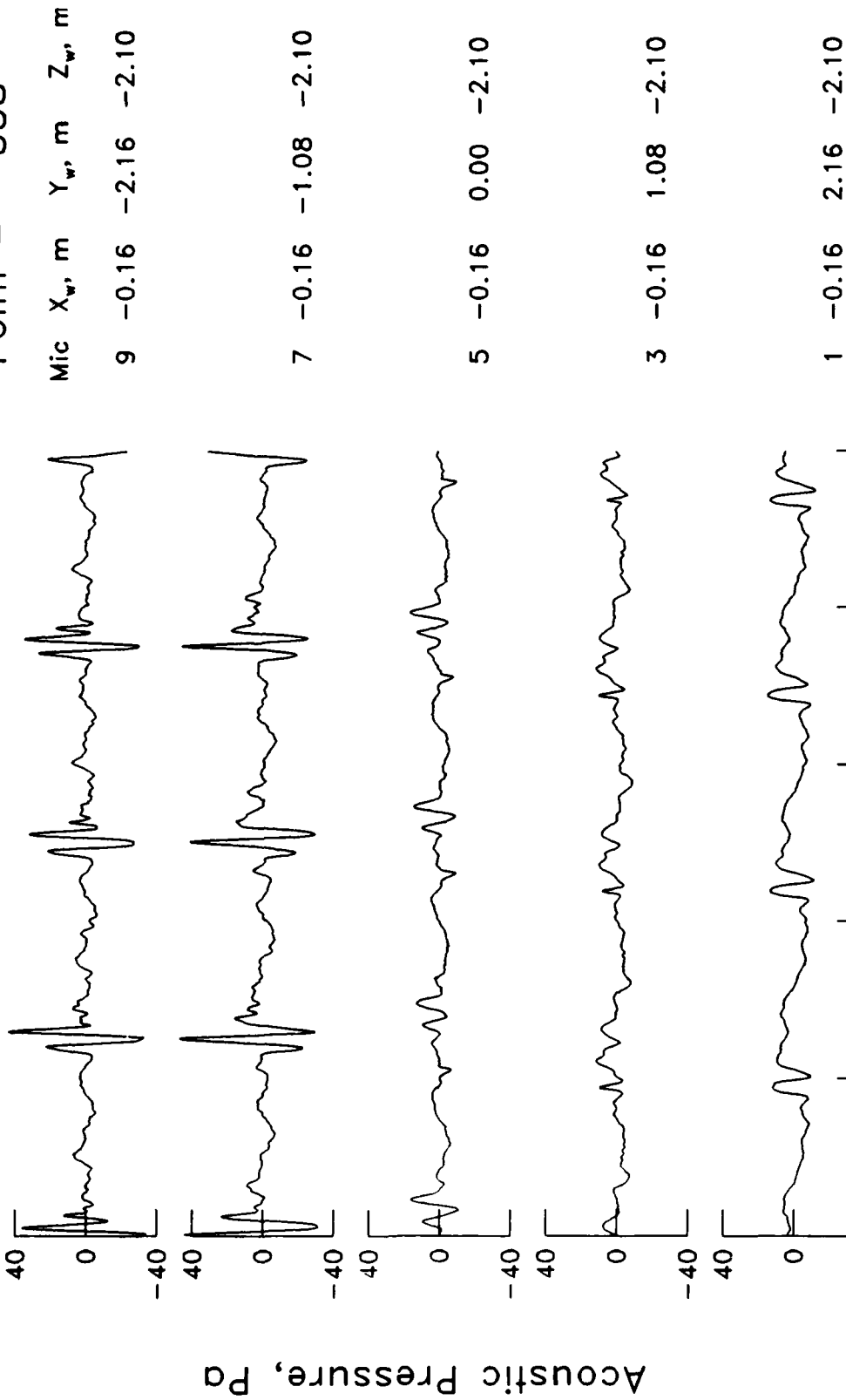
1 -0.46 2.16 -2.10



Acoustic Pressure, Pa

Time/period

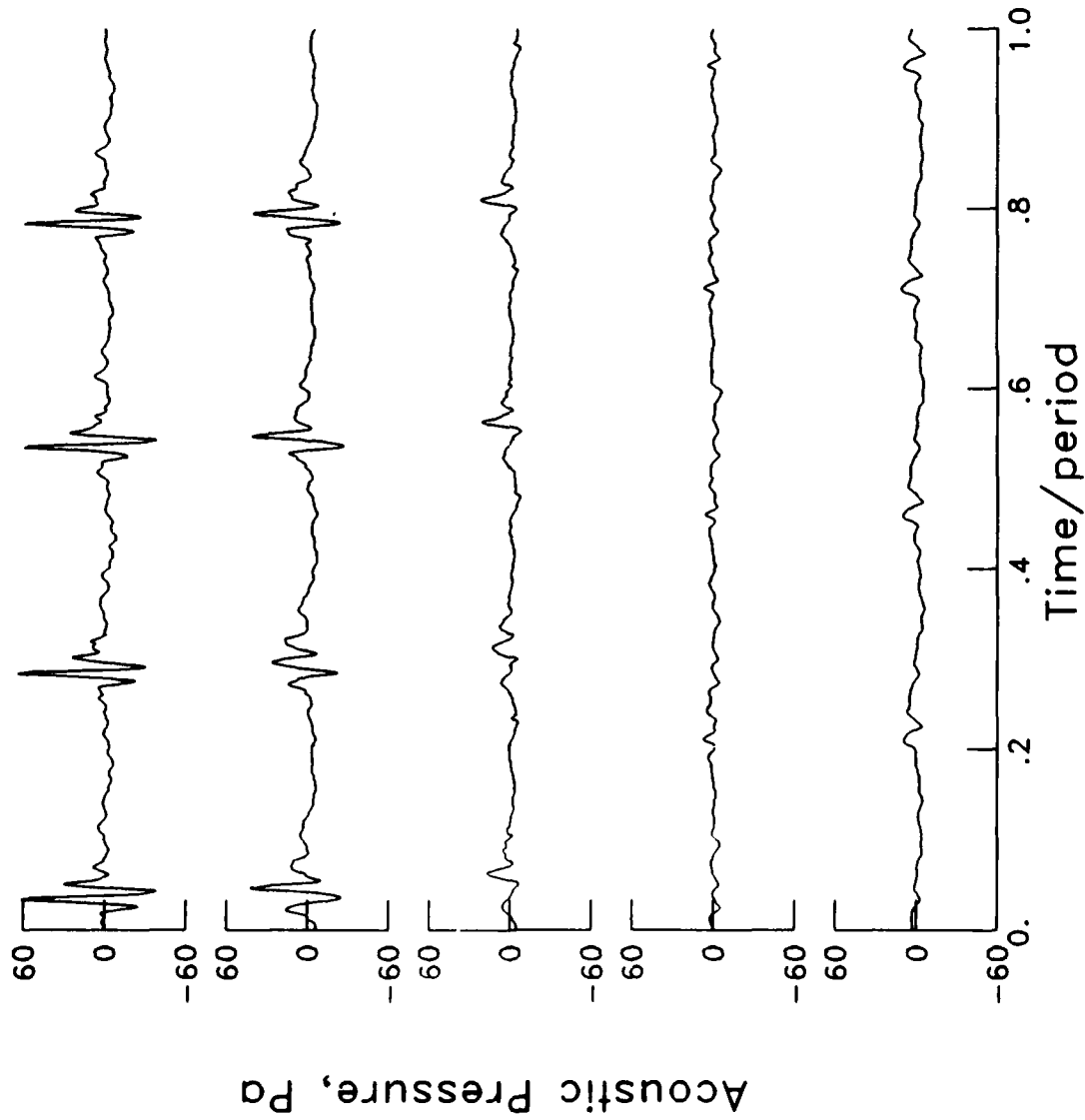
$\mu = .137$
 $\alpha_{TPP} = 3.2^\circ$
 $C_T = 0.0044$
 $M_{H_i} = 0.638$
 Point = 538



Acoustic Pressure, Pa

Time/period

$\mu = .137$
 $\alpha_{TPP} = 3.2^\circ$
 $C_T = 0.0043$
 $M_H = 0.636$
 Point = 540



Mic X_w, m Y_w, m Z_w, m
 9 0.64 -2.16 -2.10

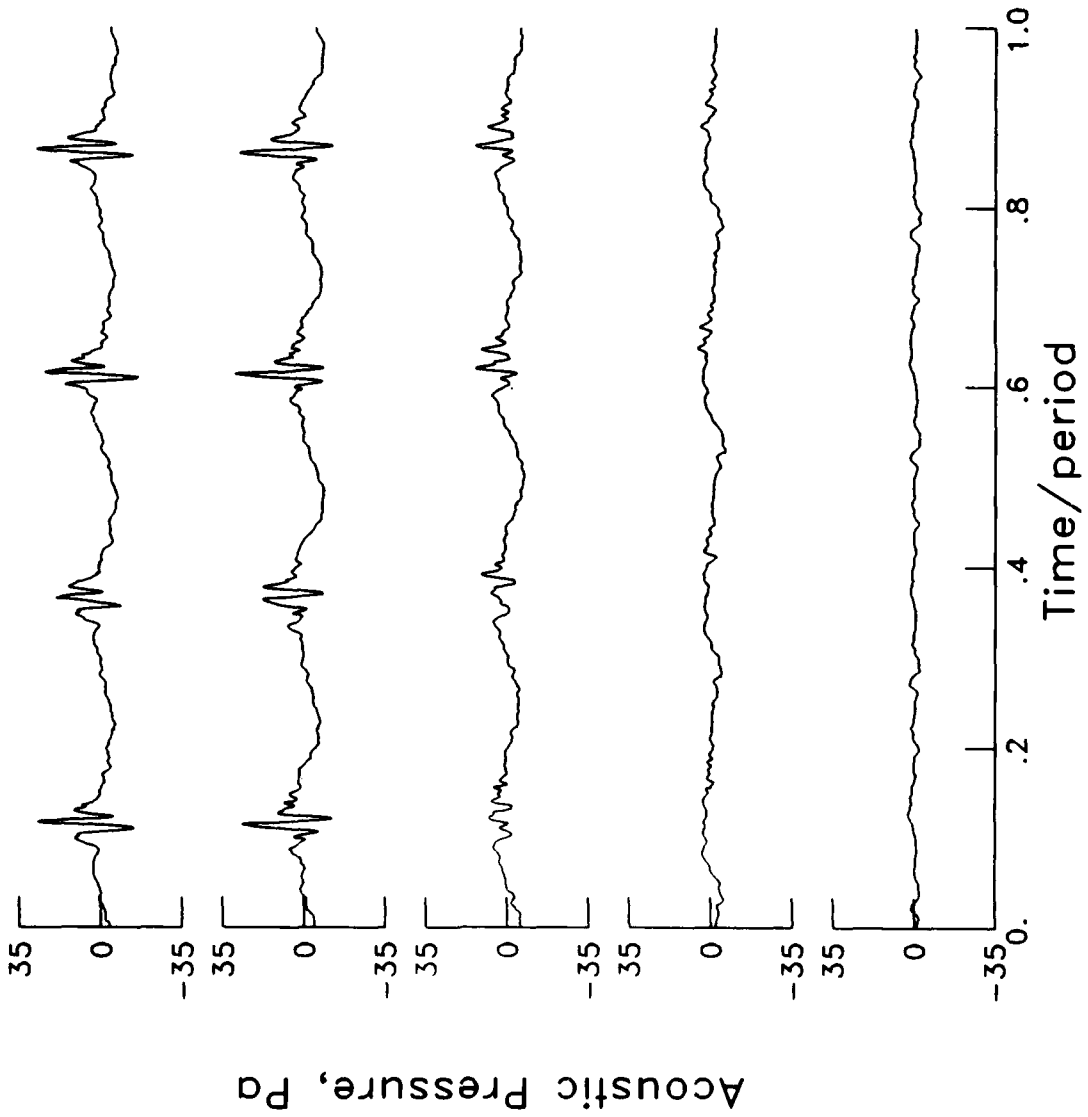
7 0.64 -1.08 -2.10

5 0.64 0.00 -2.10

3 0.64 1.08 -2.10

1 0.64 2.16 -2.10

$\mu = .138$
 $\alpha_{TPP} = 3.2^\circ$
 $C_T = 0.0043$
 $M_H = 0.636$
 Point = 542



Mic X_w , m Y_w , m Z_w , m
 9 2.24 -2.16 -2.10

7 2.24 -1.08 -2.10

5 2.24 0.00 -2.10

3 2.24 1.08 -2.10

1 2.24 2.16 -2.10

$\mu = .138$
 $\alpha_{TPP} = 3.2^\circ$
 $C_T = 0.0043$
 $M_{H,Point} = 0.637$
 $Point = 544$

Mic X_w, m Y_w, m Z_w, m

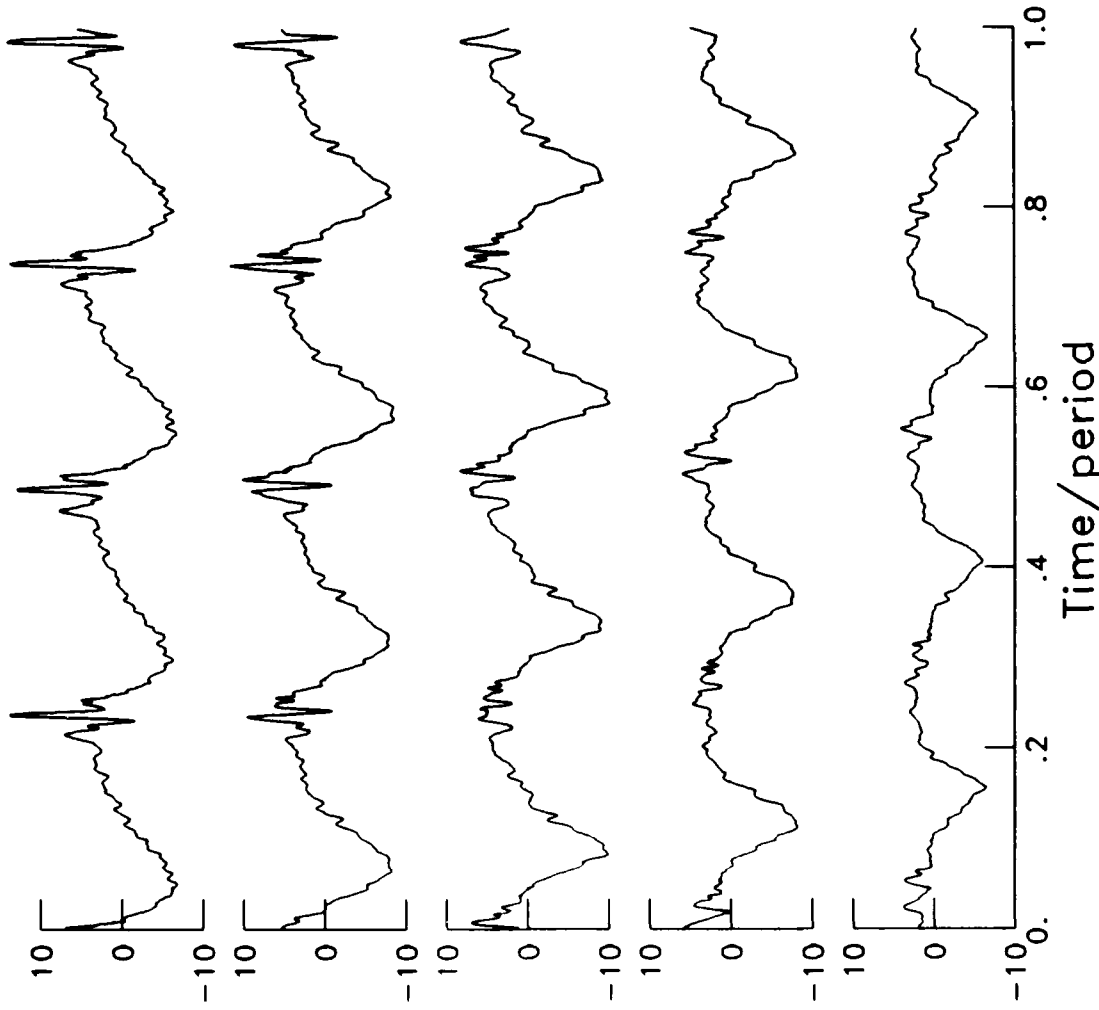
9 4.64 -2.16 -2.10

7 4.64 -1.08 -2.10

5 4.64 0.00 -2.10

3 4.64 1.08 -2.10

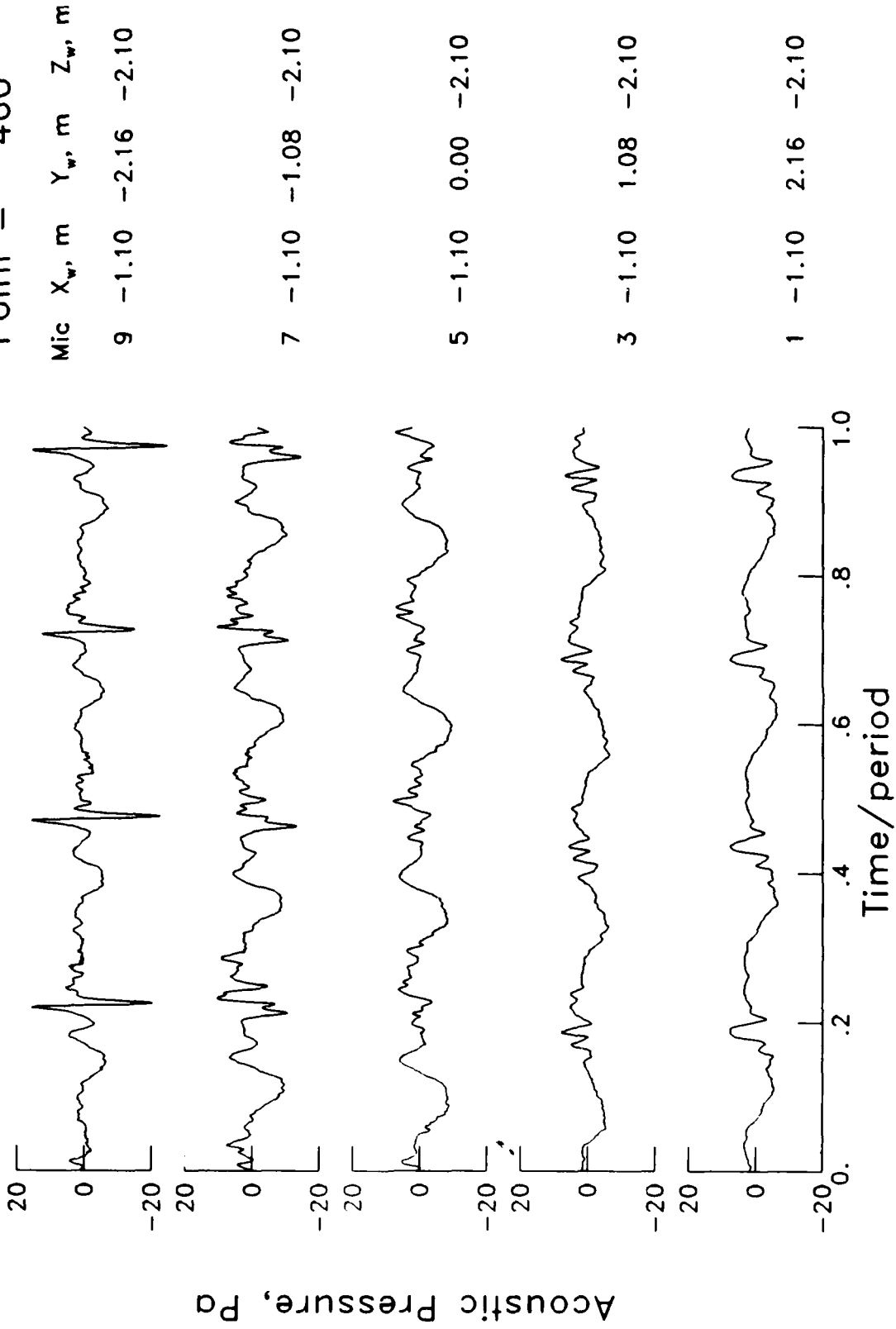
1 4.64 2.16 -2.10



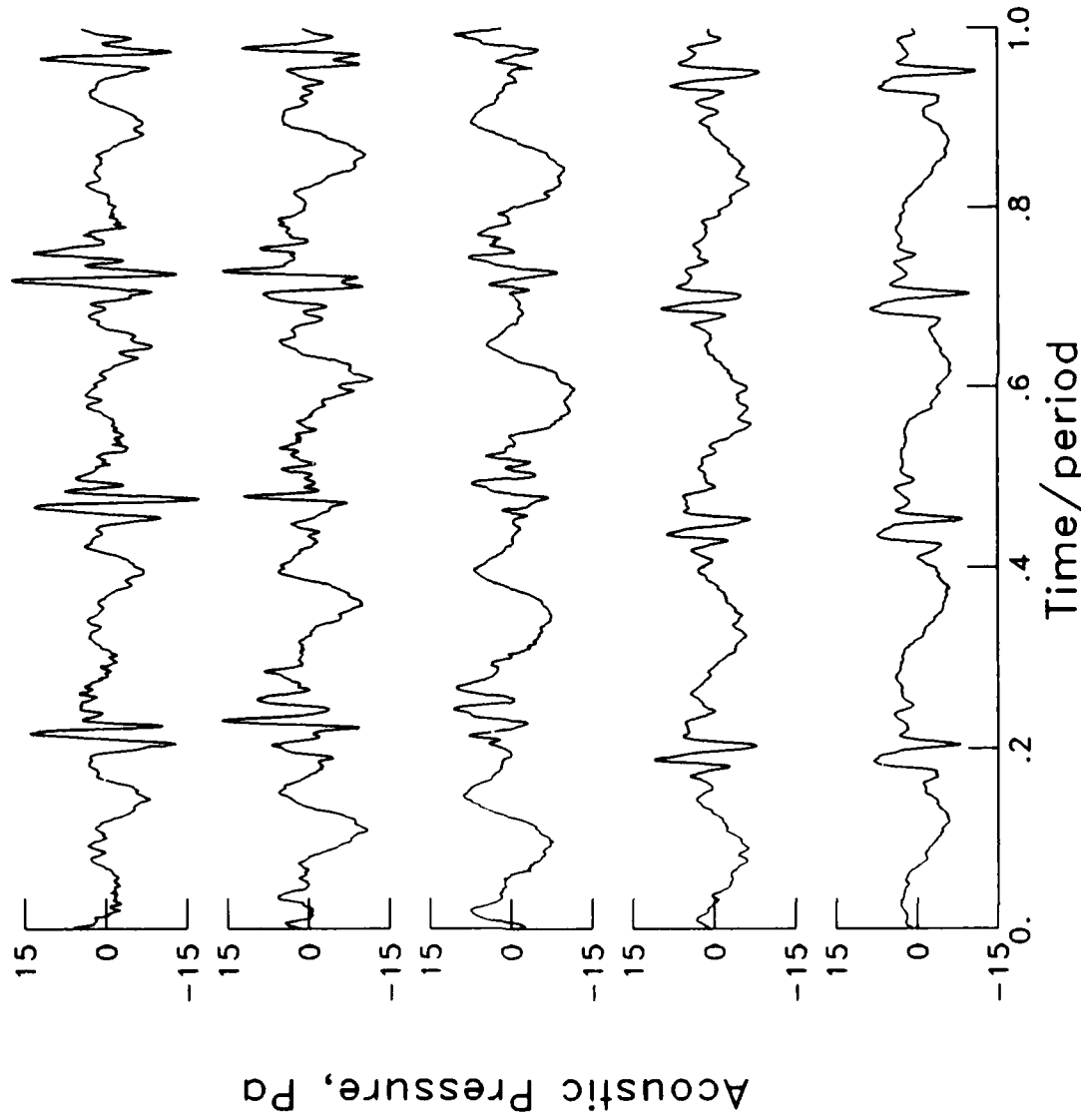
Acoustic Pressure, Pa

Time/period

$\mu = .139$
 $\alpha_{TPP} = -0.2^\circ$
 $C_T = 0.0029$
 $M_H = 0.637$
 Point = 460



$\mu = .138$
 $\alpha_{TPP} = 1.3^\circ$
 $C_T = 0.0029$
 $M_H = 0.638$
 Point = 457



Mic X_w , m Y_w , m Z_w , m
 9 -1.03 -2.16 -2.10

7 -1.03 -1.08 -2.10

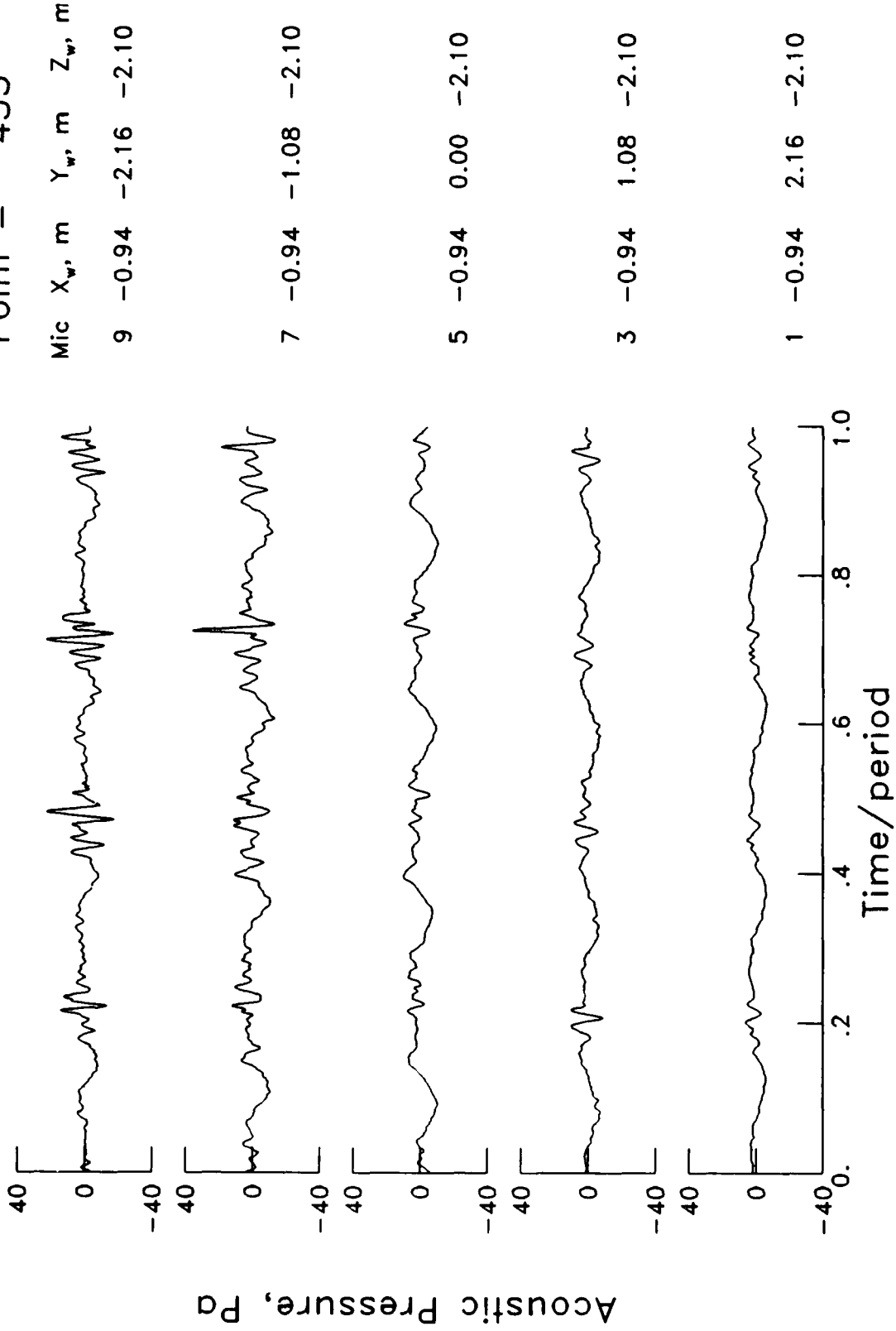
5 -1.03 0.00 -2.10

3 -1.03 1.08 -2.10

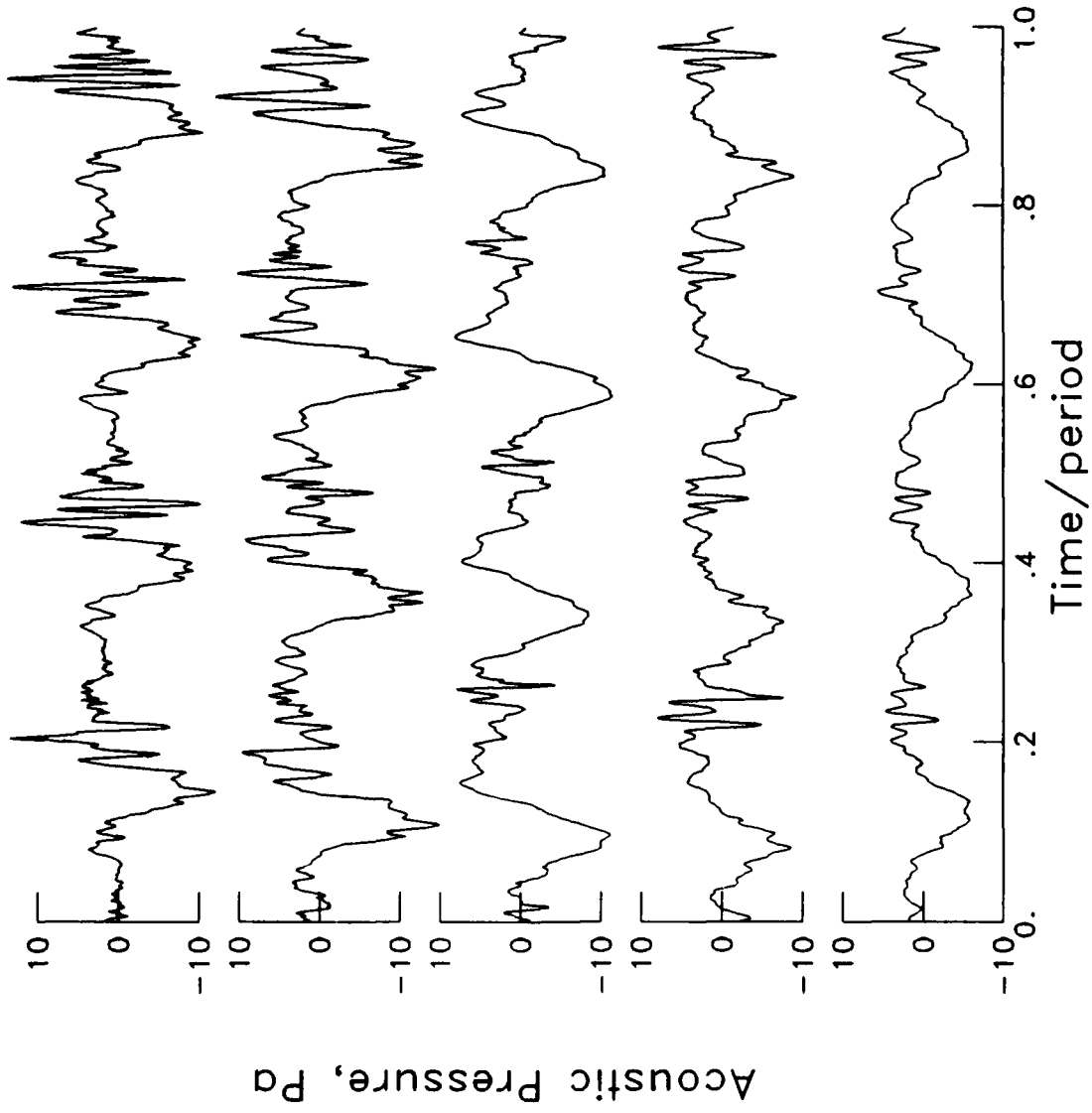
1 -1.03 2.16 -2.10

Acoustic Pressure, Pa

$\mu = .139$
 $\alpha_{TPP} = 3.4^\circ$
 $C_T = 0.0029$
 $M_{H_i} = 0.637$
 Point = 453



$\mu = .137$
 $\alpha_{TPP} = 5.9^\circ$
 $C_T = 0.0029$
 $M_H = 0.637$
 Point = 448



Mic X_w , m Y_w , m Z_w , m

9 -0.81 -2.16 -2.10

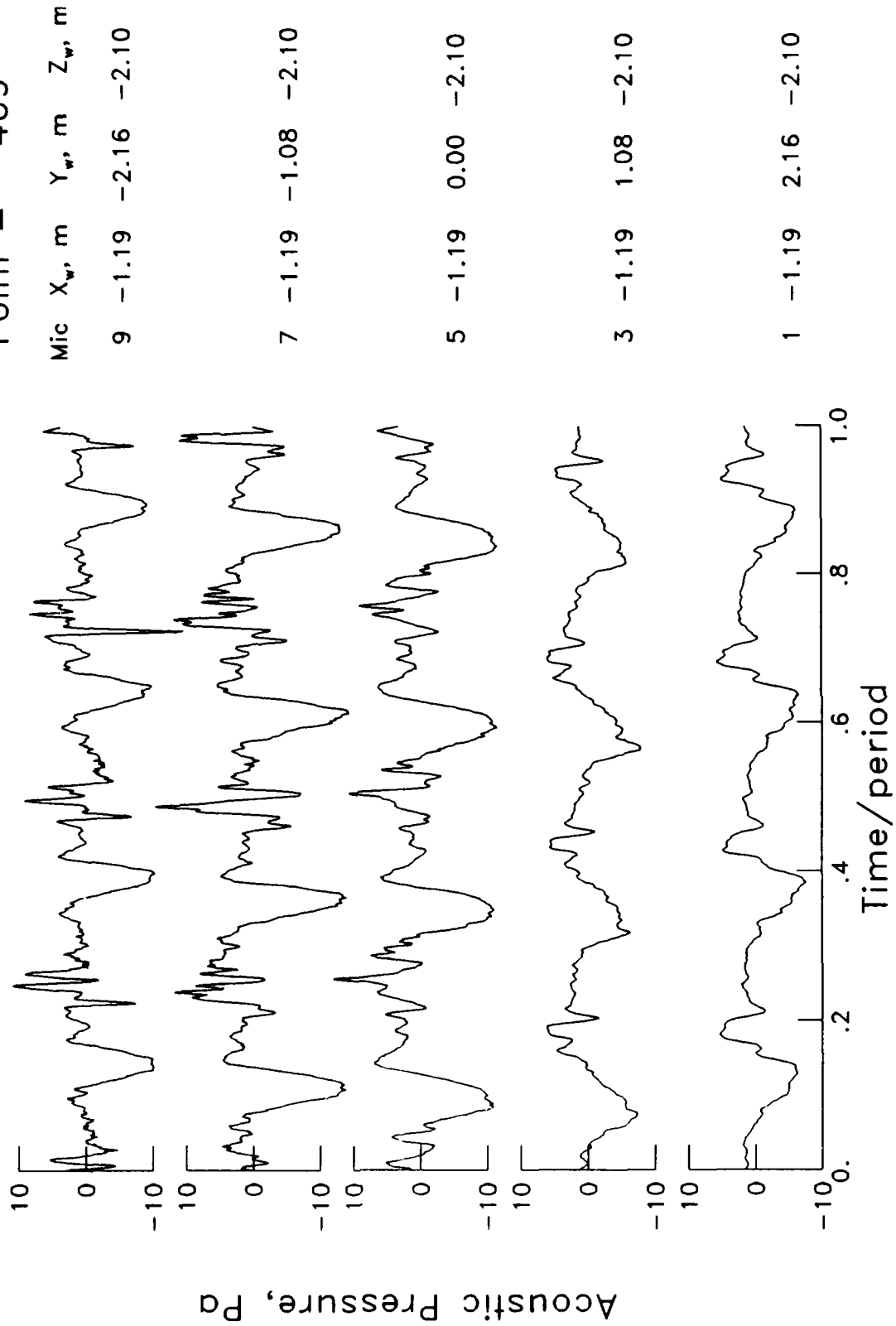
7 -0.81 -1.08 -2.10

5 -0.81 0.00 -2.10

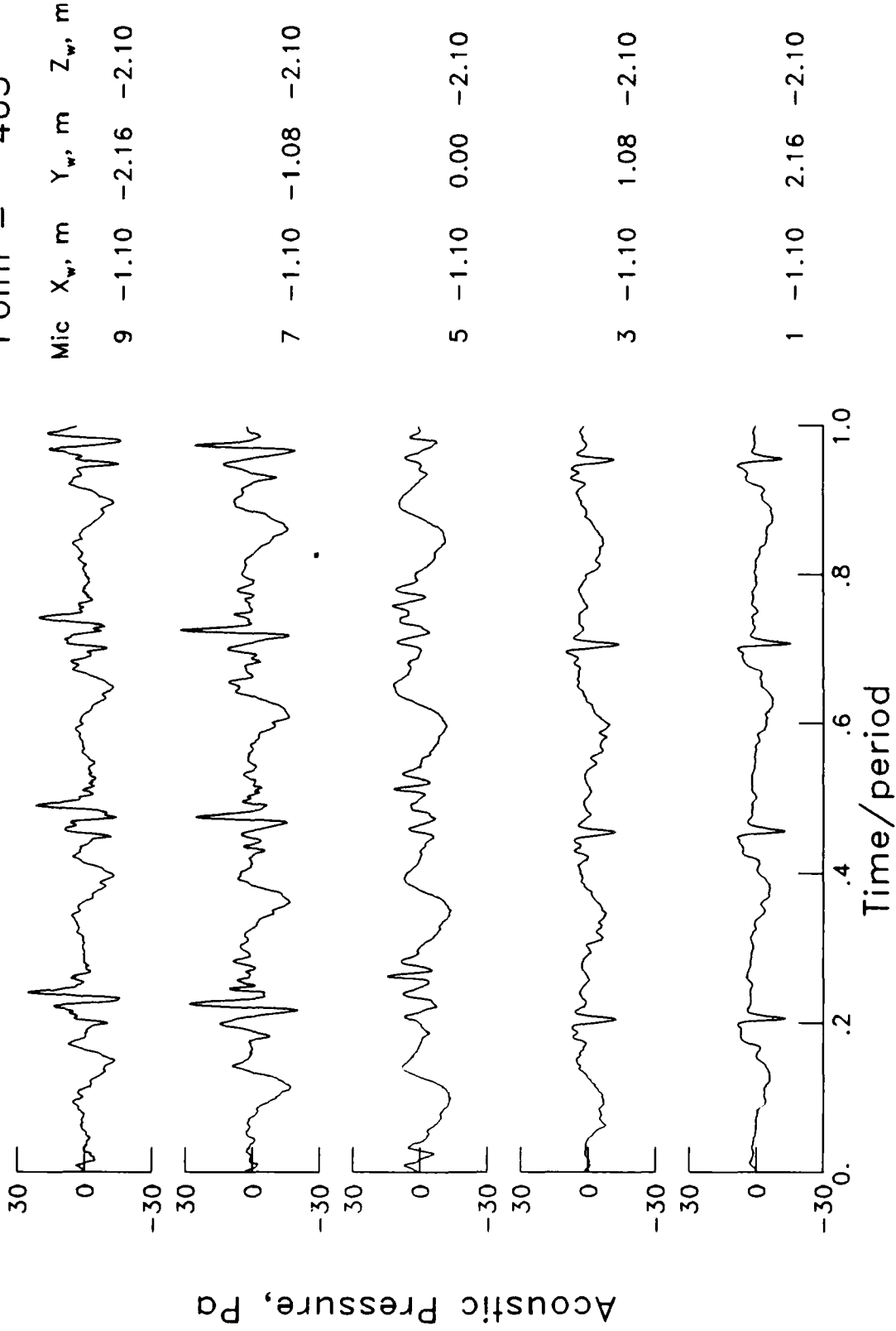
3 -0.81 1.08 -2.10

1 -0.81 2.16 -2.10

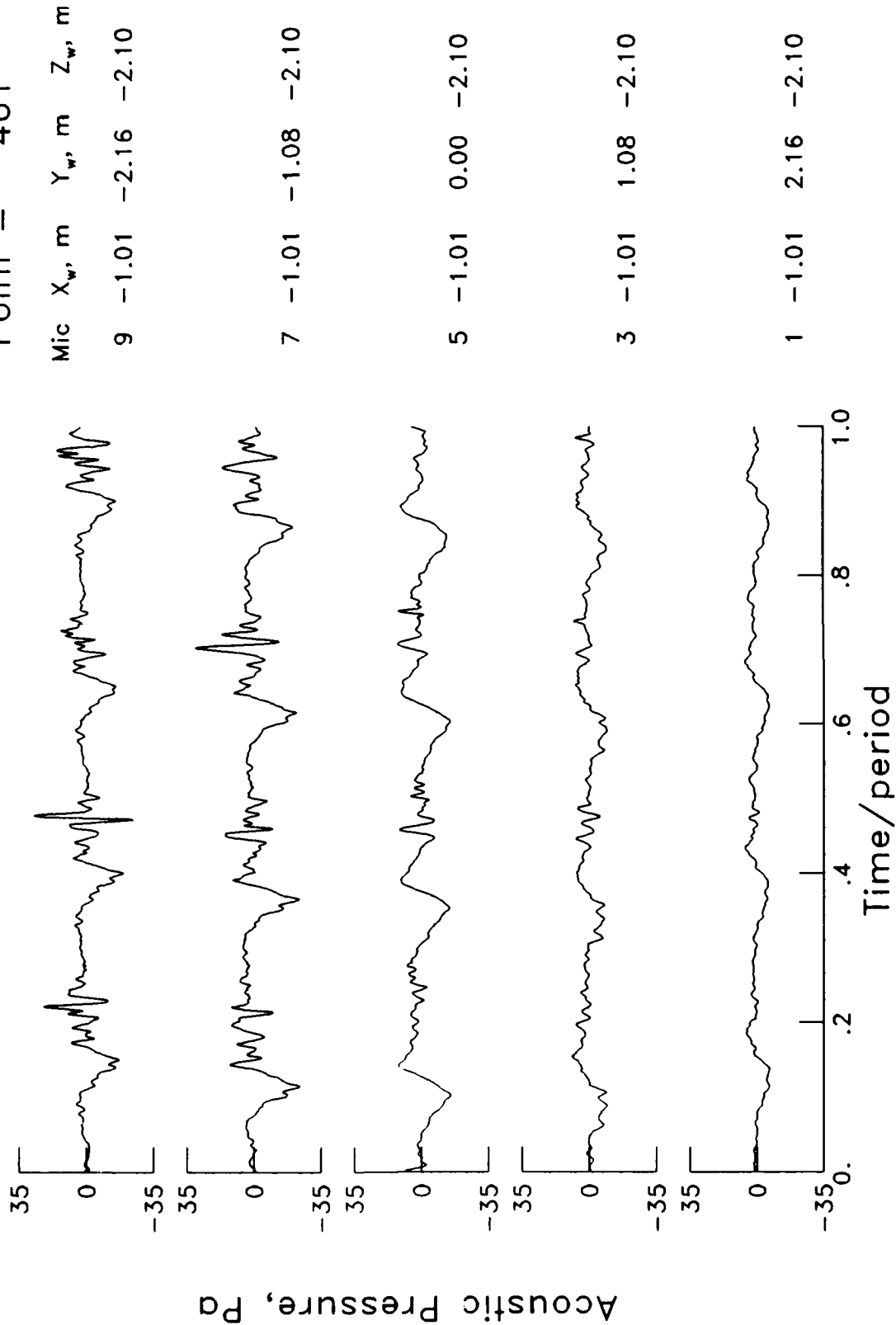
$\mu = .184$
 $\alpha_{TPP} = -1.6^\circ$
 $C_T = 0.0029$
 $M_H = 0.636$
 Point = 469



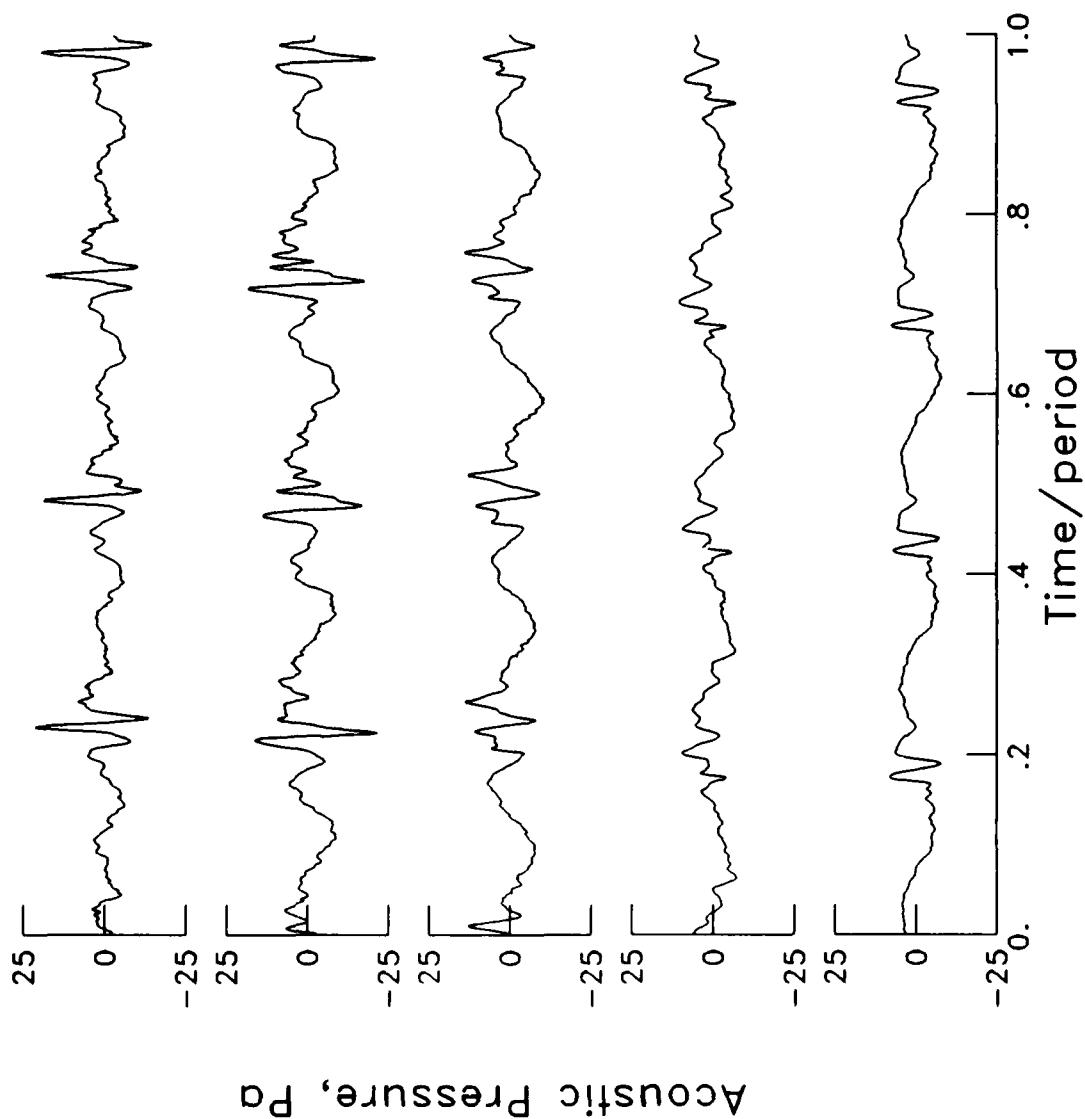
$\mu = .185$
 $\alpha_{TPP} = 0.4^\circ$
 $C_T = 0.0029$
 $M_H = 0.636$
 Point = 465



$\mu = .184$
 $\alpha_{TPP} = 2.4^\circ$
 $C_T = 0.0029$
 $M_H = 0.637$
 Point = 461

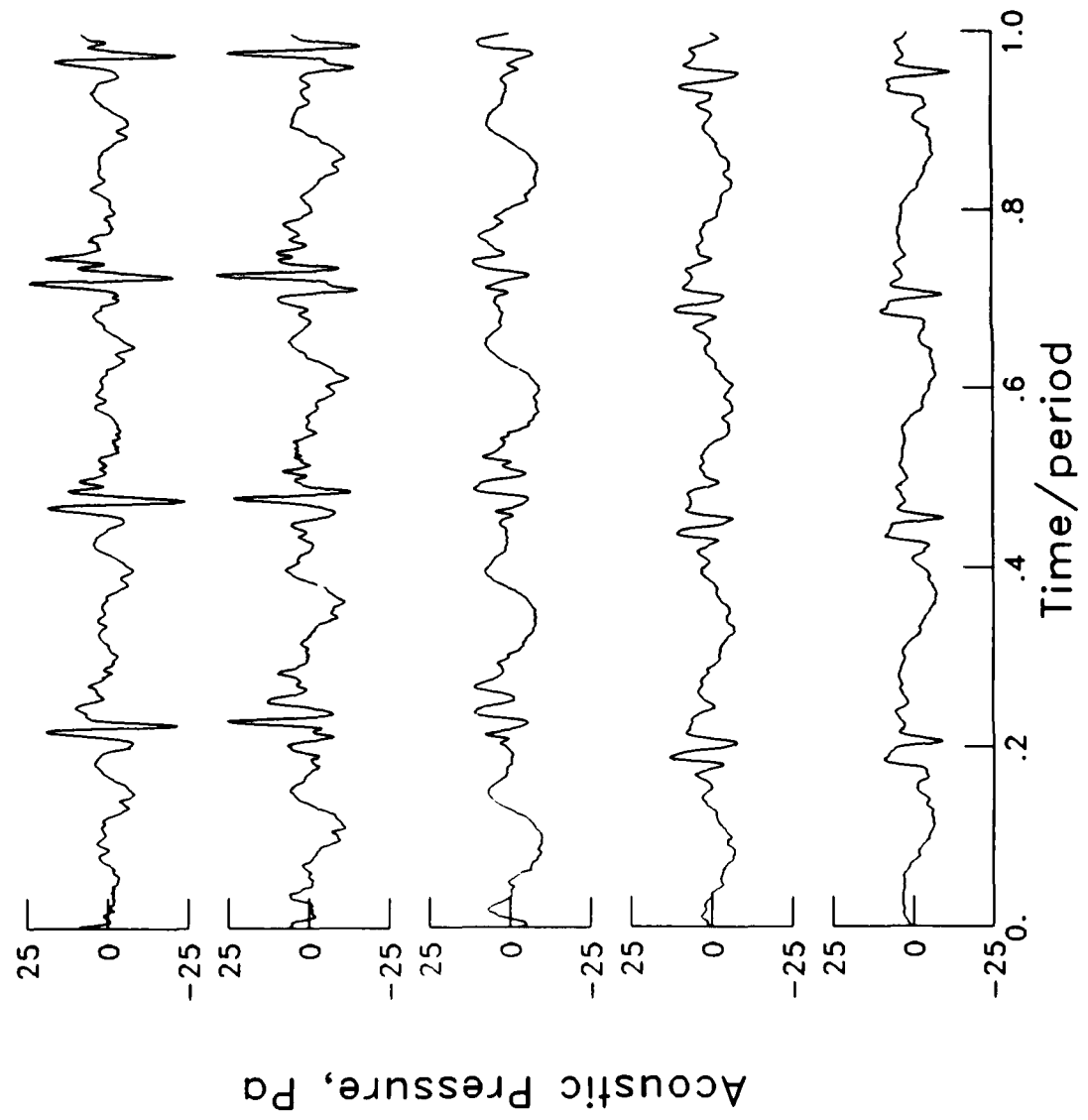


$\mu = .126^\circ$
 $\alpha_{TPP} = 1.4^\circ$
 $C_T = 0.0029$
 $M_H = 0.638$
 Point = 489

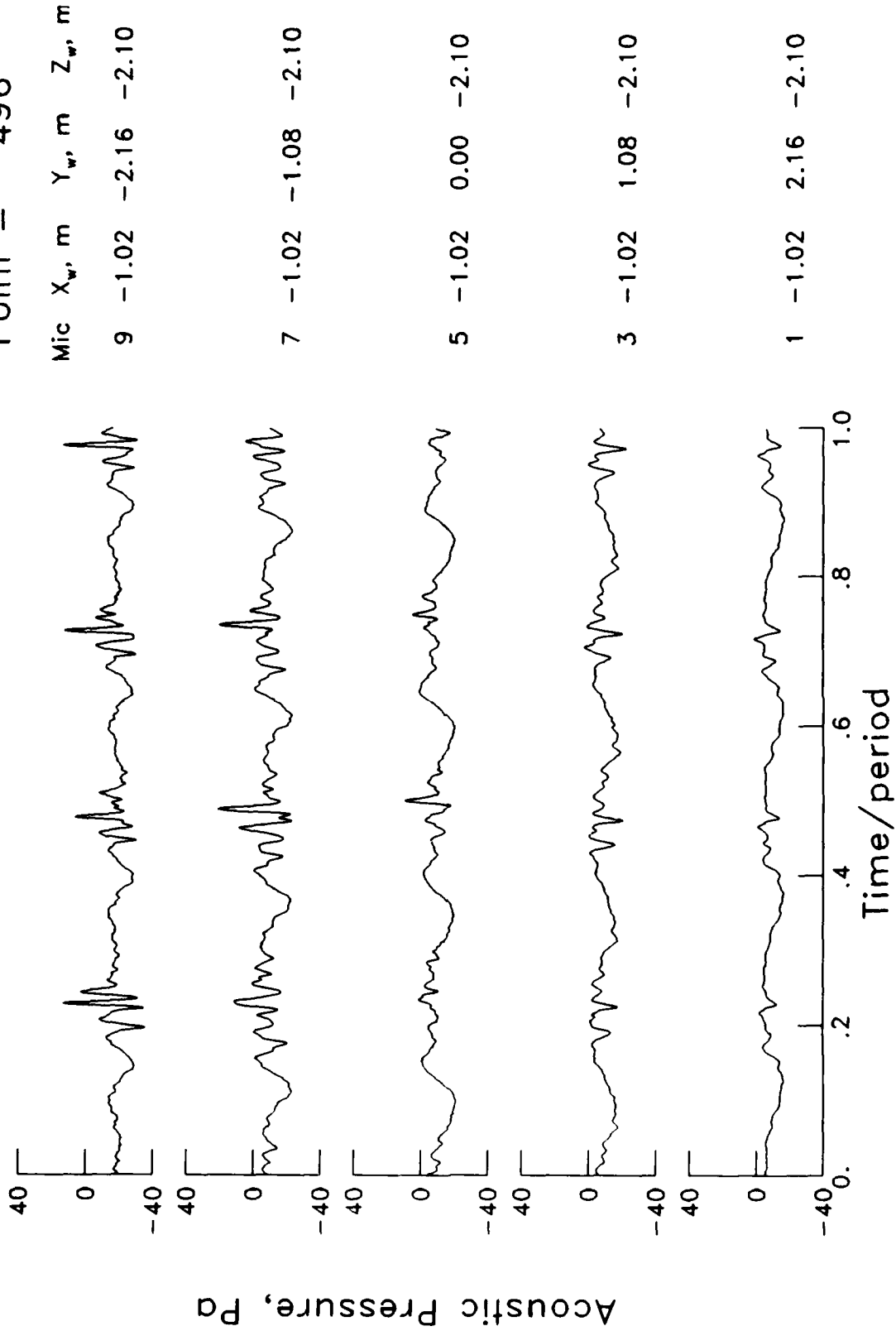


$\mu = .142$
 $\alpha_{TPP} = 1.6^\circ$
 $C_T = 0.0029$
 $M_H = 0.640$
 Point = 492

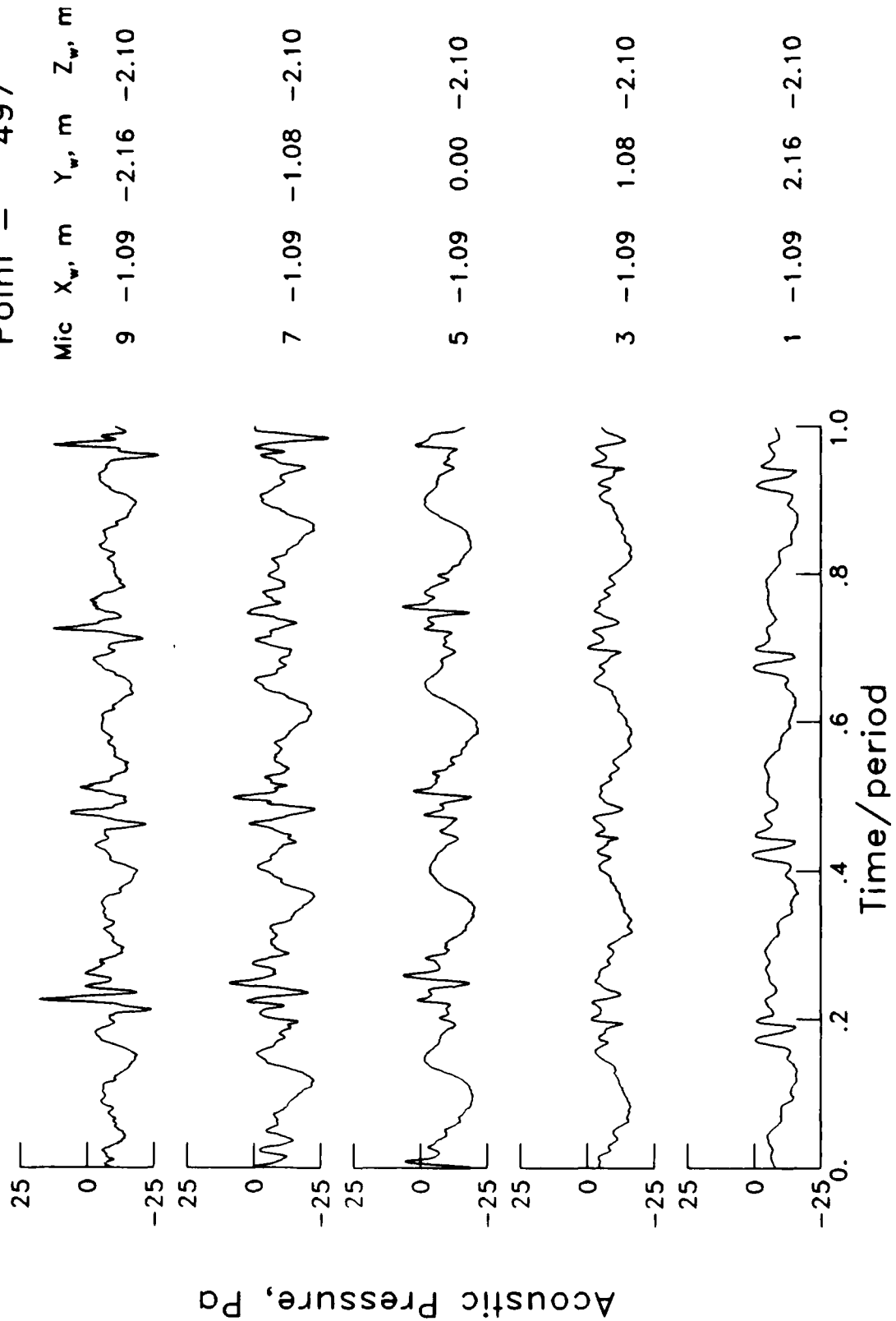
Mic	X _w , m	Y _w , m	Z _w , m
9	-1.02	-2.16	-2.10
7	-1.02	-1.08	-2.10
5	-1.02	0.00	-2.10
3	-1.02	1.08	-2.10
1	-1.02	2.16	-2.10



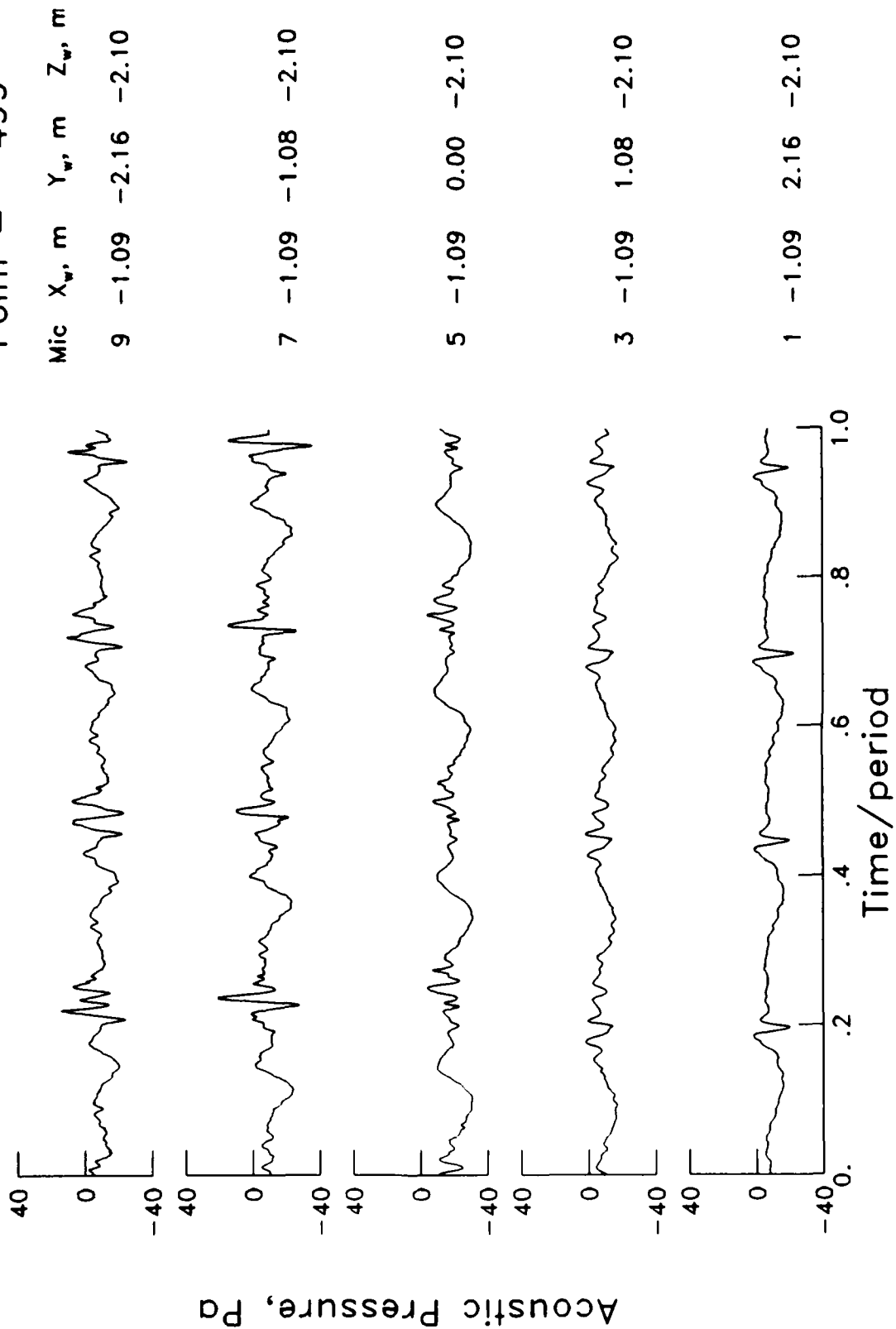
$\mu = .159$
 $\alpha_{TPP} = 1.9^\circ$
 $C_T = 0.0029$
 $M_H = 0.641$
 Point = 496



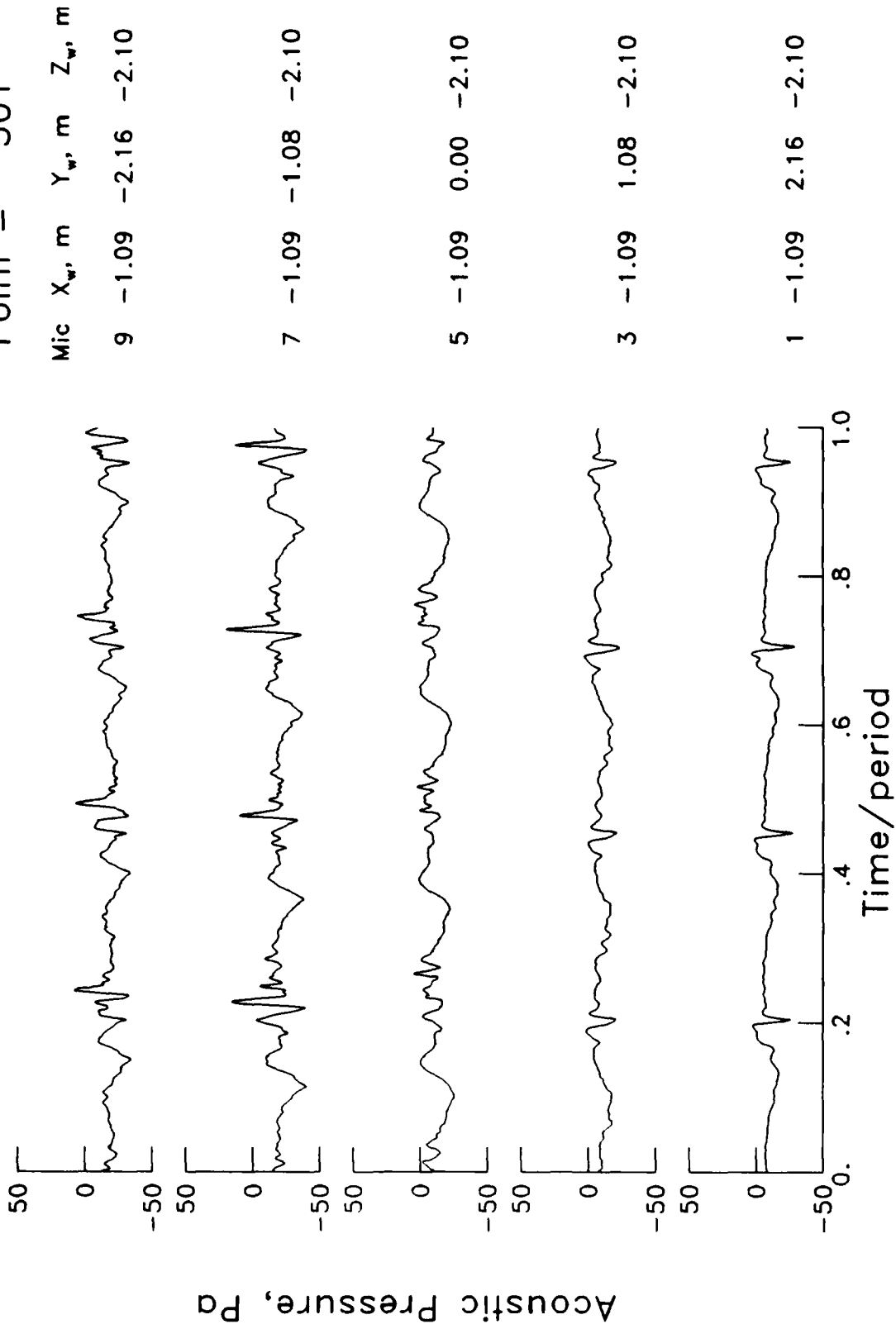
$\mu = .164$
 $\alpha_{TPP} = 0.4^\circ$
 $C_T = 0.0029$
 $M_H = 0.638$
 Point = 497



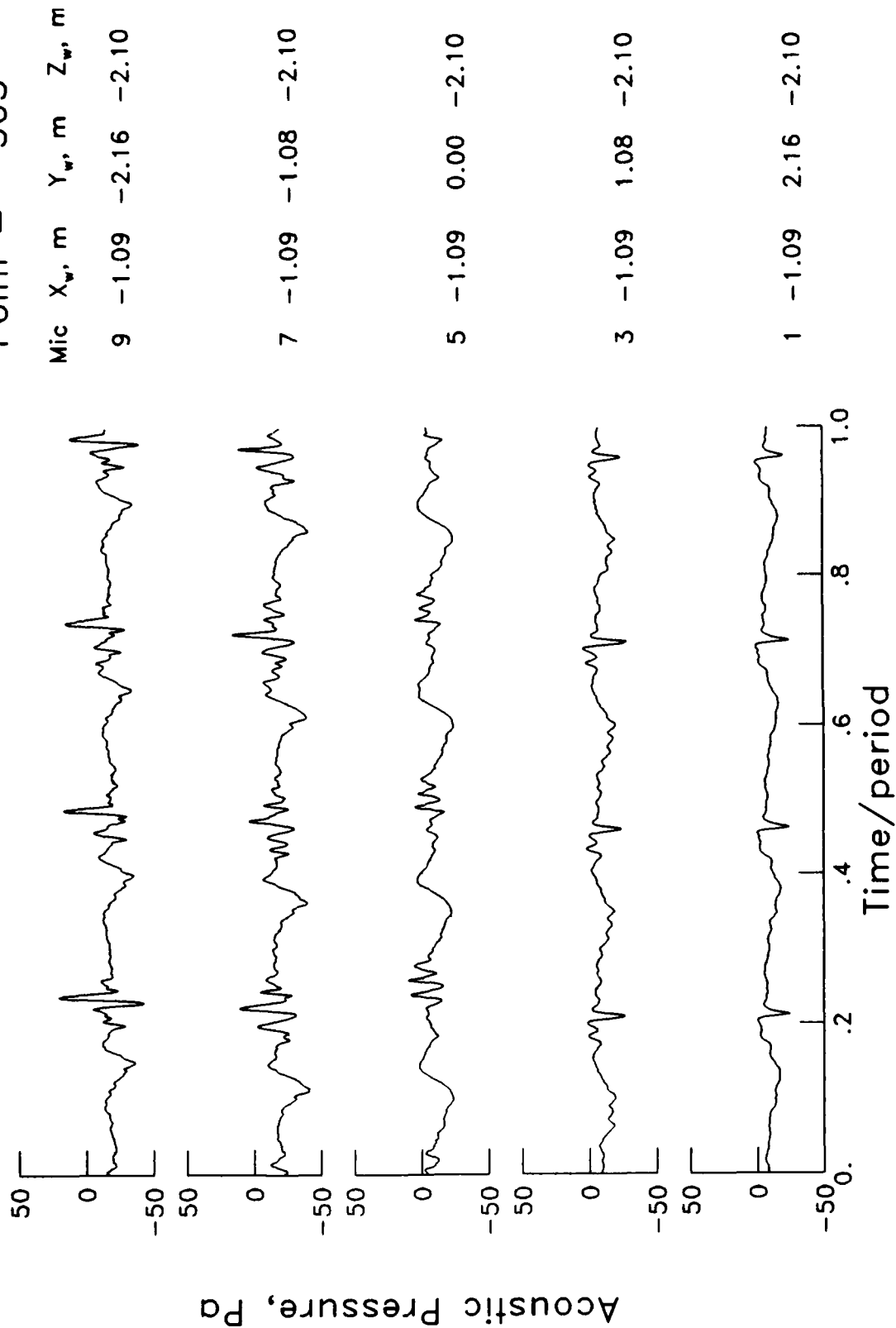
$\mu = .173$
 $\alpha_{TPP} = 0.5^\circ$
 $C_T = 0.0029$
 $M_H = 0.638$
 Point = 499



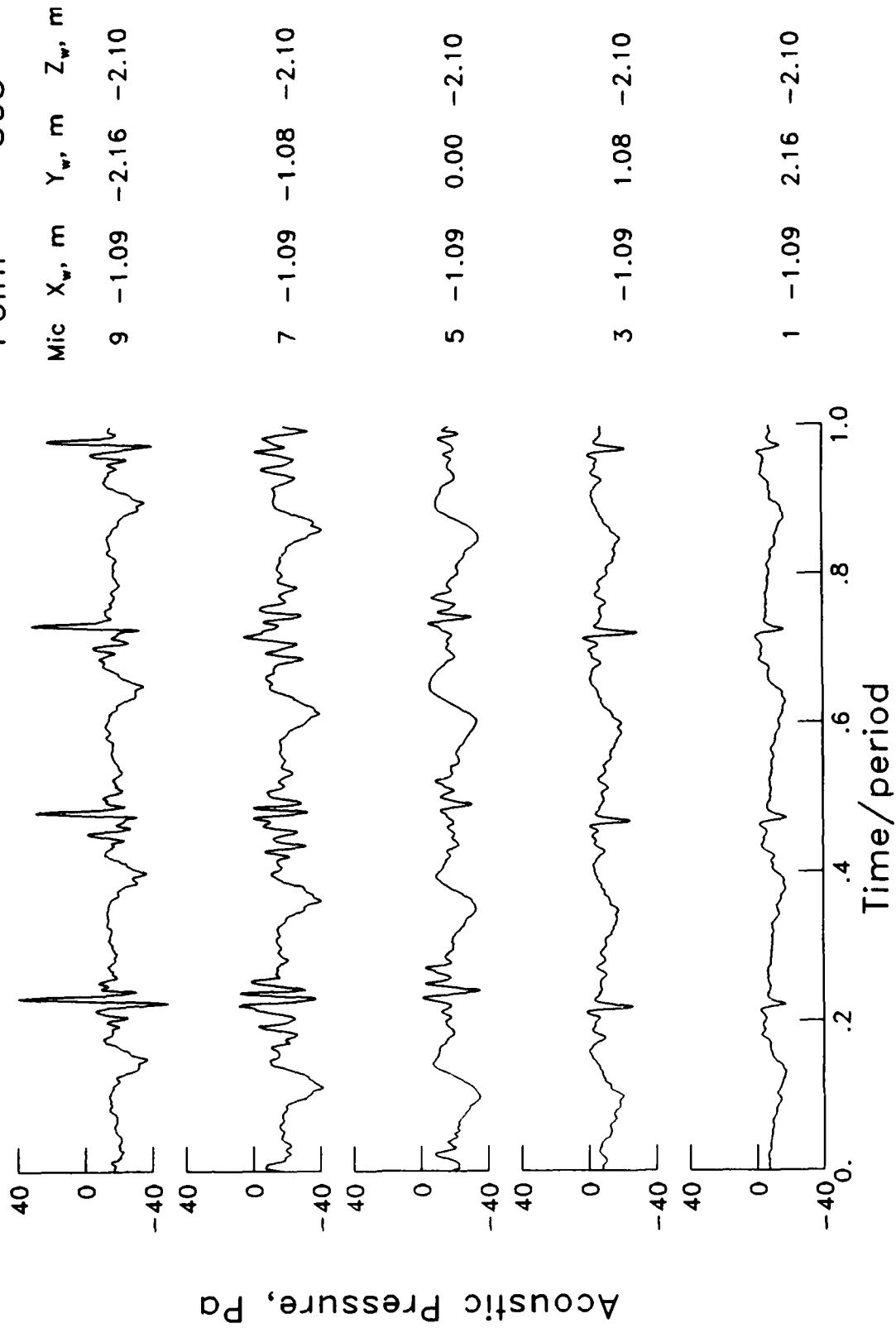
$\mu = .182$
 $\alpha_{TPP} = 0.6^\circ$
 $C_T = 0.0029$
 $M_{H_i} = 0.638$
 Point = 501



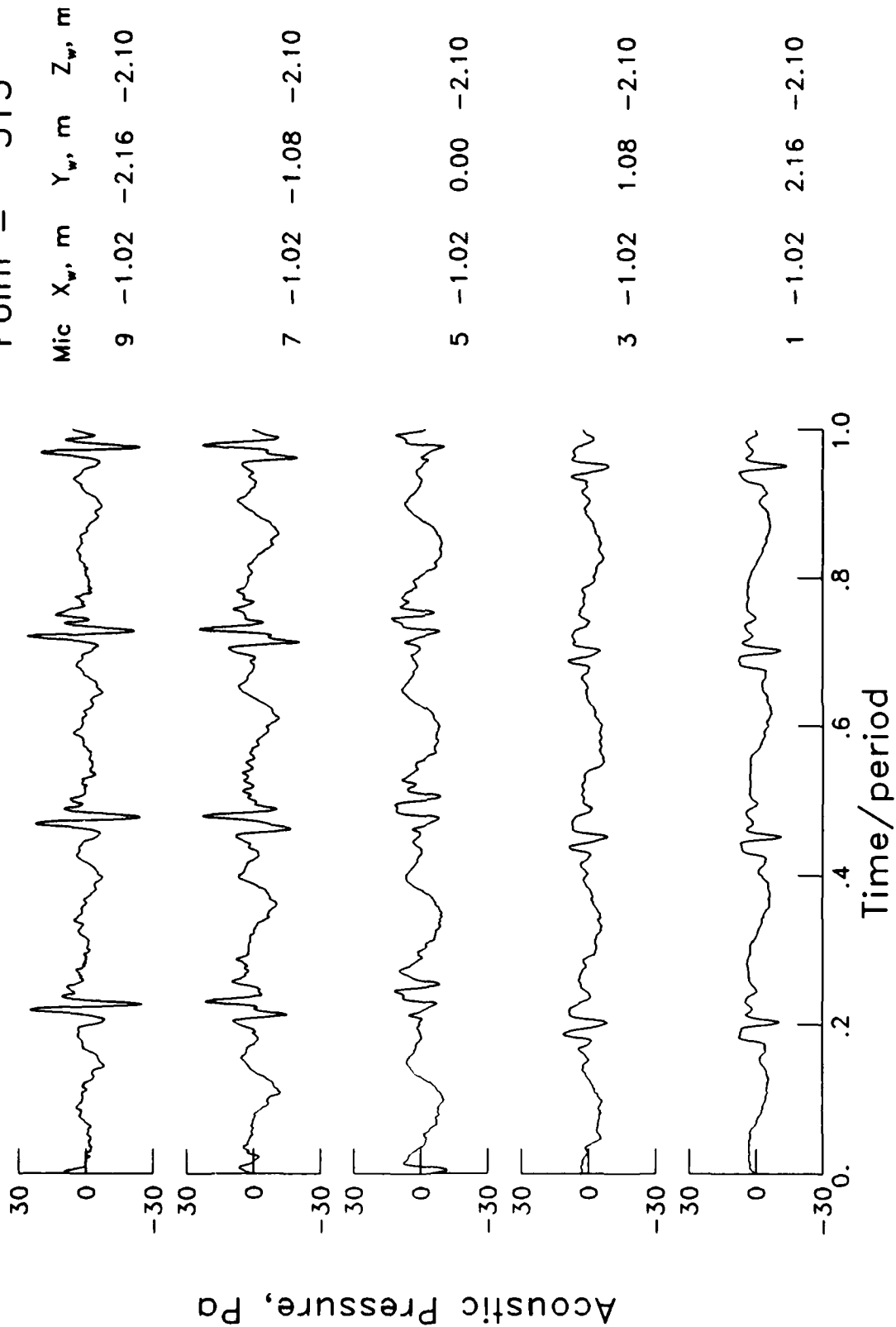
$\mu = .192$
 $\alpha_{TPP} = 0.6^\circ$
 $C_T = 0.0029$
 $M_H = 0.637$
 Point = 503



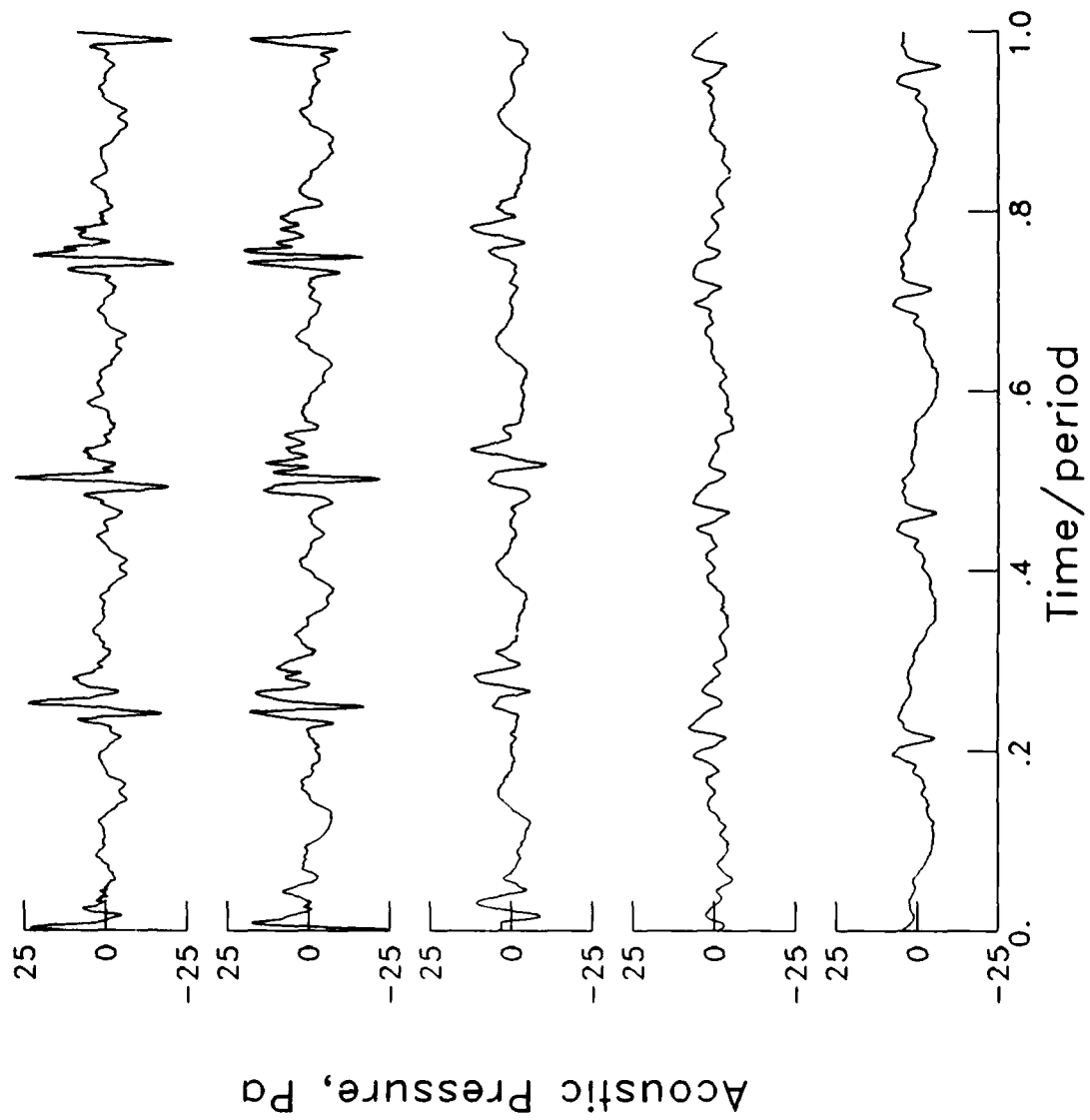
$\mu = .200$
 $\alpha_{TPP} = 0.7^\circ$
 $C_T = 0.0030$
 $M_H = 0.638$
 Point = 505



$\mu = .139$
 $\alpha_{TPP} = 1.6^\circ$
 $C_T = 0.0030$
 $M_{H_1} = 0.638$
 Point = 515

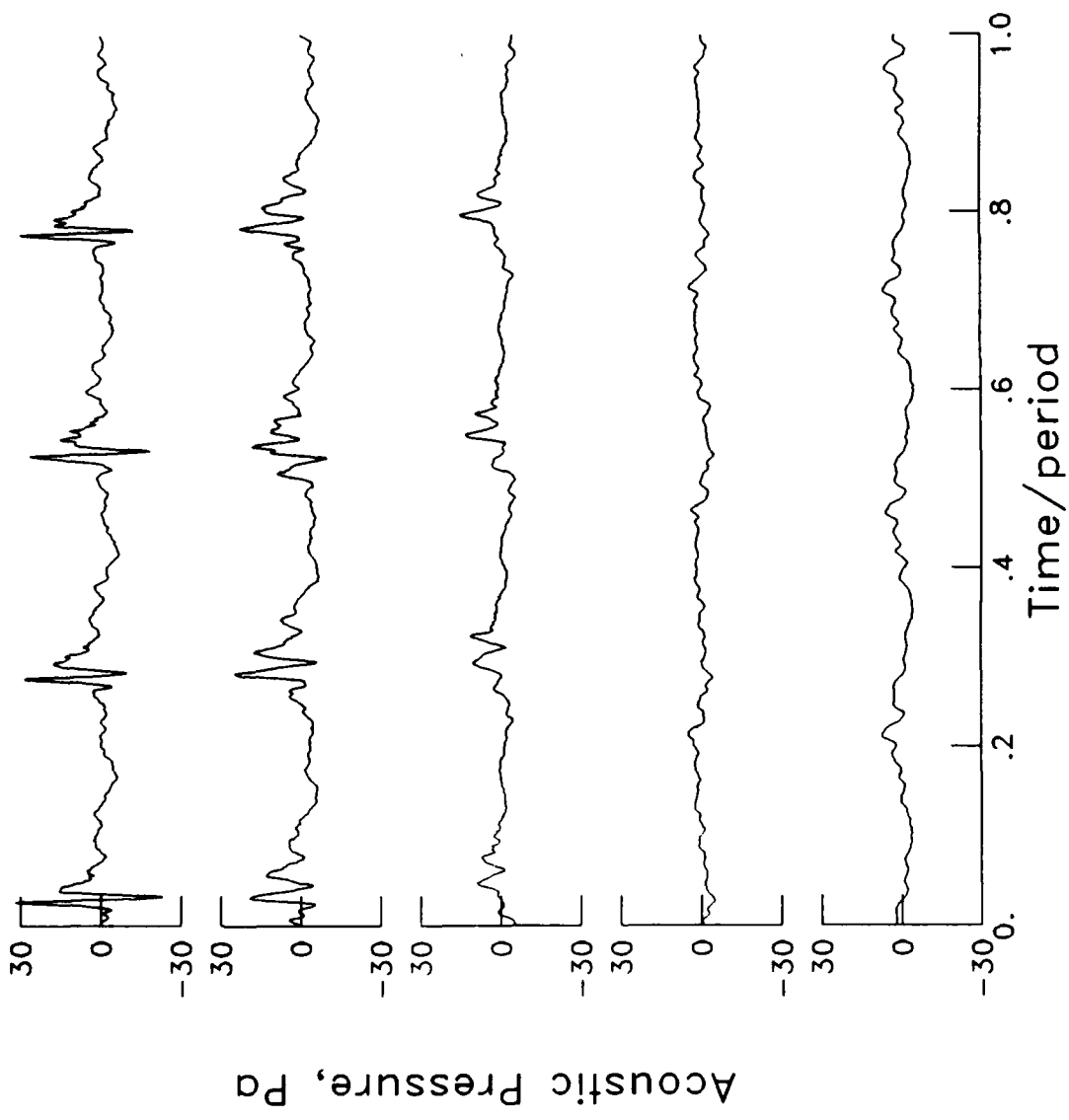


$\mu = .138$
 $\alpha_{TPP} = 1.6^\circ$
 $C_T = 0.0029$
 $M_H = 0.637$
 Point = 517



Mic	X _w , m	Y _w , m	Z _w , m
9	-0.27	-2.16	-2.10
7	-0.27	-1.08	-2.10
5	-0.27	0.00	-2.10
3	-0.27	1.08	-2.10
1	-0.27	2.16	-2.10

$\mu = .138$
 $\alpha_{TPP} = 1.6^\circ$
 $C_T = 0.0029$
 $M_H = 0.638$
 Point = 519



Mic X_w, m Y_w, m Z_w, m
 9 0.53 -2.16 -2.10

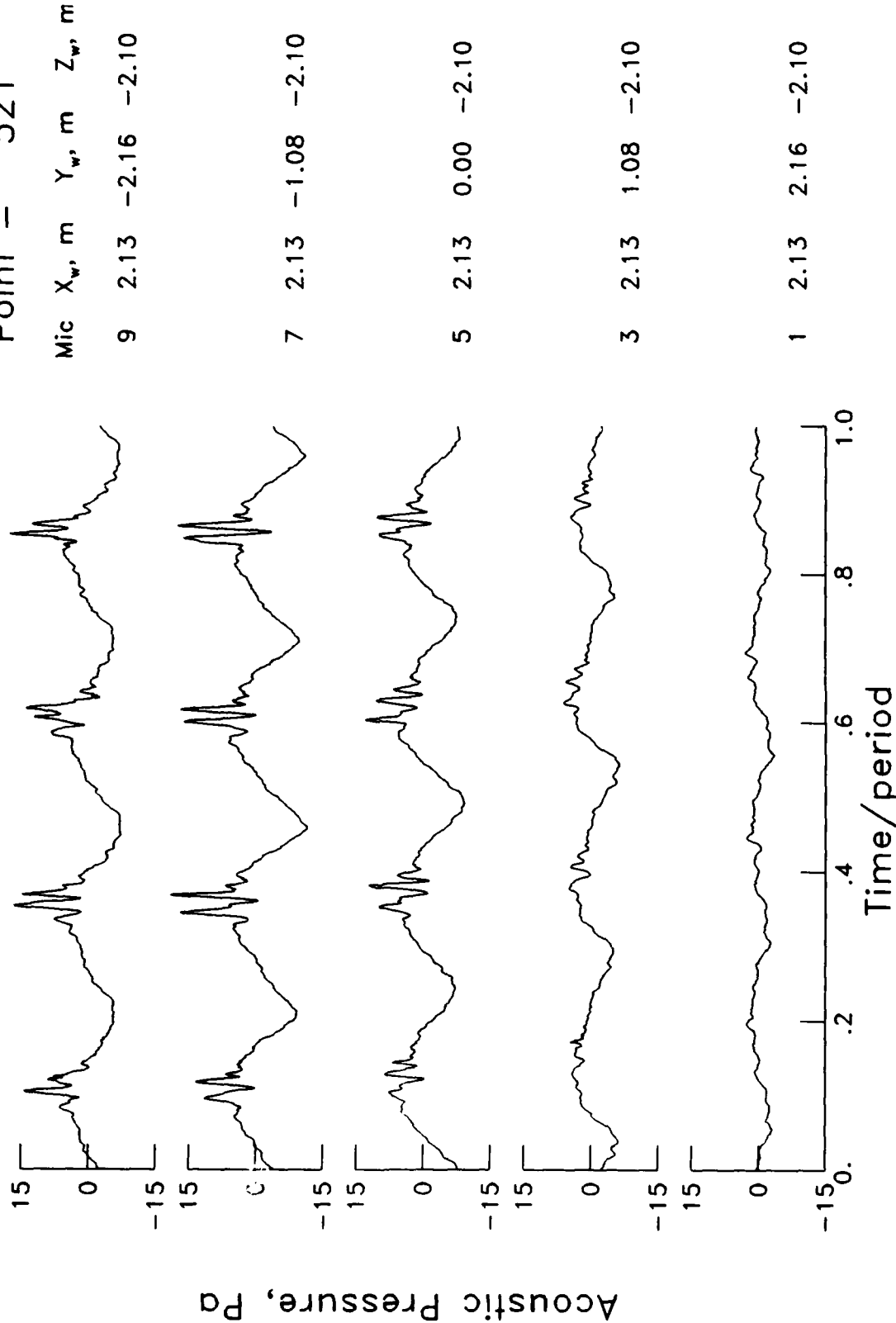
7 0.53 -1.08 -2.10

5 0.53 0.00 -2.10

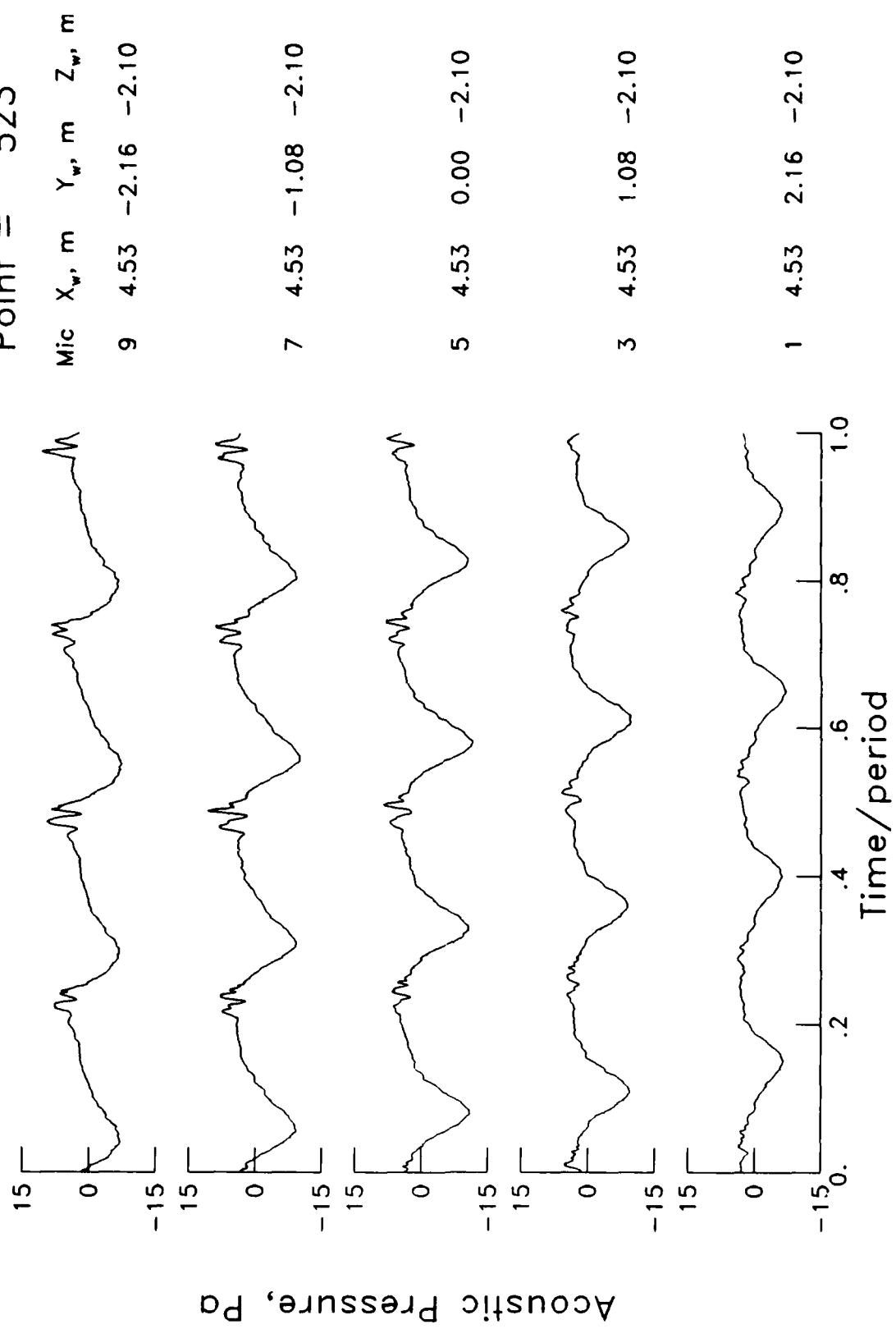
3 0.53 1.08 -2.10

1 0.53 2.16 -2.10

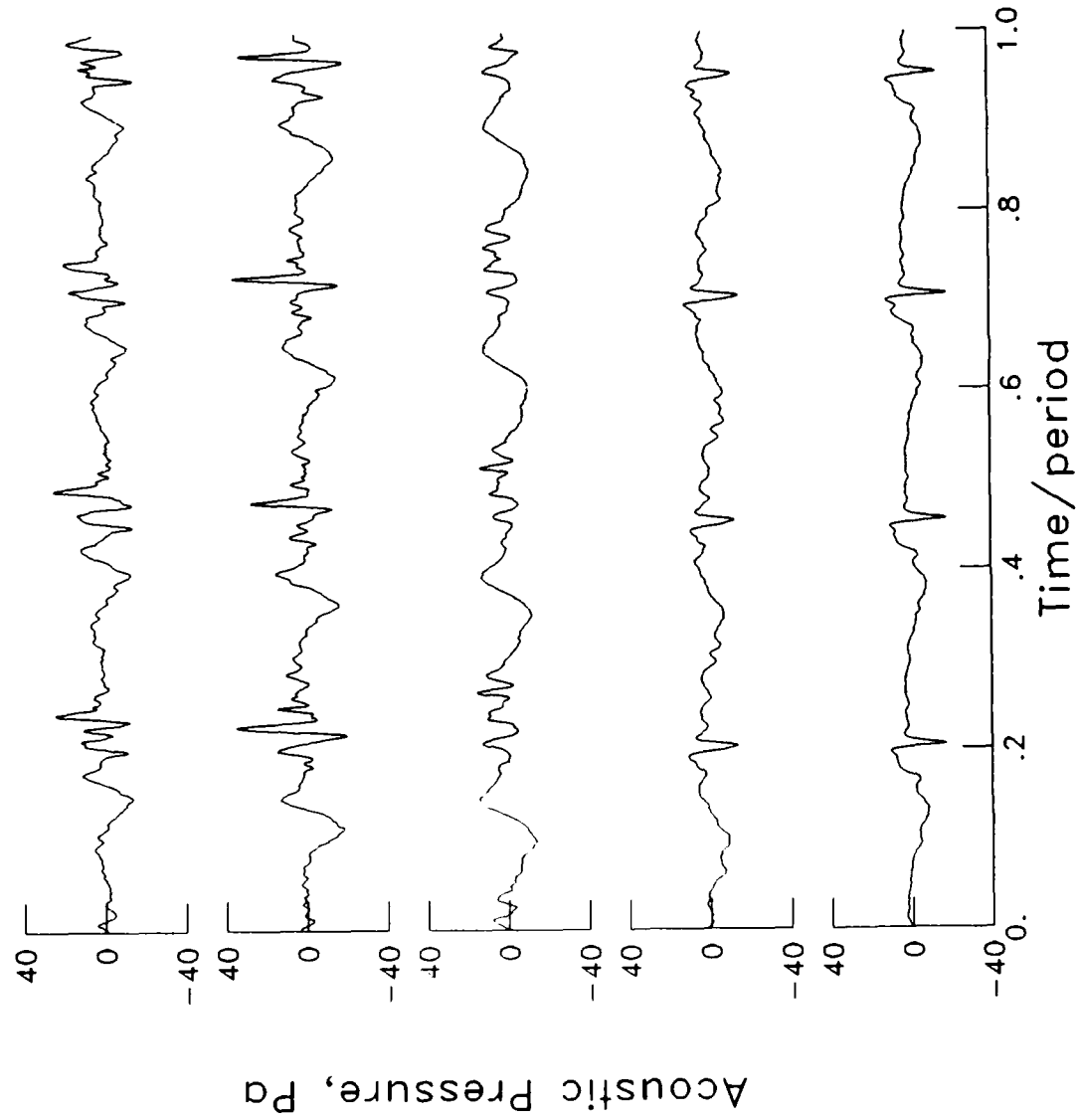
$\mu = .139$
 $\alpha_{TPP} = 1.6^\circ$
 $C_T = 0.0029$
 $M_H = 0.637$
 Point = 521



$\mu = .138$
 $\alpha_{TPP} = 1.6^\circ$
 $C_T = 0.0029$
 $M_H = 0.639$
 Point = 523

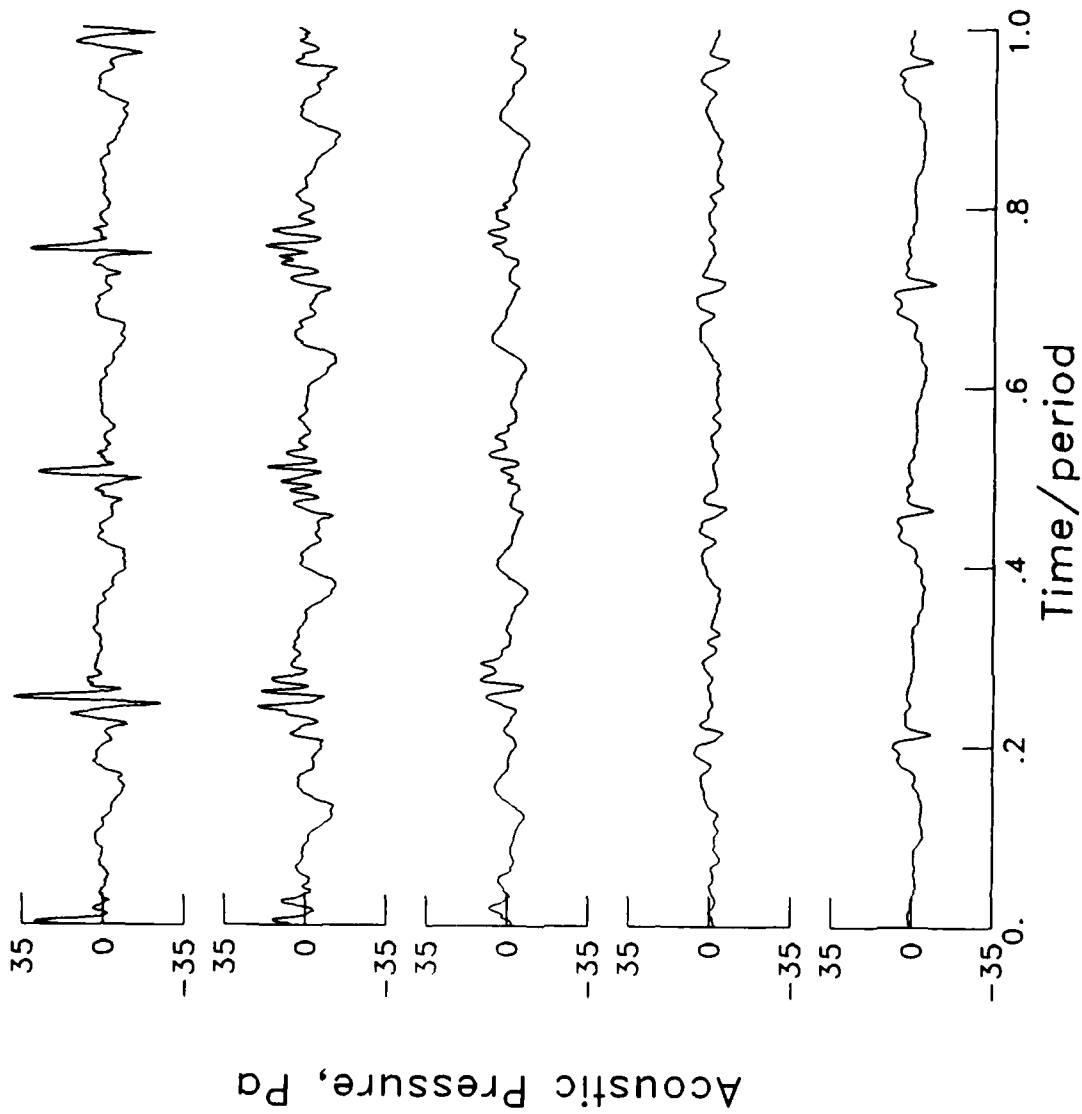


$\mu = .183$
 $\alpha_{TPP} = 0.6^\circ$
 $C_T = 0.0029$
 $M_H = 0.639$
 Point = 532



Mic	X _w , m	Y _w , m	Z _w , m
9	-1.09	-2.16	-2.10
7	-1.09	-1.08	-2.10
5	-1.09	0.00	-2.10
3	-1.09	1.08	-2.10
1	-1.09	2.16	-2.10

$\mu = .184$
 $\alpha_{TPP} = 0.6^\circ$
 $C_T = 0.0029$
 $M_H = 0.638$
 Point = 530



Mic X_w, m Y_w, m Z_w, m
 9 -0.35 -2.16 -2.10

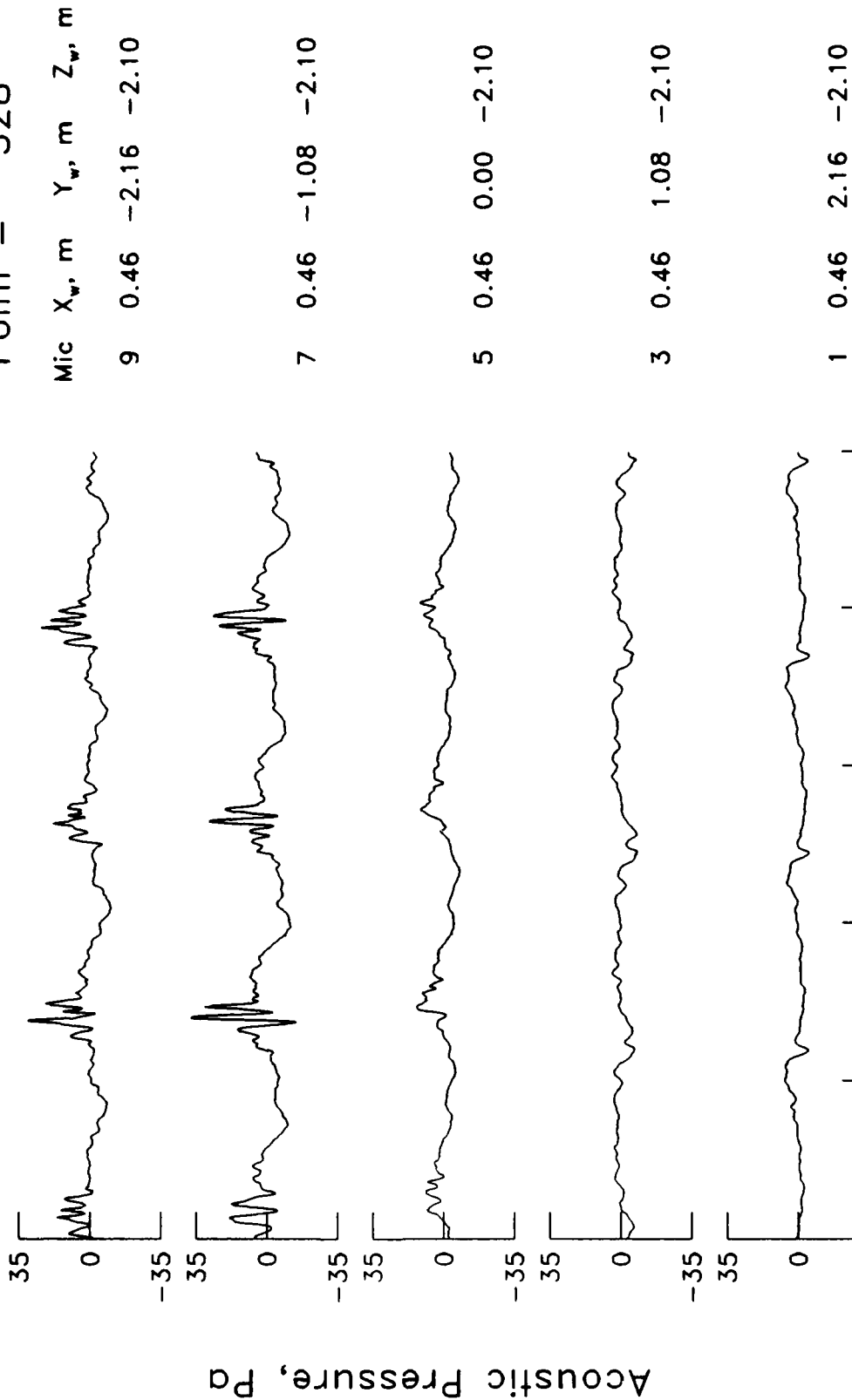
7 -0.35 -1.08 -2.10

5 -0.35 0.00 -2.10

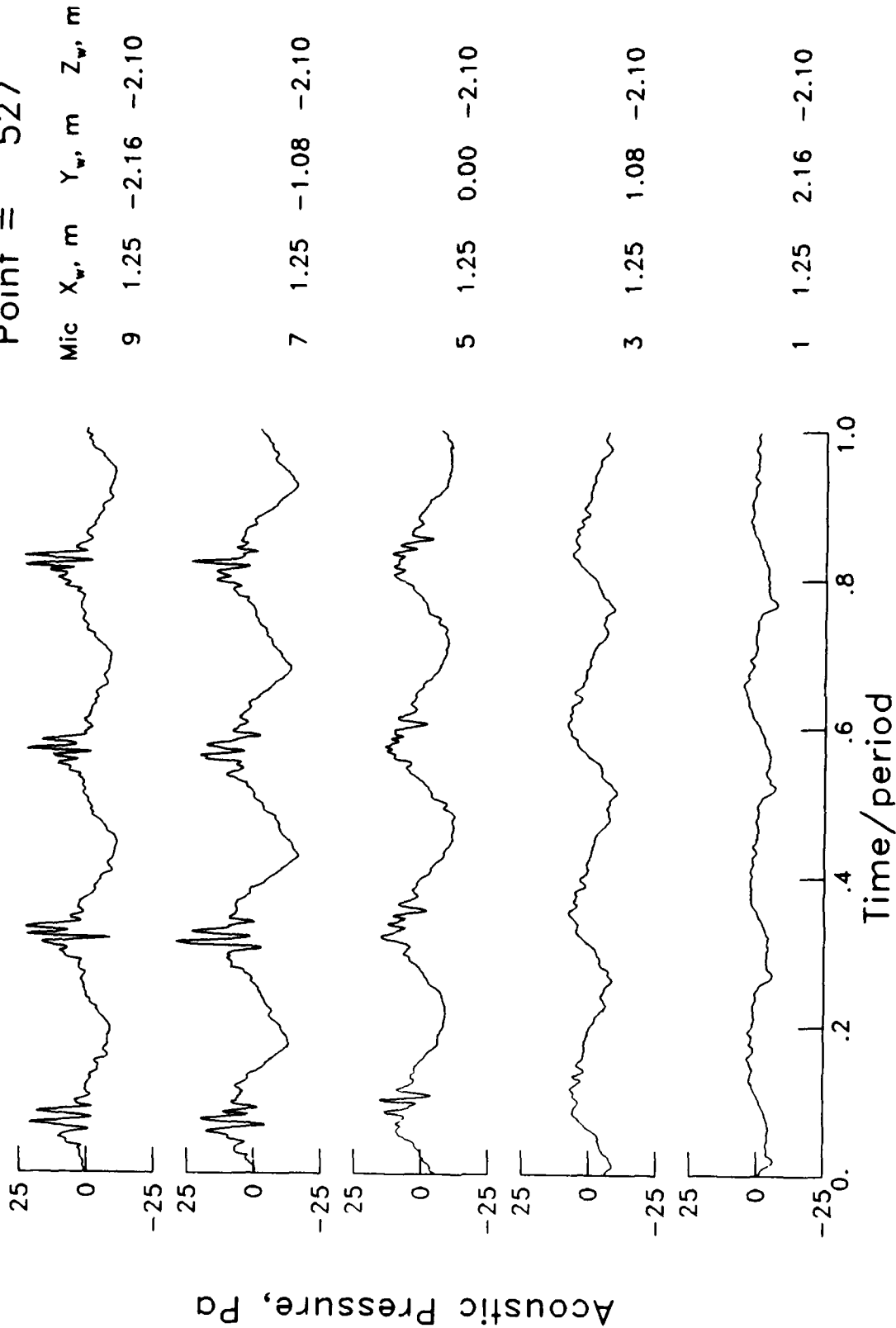
3 -0.35 1.08 -2.10

1 -0.35 2.16 -2.10

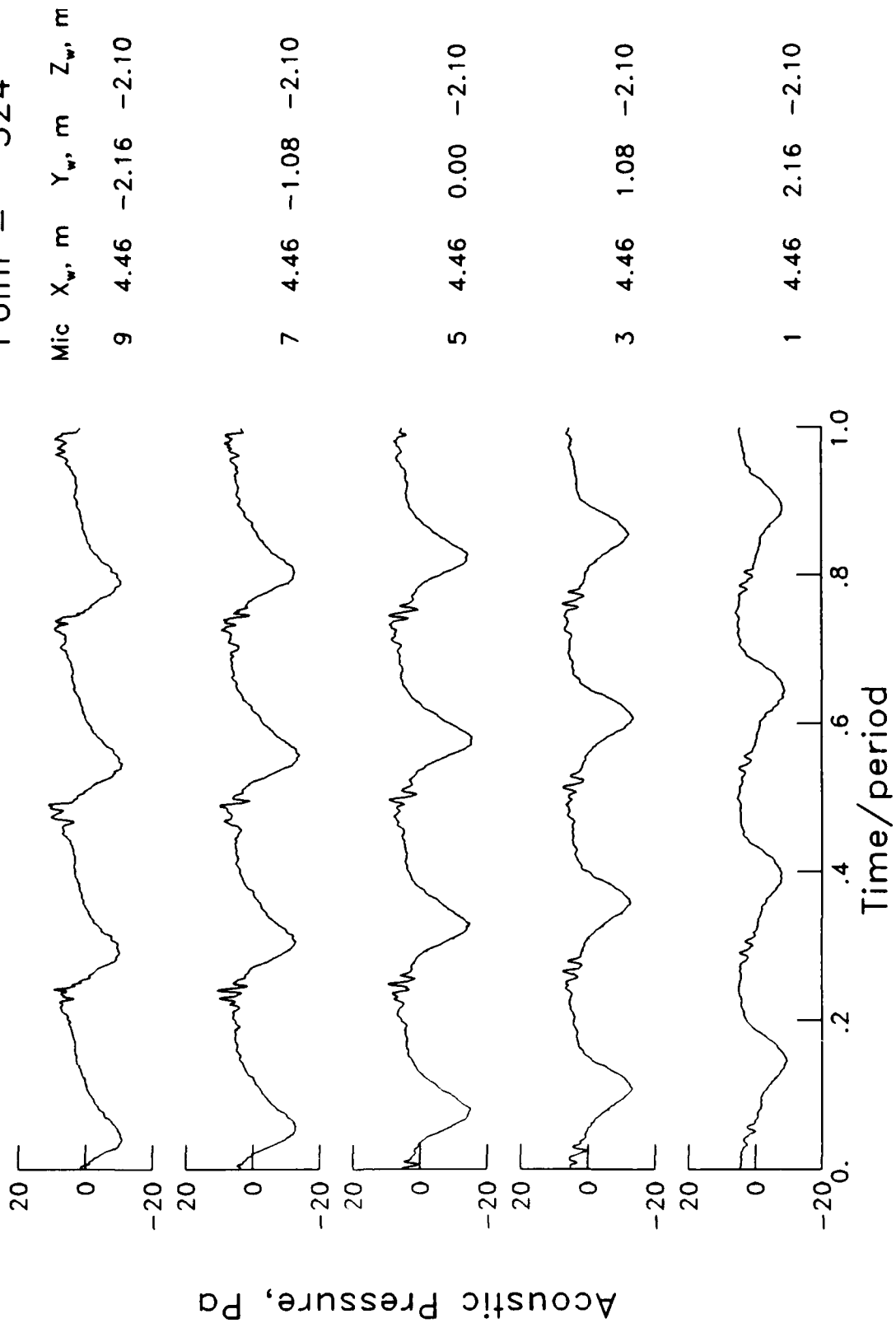
$\mu = .183$
 $\alpha_{TPP} = 0.6^\circ$
 $C_T = 0.0029$
 $M_H = 0.638$
 Point = 528



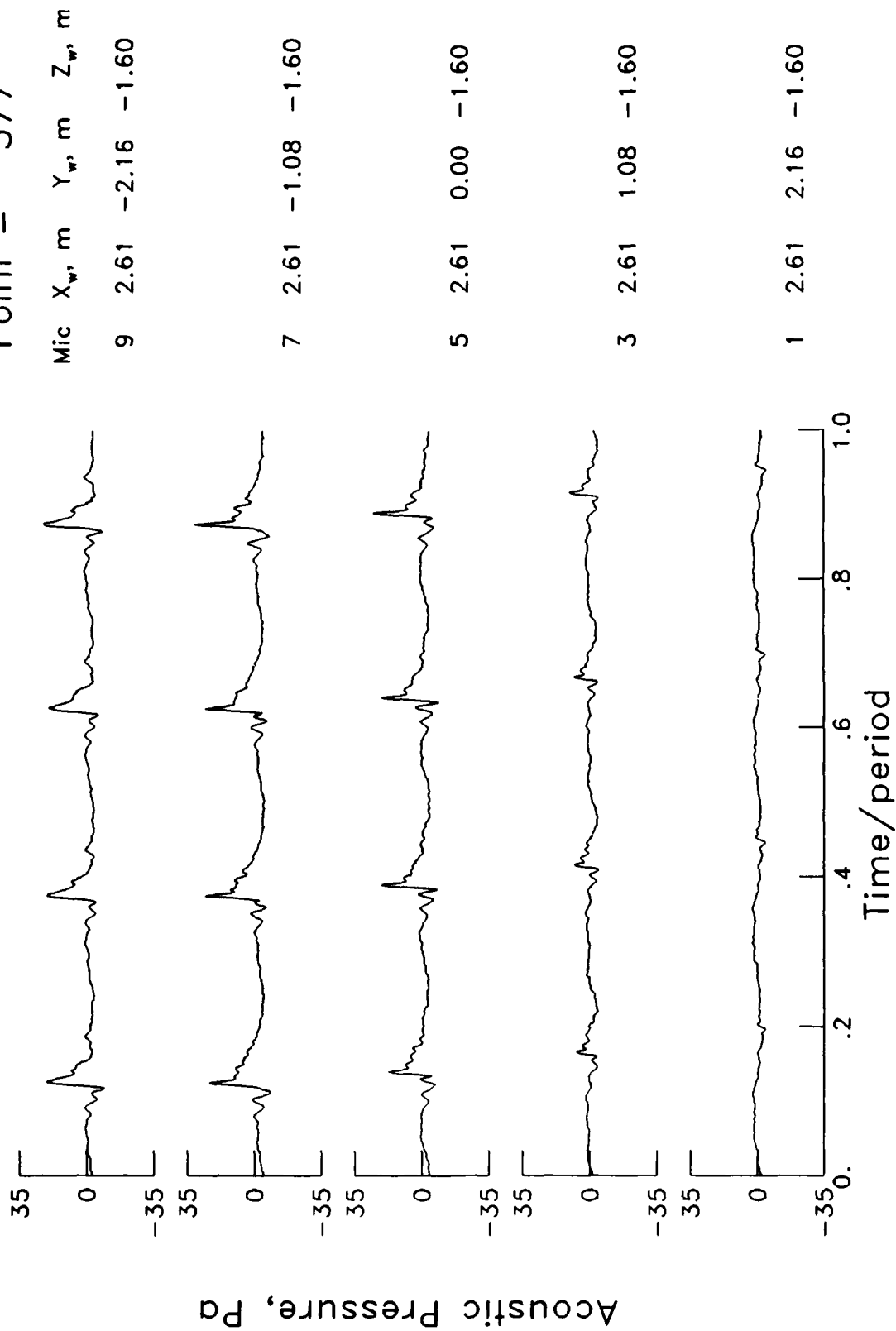
$\mu = .183$
 $\alpha_{TPP} = 0.6^\circ$
 $C_T = 0.0029$
 $M_H = 0.638$
 Point = 527



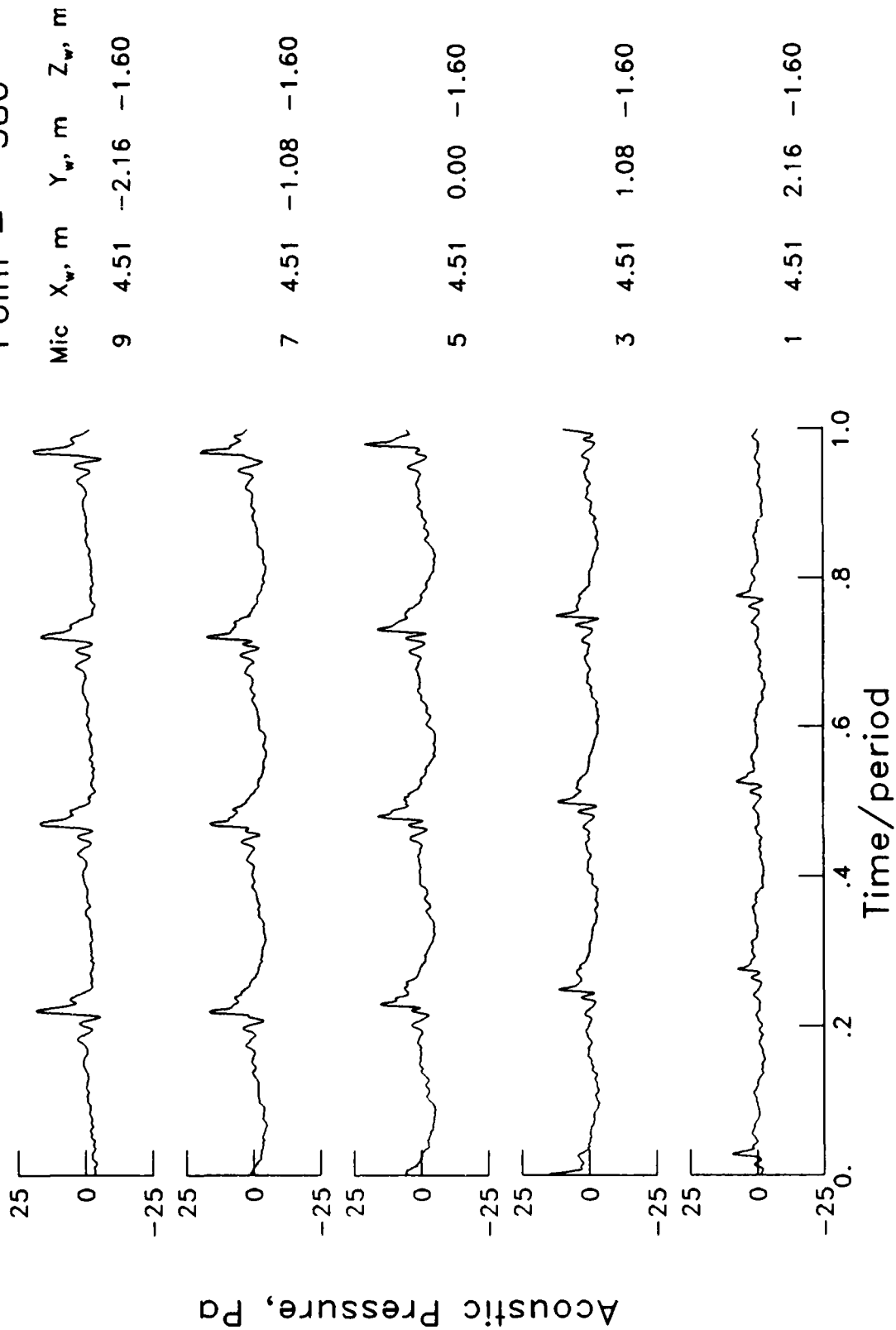
$\mu = .184$
 $\alpha_{TPP} = 0.6^\circ$
 $C_T = 0.0029$
 $M_H = 0.638$
 Point = 524



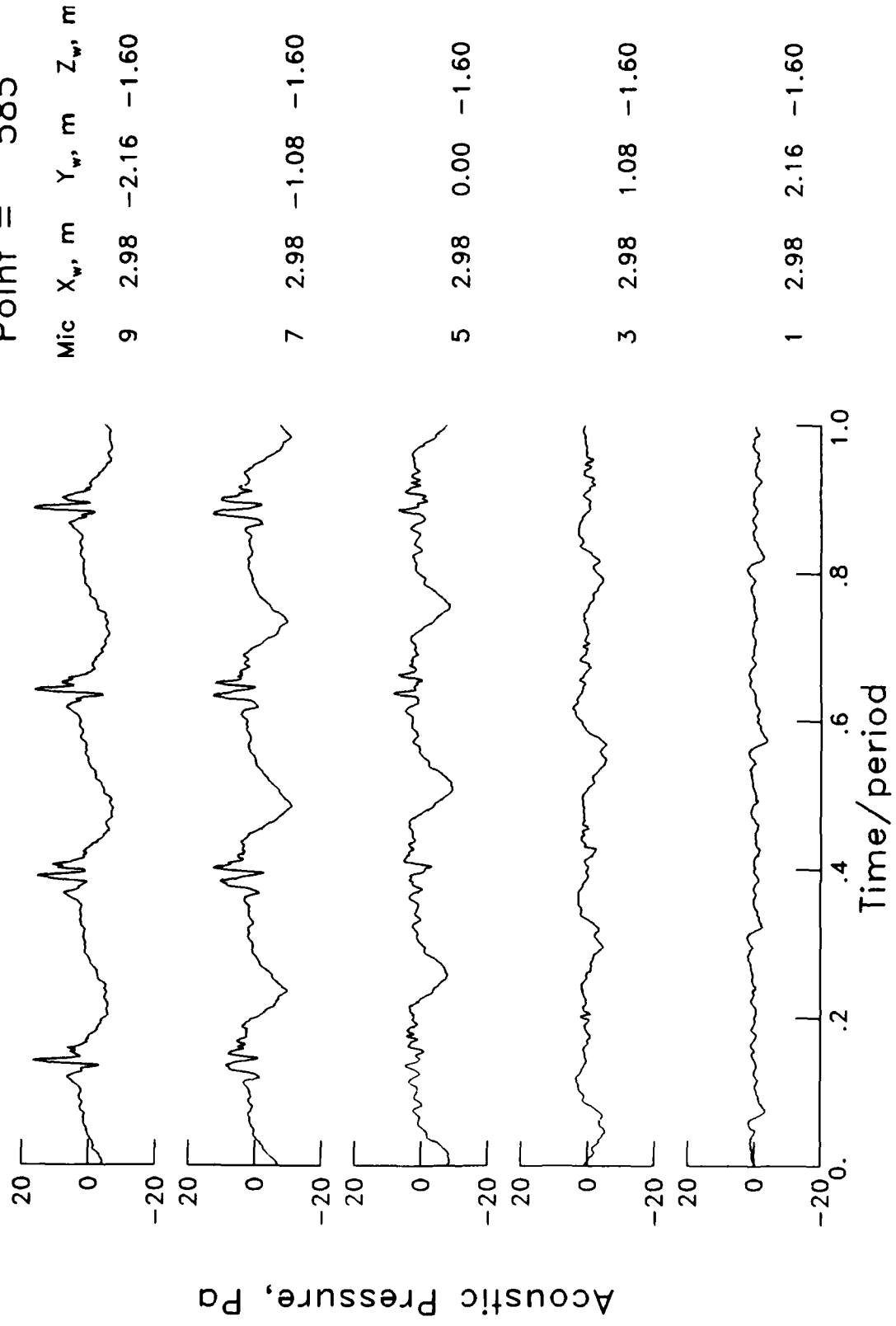
$\mu = .085$
 $\alpha_{TPP} = 5.5^\circ$
 $C_T = 0.0043$
 $M_H = 0.636$
 Point = 577



$\mu = .085$
 $\alpha_{TPP} = 5.5^\circ$
 $C_T = 0.0043$
 $M_{H_i} = 0.636$
 Point = 580



$\mu = .141$
 $\alpha_{TPP} = 3.3^\circ$
 $C_T = 0.0043$
 $M_H = 0.637$
 Point = 585



$\mu = .141$
 $\alpha_{TPP} = 3.3^\circ$
 $C_T = 0.0043$
 $M_H = 0.636$
 Point = 583

Mic X_w, m Y_w, m Z_w, m

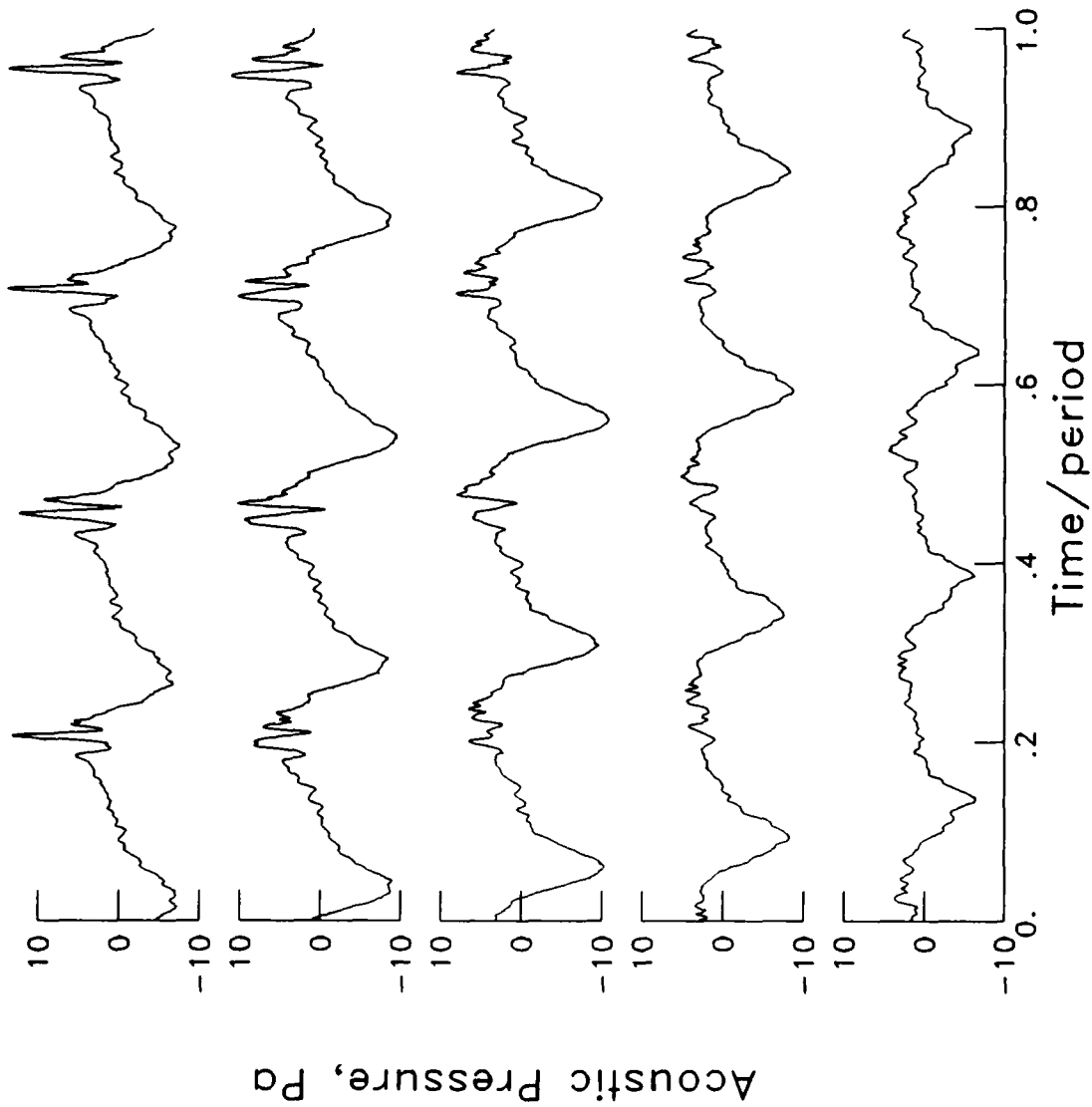
9 4.24 -2.16 -1.60

7 4.24 -1.08 -1.60

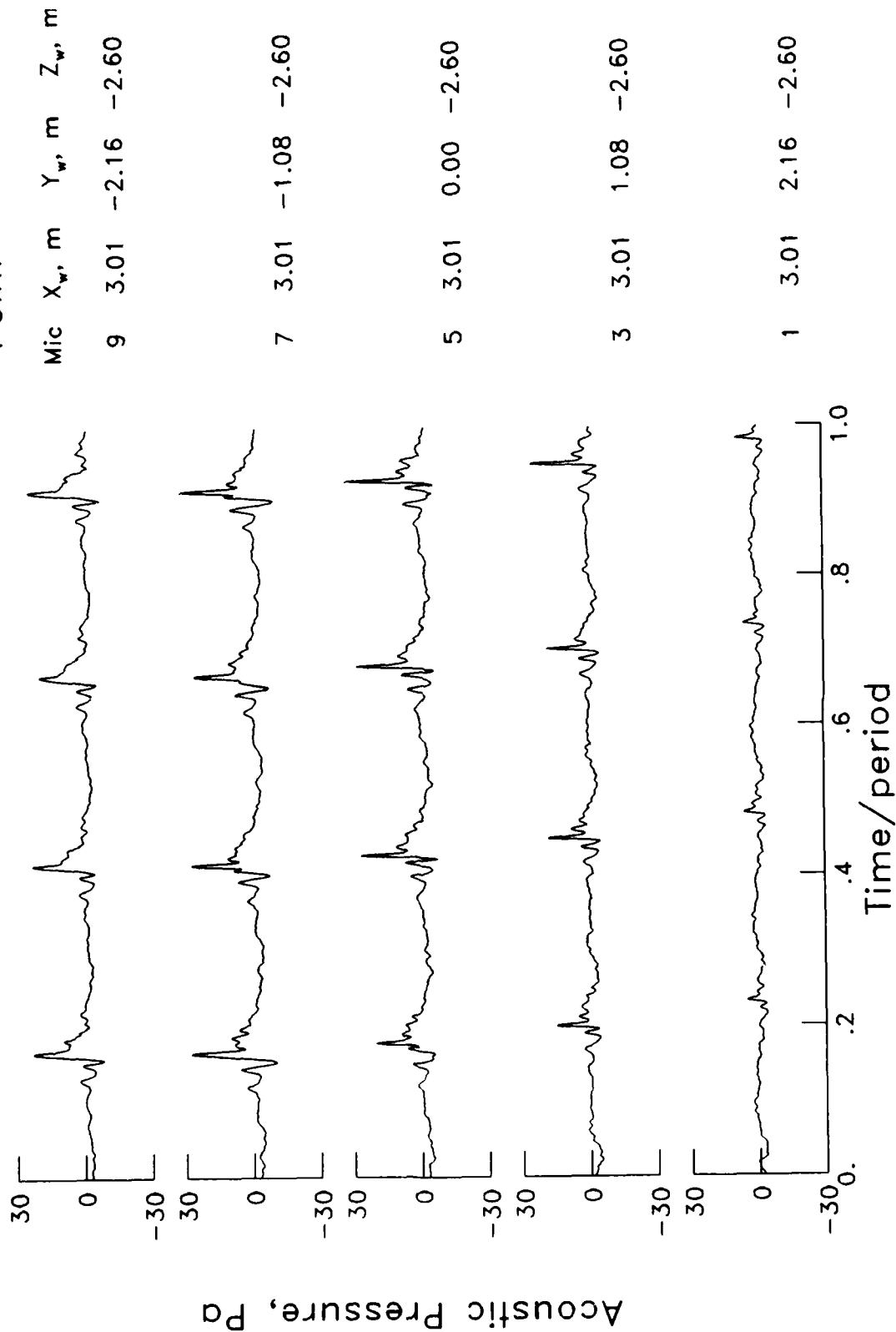
5 4.24 0.00 -1.60

3 4.24 1.08 -1.60

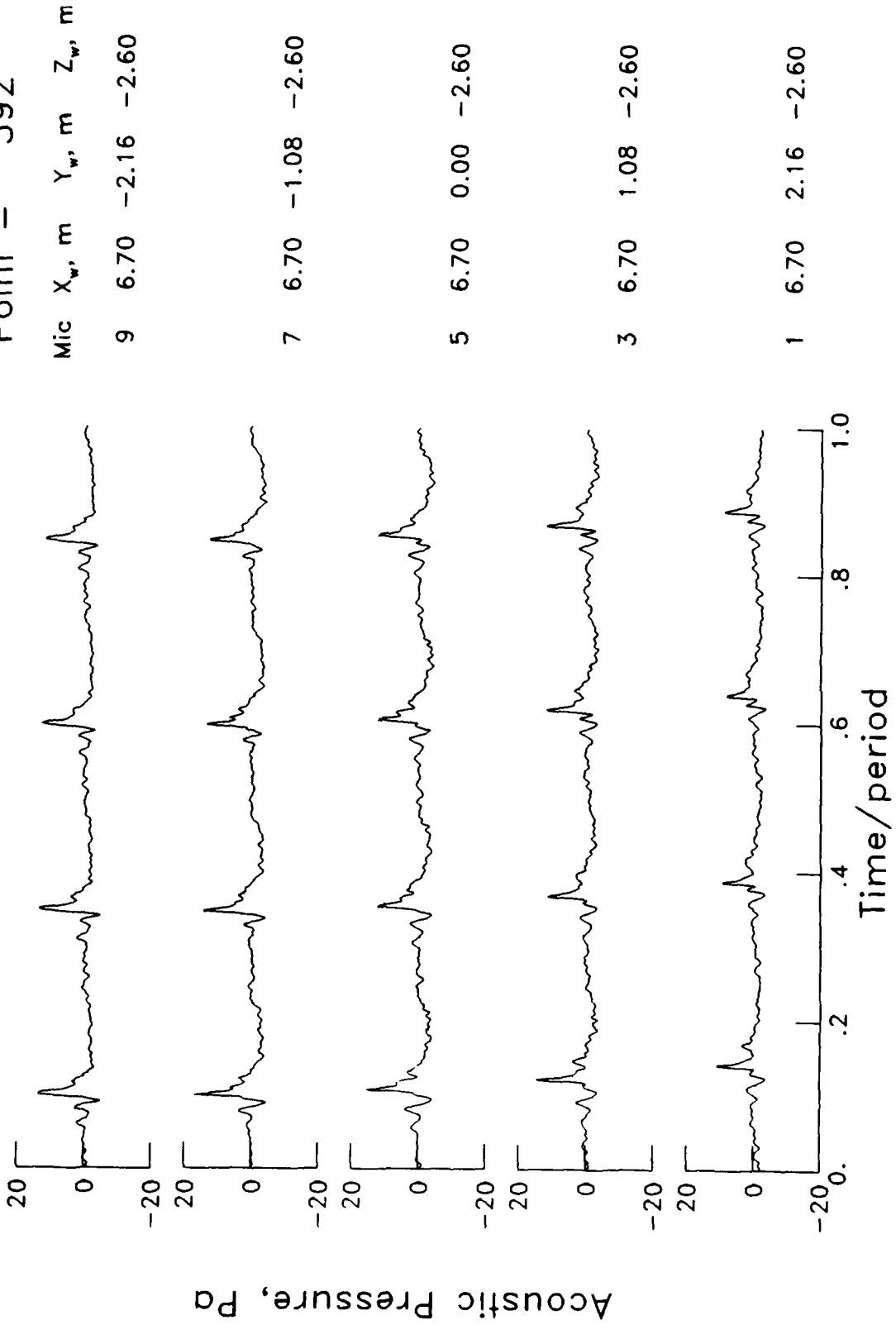
1 4.24 2.16 -1.60



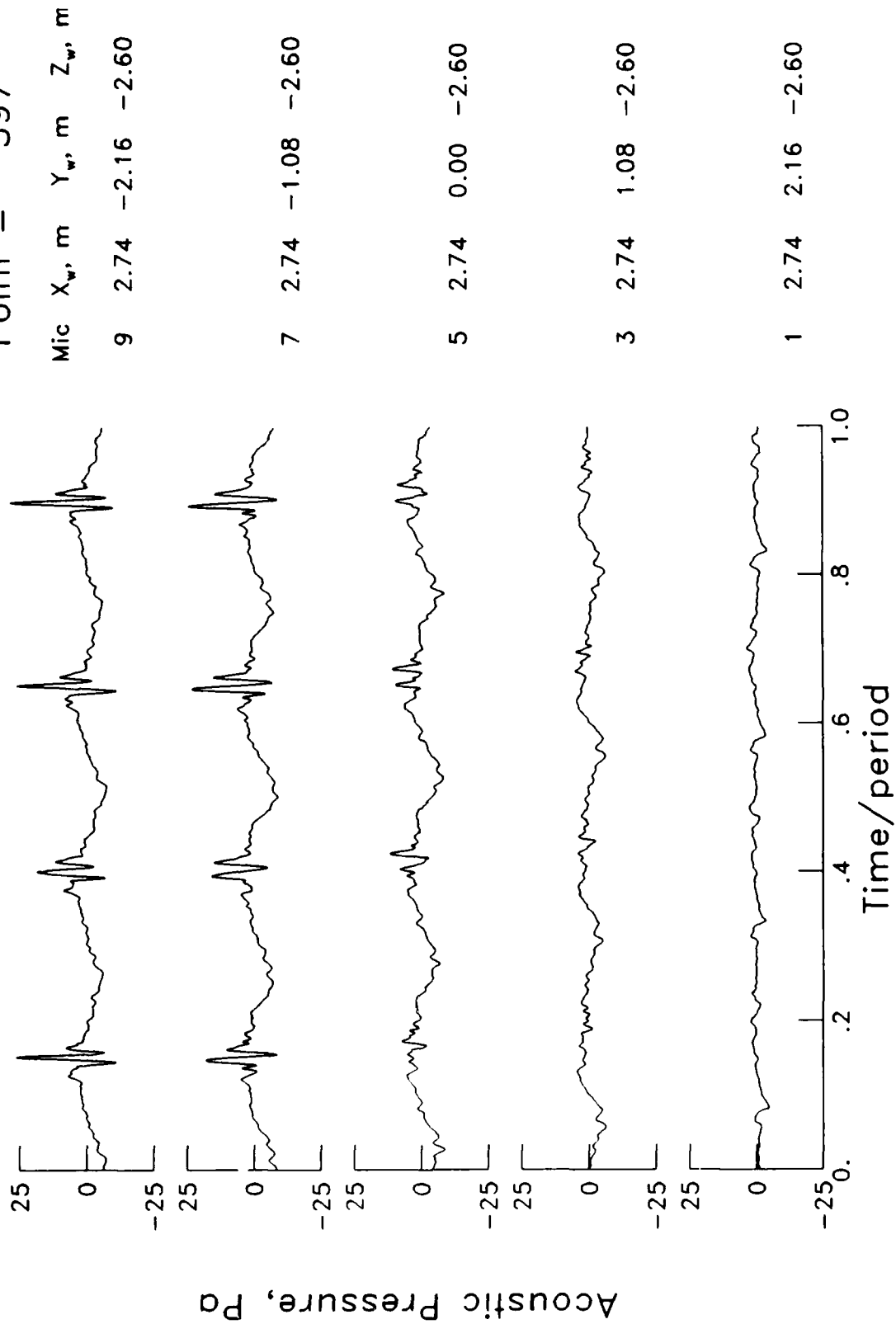
$\mu = .085$
 $\alpha_{TPP} = 5.6^\circ$
 $C_T = 0.0043$
 $M_{Hint} = 0.635$
 Point = 589



$\mu = .085$
 $\alpha_{TPP} = 5.4^\circ$
 $C_T = 0.0044$
 $M_H = 0.635$
 Point = 592



$\mu = .142$
 $\alpha_{TPP} = 3.3^\circ$
 $C_T = 0.0044$
 $M_H = 0.637$
 Point = 597



$\mu = .142$
 $\alpha_{TPP} = 3.3^\circ$
 $C_T = 0.0043$
 $M_H = 0.639$
 Point = 593

Mic X_w, m Y_w, m Z_w, m

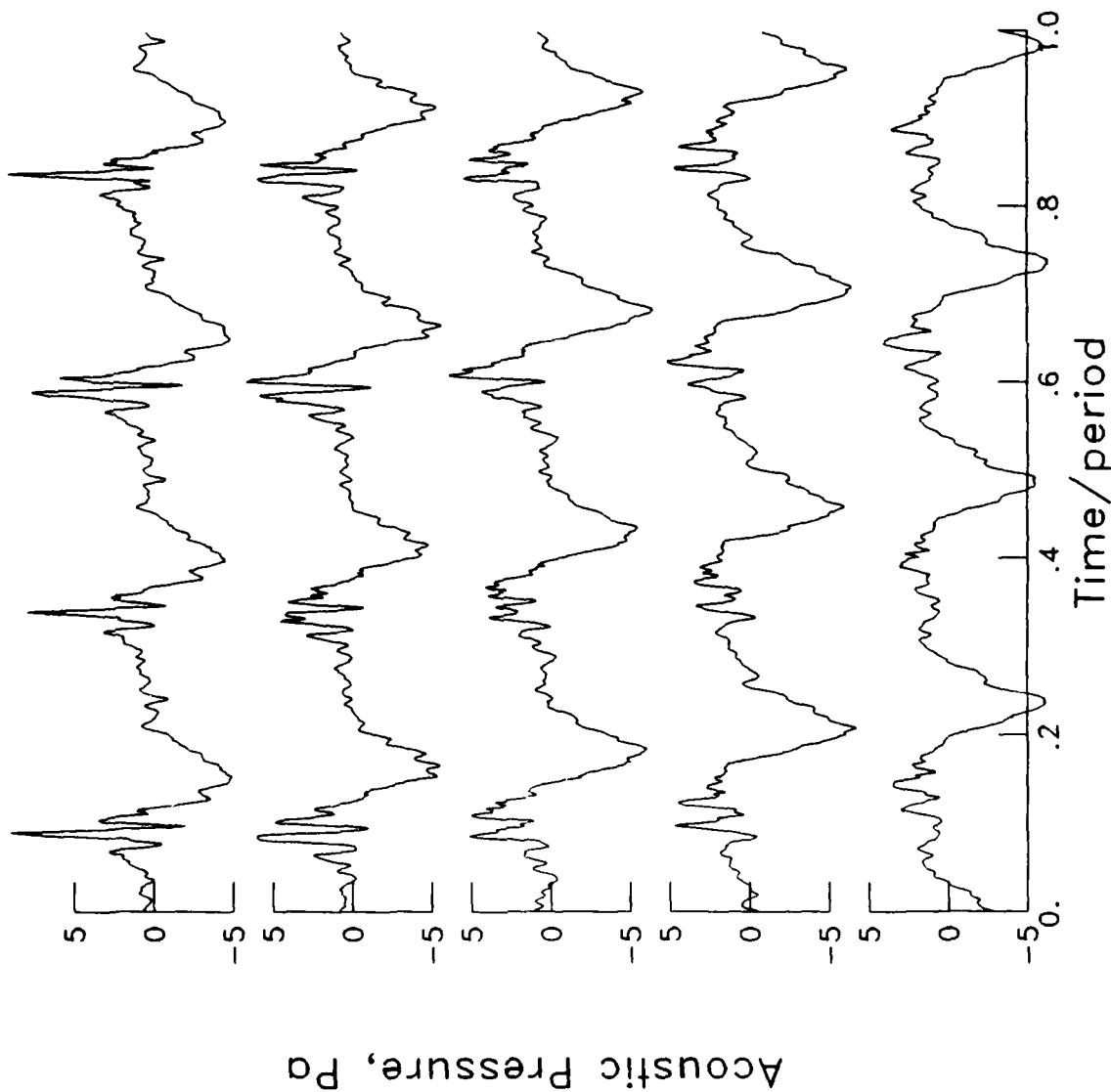
9 6.44 -2.16 -2.60

7 6.44 -1.08 -2.60

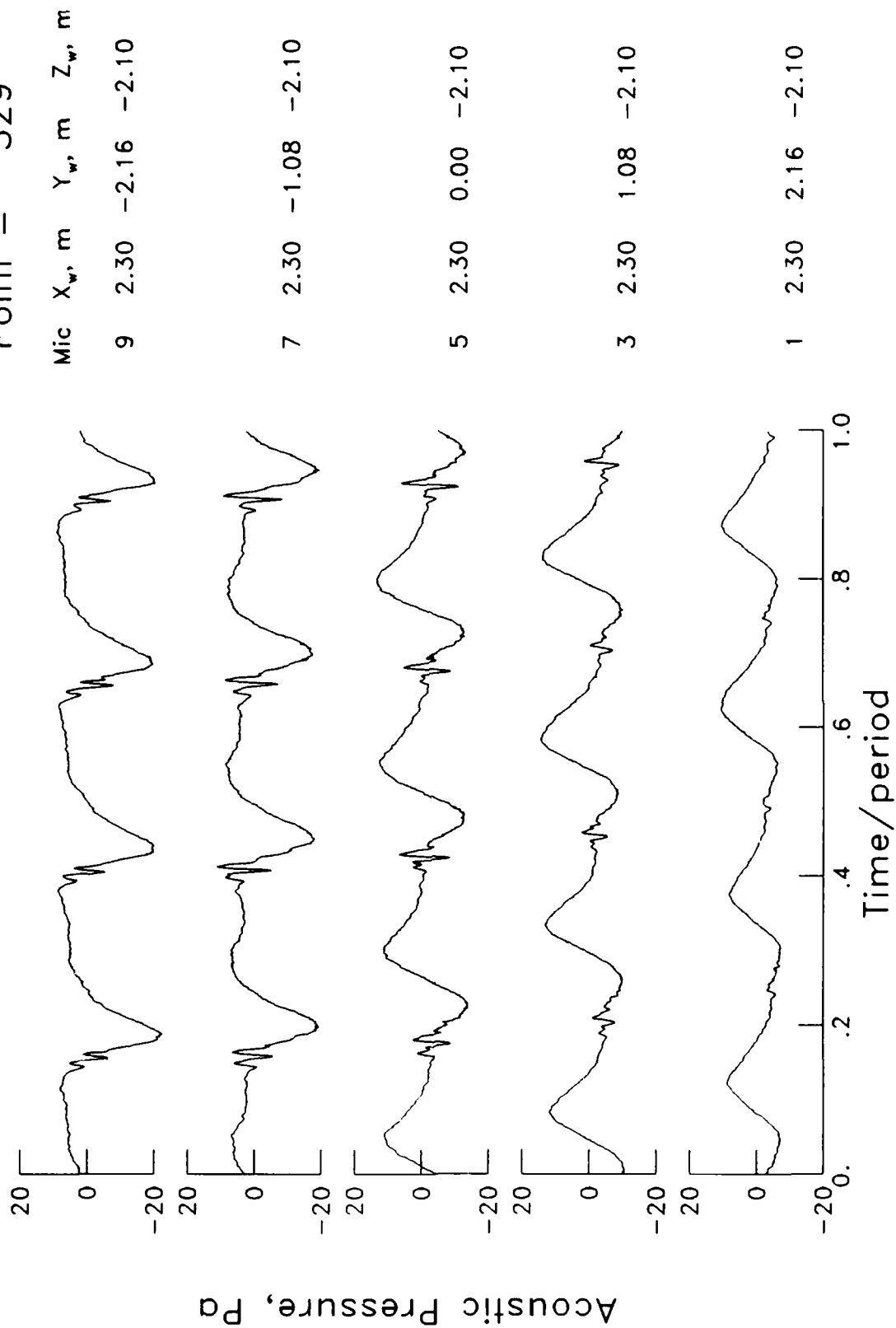
5 6.44 0.00 -2.60

3 6.44 1.08 -2.60

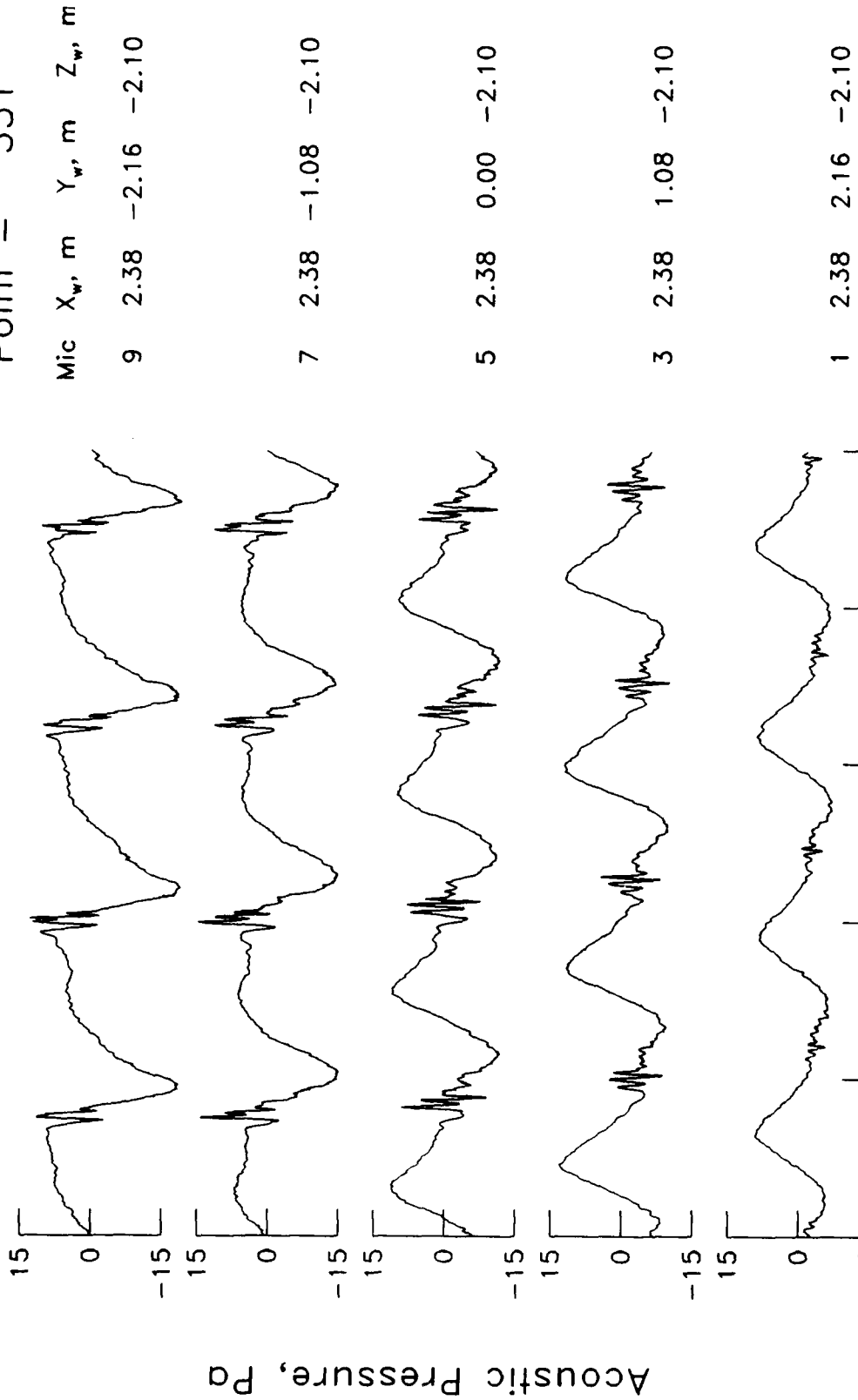
1 6.44 2.16 -2.60



$\mu = .229$
 $\alpha_{TPP} = -5.5^\circ$
 $C_T = 0.0043$
 $M_H = 0.634$
 Point = 329



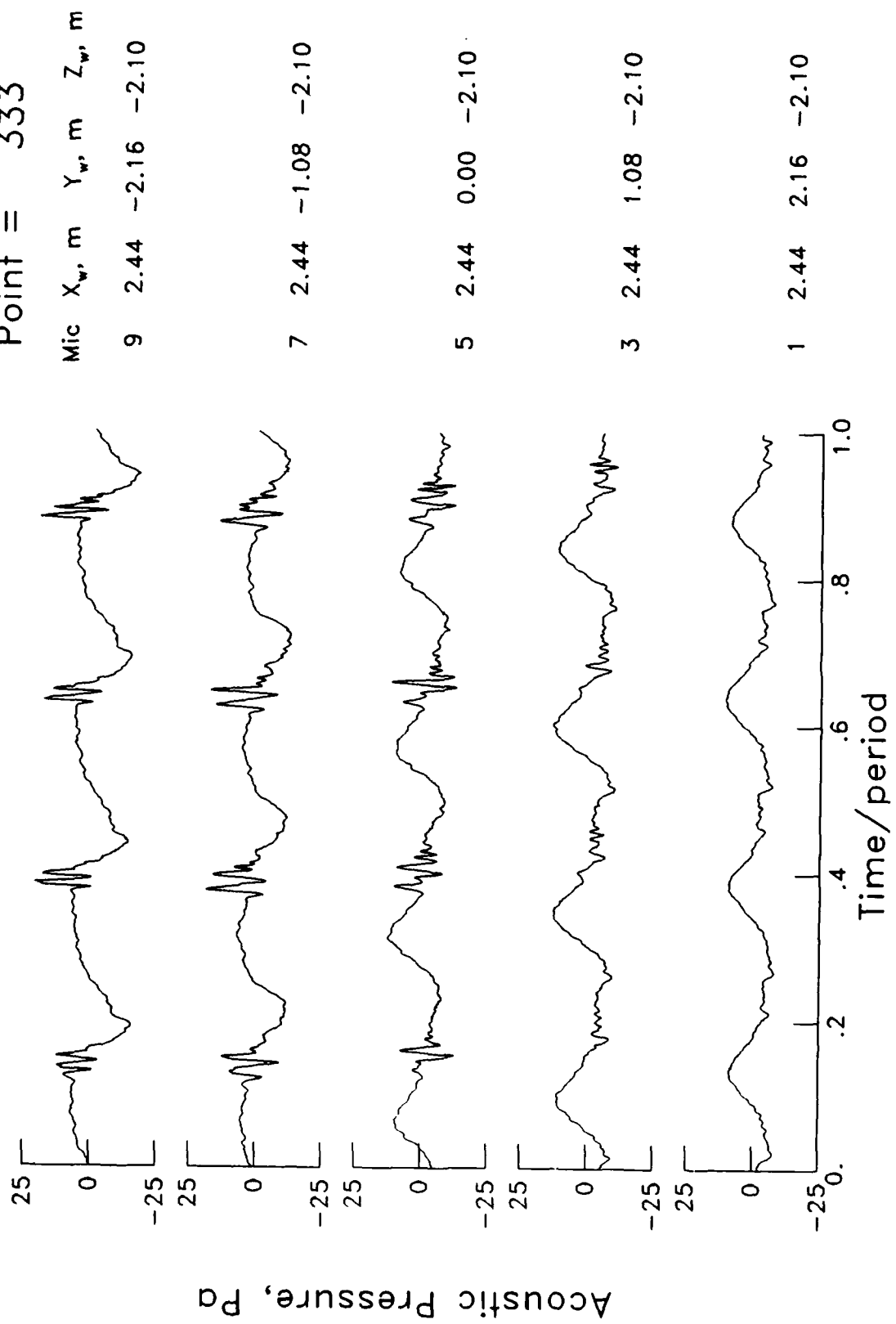
$\mu = .229$
 $\alpha_{TPP} = -3.5^\circ$
 $C_T = 0.0041$
 $M_H = 0.635$
 Point = 331



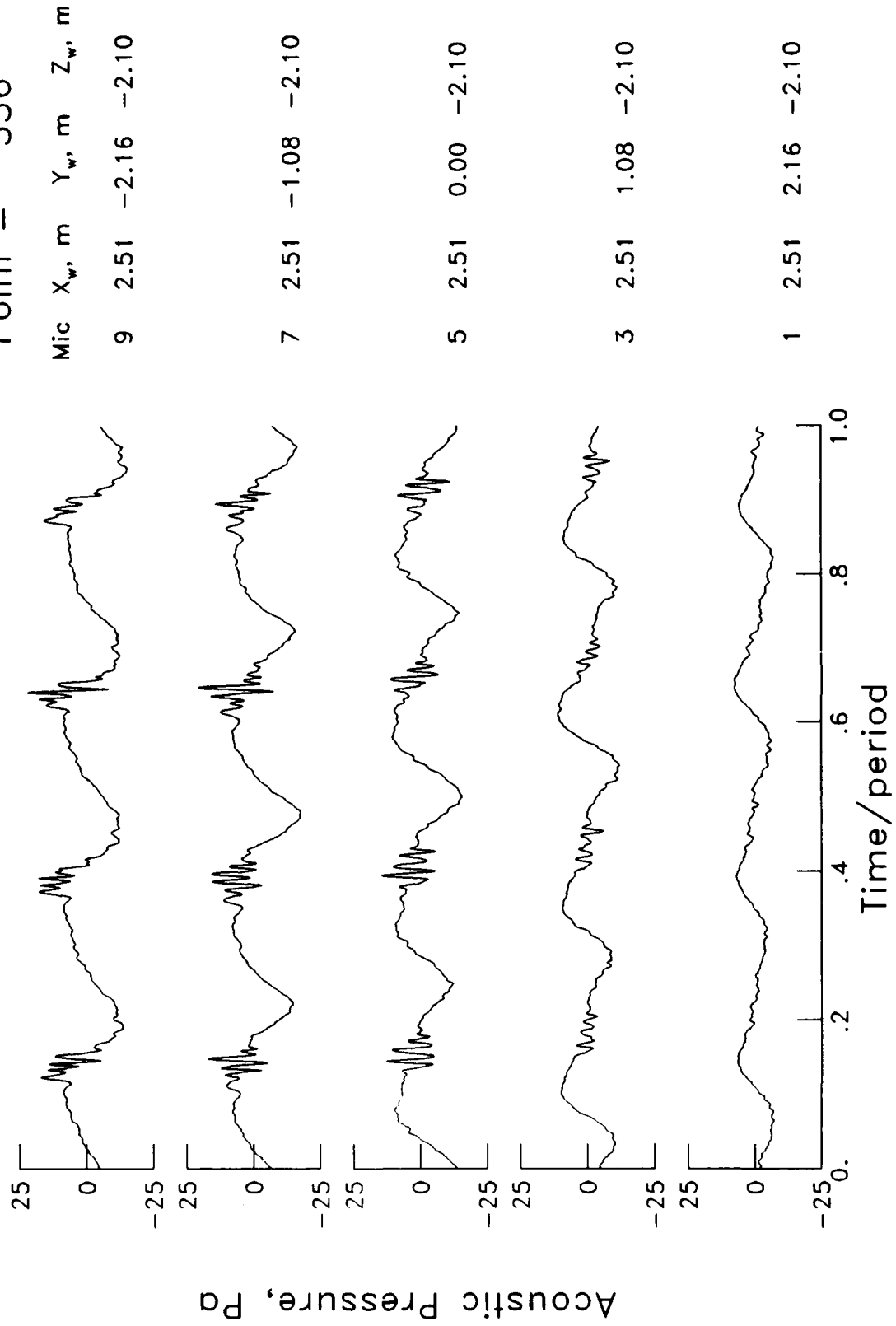
Acoustic Pressure, Pa

Time/period

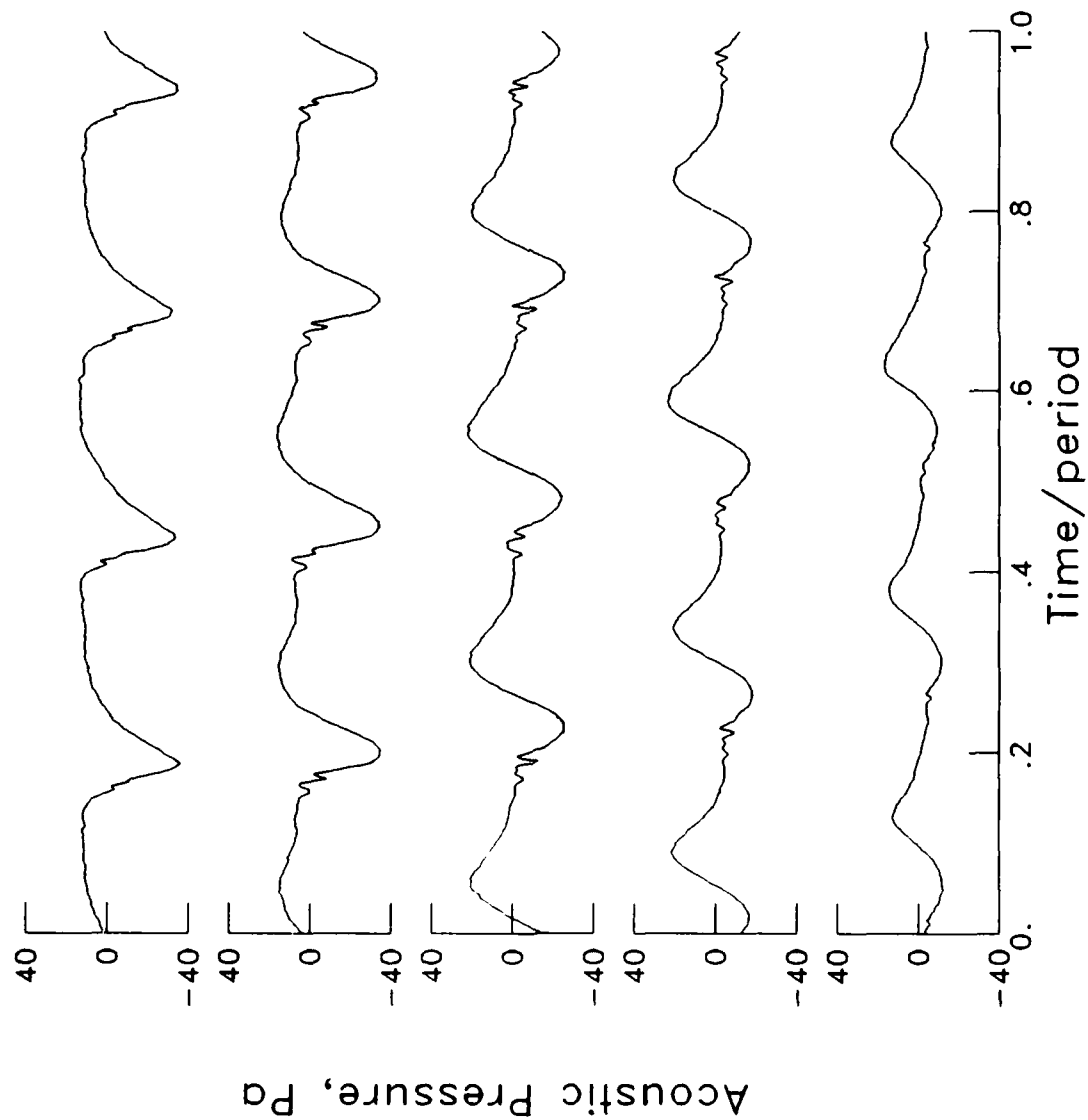
$\mu = .228$
 $\alpha_{TPP} = -1.9^\circ$
 $C_T = 0.0042$
 $M_H = 0.638$
 Point = 333



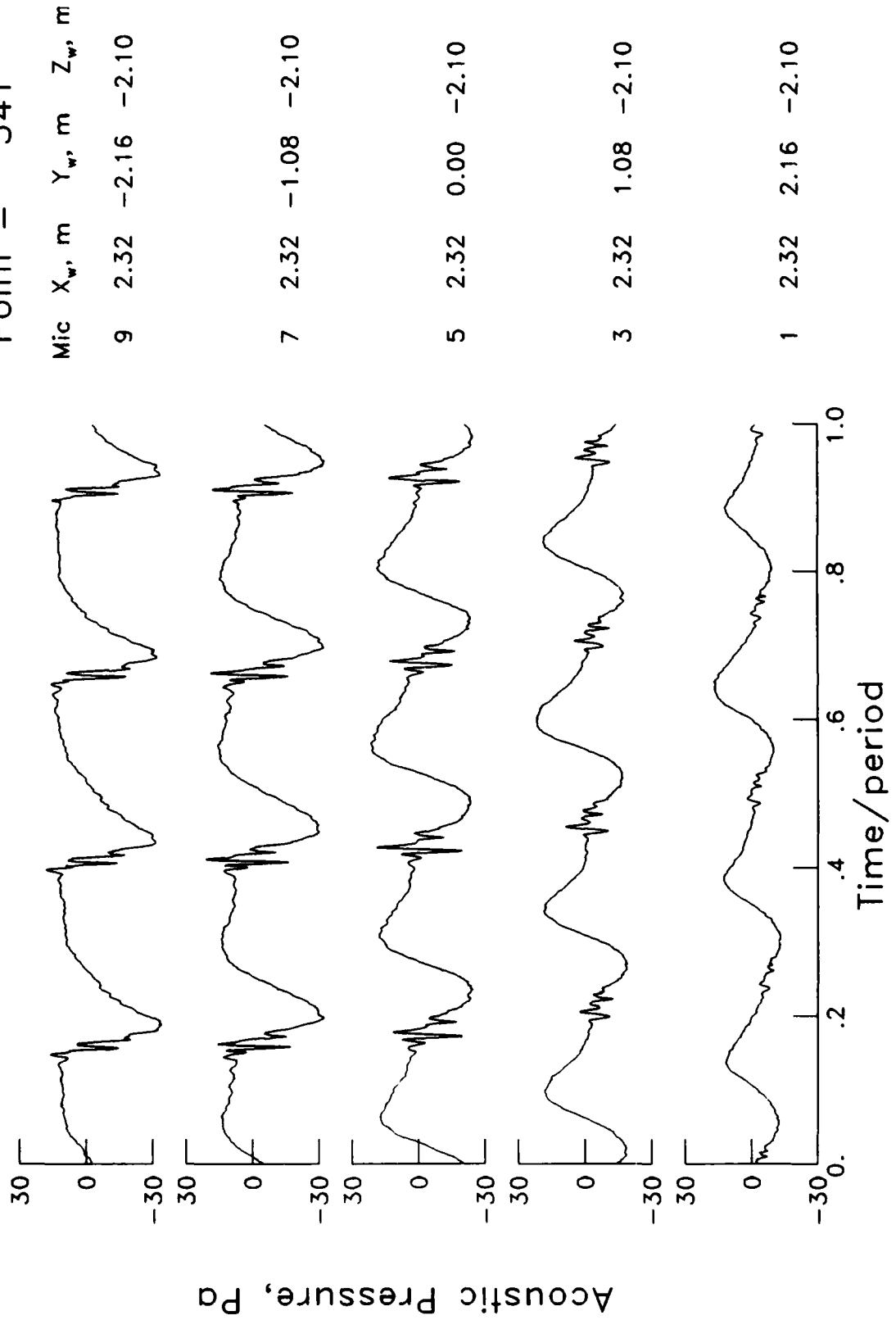
$\mu = .230$
 $\alpha_{\text{TPP}} = -0.5^\circ$
 $C_T = 0.0043$
 $M_H = 0.634$
 Point = 336



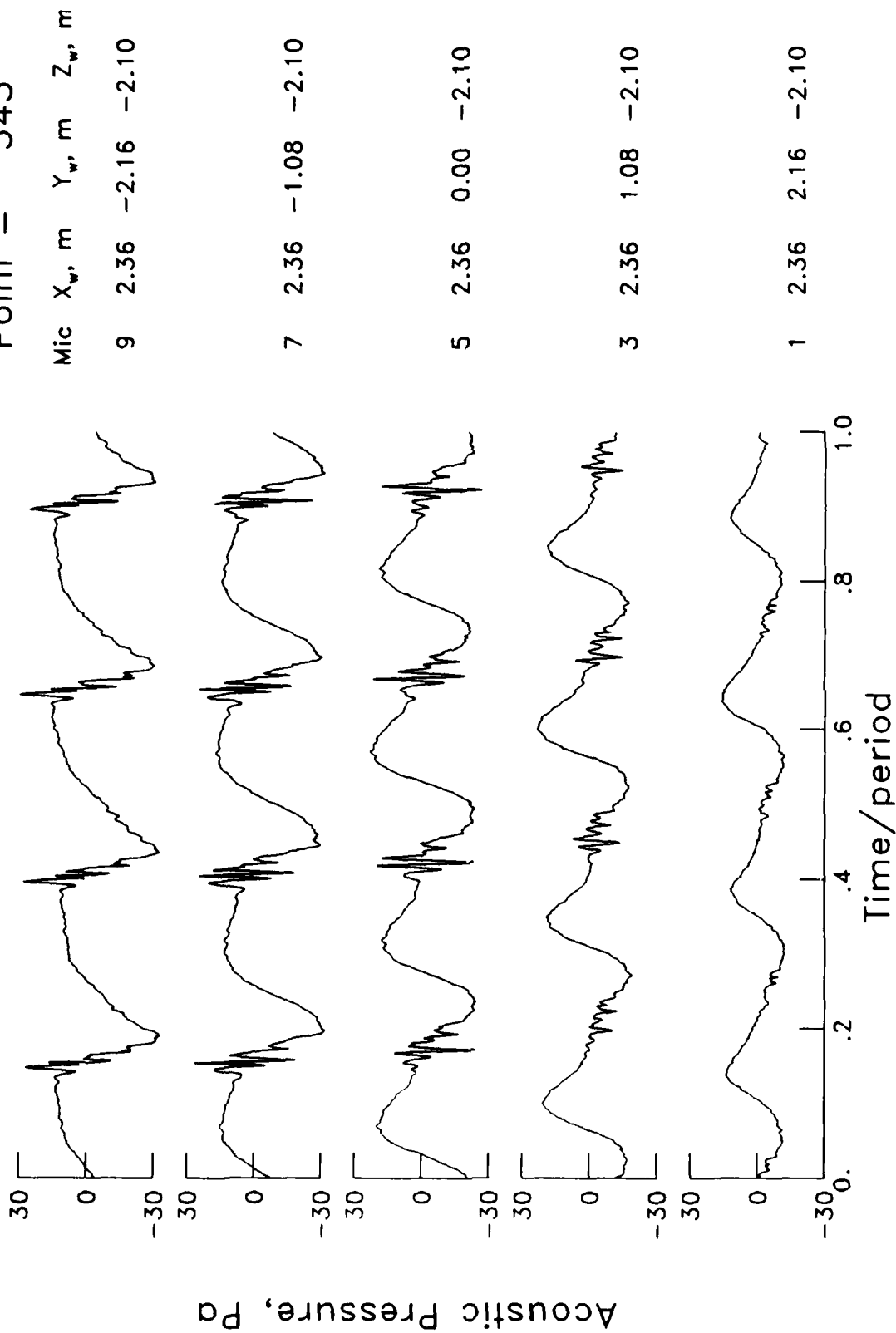
$\mu = .274$
 $\alpha_{TPP} = -7.3^\circ$
 $C_T = 0.0042$
 $M_H = 0.636$
 Point = 338



$\mu = .275$
 $\alpha_{TPP} = -4.8^\circ$
 $C_T = 0.0042$
 $M_{H_1} = 0.633$
 Point = 341

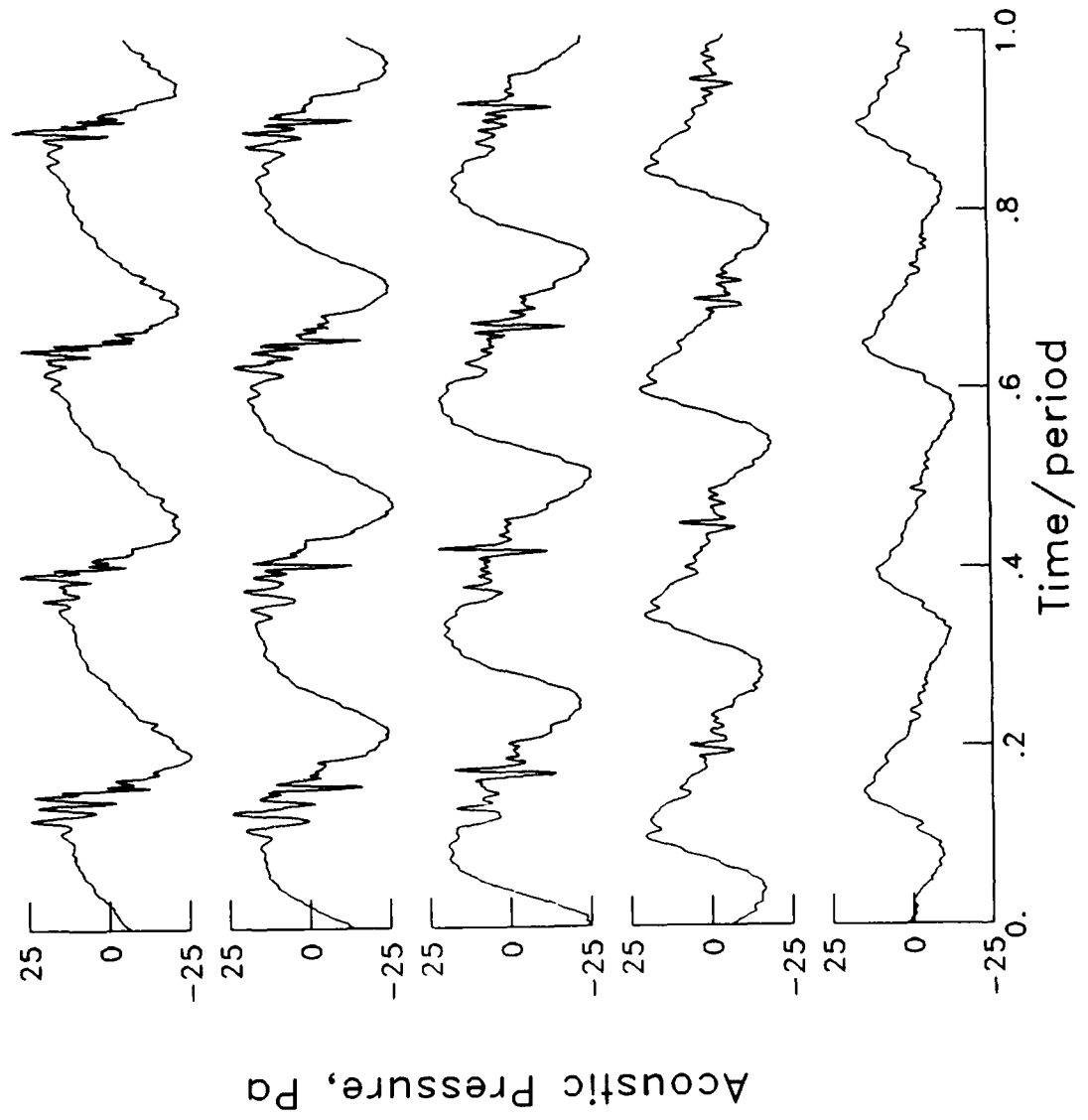


$\mu = .274$
 $\alpha_{TPP} = -3.8^\circ$
 $C_T = 0.0042$
 $M_H = 0.634$
 Point = 343

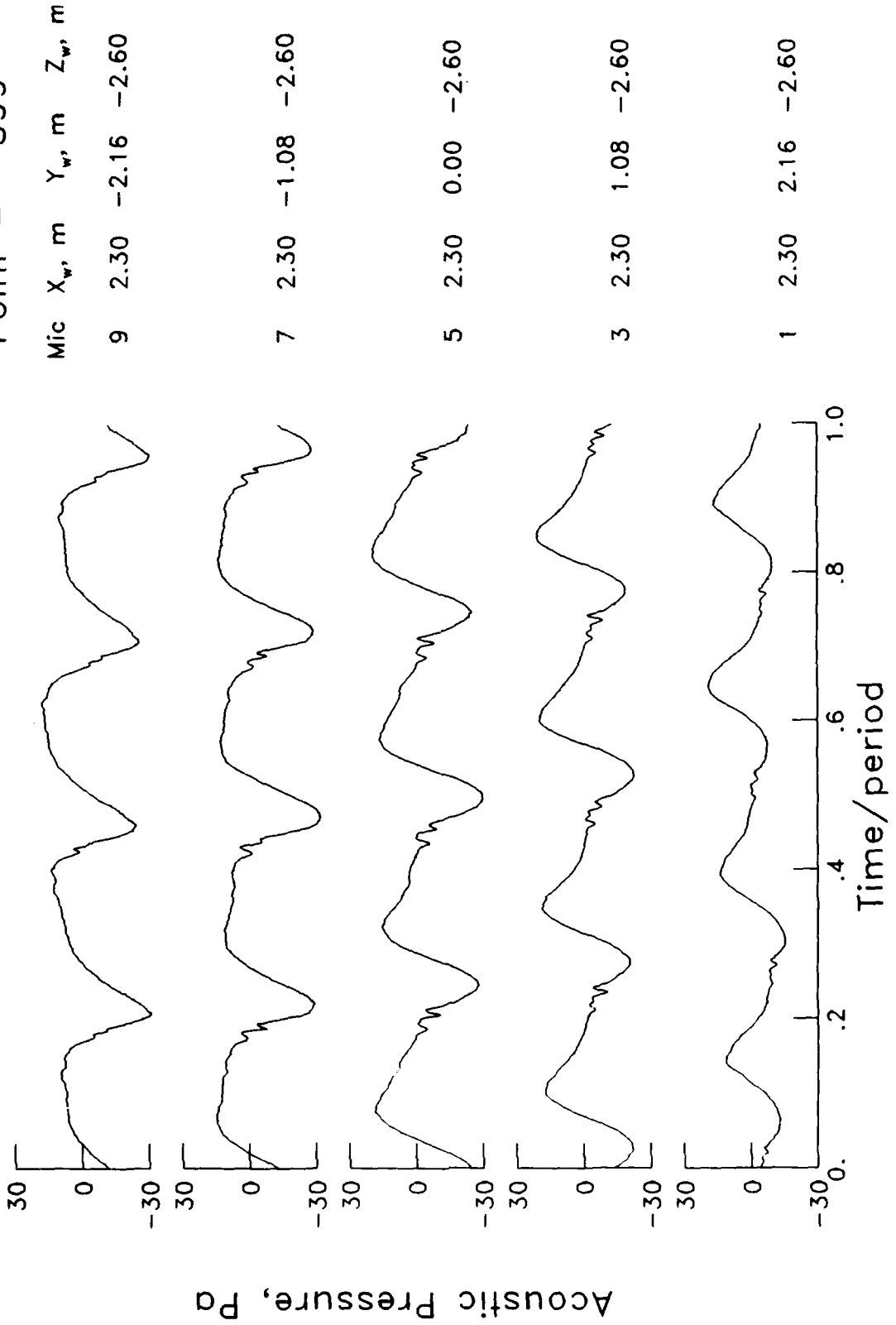


$\mu = .274$
 $\alpha_{TPP} = -1.3^\circ$
 $C_T = 0.0042$
 $M_H = 0.635$
 Point = 346

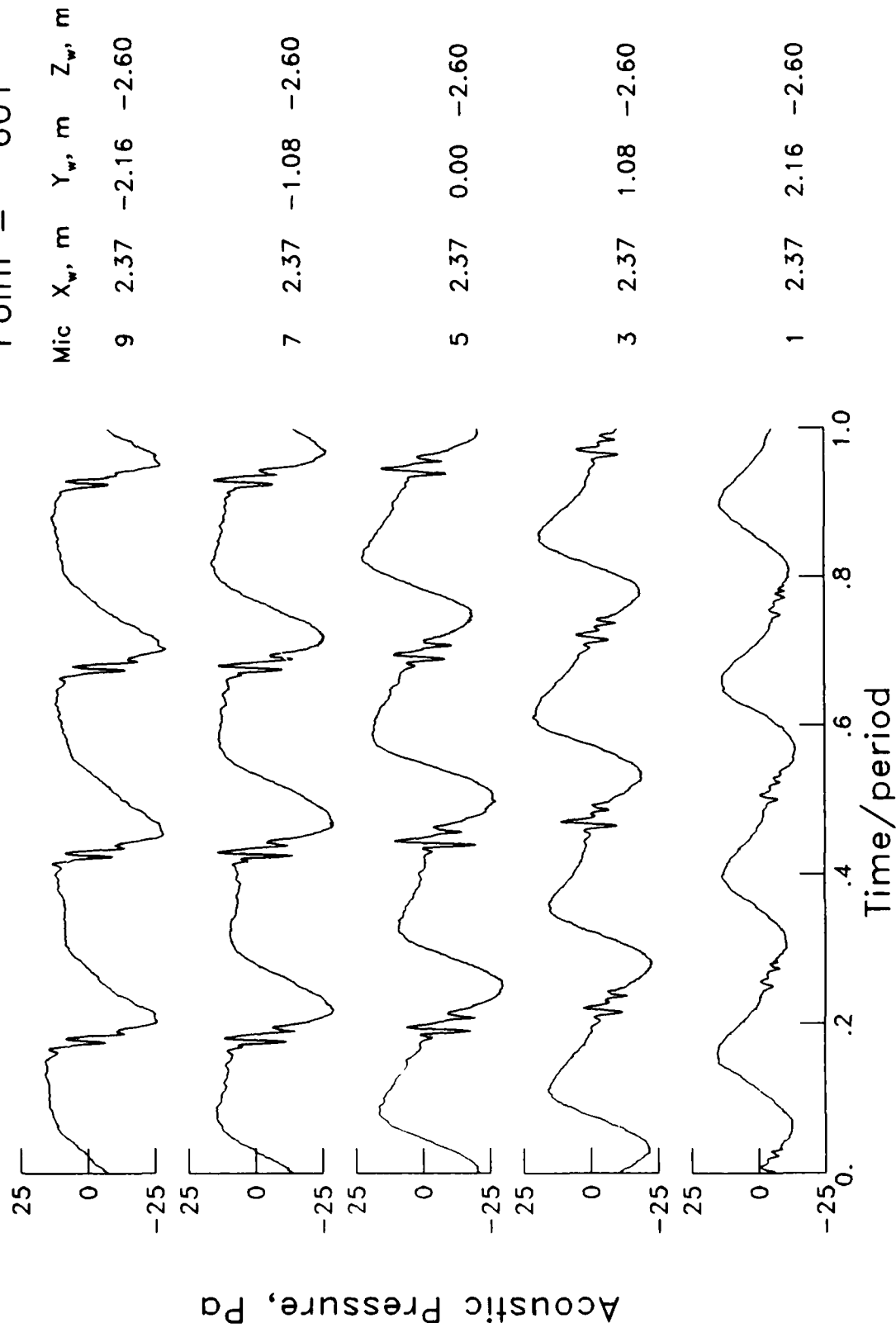
Mic	X _w , m	Y _w , m	Z _w , m
9	2.46	-2.16	-2.10
7	2.46	-1.08	-2.10
5	2.46	0.00	-2.10
3	2.46	1.08	-2.10
1	2.46	2.16	-2.10



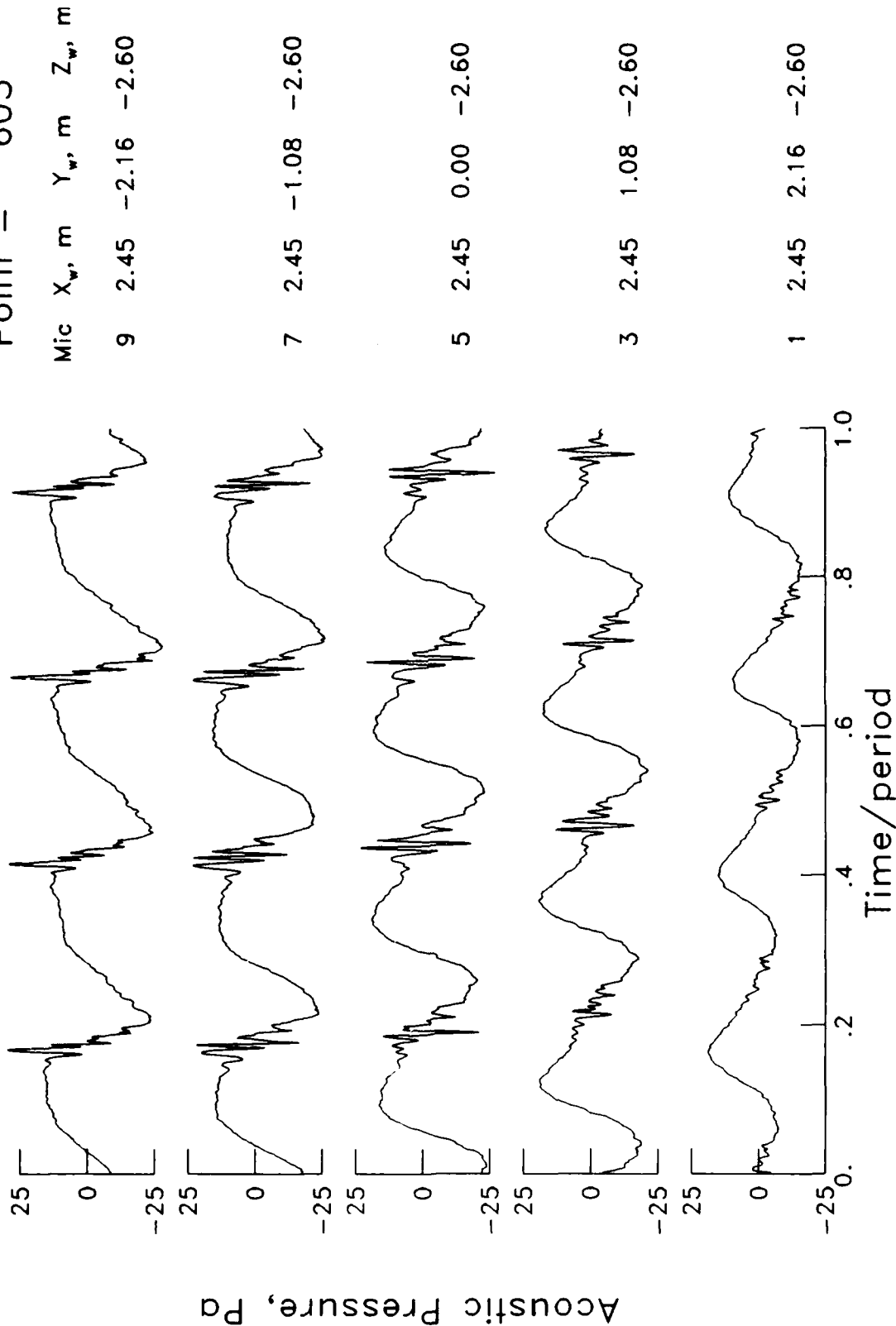
$\mu = .275$
 $\alpha_{\text{TPP}} = -7.3^\circ$
 $C_T = 0.0043$
 $M^H = 0.634$
 Point = 599



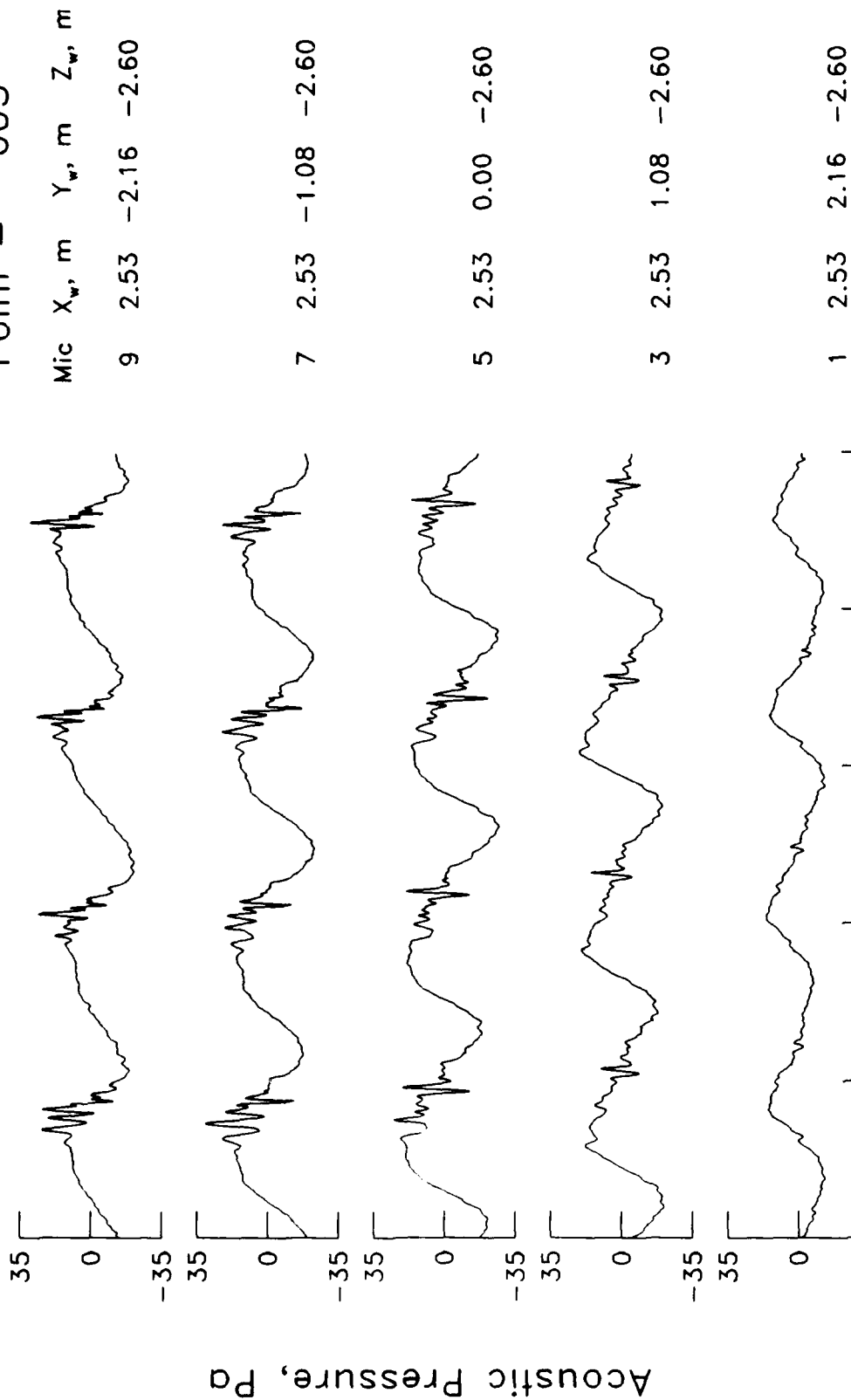
$\mu = .273$
 $\alpha_{TPP} = -5.3^\circ$
 $C_T = 0.0043$
 $M_{H,Point} = 0.636$
 $Point = 601$



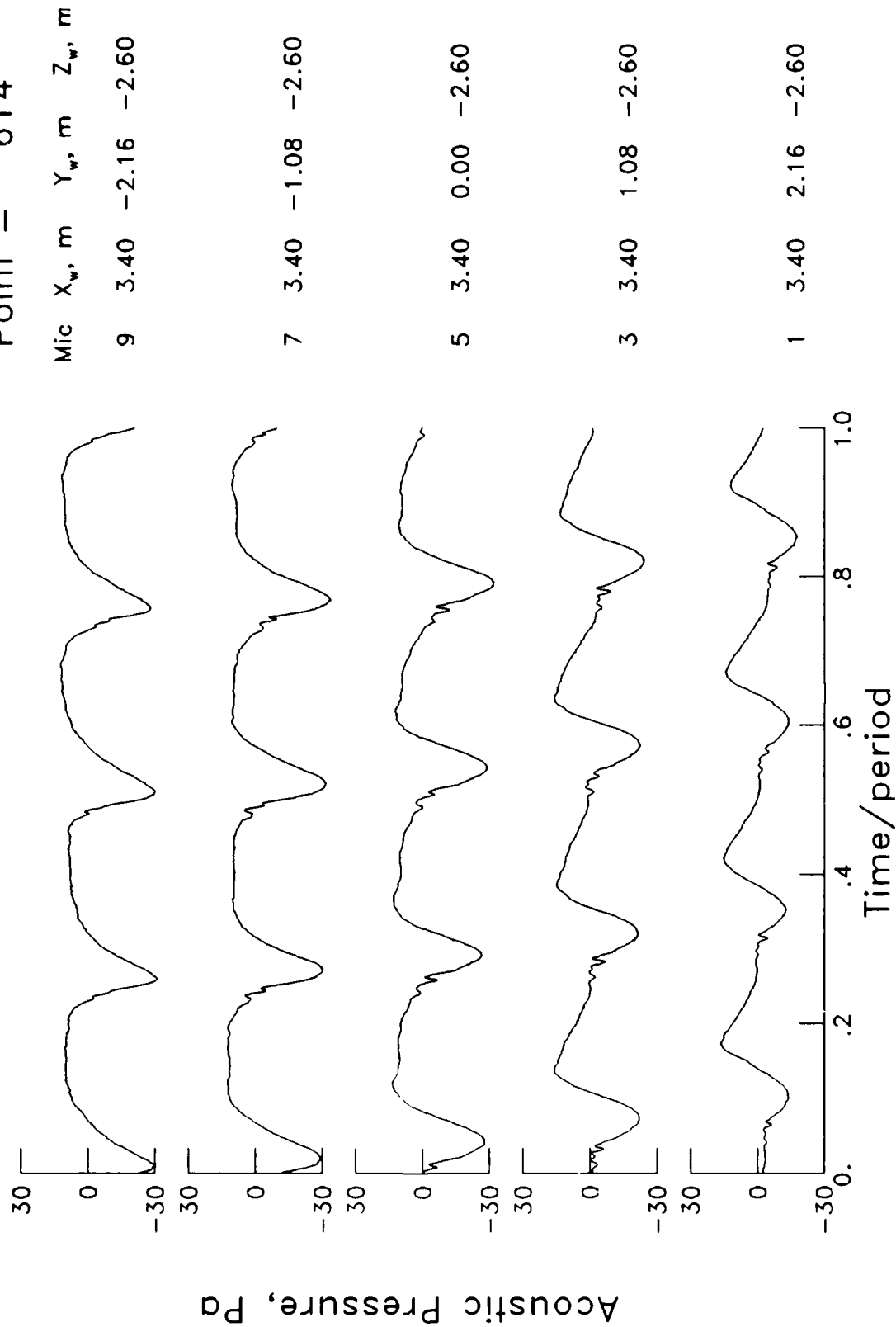
$\mu = .273$
 $\alpha_{TPP} = -3.3^\circ$
 $C_T = 0.0043$
 $M_H = 0.638$
 Point = 603



$\mu = .275$
 $\alpha_{TPP} = -1.3^\circ$
 $C_T = 0.0044$
 $M_H = 0.635$
 Point = 605

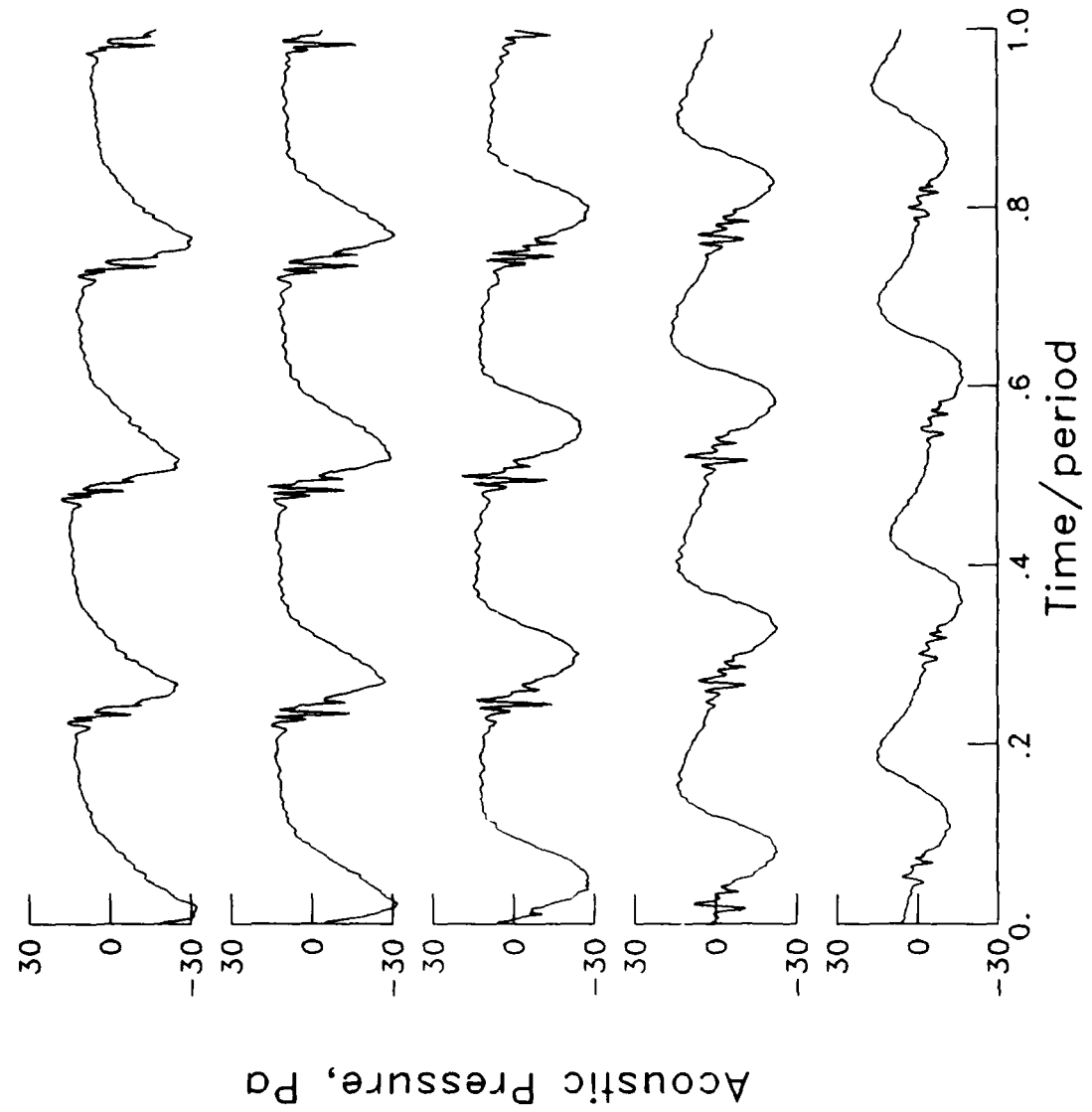


$\mu = .271$
 $\alpha_{TPP} = -7.3^\circ$
 $C_T = 0.0044$
 $M_H = 0.635$
 Point = 614

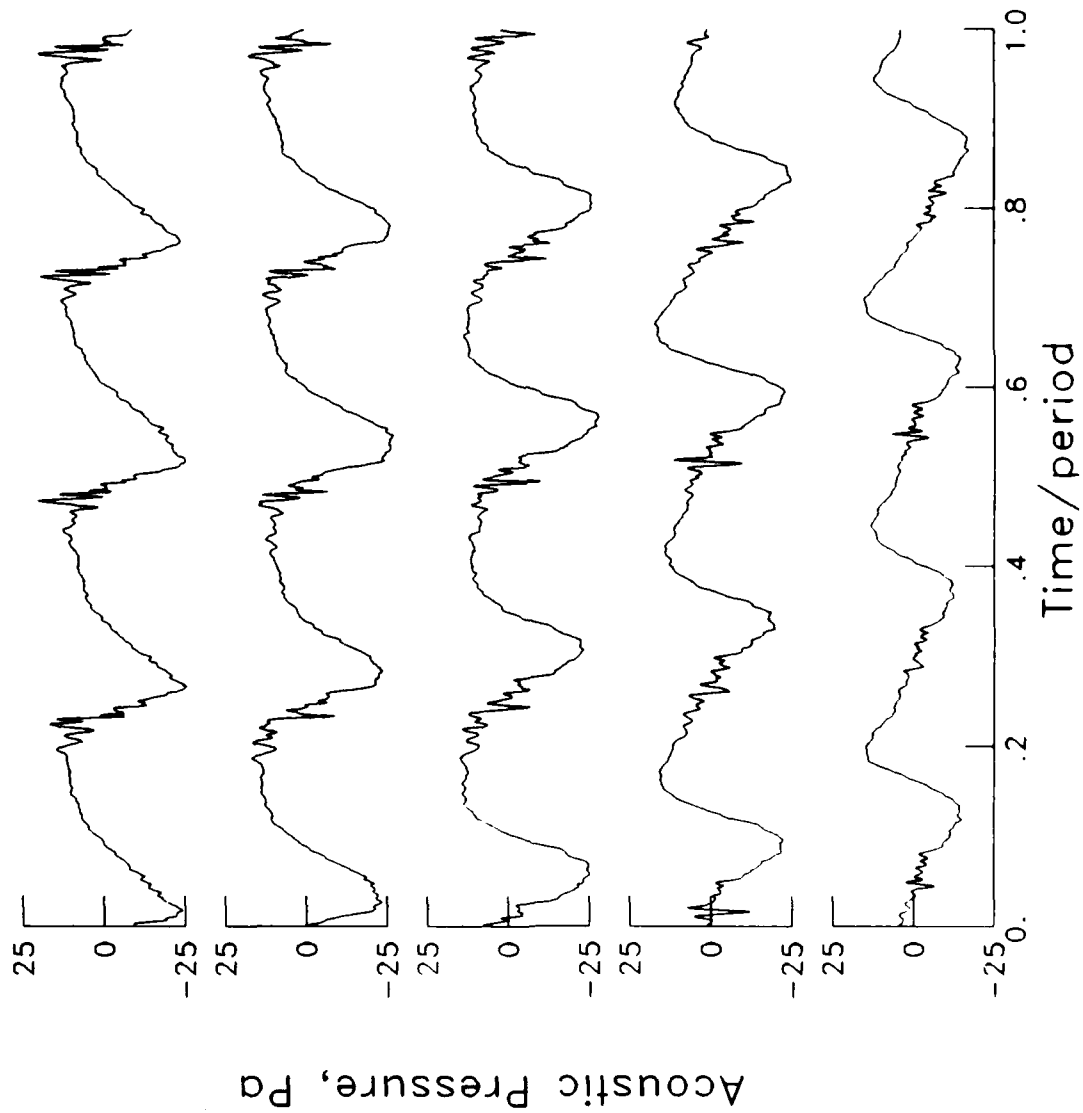


$\mu = .273$
 $\alpha_{TPP} = -4.3^\circ$
 $C_T = 0.0044$
 $M_H = 0.637$
 Point = 611

Mic	X _w , m	Y _w , m	Z _w , m
9	3.51	-2.16	-2.60
7	3.51	-1.08	-2.60
5	3.51	0.00	-2.60
3	3.51	1.08	-2.60
1	3.51	2.16	-2.60



$\mu = .272$
 $\alpha_{TPP} = -2.3^\circ$
 $C_T = 0.0043$
 $M_H = 0.637$
 Point = 609



Mic X_w, m Y_w, m Z_w, m

9 3.59 -2.16 -2.60

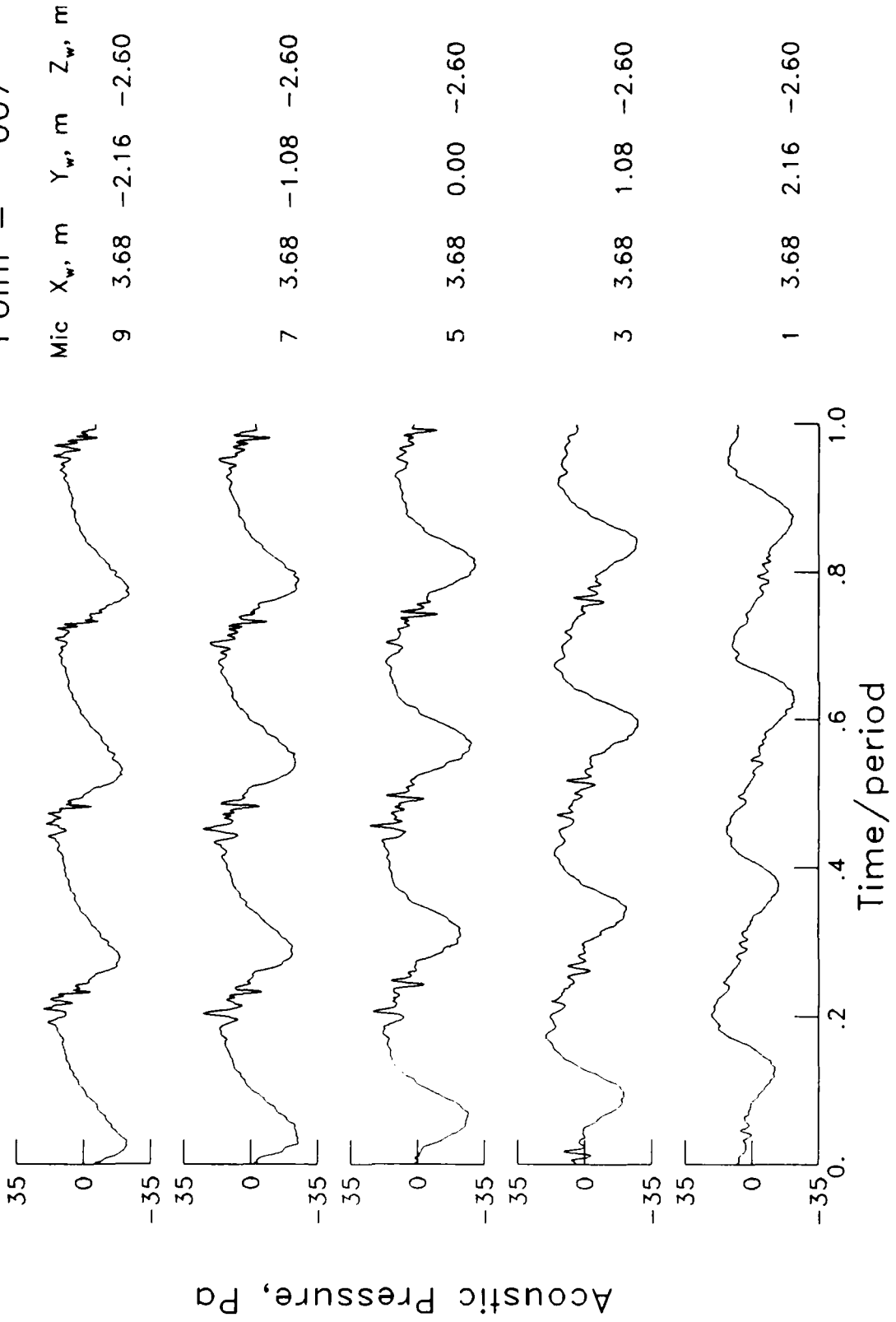
7 3.59 -1.08 -2.60

5 3.59 0.00 -2.60

3 3.59 1.08 -2.60

1 3.59 2.16 -2.60

$\mu = .274$
 $\alpha_{TPP} = -0.3^\circ$
 $C_T = 0.0043$
 $M_{H_1} = 0.636$
 Point = 607



$\mu = .142$
 $\alpha_{TPP} = 3.3$
 $C_T = 0.0044$
 $M_H = 0.559$
 Point = 545

Mic X_w, m Y_w, m Z_w, m

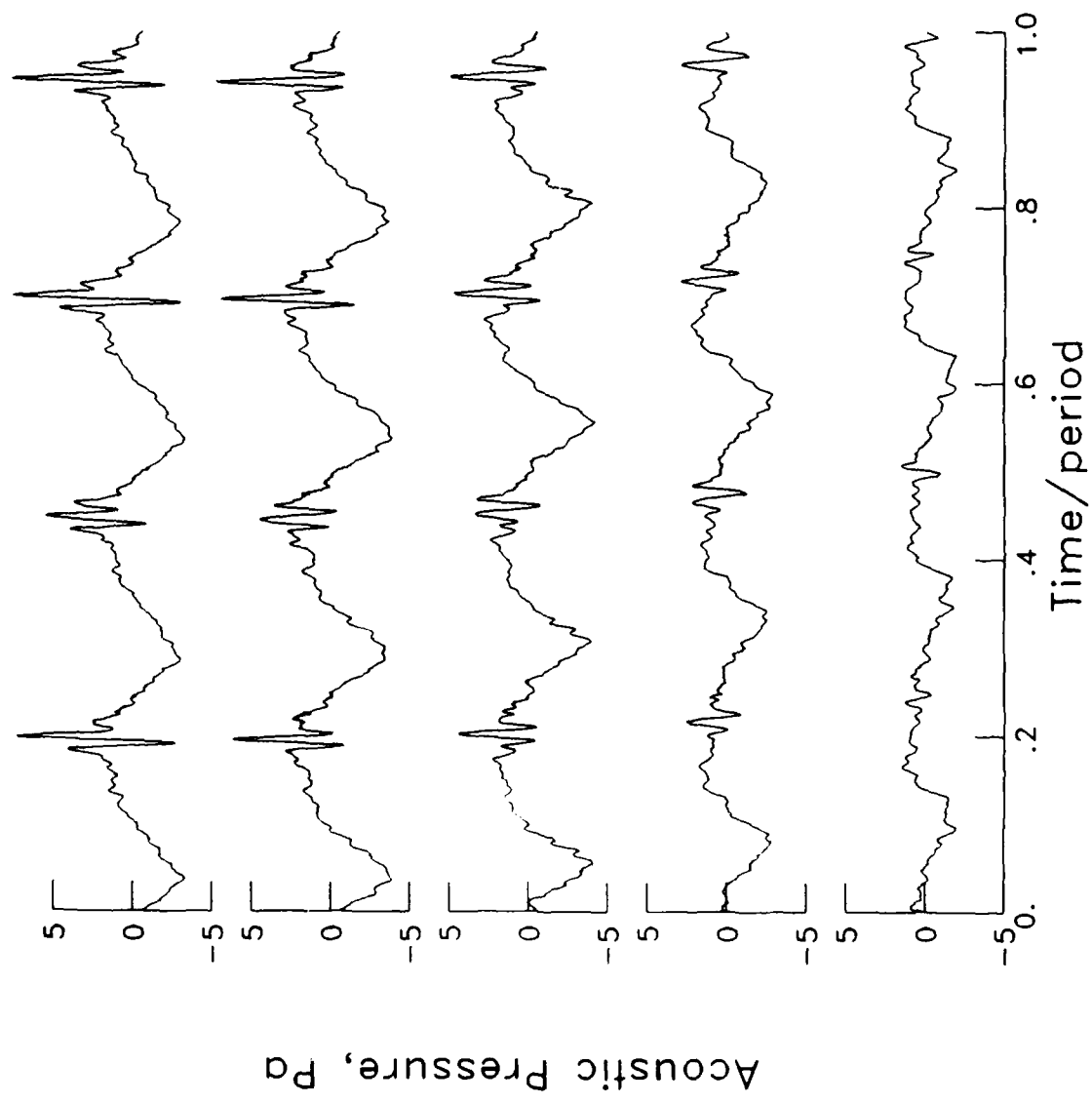
9 4.74 -2.16 -2.10

7 4.74 -1.08 -2.10

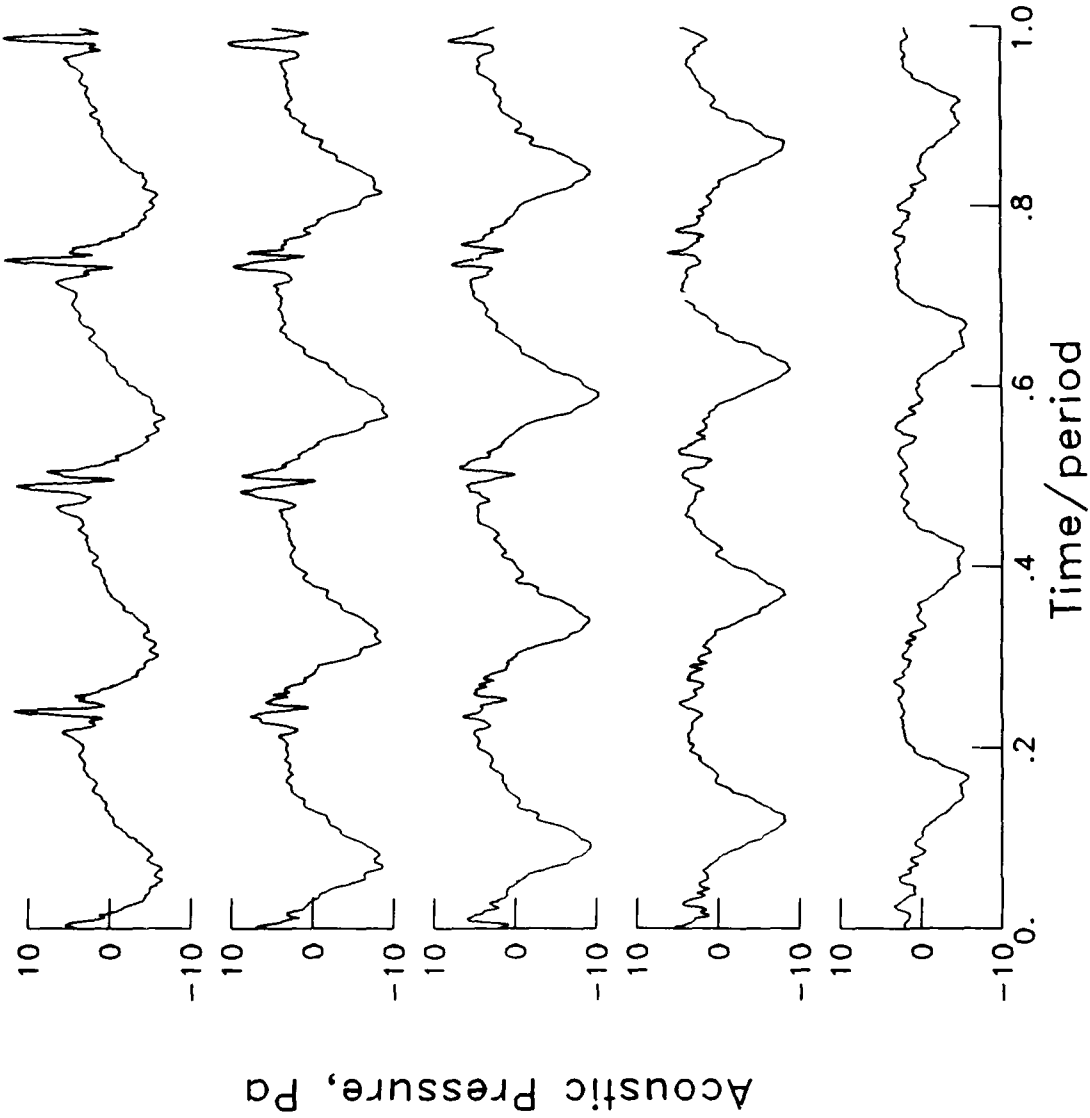
5 4.74 0.00 -2.10

3 4.74 1.08 -2.10

1 4.74 2.16 -2.10



$\mu = .141$
 $\alpha_{TPP} = 3.3^\circ$
 $C_T = 0.0043$
 $M_H = 0.636$
 Point = 547



Mic	X _w , m	Y _w , m	Z _w , m
9	4.74	-2.16	-2.10
7	4.74	-1.08	-2.10
5	4.74	0.00	-2.10
3	4.74	1.08	-2.10
1	4.74	2.16	-2.10

$\mu = .142$
 $\alpha_{TPP} = 3.4^\circ$
 $C_T = 0.0043$
 $M_H = 0.675$
 Point = 548

Mic X_w, m Y_w, m Z_w, m

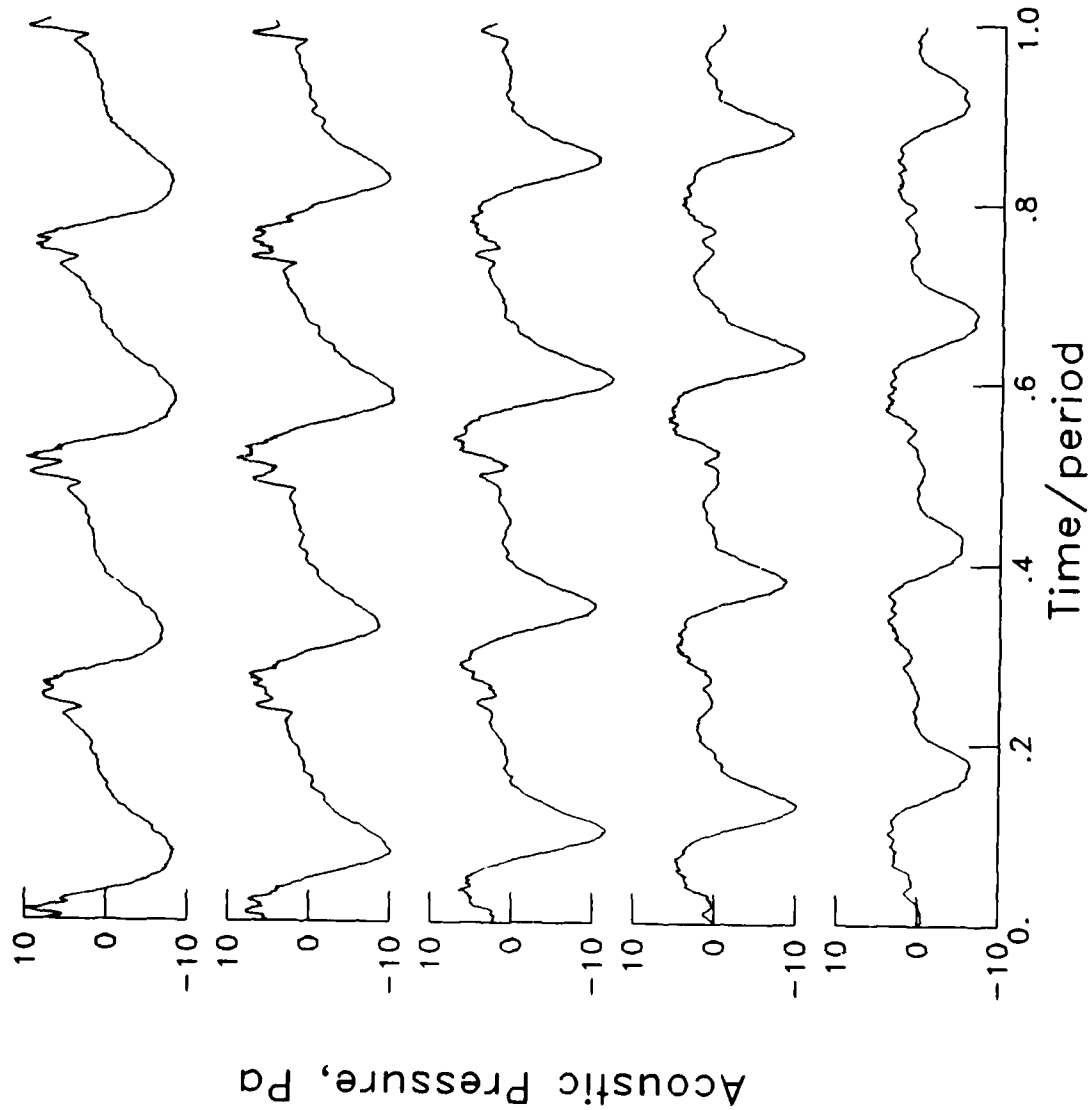
9 4.74 -2.16 -2.10

7 4.74 -1.08 -2.10

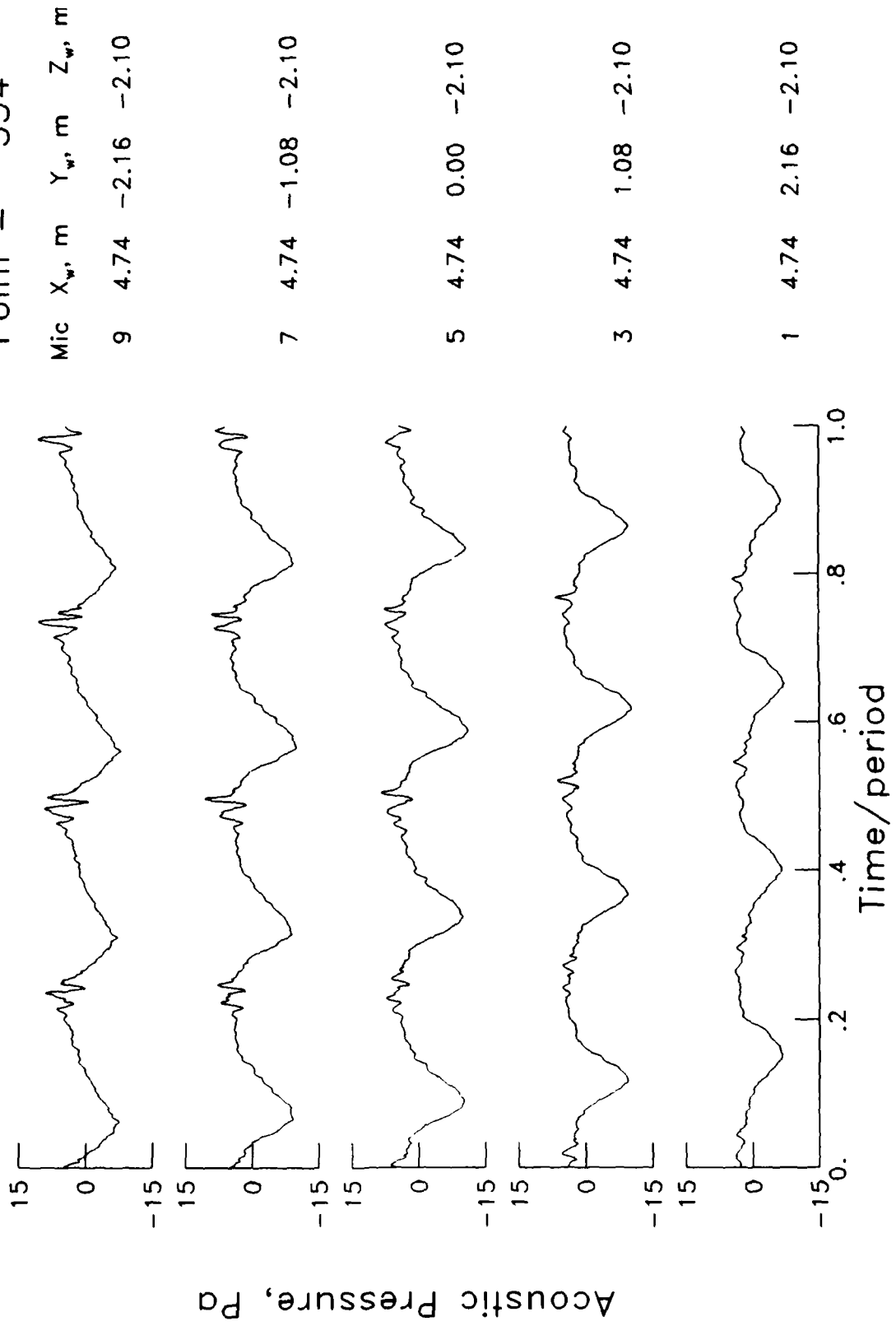
5 4.74 0.00 -2.10

3 4.74 1.08 -2.10

1 4.74 2.16 -2.10



$\mu = .143$
 $\alpha_{TPP} = 3.6^\circ$
 $C_T = 0.0036$
 $M_H = 0.635$
 Point = 554



$\mu = .142$
 $\alpha_{TPP} = 3.5^\circ$
 $C_T = 0.0040$
 $M_{H_i} = 0.637$
 Point = 553

Mic X_w, m Y_w, m Z_w, m

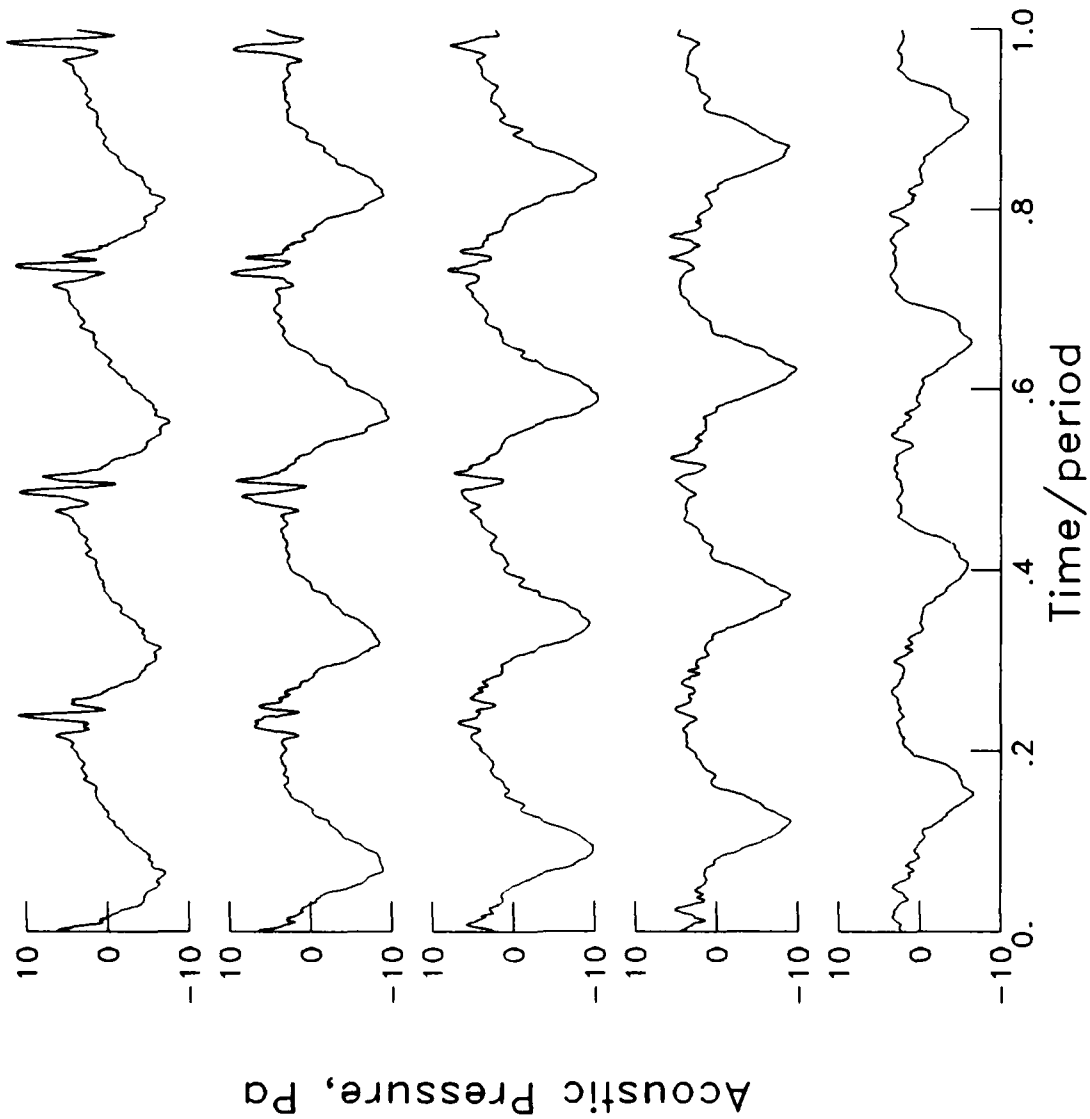
9 4.74 -2.16 -2.10

7 4.74 -1.08 -2.10

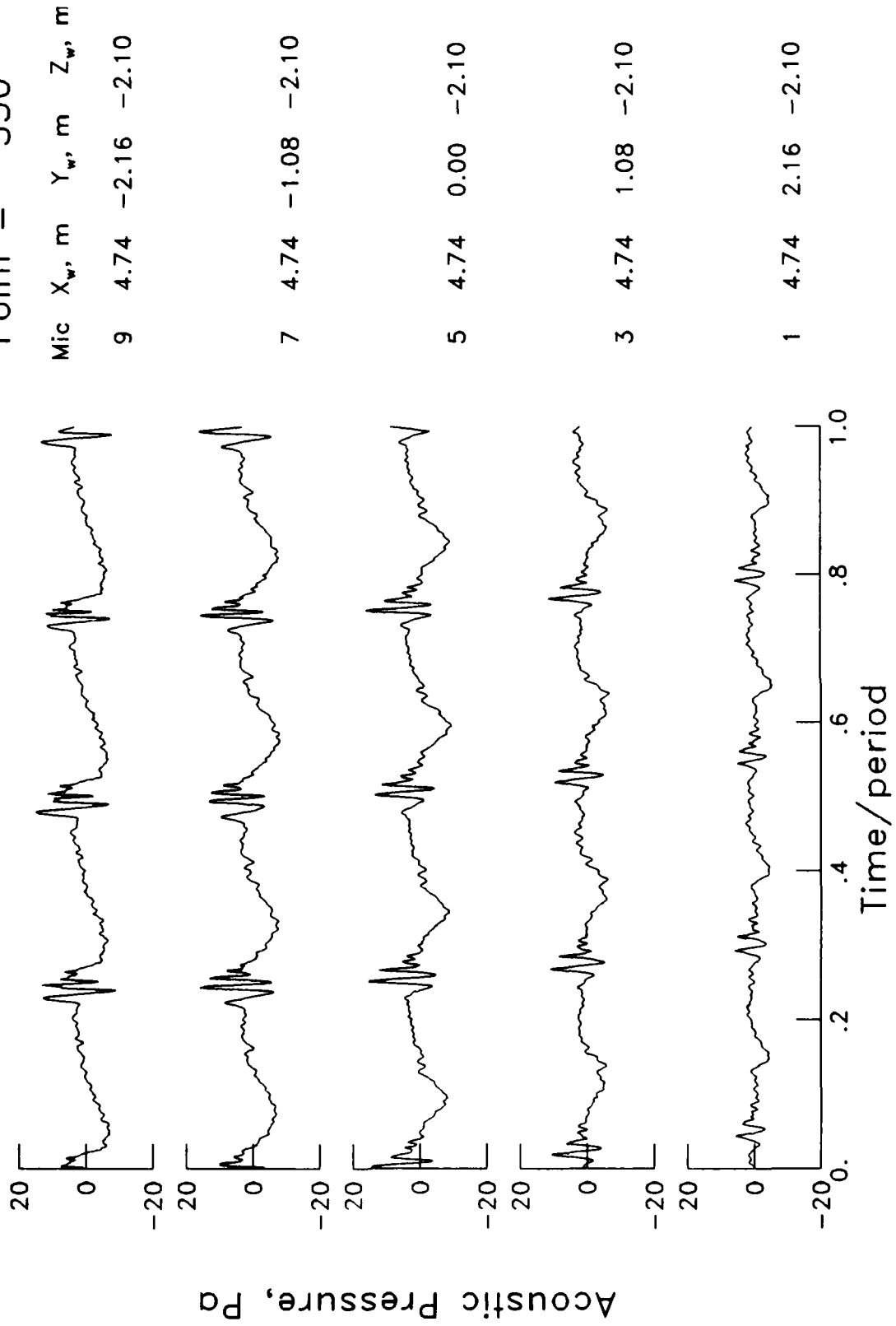
5 4.74 0.00 -2.10

3 4.74 1.08 -2.10

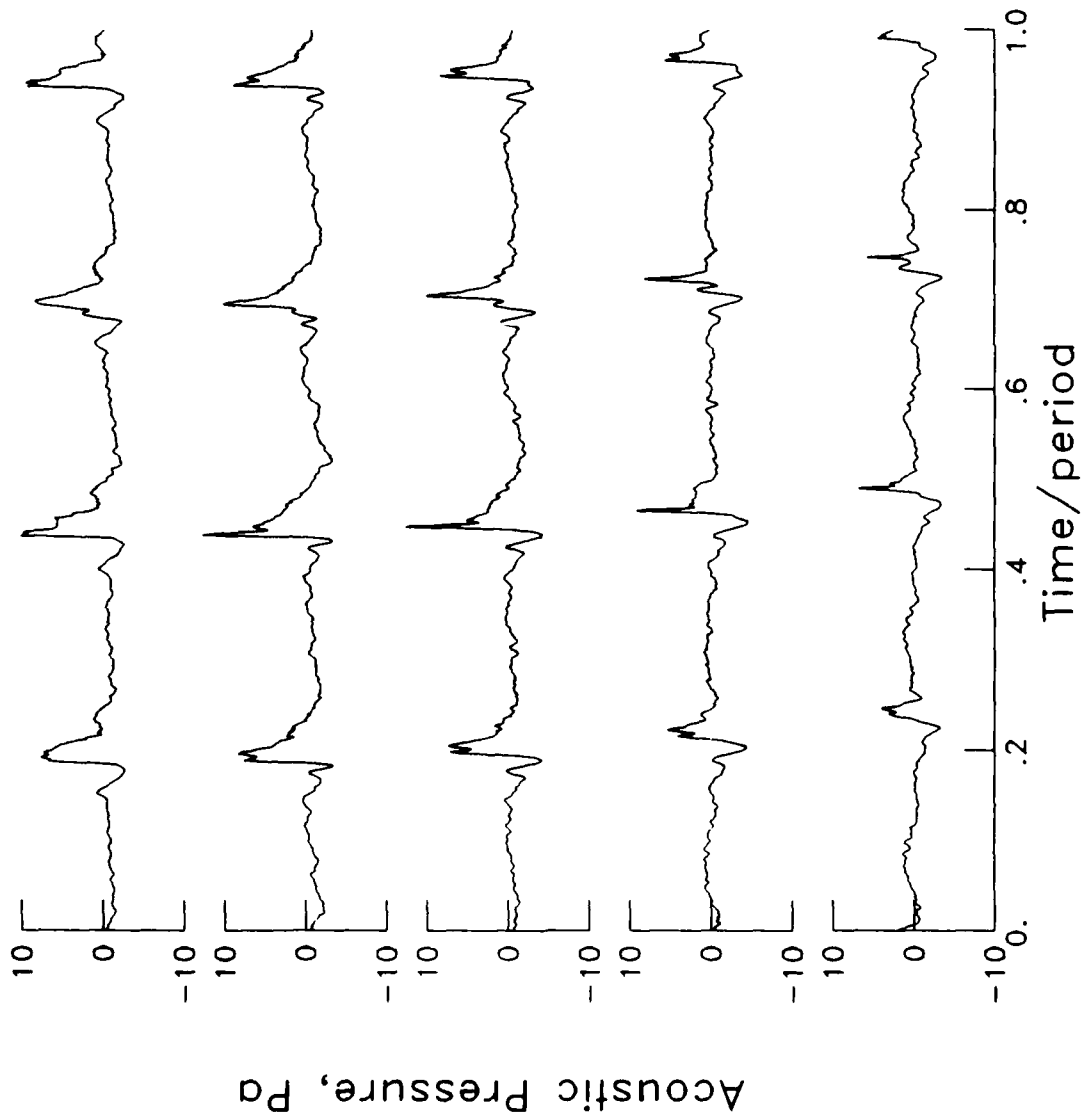
1 4.74 2.16 -2.10



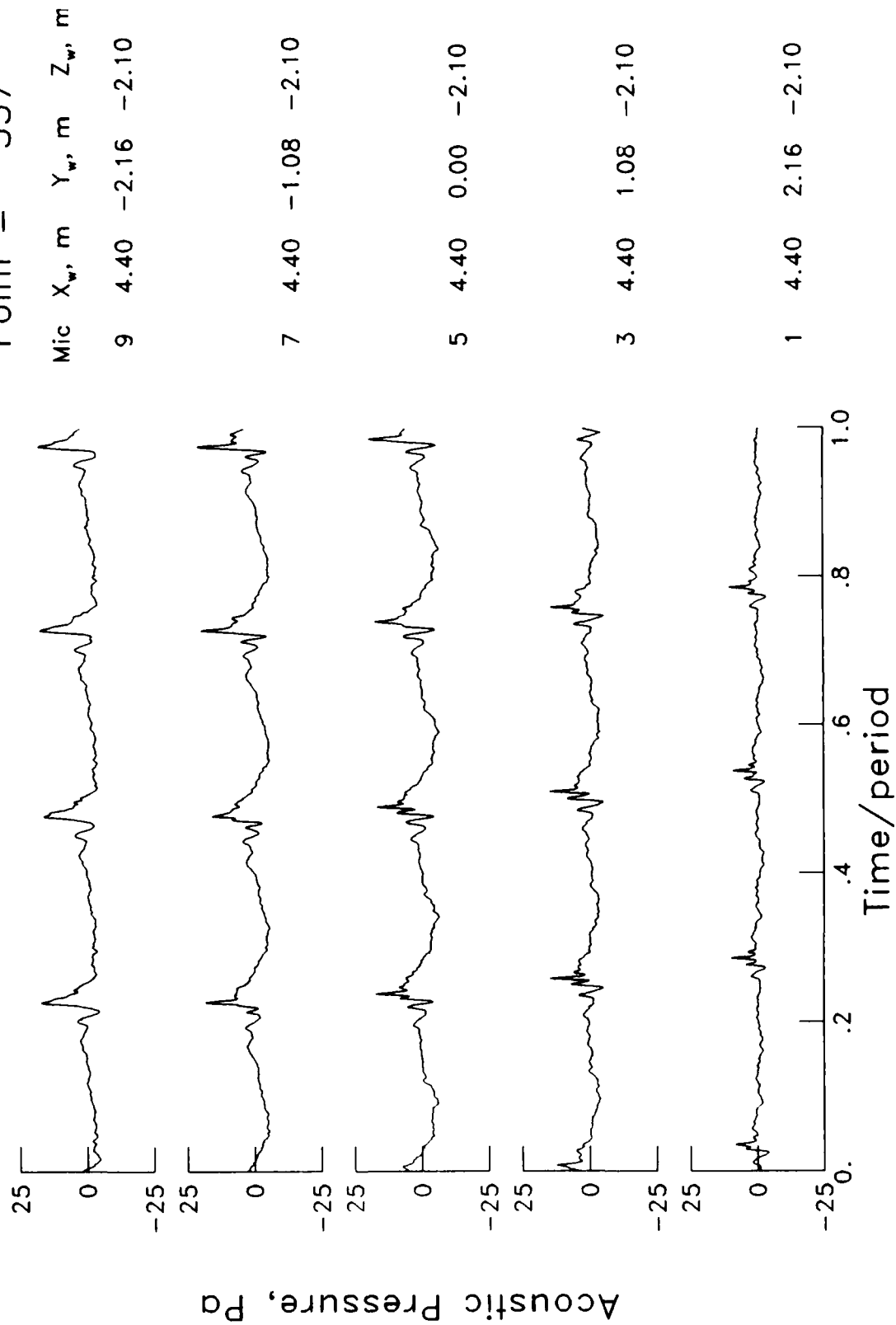
$\mu = .141$
 $\alpha_{TPP} = 2.9^\circ$
 $C_T = 0.0055$
 $M^H = 0.637$
 Point = 550



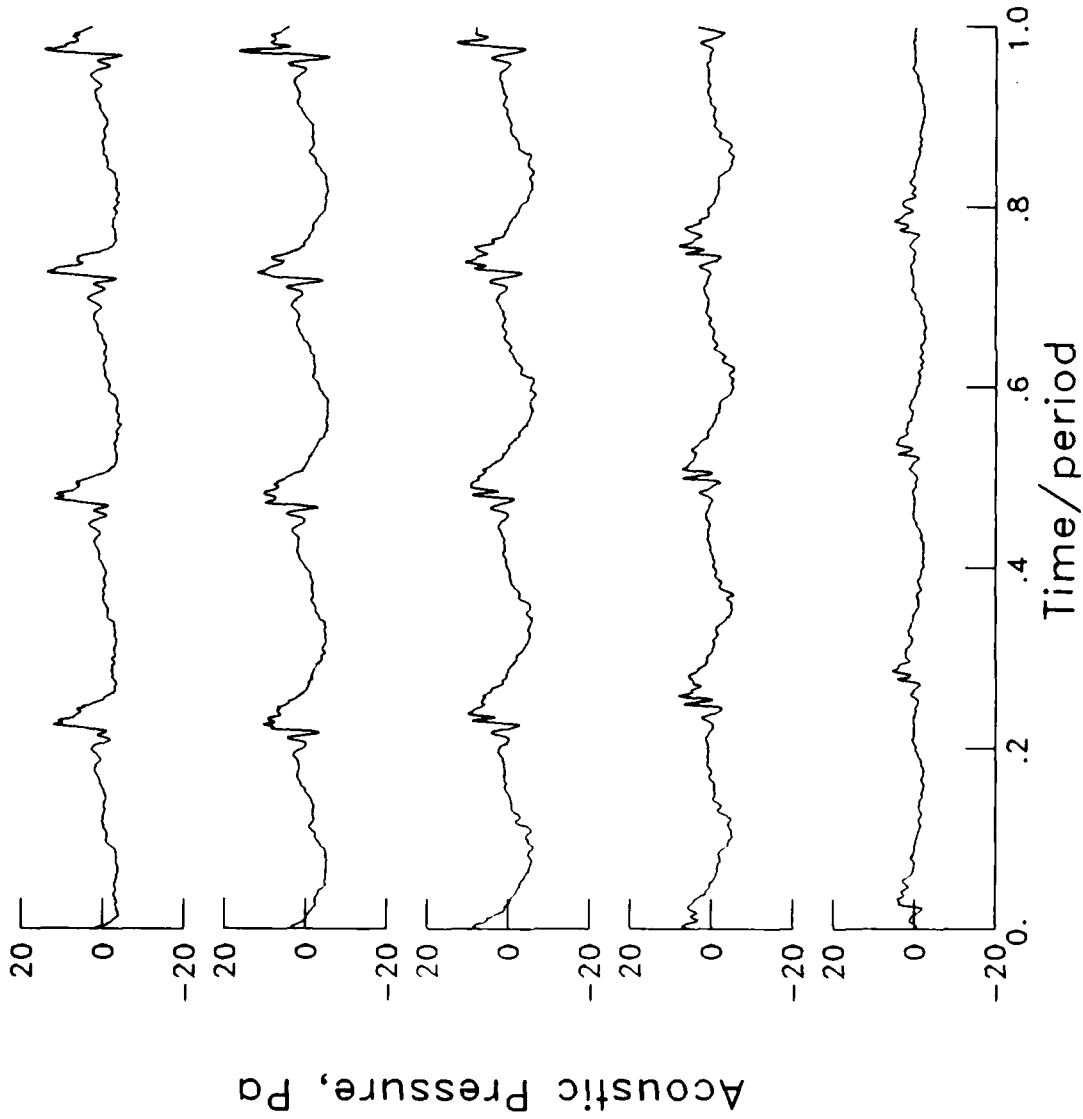
$\mu = .089$
 $\alpha_{TPP} = 4.2^\circ$
 $C_T = 0.0039$
 $M_H = 0.557$
 Point = 555



$\mu = .091$
 $\alpha_{TPP} = 4.0^\circ$
 $C_T = 0.0043$
 $M_{H_i} = 0.636$
 Point = 557



$\mu = .091$
 $\alpha_{TPP} = 4.6^\circ$
 $C_T = 0.0036$
 $M_H = 0.639$
 Point = 560



Mic X_w, m Y_w, m Z_w, m

9 4.39 -2.16 -2.10

7 4.39 -1.08 -2.10

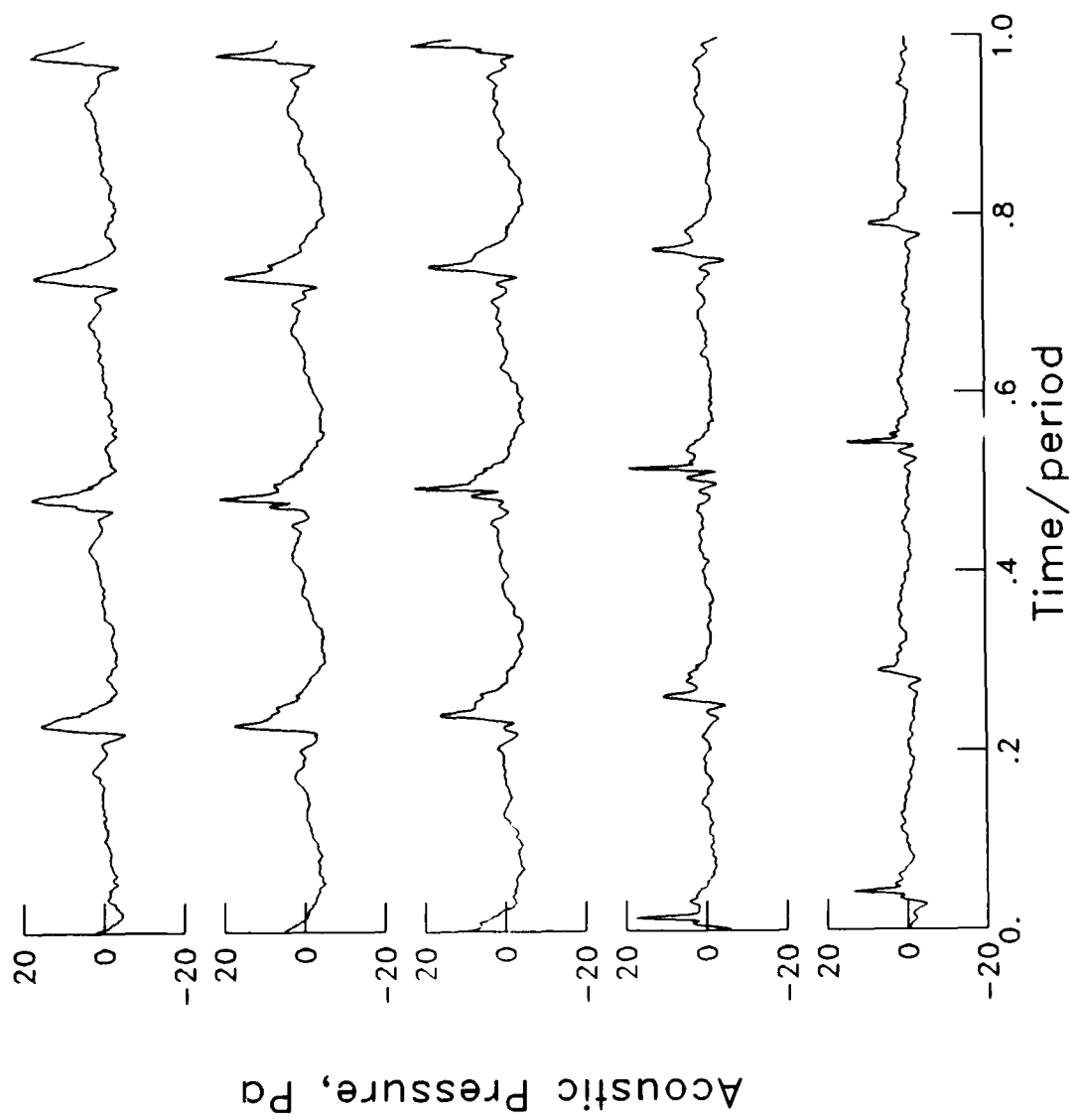
5 4.39 0.00 -2.10

3 4.39 1.08 -2.10

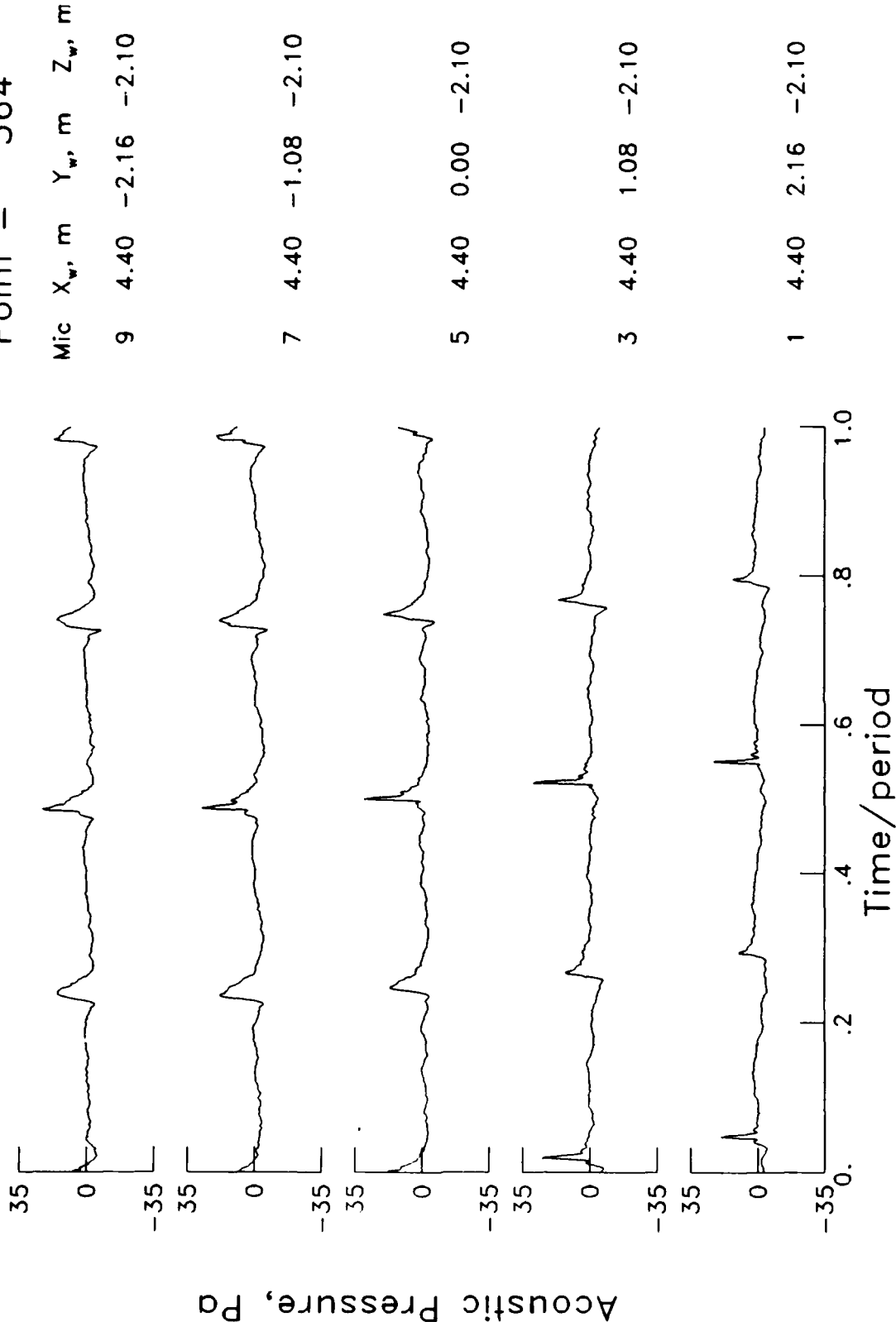
1 4.39 2.16 -2.10

$\mu = .090$
 $\alpha_{TPP} = 3.6^\circ$
 $C_T = 0.0047$
 $M_H = 0.636$
 Point = 562

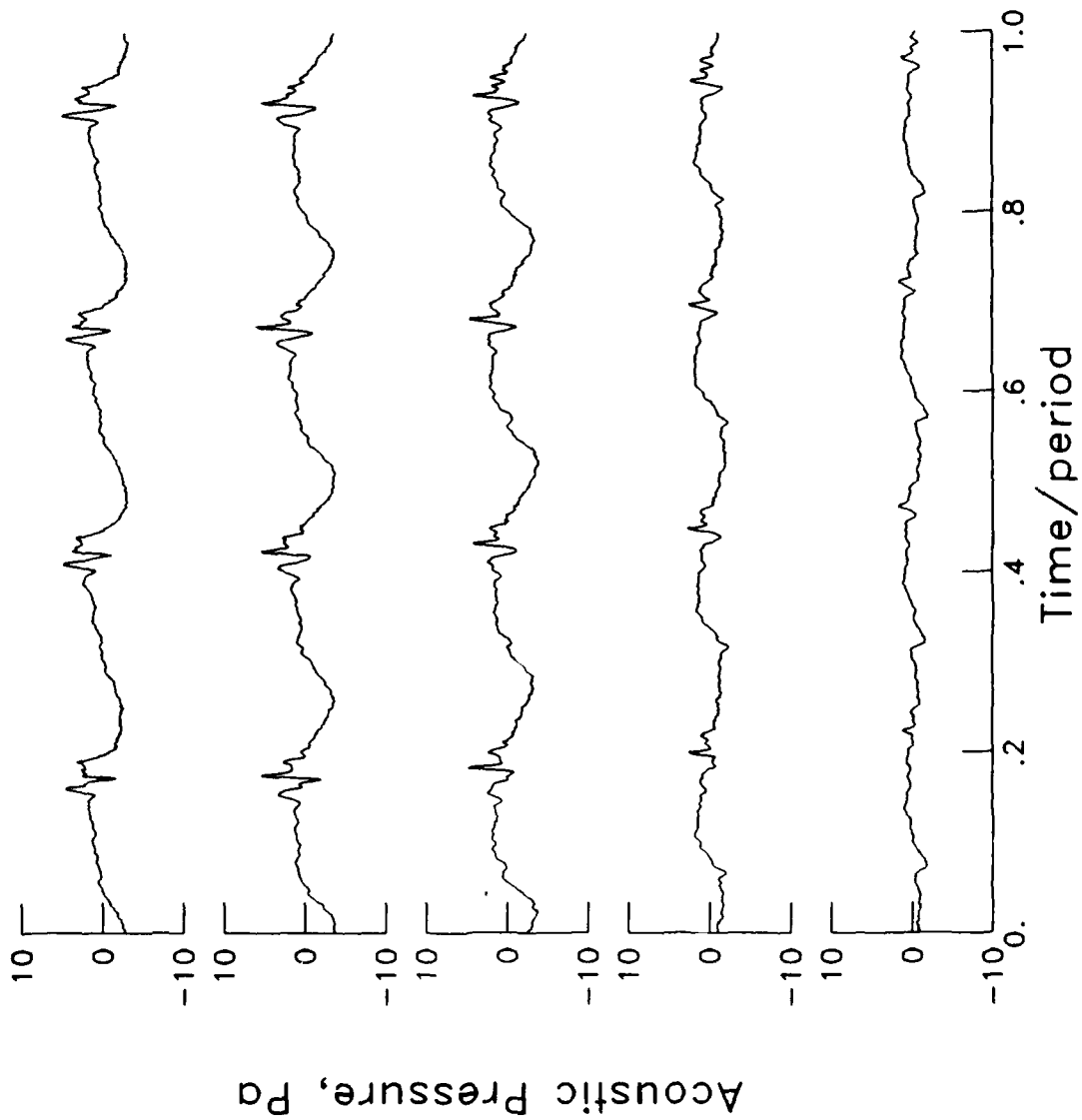
Mic	X _w , m	Y _w , m	Z _w , m
9	4.40	-2.16	-2.10
7	4.40	-1.08	-2.10
5	4.40	0.00	-2.10
3	4.40	1.08	-2.10
1	4.40	2.16	-2.10



$\mu = .091$
 $\alpha_{TPP} = 2.9^\circ$
 $C_T = 0.0055$
 $M_{H_i} = 0.635$
 Point = 564



$\mu = .175$
 $\alpha_{TPP} = -0.6^\circ$
 $C_T = 0.0043$
 $M_H = 0.559$
 Point = 565



Mic	X _w , m	Y _w , m	Z _w , m
9	4.02	-2.16	-2.10

7	4.02	-1.08	-2.10
---	------	-------	-------

5	4.02	0.00	-2.10
---	------	------	-------

3	4.02	1.08	-2.10
---	------	------	-------

1	4.02	2.16	-2.10
---	------	------	-------

$\mu = .175$
 $\alpha_{TPP} = -0.5^\circ$
 $C_T = 0.0044$
 $M_H = 0.635$
 Point = 567

Mic X_w , m Y_w , m Z_w , m

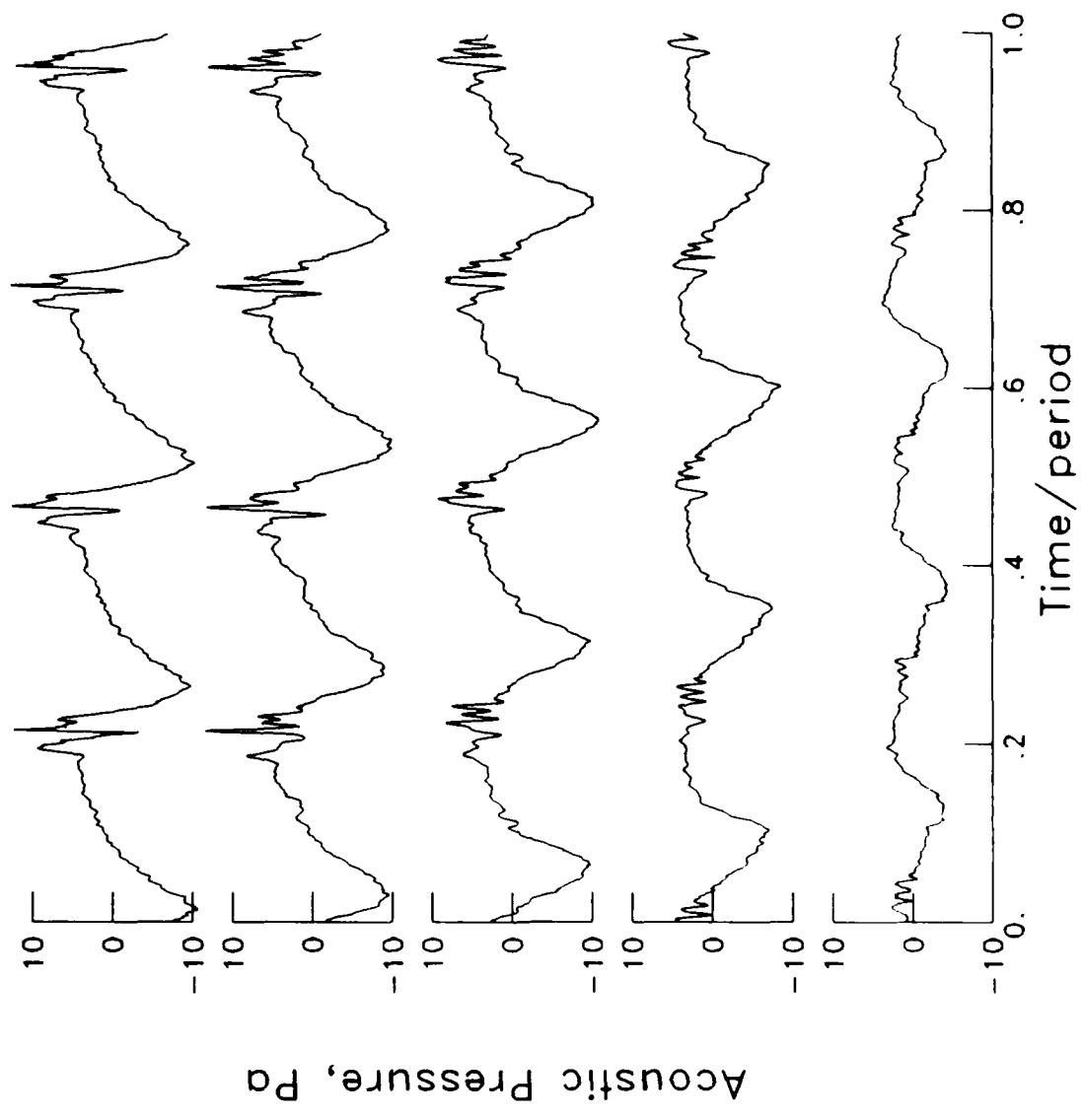
9 4.02 -2.16 -2.10

7 4.02 -1.08 -2.10

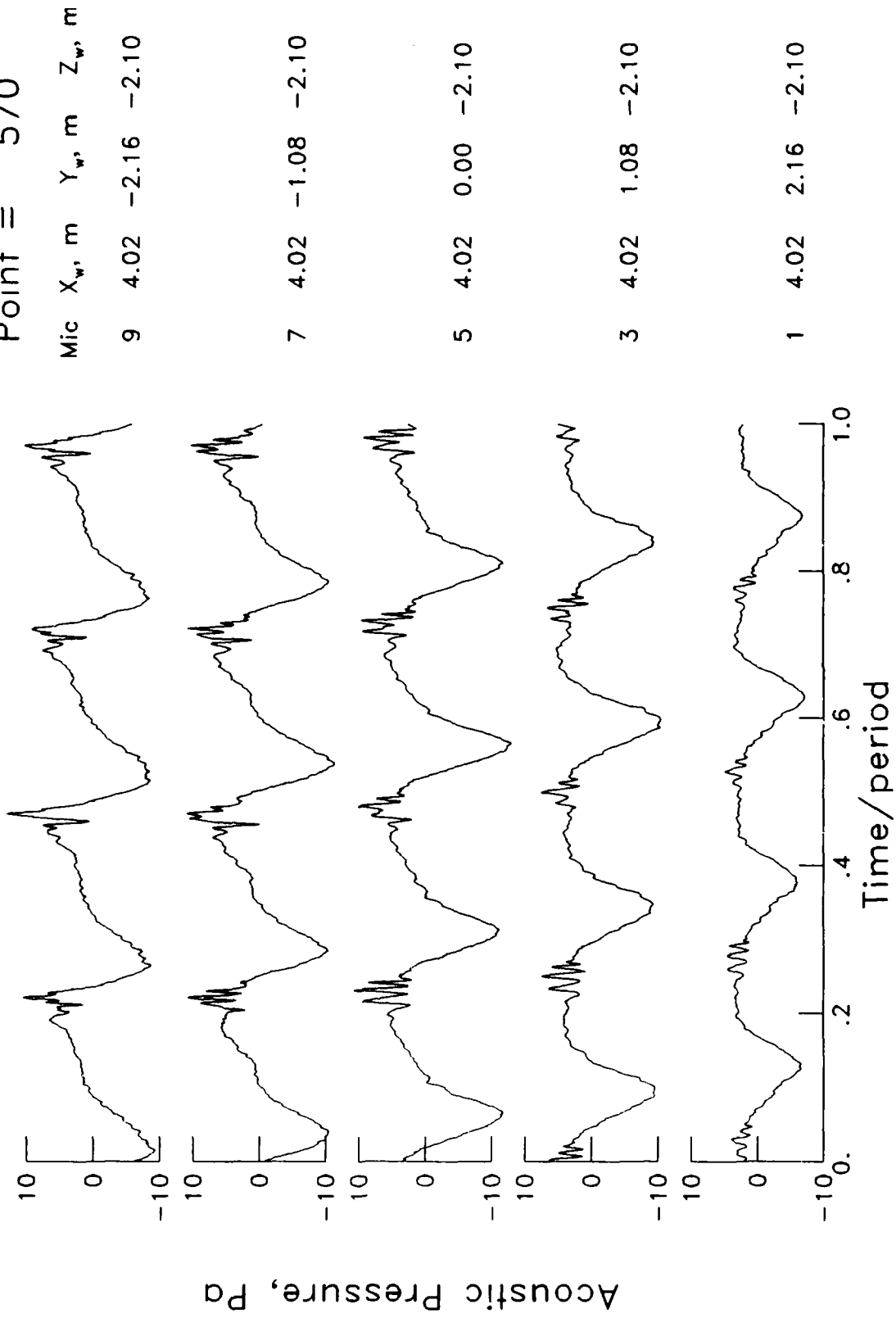
5 4.02 0.00 -2.10

3 4.02 1.08 -2.10

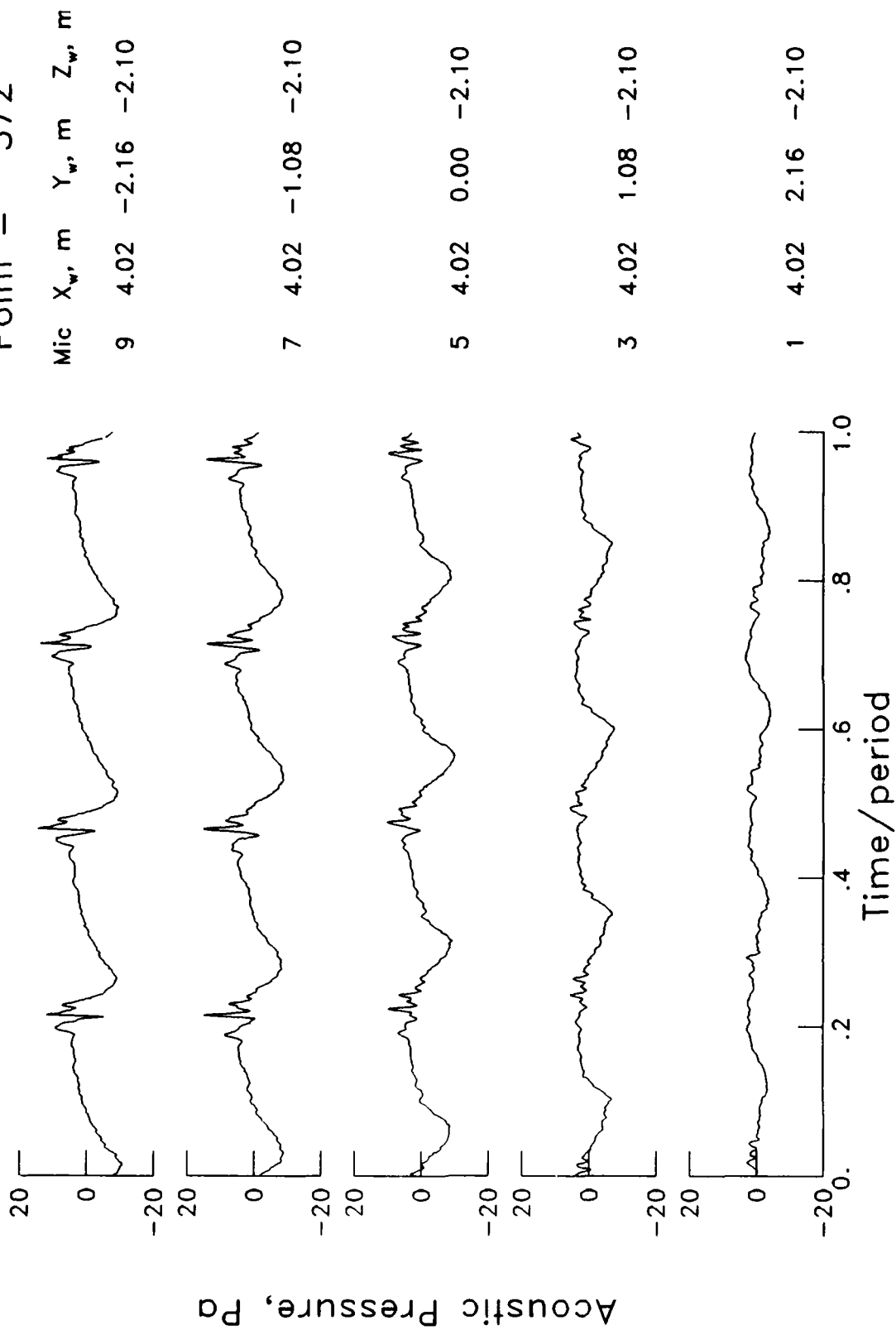
1 4.02 2.16 -2.10



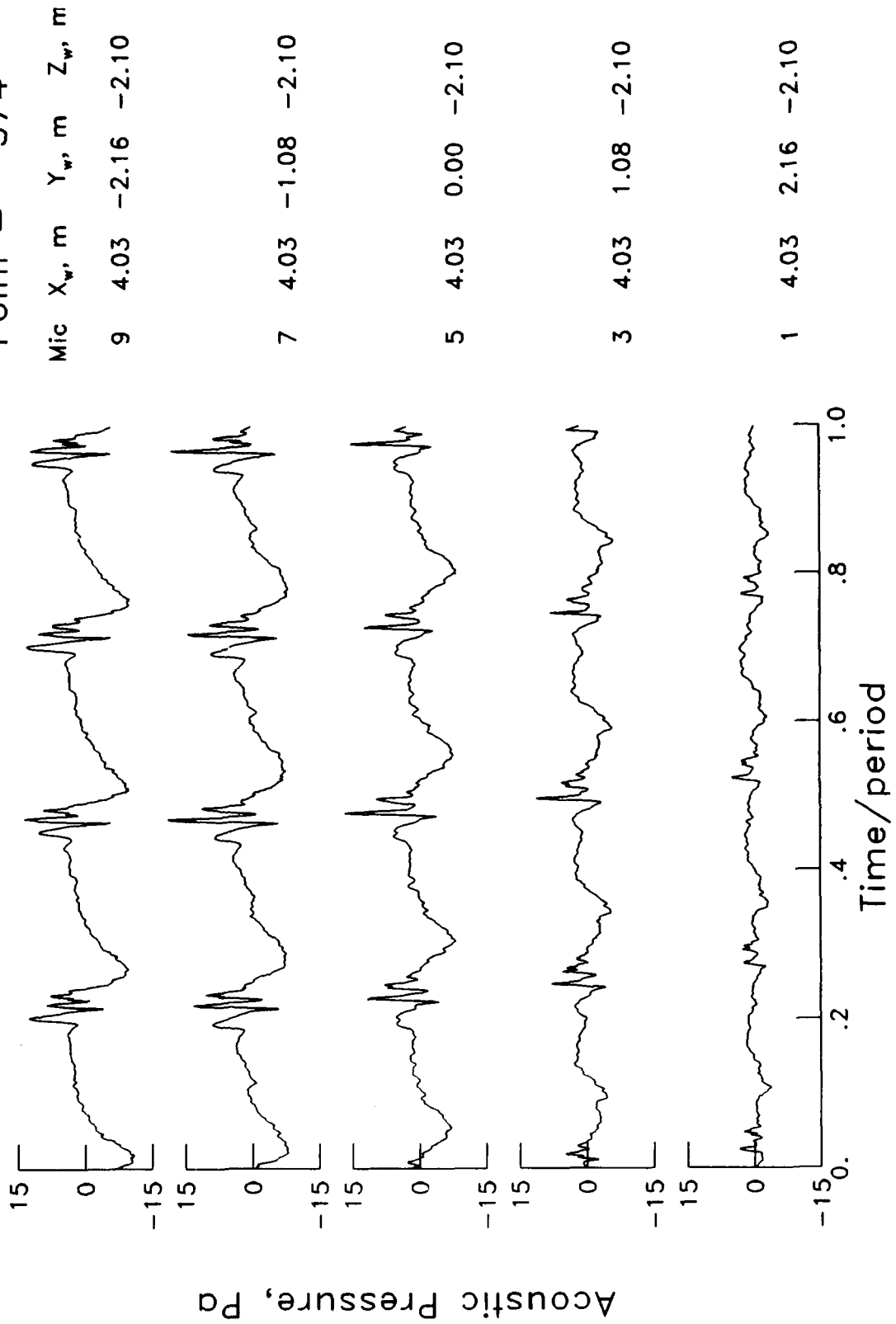
$\mu = .174$
 $\alpha_{TPP} = -0.3^\circ$
 $C_T = 0.0035$
 $M_H = 0.638$
 Point = 570



$\mu = .175$
 $\alpha_{TPP} = -0.6^\circ$
 $C_T = 0.0047$
 $M_H = 0.634$
 Point = 572



$\mu = .175$
 $\alpha_{TPP} = -0.8^\circ$
 $C_T = 0.0055$
 $M_{H_i} = 0.635$
 Point = 574





Report Documentation Page

1. Report No. NASA TM-4024 AVSCOM TR 87-B-4		2. Government Accession No.		3. Recipient's Catalog No.	
4. Title and Subtitle Acoustic Measurements From a Rotor Blade-Vortex Interaction Noise Experiment in the German-Dutch Wind Tunnel (DNW)				5. Report Date March 1988	
				6. Performing Organization Code	
7. Author(s) R. M. Martin, W. R. Splettstoesser, J. W. Elliott, and K.-J. Schultz				8. Performing Organization Report No. L-16368	
9. Performing Organization Name and Address Aerostructures Directorate USA ARTA-AVSCOM Langley Research Center Hampton, VA 23665-5225				10. Work Unit No. 505-61-51-06	
				11. Contract or Grant No.	
12. Sponsoring Agency Name and Address National Aeronautics and Space Administration Washington, DC 20546-0001 and U.S. Army Aviation Systems Command St. Louis, MO 63120-1798				13. Type of Report and Period Covered Technical Memorandum	
				14. Army Project No. 1L161102AH45	
15. Supplementary Notes R. M. Martin: Langley Research Center, Hampton, Virginia. W. R. Splettstoesser and K.-J. Schultz: DFVLR, Braunschweig, West Germany. J. W. Elliott: Aerostructures Directorate, USAARTA-AVSCOM, Langley Research Center, Hampton, Virginia.					
16. Abstract Acoustic data are presented from a 40-percent-scale model of the four-bladed BO-105 helicopter main rotor, tested in a large aeroacoustic wind tunnel. Rotor blade-vortex interaction (BVI) noise data in the low-speed flight range were acquired using a traversing in-flow microphone array. The experimental apparatus, testing procedures, calibration results, and experimental objectives are fully described. A large representative set of averaged acoustic signals are presented.					
17. Key Words (Suggested by Author(s)) Rotor acoustics Blade-vortex interaction noise Acoustic directivity				18. Distribution Statement Unclassified - Unlimited Subject Category 71	
19. Security Classif.(of this report) Unclassified		20. Security Classif.(of this page) Unclassified		21. No. of Pages 181	22. Price A05